NOVEL MICROBIAL PLATFORM FOR DEGRADATION OF HAZARDOUS ORGANIC CONTAMINANTS AND PRODUCTION OF SUSTAINABLE BIOPLASTICS

A Dissertation

Presented to

The Academic Faculty

By

Ramanan Sekar

In Partial Fulfillment

of the Requirements for the Degree

Doctor of Philosophy in the

School of Biology

Georgia Institute of Technology

May 2016

NOVEL MICROBIAL PLATFORM FOR DEGRADATION OF HAZARDOUS ORGANIC CONTAMINANTS AND PRODUCTION OF SUSTAINABLE BIOPLASTICS

Approved by:

Dr. Thomas DiChristina, Advisor
School of Biology
Georgia Institute of Technology

Dr. Yuanzhi Tang
School of Earth and Atmospheric Sciences
Georgia Institute of Technology

Dr. Martial Taillefert
School of Earth and Atmospheric Sciences
Georgia Institute of Technology

Dr. Brian Hammer
School of Biology
Georgia Institute of Technology

Dr. Roger Wartell
School of Biology
Georgia Institute of Technology

Date Approved: 30 March 2016

To my dearest parents,

For their unconditional love and support

To my wife Nita,

For her love, encouragement and patience without which none of this would be possible

To my dear Shevy,

For all the amazing moments and always being for me throughout this journey

ACKNOWLEDGEMENTS

Firstly, I would like to express my sincere gratitude to my advisor Dr.Thomas DiChristina. He has been a great teacher and mentor who has guided me and enabled me to rise and explore the limits of my potential. I will forever cherish all the scientific discussions and great moments we have shared over the past 5 years.

I would like to thank all my committee members Dr. Martial Taillefert, Dr. Roger Wartell, Dr. Yuanzhi Tang, and Dr. Brian Hammer for all their valuable suggestions and advise during the committee meetings. I would like to particularly thank Dr. Hyun-Dong Shin, one of the best minds and intellectuals in this field, for being a great support and a mentor par excellence throughout this journey. He has been very instrumental in guiding me through every hurdle and dealing with unforeseen and often complicated issues. He has taught me to develop solutions in a novel manner and laid the groundwork for me to develop my problem-solving skills. I hope to carry these experiences and learnings with me throughout my career.

I was very fortunate to work with former and current members of the DiChristina lab, Seng Kew Wee, Nadia Szeinbaum, Rebecca Cooper, Jennifer Goff, Jonathan Rodriguez, and Andrew Burns. I am grateful to them for all the useful ideas, discussions and fun-times that we have shared.

My life in Atlanta over the past 5 years wouldn't have been so great without all the amazing friends I have made along the way. Thanks to Manoj, Dipti, Barani, Veena, Joshua, Tiffany, Krishna and Sriram for being my second family in the USA and making me feel at home all these years.

Finally and most importantly, I would like to thank my family for their continued love and support in all my endeavors. My parents have been a big source of strength and it is their unconditional love that has brought me this far.

My wife, Nita has undoubtedly been one of the biggest inspirations and stood by me during my most trying times during the past 5 years. Our journey together as graduate students has helped me exponentially grow and has been one of the best and fun-filled years of my life. All my achievements during my PhD wouldn't have been possible without her eternal belief and encouragement. I am also blessed to have my dog Shevy with me throughout this journey who gave me unbridled joy and happiness everyday. His love and presence has given me strength and motivation to be a better human being.

Finally, I would like to thank the Department of Defense for funding my research work. I would also like to thank the Department of Biology and Georgia Tech for providing me infrastructure and support to do research on cutting edge technologies and fostering an environment of learning and innovation.

TABLE OF CONTENTS

LIST OF TABLES

LIST OF FIGURES

LIST OF ABBREVIATIONS

ABBE	Aminobenzoic butyl ester
Amp^R	Ampicillin resistant
Cat^R	Chloramphenicol resistant
CBP	Consolidated bioprocessing
CMC	Carboxymethyl cellulose
CDX	Cellodextrins
CFU	Colony forming unit
DNS	Dinitrosalicylic acid
DD	1,4-Dioxane degrading
DP	Degree of polymerization
DTT	Dithiothreitol
E.coli	*Escherichia coli*
EDTA	Ethylenediaminetetraacetic acid
G1	Glucose
G2	Cellobiose
G3	Cellotriose
G4	Cellotetraose
G5	Cellopentaose
G6	Cellohexaose
Gm^R	Gentamycin resistant
H_2O_2	Hydrogen Peroxide

HO•	Hydroxyl radical
HPLC	High pressure liquid chromatography
IPTG	Isopropyl β-D-1-thiogalactopyranoside
k_m	Michaelis-Menten constant
Km^R	Kanamycin resistant
MFS	Major facilitator superfamily
MR1	*Shewanella oneidensis*
NAD	Nicotinamide adenine dinucleotide
NADH	Reduced form of NAD
NADP	Nicotinamide adenine dinucleotide phosphate
NADPH	Reduced form of NADP
OD	Optical density
PCE	Tetrachloroethylene
PCP	Pentachlorophenol
PCR	Polymerase chain reaction
PHB	Polyhydroxybutyrate
PMSF	Phenylmethylsulfonyl fluoride
SDS-PAGE	Sodium dodecyl sulfate polyacrylamide gel electrophoresis
SSCF	Simultaneous saccharification and co-fermentation
SSF	Simultaneous saccharification and fermentation
TCA	1,1,2-trichloroethane
TCE	Trichloroethylene
UV	Ultra Violet

V_{max}	Maximum reaction rate
X1	Xylose
X2	Xylobiose
X3	Xylotriose
X4	Xylotetraose
X5	Xylopentaose
X6	Xylohexaose
XDX	Xylodextrins
XM1	Xylose-adapted *S. oneidensis* mutant

SUMMARY

Improper disposal of 1,4-dioxane and the chlorinated organic solvents trichloroethylene (TCE) and tetrachloroethylene (PCE) has resulted in widespread contamination of soil and groundwater. Current TCE and PCE remediation technologies are based on photolysis, sonolysis, and reductive transformations by iron-bearing minerals or dechlorinating microorganisms. Photolysis and sonolysis, however, are limited by UV light penetration and low energy transfer efficiency, respectively, while microbially-catalyzed reductive dehalogenation reactions are limited by microbial nutrient requirements, contaminant bioavailability, and incomplete dechlorination leading to the production of toxic intermediates. Current 1,4-dioxane remediation technologies such as carbon absorption, air stripping, and distillation are limited by problems associated with 1,4-dioxane solubility, boiling point, and vapor pressure, respectively. Other 1,4-dioxane remediation technologies such as photo-remediation by UV light and ultrasound-aided degradation are also limited by UV light penetration and low energy transfer efficiency. In the present study, a novel microbially-driven Fenton reaction system was designed to generate hydroxyl ($HO^{\bullet}$) radicals for simultaneous degradation of source zone levels of single, binary, and ternary mixtures of TCE, PCE, and 1,4-dioxane (Chapters 2 & 3). The new Fenton reaction system was driven by the Fe(III)-reducing facultative anaerobe *Shewanella oneidensis* amended with lactate, Fe(III), and contaminant mixtures and exposed to alternating anaerobic and aerobic conditions. The novel microbially-driven Fenton reaction system successfully degraded TCE, PCE, and 1,4-dioxane either as single contaminants or as binary and ternary mixtures. In

comparison to conventional (purely abiotic) Fenton reactions, the microbially-driven Fenton reaction operated at circumneutral pH and did not the require addition of exogenous H_2O_2 or UV irradiation to regenerate Fe(II) as Fenton reagents.The new microbially-driven Fenton reaction system may be applied as an *ex situ* platform for simultaneous degradation of co-mingled TCE, PCE, and 1,4-dioxane and provides valuable information for future development of *in situ* remediation technologies.

Degradation of lignocellulosic biomass was also demonstrated through the novel microbially driven fenton reaction by *S. oneidensis.* Lignocellulose is the most abundant renewable resource for the biofuel and biorefinery industry. General bioconversion process for production of biofuel or biorefinery products consists of polymer size reduction, pretreatment, enzymatic hydrolysis (saccharification), fermentation and downstream process for product recovery. Current pretreatment technologies including milling, ammonia fiber explosion, CO_2 explosion, steam explosion, ozonolysis, acid hydrolysis, alkaline hydrolysis, ionic liquids are problematic due to the requirement of big investments for facilities, pollution, safety, high energy demand and requiring detoxification of phenolic inhibitory byproducts for next biological process. In this study, we have developed a new method that combines both pretreatment and saccharification of cellulose and xylan in a microbially driven fenton reaction (Chapter 4). Wild type Fe(III)-respiring *S. oneidensis* is unable to utilize cellodextrin and xylodextrin sugars as carbon and energy source, thus enabling the use of this bacteria to accumulate large concentrations of fermentable sugars. The combined pretreatment and saccharification method for cellulose and xylan developed did not involve the addition of acid, alkali compounds or the use of hydrolyzing enzymes thus being an economically

feasible process to directly produce simple fermentable sugars from cellulose and xylan. Microbial Fe(III) reduction is a dominant anaerobic respiratory process in soil and sediments, which suggests that the microbially driven fenton reaction may play an important role in the degradation of decaying plant and woody materials in the natural environment in the presence of fluctuating redox conditions thus providing a foundation for the study of organic carbon cycle in a natural setting.

The pentose sugar xylose is one of the primary degradation products of lignocellulosic biomass and, after glucose, is the second most abundant carbohydrate in nature. Although the complete glucose metabolic pathway has been identified in *S. oneidensis* wild-type *S. oneidensis* does not metabolize xylose as sole carbon and energy source. In this study, an adaptive evolution approach was followed to generate *S. oneidensis* mutants that metabolize D-xylose as sole carbon and energy source leading to the identification of a previously unknown D-xylose catabolic pathway in *S. oneidensis* including a MFS transporter (SO_1396) and two metabolic enzymes (SO_0900 & SO_4230) through complementary genetic and biochemical techniques (Chapter 5). Finally, the xylose adapted *S. oneidensis* was genetically engineered to produce polyhydroxybutyrate (PHB), a biodegradable plastic as the secondary chemical product. This expansion of metabolic capability to convert D-xylose to a useful product such as PHB can be beneficial in biotechnological applications to couple multiple carbon sources such as glucose, glycerol and D-xylose by *S.oneidensis* to improve efficiency of electricity generation, biofuel production and bioremediation of toxic contaminants.

CHAPTER 1

INTRODUCTION

1.1 Background

1.1.1 *Shewanella oneidensis* MR-1

Dissimilatory Fe(III)-reducing bacteria occupy a central position in a variety of environmentally important processes, including the biogeochemical cycling of carbon and iron, the bioremediation of radionuclides and organohalides, and the generation of electricity in microbial fuel cells (1-4). Fe(III)-reducing bacteria are scattered and deeply rooted throughout both prokaryotic domains, an indication that microbial Fe(III) reduction may also have been one of the first respiratory processes to have evolved on early Earth (5, 6). The metal-reducing γ-proteobacterium *Shewanella oneidensis* is one of the most extensively studied Fe(III)-reducing bacteria. The Fe(III)-reducing facultative anaerobe *S. oneidensis* possesses diverse metabolic systems for coupling oxidation of a wide variety of electron donors (e.g., lactate, formate and hydrogen (7)) to the reduction of electron acceptors (O_2, fumarate, nitrate, nitrite, trimethylamine *N*-oxide, Fe(III), Mn(III/IV), dimethyl sulfoxide, sulfite, thiolsulfate, elemental sulfur (8)), thus highly adaptable to aerobic and anaerobic environments. Recently, the list of electron donors has been expanded to include glucose and glycerol through adaptive evolution and metabolic engineering (9-11). Therefore, *S. oneidensis* is one of the most popular model organisms for bioremediation of hazardous compounds, microbial fuel cell applications and more recently for the production of biofuels such as ethanol and isobutanol from substrates

such as glycerol and glucose through metabolic engineering (10-13).

1.1.2 Chemical and Microbially driven Fenton Reaction

The Fenton reaction was discovered by H.J.H Fenton in 1894. Fenton hydroxyl radicals ($HO^{\bullet}$) may be produced by the conventional Fenton reaction (eq 1) in which ferrous iron (Fe(II)) catalyzes the decomposition of hydrogen peroxide (H_2O_2) to produce Fe(III), hydroxyl ion (OH^-) and $HO^{\bullet}$ radical:

$$Fe(II) + H_2O_2 \rightarrow Fe(III) + OH^- + HO^{\bullet} \quad (1)$$

The high oxidation potential of $HO^{\bullet}$ radicals derived from conventional Fenton reactions drives oxidative degradation of a variety of compounds, including chlorinated aliphatics and aromatics (14), pentachlorophenol (PCP) (15, 16), PCE (17), TCE (18-22), 1,1,2-trichloroethane (TCA) (23), 1,4-dioxane (13), lignocellulosic biomass (24, 25) and petroleum hydrocarbons (26). Conventional Fenton reaction-driven degradation, however, is driven by the high concentrations of the Fenton reagents Fe(II) and H_2O_2 that must be continuously supplied to produce $HO^{\bullet}$ radicals and drive contaminant degradation (19, 27). At neutral pH, addition of Fe(III)-complexing ligands may improve conventional Fenton reaction efficiencies by preventing Fe(III) oxide precipitation (28). UV irradiation is often employed to induce Fe(III) re-reduction and photolytic radical production in photo-Fenton systems. The UV irradiation systems, however, are limited by UV light penetration, and H_2O_2 must still be continuously supplied to drive the conventional Fenton reaction (13).

Microbially-driven Fenton reactions that alternately produce the Fenton reagents H_2O_2 (via microbial O_2 respiration) and Fe(II) (via microbial Fe(III) reduction) alleviate

the need for continual addition of H_2O_2 and Fe(II) to drive $HO^{\bullet}$ radical production (13, 29-31). The Fe(III)-reducing facultative anaerobe *Shewanella oneidensis* was recently employed to drive the Fenton reaction for oxidative degradation of PCP and 1,4-dioxane (16). In the *S. oneidensis*-driven Fenton reaction, batch liquid cultures were amended with Fe(III) and the contaminant and subsequently exposed to alternating anaerobic and aerobic conditions. During the anaerobic period *S. oneidensis* produced Fe(II) via microbial Fe(III) reduction, while during the aerobic period, *S. oneidensis* produced H_2O_2 via microbial O_2 respiration. During the transition from anaerobic-to-aerobic conditions, Fe(II) and H_2O_2 interacted chemically via the Fenton reaction to produce $HO^{\bullet}$ radicals that completely degraded the contaminant at source zone concentrations .

1.1.3 1,4-Dioxane, Trichloroethylene and Tetrachloroethylene

The carcinogenic cyclic ether compound 1,4-dioxane is detected in a variety of contaminated surface waters and groundwaters (Fig. 1.2 & Table 1.1) (32-36). 1,4-dioxane has been employed as a stabilizing agent for chlorinated solvents in the textile and paper industries (37, 38) and as a byproduct of surfactant and polyethylene terephthalate plastic manufacturing processes (39-41). 1,4-dioxane is completely miscible in water, semi-volatile, and is thus highly mobile in water or aqueous environments. Current 1,4-dioxane remediation technologies such as carbon absorption, air stripping, and distillation are limited by problems associated with 1,4-dioxane solubility, boiling point, and vapor pressure, respectively (Table 1.1) (42). Alternate methods such as photo-remediation by UV light, ozone destruction in the presence of hydrogen peroxide (H_2O_2), and ultrasonic destruction are not cost effective remediation

strategies (43, 44).

Table 1.1. Applications, health hazards, current degradation methods and limitations of organic contaminants in this study.

Contaminant	Applications	EPA limit (nM)	Health hazards	Conventional degradation methods
1,4-Dioxane	Textile, paper industry, PET byproduct, stabilizer for chloro-organic compounds like 1,1,1-TCA	35	Carcinogenic	Carbon adsorption, air stripping, distillation, photo, ozone remediation, aerobic bacterial degradation, chemical Fenton reaction
TCE	Oil extraction, dry cleaning, degreaser for metals	38	Affects CNS, liver and kidneys	Photolysis, sonolysis with UV light, reductive dehalogenation by halorespiring bacteria, chemical Fenton reaction
PCE	Dry cleaning, paint stripping, degreasing for metals	31	Carcinogenic, dissolved fat tissue	

Bioremediation is a promising alternative method for in situ remediation of 1,4-dioxane-contaminated waters. 1,4-dioxane may be degraded microbially via metabolic or cometabolic reactions. Microbial degradation is carried out aerobically by mixed microbial communities in industrial sludge (45, 46), and 1,4-dioxane-degrading bacteria have been isolated (47, 48). Only a limited number of studies have examined microbial degradation of 1,4-dioxane under anaerobic conditions, and the degradation rates under nitrate-, iron-, and sulfate-reducing conditions are exceedingly slow (49, 50). Ex situ treatment of 1,4-dioxane-contaminated ground water involves pumping and treatment via advanced oxidation processes (AOPs) (17, 51-53).

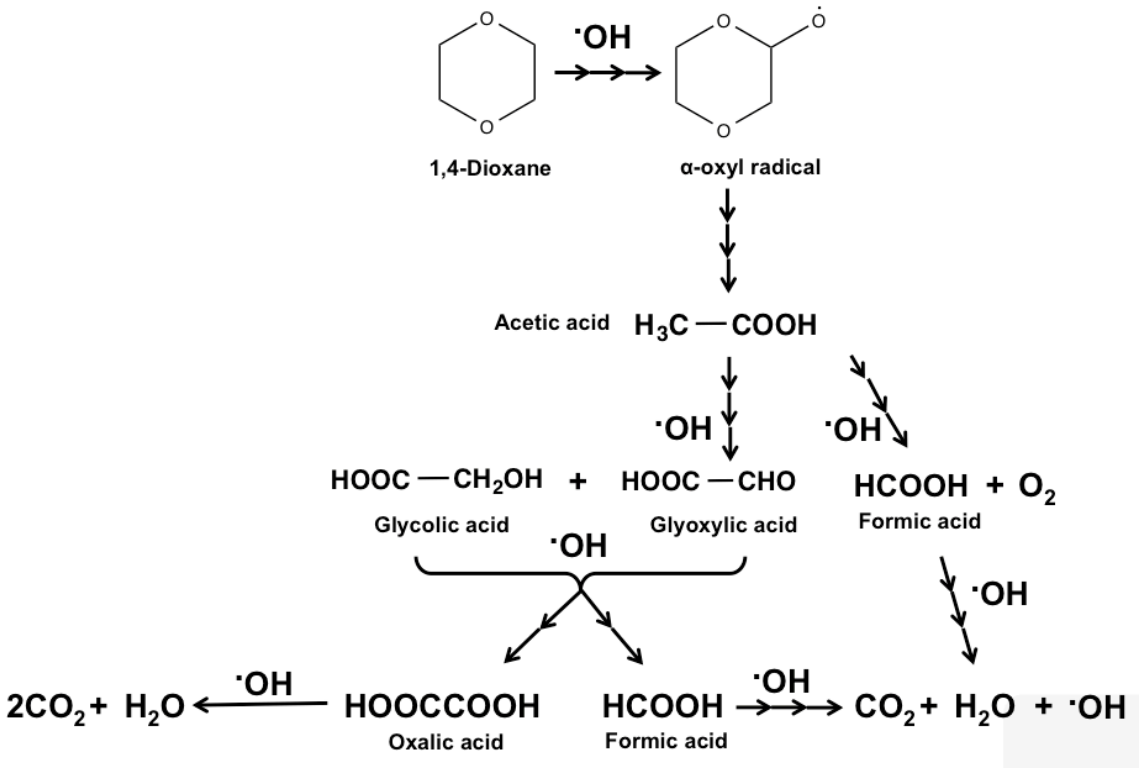

Figure. 1.1 Mechanism of 1,4-dioxane degradation by HO• radicals

1,4-Dioxane is degraded by HO• radicals and the mechanism is given in Figure 1.1. Initially, 1.4-dioxane undergoes H-abstraction to form α-oxyl radical. The α-oxyl radical is the main precursor of major intermediates during further degradation by the HO• radicals(29). The α-oxyl radical is further degraded to acetic acid through methoxyacetic acid as the transient intermediate. Acetic acid further degraded in the presence of the HO• radicals to produce formate, glyoxylate, and oxalic acids as intermediates. All the intermediates are finally degraded to CO_2 as the final product.

The chlorinated organic solvents trichloroethylene (TCE) and tetrachloroethylene (PCE) have been employed historically as solvents in a variety of industrial processes including vapor degreasing of metal surfaces, paint stripping, and dry cleaning (Table. 1.1) (19, 54). TCE and PCE are carcinogenic and improper disposal practices at industrial sites has resulted in widespread contamination of soil and ground water (Table 1.1) (19, 21, 54-57). Due to their high density and low aqueous phase solubility, TCE and PCE are also highly persistent in contaminated environments (55, 56). The potential carcinogen 1,4-dioxane is generally employed as a stabilizer for TCE and PCE in industrial processes (39-41, 58, 59), and thus TCE- and PCE-contaminated ground water is often comingled with 1,4-dioxane (29, 30, 32, 33, 41, 53, 60-63).

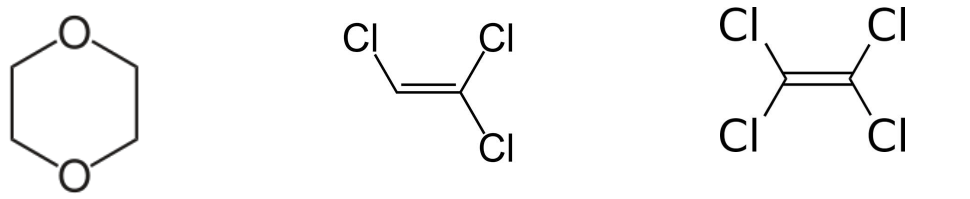

1,4-Dioxane Trichloroethylene Tetrachloroethylene

Figure 1.2. Chemical structures of organic contaminants in surface and groundwaters.

Current TCE and PCE remediation technologies are based on photolysis, sonolysis, and reductive transformation by iron-bearing minerals or dechlorinating microorganisms (18, 22, 27, 57, 64-69). Photolysis and sonolysis, however, are limited by UV light penetration and low energy transfer efficiency, respectively (70), while microbially-catalyzed reductive dehalogenation reactions are limited by microbial nutrient

requirements, contaminant bioavailability, and incomplete dechlorination leading to the production of toxic intermediates (71).

Reductive dehalogenation is a process during which a halogen substituent is removed from a molecule with concurrent addition of electrons to the molecule. Such a process requires a electron donor (reductant) (72). Reductive dehalogenation is carried out by dehalorespiring bacteria that play a key role in the transformation and detoxification of variety of halogenated compounds such as chlorophenols, chloroethenes, chlorobenzenes etc (64). Respiratory organochlorine-reducing bacteria use chlorinated compounds as terminal acceptors for energy. This process is called chlororespiration or dechlororespiration, a process limited to the availability of suitable electron donors in contaminated subsurface environments(73). Trichloroethene (TCE) and Perchloroethene (PCE) are industrial organic solvents found in soil and ground water due to improper disposal methods leading to extensive research studies of microbial reductive dechlorination of such chloroethenes over the last decade(64). First microbiologically mediated reductive chlorination of PCE and TCE was observed in the 1980s and the first report of dechlorination of PCE to ethane in 1989(74). TCE and PCE respiring bacteria isolated till date include *Desulfitobacterium, Sulfurospirillum, Desulfomonile, Desulfuromonas, Geobacter, "Dehalococcoides,"* and *Dehalobacter* (75, 76). *cis*-1,2-dichloroethene (*cis*-DCE) and *trans*-dichloroethene (trans-DCE) are the most common end products among dehalorespiring bacteria and in some cases (*Dehalococcoides*), PCE and TCE are completely reduced to ethene (64, 77).

In order to dechlorinate TCE and PCE, bacteria require suitable electron donors (organic

substrate or hydrogen) (78). Several efforts have been made to improve hydrogen concentrations at contamination sites to further activate dechlorinators. Addition of favorable electron donors has been a recent focus to improve bioremediation of PCE and TCE contaminated sites(73). In a specific study, carbon electrodes have been shown to act as sole electron donors for the dechlorination of TCE to non-chlorinated end products. Soluble redox mediators act as electron shuttles to transfer electrons between the electrode and the dechlorinating bacteria(78). Under aerobic conditions, PCE is non-biodegradable, whereas TCE is broken down to nontoxic products by enzymes such as methane monooxygenase or toluene dioxygenase(79). Under anaerobic conditions, PCE and TCE have been reductively dechlorinated by mixed cultures to less-chlorinated ethenes(80). Enzymes such as chloroethene reductive dehalogenes have been identified from several organisms. Methanogens, acetogens and sulfur reducing bacteria contain reduced transition metal factors such as corrinoids, hemes and cofactor F_{430}. In *dehalobacter restrictus*, dechlorination proceeds through a radical mechanism (81).

TCE and PCE are also degraded by the HO$^{\bullet}$ radicals (Fig. 1.3). The reaction of PCE with radiolysis-produced HO$^{\bullet}$ gives low yields of trichloro- and dichloroacetic acids. The trichloro-/dichloroacetic acid ratio in the fenton reaction is 0.6, while the same ratio in the photo-Fenton reaction is 18.5. The key step in trichloroacetic acid formation is proposed to be either (path 3) 1,2-Cl shift within the PCE-OH$^{\bullet}$ adductor (path 4) addition of Cl$^{\bullet}$ (produced in secondary reactions) to the double bond. Reaction of OH• with TCE gives 0.12% dichloroacetic acid and a trace of trichloroacetic acid, while the photo- Fenton reaction gives 2.7% dichloroacetic acid and a trace of trichloroacetic acid. The TCE pathway to dichloroacetic acid is no known, but by analogy to PCE, two routes are

plausible: (path 5) addition of HO• to the less-favored carbon, followed by 1,2-Cl shift and (path 6) addition of Cl• to the double bond.

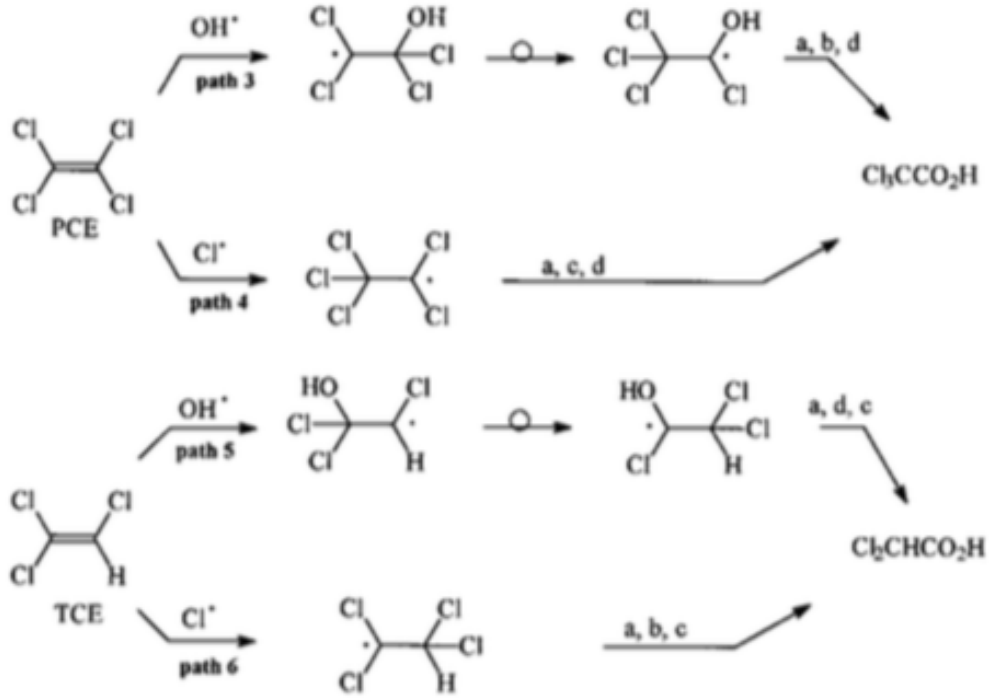

Figure. 1.3 Mechanism of TCE and PCE degradation by HO• radical. Reaction with dioxygen to give the peroxyl radical, ROO•; b, dimerization of ROO• to ROOOOR followed by decay of the tetroxide to give an acyl chloride + O_2 + 2Cl•; c, hydrolysis of the acyl chloride to the carboxylic acid; d, elimination of HO_2• to form an acyl chloride

1.1.4 Lignocellulosic Biomass

Renewable resources that replace non-renewable fossil fuels include low-cost biomass such as lignocellulose, one of the most abundant renewable feedstocks (82, 83). Lignocellulosic biomass consists of cellulose, hemicellulose, and lignin (Fig. 1.2). Cellulose is a polymer made up of multiple glucose units bonded by a 1-4 beta linkage. Xylan is a polymer made up of multiple xylose units bonded by a 1-4 beta linkage. Lignin is a hydrophobic

component made up of phenyl propanoid subunits. More importantly, lignocellulose possesses little food value and grows on non-agricultural land. Although economic benefits may be derived from producing useful products from lignocellulose, the associated production costs continue to outweigh the costs of fossil fuel production. Some of the useful products include bioethanol, butanol, 1-propanol, mesobutandiol, isoprenoids, sugar alcohols and bioplastics. Resistance of lignocellulose to chemical depolymerization reactions increases the cost of fermentable sugar production. The polymeric structure of lignocellulose is highly resistant to chemical attack and solubilization (84) and, although cellulose and hemicellulose is hydrolyzed through chemical pretreatment processes such as acidic, alkaline, or organic pulping (85), these processes often generate inhibitory byproducts that compromise downstream reactions (86, 87). Chemical pretreatment is typically followed by enzymatic hydrolysis catalyzed by endocellulases, exocellulases, and peroxidases (88, 89) that breakdown cellulosic materials to sugar monomers, which are subsequently fermented to secondary metabolites including bioethanol, butanol, and propanol. Degradation of lignocellulose to sugar monomers is the major obstacle in improving the overall yield and efficiency of secondary chemical production. Lignin degradation systems in nature are generally based on the activity of white- and brown-rot fungi (90) which produce lignolytic enzymes such as peroxidases and laccases. Brown-rot fungi hydrolyze cellulose and partially oxidize lignin via free radical-based oxidation reactions.

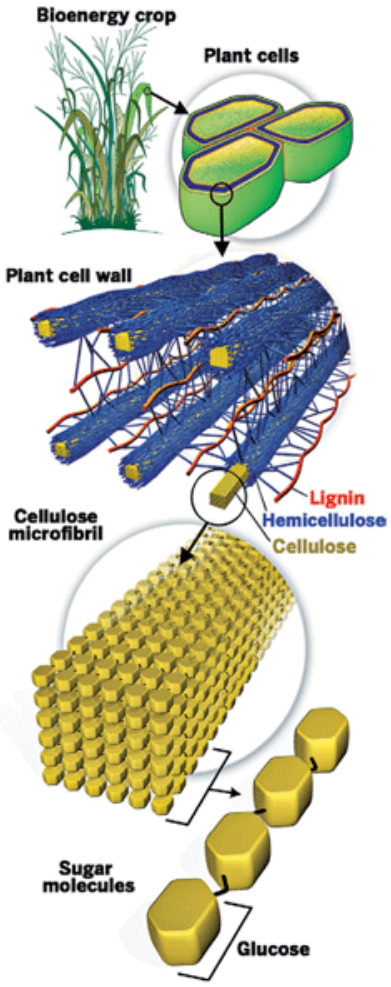

Lignocellulose

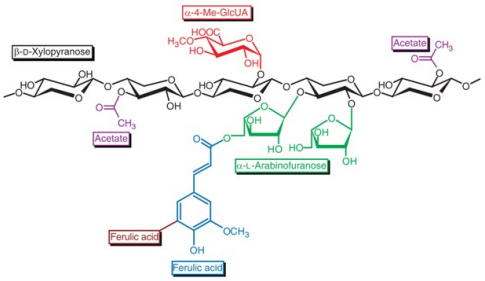

Hemicellulose

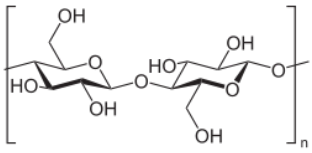

Cellulose

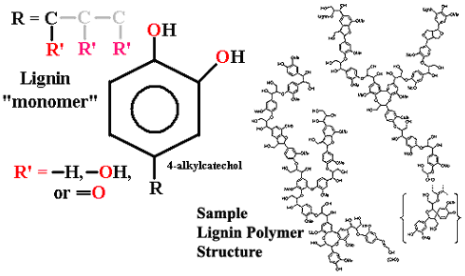

Lignin

Figure. 1.4. Illustration of lignocellulosic biomass structure and components hemicellulose, cellulose, and lignin. Adapted from Shin et al (91, 92)

1.1.5 Polyhydroxyalkanoate (PHA)-based bioplastics

Polyhydroxyalkanoates consist of linear polyesters with repeating monomeric units of hydroxyalkanoate. PHAs are produced by microorganisms (93-95) such as

Alcaligenes eutrophus (96), *Pseudomonas aeruginosa* (97) and *Bacillus subtilis* (98) as a means of storing carbon and energy source. The chemical structure of the major PHAs are given in Fig. 1.3 (93). The chemical properties of these biorenewable polymers are comparable to that of conventional plastics, thus PHAs are attractive alternative materials for production of biodegradable plastics.

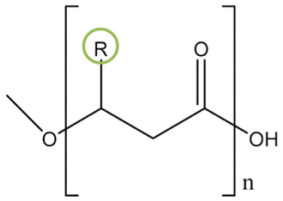

R-Group	PHA name	Abbreviation
-H	Polyhydroxypropionate	PHP
$-CH_3$	Polyhydroxybutyrate	PHB
$-CH_2CH_3$	Polyhydroxyvalerate	PHV
$-CH_2CH_2CH_3$	Polyhydroxyhexanoate	PHH

Figure. 1.5. General structure of PHAs. Structure and chemical properties are based on the composition of the attached R-group (93), where n indicates the number of monomeric units of each polymer chain (varying between 100-30,000) and R is the side chain that includes alkyl groups that vary from methyl (C1) to tridecyl (C13) (93).

PHB is the most common type of PHA synthesized and accumulated intracellularly by PHB-synthesizing microorganisms such as *Ralstonia eutropha* (previously known as *Cupriavidus necator*, *Wautersia eutropha*, and *A. eutrophus*) as carbon and energy storage material in response to conditions of physiological stress (99). PHB is a linear polyester of the monomer, (R)-3-hydroxybutyric acid that belongs to the group of short chain length PHAs consisting of C3-C5 hydroxyacid monomers (100). The

PHB biosynthetic pathway involves three enzymes that carry out a set of three sequential reactions (101). Lactate, glucose, and xylose metabolism produces acetyl-CoA as intermediate by-product. The first enzyme of the PHB pathway is acetyl-CoA-acetyltransferase (encoded by *phaA*), which catalyzes the condensation of two acetyl-CoA molecules to form acetoacetyl-CoA. This step is followed by reduction of acetoacetyl-CoA to (R)-3-hydroxybutyryl-CoA by NADPH-dependent acetoacetyl-CoA reductase (encoded by *phaB*). Finally, PHA synthase (encoded by *phaC*) catalyzes the polymerization of (R)-3-hydroxybutyryl-CoA monomers to PHB (102).

1.1.6 Xylose metabolism

Xylose is one of the primary products of lignocellulose degradation and, after glucose, is the second most abundant carbohydrate in nature. The xylose polymer xylan is the primary constituent of hemicellulose that comprises approximately 17% of dry weight of hardwoods and up to 31% of plants (103). Xylose catabolism is a key component of sustainable processes that produce useful secondary products from lignocellulosic biomass (104-106). Xylose catabolism is also of commercial interest because xylose conversion to useful secondary chemicals such as bioethanol and biodegradable plastics can reduce losses associated with lignocellulose bioprocessing (107, 108). Industrially important byproducts of xylose metabolism include xylitol, which is used as a natural sweetener in the food and confectionary industries (109).

Xylose metabolic pathways include the oxido-reductase, isomerase, and Weimberg-Dahms pathways (Fig. 1) (103, 110). Extracellular xylose is transported inside the cell via the ATP-binding cassette (ABC) or major facilitator superfamily (MFS) xylose transporters XylFGH and XylE, respectively (111, 112). In the oxido-reductase pathway of yeast (113),

NAD(P)H dependent D-xylose (referred to below as xylose) reductase converts intracellular xylose to xylitol, which is then oxidized to xylulose by D-xylitol dehydrogenase. Xylulose is then phosphorylated by xylulokinase to xylulose 5-phosphate, which enters the pentose phosphate pathway. In the xylose isomerase pathway of *Escherichia coli* (113), xylose isomerase converts xylose to xylulose, which enters the pentose phosphate pathway similar to the oxidoreductase pathway (103, 114). In the Weimberg-Dahms pathway of *Caulobacter crescentus*, xylose dehydrogenase catalyzes the conversion of xylose to xylonolactone, which is then converted to either α-ketoglutaric semialdehyde via the Weimburg pathway or to glucoaldehyde and pyruvate via the Dahms pathway (110).

The metal-reducing facultative anaerobe *Shewanella oneidensis* displays a variety of diverse metabolic systems that couple the oxidation of a wide variety of electron donors (7) to the reduction of a set of electron acceptors whose redox potentials span nearly the entire continuum of potentials encountered in nature (8). Recently, the list of electron donors has been expanded to include glucose and glycerol through adaptive evolution and metabolic engineering (9-11). Genes encoding canonical xylose metabolic pathways, however, are missing from the *S. oneidensis* genome (115).

1.1.7 Adaptive evolution

Adaptive evolution is the process by which stresses that are not directly mutagenic activate mechanisms for inducing mutations, even in non-growing cells (stress-induced or stationary-phase mutagenesis). In adaptive evolution, mutations arise under selective pressure and a subset of the cell population acquires a mutation that facilitates growth under new environmental conditions (116). Adaptive evolution is extremely useful for strain improvement in the field of metabolic engineering (117-119)

since apriori knowledge of the targeted metabolic process is not required (108). Organisms incubated in the presence of non-natural carbon sources, for example, may develop a mutator population that acquires genetic mutations at high frequency. Mutator cells include 'growth advantage in stationary phase' (GASP) mutants in which genetic alterations in small cell populations display a higher competitive advantage over weaker cells (120). Therefore, existing metabolic pathways in organisms can be modified to utilize novel carbon sources. The acquisition of new metabolic functions requires mutations that occur during adaptive evolution process(121).

Adaptive evolution approach can be applied to generate *S. oneidensis* mutants that metabolize xylose as sole carbon and energy source. In adaptive evolution, mutations arise under selective pressure and a subset of the cell population acquires a mutation that facilitates growth under a new set of environmental conditions (116). Adaptive evolution is a useful strategy for strain improvement in metabolic engineering (117-119) since apriori knowledge of the targeted metabolic process is not required (108). The remarkable metabolic flexibility displayed by *S. oneidensis* (122) led us to hypothesize that under selective growth conditions *S. oneidensis* mutator cells may acquire xylose metabolic capability.

1.2 Research objectives

The main objectives of this thesis were,

Chapter 2:

i) design a microbially-driven Fenton reaction that autocatalytically generated HO• radicals and degraded 1,4-dioxane at circumneutral pH without the need for continual addition of

exogenous H_2O_2 or UV irradiation to regenerate Fe(II), ii) optimize the 1,4-dioxane degradation rates by varying the duration and frequency of the aerobic and anaerobic incubation periods, and iii) determine the pathway for 1,4-dioxane degradation by identifying the transient intermediates produced during the microbially-driven 1,4-dioxane degradation process.

Chapter 3:

(i) design a new fed batch, microbially-driven Fenton reaction system that minimizes contaminant loss due to volatility by separating the Fe(II)-generating, H_2O_2-generating, and contaminant degradation phases and ii) apply the new microbially-driven Fenton reaction system to simultaneously degrade single, binary, and ternary mixtures of TCE, PCE, and 1,4-dioxane.

Chapter 4:

(i) Apply a microbially-driven Fenton reactor system to directly pretreat and hydrolyze cellulose and hemicellulose to produce monomers including glucose and xylose as major products

Chapter 5:

(i) Adaptively evolve *S. oneidensis* to metabolize xylose as carbon and energy source, (ii) identify the enzymes mutated in the adaptively evolved xylose catabolic pathway in *S. oneidensis*, (iii) determine the ability of the xylose-adapted strain to grow aerobic and anaerobically with xylose as sole electron donor, and (iv) genetically engineer xylose-

adapted *S. oneidensis* mutants to express the PHB biosynthesis genes (*phaCAB*) of *R. eutropha* and produce PHB with xylose as carbon and energy source.

1.3 Scope of thesis

In the present study, we have successfully designed a novel microbially-driven Fenton reaction system to generate hydroxyl ($HO^{\bullet}$) radicals for the degradation of organic contaminants including 1,4-dioxane, TCE and PCE and the degradation of lignocellulosic biomass to produce simple sugars. The new Fenton reaction system was driven by the Fe(III)-reducing facultative anaerobe *Shewanella oneidensis* amended with lactate, Fe(III), and contaminant mixtures and exposed to alternating anaerobic and aerobic conditions. Chapter 2 describes the microbially driven fenton degradation of 1,4-dioxane to produce transient intermediates including acetate and oxalate. Chapter 3 describes the design of a novel fed batch microbially driven fenton reaction to simultaneously degrade mixtures of 1,4-dioxane and volatile organic contaminants TCE and PCE. Chapter 4 describes the application of the designed microbially driven fenton reaction to pretreat and hydrolyze cellulose and hemicellulose to produce short-chain sugar oligosaccharides. Chapter 5 describes the activation of an otherwise silent xylose metabolic pathway in *S. oneidensis*. This work also includes the production of polyhydroxybutyrate (PHB) from a xylose-adapted *S. oneidensis* with D-xylose as the sole carbon and energy source.

1.4 References

1. **Logan BE.** 2009. Exoelectrogenic bacteria that power microbial fuel cells. Nature Reviews Microbiology **7:**375-381.

2. **Lovley DR, Holmes DE, Nevin KP.** 2004. Dissimilatory Fe(III) and Mn(IV) reduction. Advances in Microbial Physiology, Vol 49 **49:**219-286.

3. **Thamdrup B.** 2000. *Bacterial manganese and iron reduction in aquatic sediments*, p 86-103. *In* Schink B (ed), *Advances in Microbial Ecology*. Kluwer Academic Publishers, Dordrecht.

4. **Lovley DR, Coates JD.** 1997. Bioremediation of metal contamination. Current Opinion in Biotechnology **8:**285-289.

5. **Lonergan DJ, Jenter HL, Coates JD, Phillips EJP, Schmidt TM, Lovley DR.** 1996. Phylogenetic analysis of dissimilatory Fe(III)-reducing bacteria. Journal of Bacteriology **178:**2402-2408.

6. **Vargas M, Kashefi K, Blunt-Harris EL, Lovley DR.** 1998. Microbiological evidence for Fe(III) reduction on early Earth. Nature **395:**65-67.

7. **Szeinbaum N, Burns JL, DiChristina TJ.** 2014. Electron transport and protein secretion pathways involved in Mn(III) reduction by Shewanella oneidensis. Environ Microbiol Rep **6:**490-500.

8. **Wee SK, Burns JL, DiChristina TJ.** 2014. Identification of a molecular signature unique to metal-reducing Gammaproteobacteria. FEMS Microbiol Lett **350:**90-99.

9. **Howard EC, Hamdan LJ, Lizewski SE, Ringeisen BR.** 2012. High frequency of glucose-utilizing mutants in Shewanella oneidensis MR-1. FEMS Microbiol Lett **327:**9-14.

10. **Choi D, Lee SB, Kim S, Min B, Choi IG, Chang IS.** 2014. Metabolically engineered glucose-utilizing Shewanella strains under anaerobic conditions. Bioresour Technol **154:**59-66.

11. **Flynn JM, Ross DE, Hunt KA, Bond DR, Gralnick JA.** 2010. Enabling unbalanced fermentations by using engineered electrode-interfaced bacteria. MBio **1**.

12. **Jeon JM, Park H, Seo HM, Kim JH, Bhatia SK, Sathiyanarayanan G, Song HS, Park SH, Choi KY, Sang BI, Yang YH.** 2015. Isobutanol production from an engineered Shewanella oneidensis MR-1. Bioprocess Biosyst Eng **38:**2147-2154.

13. **Sekar R, DiChristina TJ.** 2014. Microbially driven fenton reaction for degradation of the widespread environmental contaminant 1,4-dioxane. Environ Sci Technol **48:**12858-12867.

14. **Tyre BW, Watts RJ, Miller GC.** 1991. Treatment of 4 Biorefractory Contaminants in Soils Using Catalyzed Hydrogen-Peroxide. Journal of Environmental Quality **20:**832-838.

15. **Barbeni M, Minero C, Pelizzetti E, Borgarello E, Serpone N.** 1987. Chemical Degradation of Chlorophenols with Fenton Reagent (Fe-2++H2O2). Chemosphere **16:**2225-2237.

16. **McKinzi AM, Dichristina TJ.** 1999. Microbially driven Fenton reaction for transformation of pentachlorophenol. Environmental Science & Technology **33:**1886-1891.

17. **Jho EH, Singhal N, Turner S.** 2010. Fenton degradation of tetrachloroethene and hexachloroethane in Fe(II) catalyzed systems. Journal of hazardous materials **184:**234-240.

18. **Tsai TT, Kao CM, Surampalli RY, Weng CH, Liang SH.** 2010. Treatment of TCE-Contaminated Groundwater Using Fenton-Like Oxidation Activated with Basic Oxygen Furnace Slag. Journal of Environmental Engineering-Asce **136:**288-294.

19. **Teel AL, Warberg CR, Atkinson DA, Watts RJ.** 2001. Comparison of mineral and soluble iron Fenton's catalysts for the treatment of trichloroethylene. Water Res **35:**977-984.

20. **Che H, Bae S, Lee W.** 2011. Degradation of trichloroethylene by Fenton reaction in pyrite suspension. J Hazard Mater **185:**1355-1361.

21. **Choi K, Lee W.** 2012. Enhanced degradation of trichloroethylene in nano-scale zero-valent iron Fenton system with Cu(II). J Hazard Mater **211-212:**146-153.

22. **Yeh KJ, Chen TC, Young WL.** 2013. Competitive Removal of Two Contaminants in a Goethite-Catalyzed Fenton Process at Neutral pH. Environmental Engineering Science **30:**47-52.

23. **Pignatello J, Liu D, Huston P.** 1999. Evidence for an Additional Oxidant in the Photoassisted Fenton Reaction. Environmental Science & Technology **33:**1832-1839.

24. **Baures MA, Krier CA, Cox HW.** 2008. Systems, compositions, and/or methods for depolymerizing cellulose and/or starch. Google Patents.

25. **Kato DM, Elia N, Flythe M, Lynn BC.** 2014. Pretreatment of lignocellulosic biomass using Fenton chemistry. Bioresource Technology **162:**273-278.

26. **Ojinnaka C, Osuji L, Achugasim O.** 2012. Remediation of hydrocarbons in crude oil-contaminated soils using Fenton's reagent. Environ Monit Assess **184:**6527-6540.

27. **Jho EH, Singhal N, Turner S.** 2010. Fenton degradation of tetrachloroethene and hexachloroethane in Fe(II) catalyzed systems. J Hazard Mater **184:**234-240.

28. **Lewis S, Lynch A, Bachas L, Hampson S, Ormsbee L, Bhattacharyya D.** 2009. Chelate-Modified Fenton Reaction for the Degradation of Trichloroethylene in Aqueous and Two-Phase Systems. Environ Eng Sci **26:**849-859.

29. **Stefan MI, Bolton JR.** 1998. Mechanism of the degradation of 1,4-dioxane in dilute aqueous solution using the UV hydrogen peroxide process. Environmental Science & Technology **32:**1588-1595.

30. **Coleman HM, Vimonses V, Leslie G, Amal R.** 2007. Degradation of 1,4-dioxane in water using TiO2 based photocatalytic and H2O2/UV processes. Journal of Hazardous Materials **146:**496-501.

31. **Kim CG, Seo HJ, Lee BR.** 2006. Decomposition of 1,4-dioxane by advanced oxidation and biochemical process. J Environ Sci Health A Tox Hazard Subst Environ Eng **41:**599-611.

32. **Stickney JA, Sager SL, Clarkson JR, Smith LA, Locey BJ, Bock MJ, Hartung R, Olp SF.** 2003. An updated evaluation of the carcinogenic potential of 1,4-dioxane. Reg Tox Pharm **38:**183-195.

33. **Mahendra S, Alvarez-Cohen L.** 2006. Kinetics of 1,4-dioxane biodegradation by monooxygenase-expressing bacteria. Environmental Science & Technology **40:**5435-5442.

34. **DeRosa CT, Wilbur S, Holler J, Richter P, Stevens YW.** 1996. Health evaluation of 1,4-dioxane. Toxicol Ind Health **12:**1-43.

35. **Mohr TKG, Stickney JA, DiGuiseppi WH.** 2010. Environmental Investigation and Remediation: 1,4-Dioxane and other Solvent Stabilizers. CRC Press.

36. **Kratschmar D, Wallner S, Florenski S, Schmid D, Kuhn R.** 1999. Analysis of Oligosaccharides by MEKC with Aminobenzoic Alkyl Esters as Derivatization Agents. Chromatographia **50:**596-600.

37. **Abe A.** 1999. Distribution of 1,4-dioxane in relation to possible sources in the water environment. The Science of the total environment **227:**41-47.

38. **Jackson RE, Dwarkanath V.** 1999. Chlorinated degreasing solvents:physical-chemical properties affecting aquifer contamiants and remediation. Ground Water Monit Rem **19:**102-110.

39. **Lanigan RS.** 2000. Addendum to the final report on the safety assessment of polysorbates. Int J Toxicol **19:**43-89.

40. **Zenker MJ, Borden RC, Barlaz MA.** 2003. Occurence and treatment of 1,4-dioxane in aqueous environments. Environ Eng Sci **20:**423-432.

41. **Sei K, Kakinoki T, Inoue D, Soda S, Fujita M, Ike M.** 2010. Evaluation of the biodegradation potential of 1,4-dioxane in river, soil and activated sludge samples. Biodegradation **21:**585-591.

42. **Adams CD, Scanian PA, Secrist ND.** 1998. Oxidation and biodegradability enhancement of 1,4-dioxane using hydroxide peroxide and ozone. Environ Sci Technol **28:**1812-1816.

43. **Hill RR, Jeffs GE, Roberts DR.** 1997. Photocatalytic degradation of 1,4-dioxane in aqueous solution. J Photochem Photobiol A **108:**55-58.

44. **Beckett MA, Hua I.** 2003. Enhanced sonochemical decomposition of 1,4-dioxane by ferrous iron. Water Research **37:**2372-2376.

45. **Roy D, Anagnostu G, Chaphalkar P.** 1994. Biodegradation of dioxane and diglyme in industrial waste. J Environ Sci Health Part A Environ Sci Eng **29:**129-147.

46. **Chidambara Raj CB, Ramkumar N, Haja jahabar siraj A, Chidambaram SP.** 1997. Biodegradation of acetic, benzoic, isophthalic, toluic and terephthalic acids using a mixed culture: effluents of PTA production. Process saf Environ Prot **75:**245-256.

47. **Vainberg S, McClay K, Masuda H, Root D, Condee C, Zylstra GJ, Steffan RJ.** 2006. Biodegradation of ether pollutants by Pseudonocardia sp. strain ENV478. Appl Environ Microbiol **72:**5218-5224.

48. **Mahendra S, Alvarez-Cohen L.** 2005. Pseudonocardia dioxanivorans sp. nov., a novel actinomycete that grows on 1,4-dioxane. Int J Syst Evol Microbiol **55:**593-598.

49. **Steffan R.** 2007. Biodegradation of 1,4-Dioxane. SERDP **August**.

50. **Shen W, Chen H, Pan S.** 2008. Anaerobic biodegradation of 1,4-dioxane by sludge enriched with iron-reducing microorganisms. Bioresour Technol **99:**2483-2487.

51. **Richard J. Watts, Brett C. Bottenberg, Thomas F. Hess, Mark D. Jensen, Teel. AL.** 1999. Role of reductants in the enhanced desorption and transformation of chloroaliphatic compounds by modified Fenton's reactions. Environmental Science & Technology **33:**3432-3437.

52. **Kinne M, Poraj-Kobielska M, Ralph SA, Ullrich R, Hofrichter M, Hammel KE.** 2009. Oxidative cleavage of diverse ethers by an extracellular fungal peroxygenase. The Journal of biological chemistry **284:**29343-29349.

53. **Vescovi T, Coleman HM, Amal R.** 2010. The effect of pH on UV-based advanced oxidation technologies--1,4-dioxane degradation. Journal of hazardous materials **182:**75-79.

54. **Wu X, Gu X, Lu S, Qiu Z, Sui Q, Zang X, Miao Z, Xu M, Danish M.** 2015. Accelerated degradation of tetrachloroethylene by Fe(II) activated persulfate process with hydroxylamine for enhancing Fe(II) regeneration Journal of Chemical Technology and Biotechnology doi:10.1002/jctb.4718.

55. **Chawla RC, Doura KF, McKay D.** 2001. Effect of Alcohol Cosolvents on the Aqueous Solubility of Trichloroethylene. Proceedings of the 2001 Conference on Environmental Research**:**52-66.

56. **Tsai TT, Kao CM, Hong A.** 2009. Treatment of tetrachloroethylene-contaminated groundwater by surfactant-enhanced persulfate/BOF slag oxidation--a laboratory feasibility study. J Hazard Mater **171:**571-576.

57. **Kang JW, Khan Z, Doty SL.** 2012. Biodegradation of trichloroethylene by an endophyte of hybrid poplar. Appl Environ Microbiol **78:**3504-3507.

58. **Abe A.** 1999. Distribution of 1,4-dioxane in relation to possible sources in the water environment. Sci Total Environ **227:**41-47.

59. **Jackson RE, Dwarakanath V.** 1999. Chlorinated degreasing solvents: Physical-chemical properties affecting aquifer contamination and remediation. Ground Water Monitoring and Remediation **19:**102-110.

60. **Sun BZ, Ko K, Ramsay JA.** 2011. Biodegradation of 1,4-dioxane by a Flavobacterium. Biodegradation **22:**651-659.

61. **Kim YM, Jeon JR, Murugesan K, Kim EJ, Chang YS.** 2009. Biodegradation of 1,4-dioxane and transformation of related cyclic compounds by a newly isolated Mycobacterium sp. PH-06. Biodegradation **20:**511-519.

62. **Anderson RH, Anderson JK, Bower PA.** 2012. Co-occurrence of 1,4-dioxane with trichloroethylene in chlorinated solvent groundwater plumes at US Air Force installations: Fact or fiction. Integrated Environmental Assessment and Management **8:**731-737.

63. **USEPA.** 2014. Technical Fact Sheet - 1,4-Dioxane. Response OoSWaE,

64. **Cheng D, He J.** 2009. Isolation and characterization of "Dehalococcoides" sp. strain MB, which dechlorinates tetrachloroethene to trans-1,2-dichloroethene. Appl Environ Microbiol **75:**5910-5918.

65. **Liang SH, Wang SY, Chang YM, Kao CM.** 2015. Treatment of TCE-contaminated Groundwater using In Situ Potassium Permanganate Oxidation: Effects and Kinetics Evaluation. Research Journal of Biotechnology **10:**20-24.

66. **Weir BA, McLane CR, Leger RJ.** 1996. Design of a UV oxidation system for treatment of TCE-contaminated groundwater. Environmental Progress **15:**179-186.

67. **Yeh CK, Hsu CY, Chiu CH, Huang KL.** 2008. Reaction efficiencies and rate constants for the goethite-catalyzed Fenton-like reaction of NAPL-form aromatic hydrocarbons and chloroethylenes. J Hazard Mater **151:**562-569.

68. **Everett JL, Kennedy LG, Gonzales J.** 2006. Natural attenuation assessment using mineral data. Pract Periodical Hazard, Toxic, Radioact Waste Manage **10:**256-263.

69. **Shen H, Wilson JT.** 2007. Trichloroethylene removal from groundwater in flow-through columns simulating a permeable reactive barrier constructed with plant mulch. Environmental Science & Technology **41:**4077-4083.

70. **Rashid MM, Sato C.** 2012. Degradation of Trichloroethylene and Tetrachloroethylene in Simulated Groundwater in a Flow-Through Photosono Reactor. Journal of Environmental Engineering-Asce **138:**1179-1185.

71. **Pavlostathis SP, Prytula MT, Yeh DH.** 2003. Potential and limitations of microbial reductive dechlorination for bioremediation applications. Water, Air and Soil Pollution: Focus **3:**117-129.

72. **Mohn WW, Tiedje JM.** 1992. Microbial reductive dehalogenation. Microbiol Rev **56:**482-507.

73. **He J, Sung Y, Dollhopf ME, Fathepure BZ, Tiedje JM, Loffler FE.** 2002. Acetate versus hydrogen as direct electron donors to stimulate the microbial reductive dechlorination process at chloroethene-contaminated sites. Environ Sci Technol **36:**3945-3952.

74. **Sutherson SS.** 2002. Natural and enhanced remediation systems. CRC Press, Inc, Boca Raton, Florida.

75. **Hiraishi A.** 2008. Biodiversity of dehalorespiring bacteria with special emphasis on polychlorinated biphenyl/dioxin dechlorinators. Microbes Environ **23:**1-12.

76. **Smidt H, de Vos WM.** 2004. Anaerobic microbial dehalogenation. Annu Rev Microbiol **58:**43-73.

77. **Griffin BM, Tiedje JM, Loffler FE.** 2004. Anaerobic microbial reductive dechlorination of tetrachloroethene to predominately trans-1,2-dichloroethene. Environ Sci Technol **38:**4300-4303.

78. **Aulenta F, Canosa A, Reale P, Rossetti S, Panero S, Majone M.** 2009. Microbial reductive dechlorination of trichloroethene to ethene with electrodes serving as electron donors without the external addition of redox mediators. Biotechnol Bioeng **103:**85-91.

79. **Maymo-Gatell X, Anguish T, Zinder SH.** 1999. Reductive dechlorination of chlorinated ethenes and 1, 2-dichloroethane by "Dehalococcoides ethenogenes" 195. Appl Environ Microbiol **65:**3108-3113.

80. **Vogel TM, Criddle CS, McCarty PL.** 1987. ES Critical Reviews: Transformations of halogenated aliphatic compounds. Environ Sci Technol **21:**722-736.

81. **Maillard J, Schumacher W, Vazquez F, Regeard C, Hagen WR, Holliger C.** 2003. Characterization of the corrinoid iron-sulfur protein tetrachloroethene reductive dehalogenase of Dehalobacter restrictus. Appl Environ Microbiol **69:**4628-4638.

82. **Bothast RJ, Schlicher MA.** 2005. Biotechnological processes for conversion of corn into ethanol. Applied Microbiology and Biotechnology **67:**19-25.

83. **Demirbas A.** 2009. Political, economic and environmental impacts of biofuels: A review. Applied energy **86:**S108-S117.

84. **Himmel ME, Ding SY, Johnson DK, Adney WS, Nimlos MR, Brady JW, Foust TD.** 2007. Biomass recalcitrance: Engineering plants and enzymes for biofuels production. Science **315:**804-807.

85. **Wyman CE, Dale BE, Elander RT, Holtzapple M, Ladisch MR, Lee YY.** 2005. Coordinated development of leading biomass pretreatment technologies. Bioresource Technology **96:**1959-1966.

86. **Sarrouh BF, Branco RD, da Silva SS.** 2009. Biotechnological Production of Xylitol: Enhancement of Monosaccharide Production by Post-Hydrolysis of Dilute Acid Sugarcane Hydrolysate. Applied Biochemistry and Biotechnology **153:**163-170.

87. **Zhuang JP, Liu Y, Wu Z, Sun Y, Lin L.** 2009. Hydrolysis of Wheat Straw Hemicellulose and Detoxification of the Hydrolysate for Xylitol Production. Bioresources **4:**674-686.

88. **Ramachandra M, Crawford DL, Hertel G.** 1988. Characterization of an Extracellular Lignin Peroxidase of the Lignocellulolytic Actinomycete Streptomyces-Viridosporus. Applied and environmental microbiology **54:**3057-3063.

89. **Shaw AJ, Jenney FE, Adams MWW, Lynd LR.** 2008. End-product pathways in the xylose fermenting bacterium, Thermoanaerobacterium saccharolyticum. Enzyme and Microbial Technology **42:**453-458.

90. **Sanchez C.** 2009. Lignocellulosic residues: Biodegradation and bioconversion by fungi. Biotechnology Advances **27:**185-194.

91. **Shin HD, McClendon S, Vo T, Chen RR.** 2010. Escherichia coli Binary Culture Engineered for Direct Fermentation of Hemicellulose to a Biofuel. Applied and Environmental Microbiology **76:**8150-8159.

92. **Wyman CE, Yang B.** 2009. Cellulosic biomass could help meet California's transportation fuel needs. California Agriculture **63:**185-190.

93. **Green R.** 2010. Current strategies for optimizing polyhydroxyalkanoate production in bacteria systems. MMG 445 Basic Biotechnol eJournal **6:**1-6.

94. **Khanna S, Srivastava A.** 2005. Recent advances in microbial polyhydroxyalkanoates. Process Biochem **40:**607-619.

95. **Akaraonye E, Keshavarz T, I. R.** 2010. Production of polyhydroxyalkanoates: the future green materials of choice. J Chem Technol Biotechnol **85:**732-743.

96. **Doi Y, Kawaguchi Y, Koyama N, Nakamura S, Hiramitsu M, Yoshida Y, H K.** 1992. Synthesis and degradation of polyhydroxyalkanoates in Alcaligenes eutrophus. FEMS Microbiol Lett **103:**103-108.

97. **Pham TH, Webb JS, BHA R.** 2004. The role of polyhydroxyalkanoate biosynthesis by Pseudomonas aeruginosa in rhamnolipid and alginate production as well as stress tolerance and biofilm formation. Microbiological Research **150:**3405-3413.

98. **Singh M, Patel S, V K.** 2009. Bacillus subtilis as potential producer for polyhydroxyalkanoates. Microb Cell Fact **8:**38.

99. **Steinbuchel A, Hustede E, Liebergesell M, Pieper U, Timm A, Valentin H.** 1993. Molecular basis for biosynthesis and accumulation of polyhydroxyalkanoic acids in bacteria. FEMS Microbiol Rev **10:**347-350.

100. **Hankermeyer CR, RS T.** 1999. Polyhydroxybutyrate: Plastic made and degraded by microorganisms, vol 159. Springer, New York.

101. **A Sc.** 2001. Perspectives for biotechnological production and utilization of biopolymers: Metabolic engineering of polyhydroxyalkanoate biosynthesis pathways as a successful example. Macromol Biosci **1:**1-24.

102. **Peoples OP, Sinskey AJ.** 1989. Poly-beta-hydroxybutyrate (PHB) biosynthesis in Alcaligenes eutrophus H16. Identification and characterization of the PHB polymerase gene (phbC). J Biol Chem **264:**15298-15303.

103. **Jackson S, Nicolson SW.** 2002. Xylose as a nectar sugar: from biochemistry to ecology. Comparative Biochemistry and Physiology Part B: Biochemistry and Molecular Biology **131:**613-620.

104. **Lia X, Parka A, Estrelaa R, Kimb S, Jin Y, Cate J.** 2016. Comparison of xylose fermentation by two high-performance engineered strains of Saccharomyces cerevisiae. Biotechnology Reports **9:**53-56.

105. **Li P, Sun H, Chen Z, Li Y, Zhu T.** 2015. Construction of efficient xylose utilizing Pichia pastoris for industrial enzyme production. Microb Cell Fact **14:**22.

106. **Lee SJ, Lee SJ, Lee DW.** 2013. Design and development of synthetic microbial platform cells for bioenergy. Front Microbiol **4:**92.

107. **Sandstrom AG, Munoz de Las Heras A, Portugal-Nunes D, Gorwa-Grauslund MF.** 2015. Engineering of Saccharomyces cerevisiae for the production of poly-3-d-hydroxybutyrate from xylose. AMB Express **5:**14.

108. **Agrawal M, Mao ZC, Chen RR.** 2011. Adaptation Yields a Highly Efficient Xylose-Fermenting Zymomonas mobilis Strain. Biotechnology and Bioengineering **108:**777-785.

109. **Ko BS, Kim J, Kim JH.** 2006. Production of xylitol from D-xylose by a xylitol dehydrogenase gene-disrupted mutant of Candida tropicalis. Appl Environ Microbiol **72:**4207-4213.

110. **Stephens C, Christen B, Fuchs T, Sundaram V, Watanabe K, Jenal U.** 2007. Genetic analysis of a novel pathway for D-xylose metabolism in Caulobacter crescentus. J Bacteriol **189:**2181-2185.

111. **Young E, Poucher A, Comer A, Bailey A, Alper H.** 2011. Functional Survey for Heterologous Sugar Transport Proteins, Using Saccharomyces cerevisiae as a Host. Applied and Environmental Microbiology **77:**3311-3319.

112. **Gu Y, Ding Y, Ren C, Sun Z, Rodionov DA, Zhang W, Yang S, Yang C, Jiang W.** 2010. Reconstruction of xylose utilization pathway and regulons in Firmicutes. BMC Genomics **11:**255.

113. **Ceroni F, Carbonell P, Francois JM, Haynes KA.** 2015. Editorial - Synthetic Biology: Engineering Complexity and Refactoring Cell Capabilities. Front Bioeng Biotechnol **3:**120.

114. **Lee SM, Jellison T, Alper HS.** 2012. Directed evolution of xylose isomerase for improved xylose catabolism and fermentation in the yeast Saccharomyces cerevisiae. Appl Environ Microbiol **78:**5708-5716.

115. **Rodionov DA, Yang C, Li X, Rodionova IA, Wang Y, Obraztsova AY, Zagnitko OP, Overbeek R, Romine MF, Reed S, Fredrickson JK, Nealson KH, Osterman AL.** 2010. Genomic encyclopedia of sugar utilization pathways in the Shewanella genus. BMC Genomics **11:**494.

116. **Roth JR, Kugelberg E, Reams AB, Kofoid E, Andersson DI.** 2006. Origin of mutations under selection: the adaptive mutation controversy. Annu Rev Microbiol **60:**477-501.

117. **Fong SS, Marciniak JY, Palsson BO.** 2003. Description and interpretation of adaptive evolution of Escherichia coli K-12 MG1655 by using a genome-scale in silico metabolic model. J Bacteriol **185:**6400-6408.

118. **Kuyper M, Toirkens MJ, Diderich JA, Winkler AA, van Dijken JP, Pronk JT.** 2005. Evolutionary engineering of mixed-sugar utilization by a xylose-fermenting Saccharomyces cerevisiae strain. FEMS Yeast Res **5:**925-934.

CHAPTER 2

MICROBIALLY DRIVEN FENTON REACTION FOR DEGRADATION OF THE WIDESPREAD ENVIRONMENTAL CONTAMINANT 1,4-DIOXANE

Abstract

The carcinogenic cyclic ether compound 1,4-dioxane is employed as a stabilizer of chlorinated industrial solvents and is a widespread environmental contaminant in surface water and groundwater. In the present study, a microbially-driven Fenton reaction was designed to autocatalytically generate hydroxyl ($HO^{\bullet}$) radicals that degrade 1,4-dioxane. In comparison to conventional (purely abiotic) Fenton reactions, the microbially-driven Fenton reaction operated at circumneutral pH and did not the require addition of exogenous H_2O_2 or UV irradiation to regenerate Fe(II) as Fenton reagents. The 1,4-dioxane degradation process was driven by pure cultures of the Fe(III)-reducing facultative anaerobe *Shewanella oneidensis* manipulated under controlled laboratory conditions. *S. oneidensis* batch cultures were provided with lactate, Fe(III), and 1,4-dioxane and were exposed to alternating aerobic and anaerobic conditions. The microbially driven Fenton reaction completely degraded 1,4-dioxane (10 mM initial concentration) in 53 h with an optimal aerobic-anaerobic cycling period of 3 h. Acetate and oxalate were detected as transient intermediates during the microbially-driven Fenton degradation of 1,4-dioxane, an indication that conventional and microbially-driven Fenton degradation processes follow similar reaction pathways. The microbially-driven Fenton reaction provides the foundation for development of alternative in situ remediation technologies to degrade environmental contaminants susceptible to attack by $HO^{\bullet}$ radicals generated by the

Fenton reaction.

2.1 Introduction

The carcinogenic cyclic ether compound 1,4-dioxane is detected in a variety of contaminated surface waters and groundwaters(1-5). 1,4-dioxane has been employed as a stabilizing agent for chlorinated solvents in the textile and paper industries(6, 7) and as a byproduct of surfactant and polyethylene terephthalate plastic manufacturing processes(8-10). 1,4-dioxane is completely miscible in water, semi-volatile, and is thus highly mobile in water or aqueous environments. Current 1,4-dioxane remediation technologies such as carbon absorption, air stripping, and distillation are limited by problems associated with 1,4-dioxane solubility, boiling point, and vapor pressure, respectively(11). Alternate methods such as photo-remediation by UV light, ozone destruction in the presence of hydrogen peroxide (H_2O_2), and ultrasonic destruction are not cost effective remediation strategies(12, 13).

Bioremediation is a promising alternative method for in situ remediation of 1,4-dioxane-contaminated waters. 1,4-dioxane may be degraded microbially via metabolic or cometabolic reactions. Microbial degradation is carried out aerobically by mixed microbial communities in industrial sludge(14, 15), and 1,4-dioxane-degrading bacteria have been isolated.(16-19) Only a limited number of studies have examined microbial degradation of 1,4-dioxane under anaerobic conditions, and the degradation rates under nitrate-, iron-, and sulfate-reducing conditions are exceedingly slow(20). Ex situ treatment of 1,4-dioxane-contaminated ground water involves pumping and treatment via advanced oxidation processes (AOPs)(21-24). In the Fenton reaction (equation 1), H_2O_2 reacts with ferrous iron (Fe(II)) to produce ferric iron (Fe(III)), hydroxyl ion (OH^-), and hydroxyl radical ($HO^\bullet$):

$$Fe(II) + H_2O_2 \rightarrow Fe(III) + {}^{-}OH + HO^{\bullet} \quad (1)$$

Due to their high oxidation potential, Fenton reaction-generated $HO^{\bullet}$ radicals oxidatively degrade a wide variety of hazardous organic compounds, including landfill leachates(25), chlorinated aliphatics and aromatics(26), dry-cleaning solvents(27), pharmaceuticals(28), pentachlorophenol (PCP)(29, 30), tetrachloroethene (PCE)(23), trichloroethene (TCE)(31) and 1,1,2-trichloroethane (TCA)(32). Fenton reaction-driven AOPs have also recently attracted attention as an alternative means for degrading 1,4-dioxane(33-36). Fenton reaction-driven AOPs are expensive, however, since the Fenton reagents Fe(II) and H_2O_2 must be continuously supplied to drive the chemical degradation reaction. UV irradiation is often employed to induce Fe(III) reduction and photolytic radical production in photo-Fenton systems. The UV irradiation systems, however, are limited by UV light penetration(37), and H_2O_2 must still be continuously supplied to drive the Fenton degradation reaction.

Microbially-driven Fenton reactions based on production of H_2O_2 via microbial O_2 respiration and Fe(II) via microbial Fe(III) reduction alleviate the need for continual addition of H_2O_2 and Fe(II) that drive the chemical Fenton reaction(36, 38, 39). The microbially-driven Fenton reaction designed in the present study was based on the original observation that the Fe(III)-reducing facultative anaerobe *Shewanella oneidensis* liquefied the agar support directly beneath colonies grown aerobically on solid growth medium supplemented with Fe(III)(40). Under such conditions, high microbial O_2 consumption rates directly beneath the colony effectively lower the O_2 concentrations to levels that permit simultaneous microbial Fe(III) reduction(41), concomitant production of the Fenton substrates H_2O_2 and Fe(II), and agar liquefaction via the resulting $HO^{\bullet}$ radicals (Fig. 2.1). The agar liquefaction phenotype was subsequently employed as the basis of a genetic screening technique for

identification of Fe(III) reduction-deficient mutant strains and the corresponding genes required for microbial Fe(III) reduction(40, 42).

The main objectives of the present study were to i) design a microbially-driven Fenton reaction that autocatalytically generated $HO^{\bullet}$ radicals and degraded 1,4-dioxane at circumneutral pH without the need for continual addition of exogenous H_2O_2 or UV irradiation to regenerate Fe(II), ii) optimize the 1,4-dioxane degradation rates by varying the duration and frequency of the aerobic and anaerobic incubation periods, and iii) determine the pathway for 1,4-dioxane degradation by identifying the transient intermediates produced during the microbially-driven 1,4-dioxane degradation process.

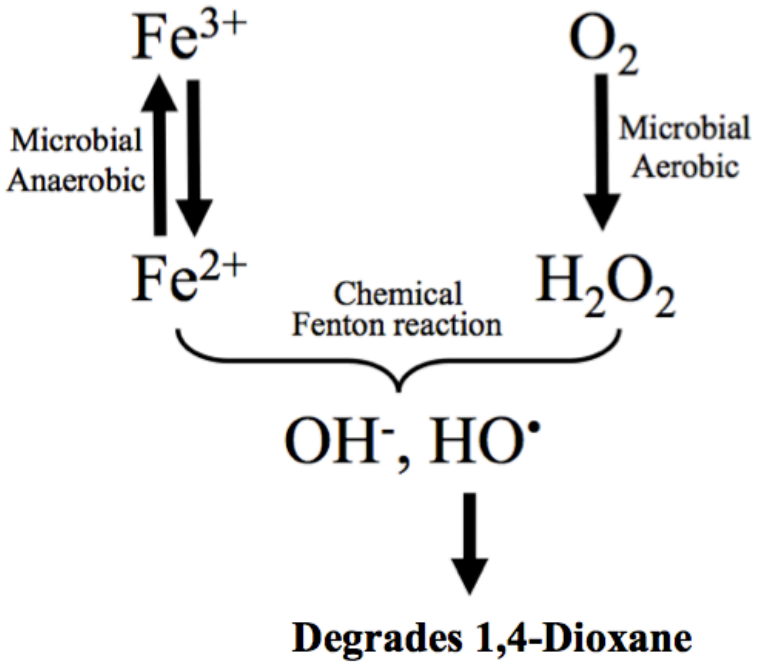

Figure 2.1. Overall strategy for generation of $HO^{\bullet}$ radicals by the *S. oneidensis*-driven Fenton reaction. Fe(II) produced during anaerobic phases interacts chemically via the Fenton reaction with H_2O_2 produced during aerobic phases to yield $HO^{\bullet}$ radicals that oxidatively degrade 1,4-dioxane.

2.2 Materials And Methods

Culture Medium and Chemical Reagents. *S. oneidensis* was routinely cultured aerobically on LB medium (10 g/L tryptone, 5 g/L yeast extract, and 10 g/L NaCl)(43). 1,4-dioxane degradation experiments were conducted in a lactate (10 mM)-supplemented minimal salt solution (LS; pH 7.0, Supplementary Table 2.S4)(30, 44). Fe(III) citrate was prepared by previously described methods(40) and added at a final concentration of 10 mM. 1,4-dioxane, acetonitrile, sodium glyoxylate, ferrozine, heptafluorobutyric acid, tetrabutylammonium hydroxide, mannitol, sodium acetate, sodium oxalate, sodium lactate, sodium formate and thiourea were obtained from Sigma-Aldrich. Sodium glycolate was obtained from Acros Organics. Ethylene glycol diformate were obtained from Frinton Laboratories, Inc.

Design of a Microbially Driven Fenton Reaction for 1,4-Dioxane Degradation. The toxicity of 1,4-dioxane to *S. oneidensis* was tested by growing batch cell cultures in the presence of potential source zone levels (10 mM) of 1,4-dioxane in LS medium under aerobic conditions for 48 h. Culture samples were withdrawn periodically during the toxicity tests and the number of colony forming units (CFUs) were measured to monitor cell viability. The experimental conditions for the microbially-driven Fenton degradation of 1,4-dioxane (designated DD conditions in the remainder of the present study) consisted of *S. oneidensis* batch cultures amended with Fe(III) and 1,4-dioxane and exposed to different aerobic/anaerobic cycling periods. *S. oneidensis* was grown aerobically in LB on a rotary shaker (200 rpm, 30 °C) to early stationary phase (OD_{600} = 1.5), harvested by centrifugation at 6000 x g, washed and resuspended in LS medium to a final cell density of 1 x 10^9 cells per ml. Anaerobic stock solutions of Fe(III) citrate and 1,4-dioxane were added to final concentrations of 10 mM each. The cell culture was allowed to reduce Fe(III) citrate for pre-selected time periods (45 min, 1.5 h,

3 h, and 6 h) under anaerobic conditions maintained by continuously sparging with hydrated high-purity nitrogen. Reactor temperature (25°C) and pH (7.0) were held constant in all experiments. Aerobic conditions were initiated by sparging the culture with hydrated compressed air for pre-selected time periods (45 min, 1.5 h, 3 h, and 6 h). Cell density was monitored by determining CFUs on LB agar plates incubated at 30 °C for 72 h.

Analytical Techniques. HCl-extracted Fe(II) concentrations were determined with a previously described Ferrozine-based detection technique(45). H_2O_2 concentrations were determined using a previously described spectrophotometric assay(46): a solution consisting of 400 mM KI, 50 mM NaOH, and 170 μM of ammonium molybdate tetrahydrate was mixed with equal volume of 100 mM potassium hydrogen phthalate. Samples were added and absorbance of the resulting solution was measured at 350 nm to determine H_2O_2 concentration. H_2O_2 spectrophotometric measurements were not possible in Fe(III)-containing LS medium due to Fe(III) interference. Calibration curves were generated from standards to determine the H_2O_2 concentrations. H_2O_2 concentrations were monitored under a variety of conditions, including i) DD conditions with Fe(III) omitted and aerobic/anaerobic cycling periods of 45 min, 1.5 h, 3 h, 6 h, ii) strictly aerobic conditions, and iii) abiotic Fe(II) oxidation experiments in which 10 mM bacterially-produced Fe(II)(obtained by microbial Fe(III) reduction) was subjected to strictly aerobic conditions for 74 h.

Chemical Analysis of 1,4-Dioxane, Lactate, and Transient Degradation Products. Samples were withdrawn and centrifuged at 6000 x g for 10 min. 1,4-dioxane and ethylene glycol diformate were analyzed via liquid chromatography (LC) using a ZORBAX SB-C18 column with 20% aqueous acetonitrile as the mobile phase and a constant flow rate of 1.0 ml/min(18). Chromatograms were generated at 190 nm for 1,4-dioxane at a retention time of 2.4

min and at 210 nm for ethylene glycol diformate at a retention time of 3.1 min(24). Lactate, acetate, formate, glyoxylate, glycolate and oxalate were analyzed via an ion chromatograph (IC) (Dionex, DX-300 Series) equipped with a Dionex IonPac® ICE-AS6 chromatography column and AMMS® ICE 300 suppressor. The Dionex DX-300 uses a CDM II detector with suppressed conductivity detection. Anion analysis was performed with 0.4 mM heptafluorobutyric acid as eluent and 5 mM tetrabutylammonium hydroxide as regenerant. Chromatograms were generated for lactate, acetate, oxalate, formate, glyoxylate, and glycolate at retention times of 10.0, 13.3, 4.3, 9.3, 6.5, and 9.0 min, respectively. Calibration curves were generated from standards to determine the concentrations of each compound.

Inhibition of the Microbially-Driven Fenton Reaction. A series of five control experiments were carried out to confirm that 1,4-dioxane was degraded by $HO^{\bullet}$ radicals generated by the *S. oneidensis*-driven Fenton reaction. All five control experiments were carried out under DD conditions, with the following noted changes: In the first set of control experiments, 1,4-dioxane degradation was monitored under identical alternating aerobic/anaerobic periods with 15 mM NO_3^- replacing Fe(III) as electron acceptor. In the second set of control experiments, the $HO^{\bullet}$ radical scavenging compounds mannitol (120 mM) and thiourea (40 mM) were added to reactors carrying out an otherwise identical 1,4-dioxane degradation process.(30) The toxicity of mannitol (120 mM) and thiourea (40 mM) to *S. oneidensis* was tested by growing batch cell cultures in the presence of the $HO^{\bullet}$ radical scavenging compounds in LS medium under aerobic conditions for 48 h. In the third set of control experiments, 1,4-dioxane degradation was monitored under DD conditions with either Fe(III) citrate, 1,4-dioxane, or cells (abiotic control) omitted. In the fourth set of control experiments, 1,4-dioxane concentration was monitored in abiotic sealed anaerobic bottles to

examine the effects of hydrated compressed air and nitrogen gas flow on volatilization of 1,4-dioxane during the aerobic and anaerobic phases, respectively. In the fifth set of control experiments, 1,4-dioxane concentrations were monitored under strictly aerobic conditions for 74 h.

2.3 Results

H_2O_2 production by *S. oneidensis*. In iron-free LS medium, *S. oneidensis* batch cultures produced approximately 24.5 μM H_2O_2 (presumably as a by-product of microbial aerobic respiration) under either strictly aerobic conditions for 74 h or with alternating aerobic/anaerobic periods of 3 h and 6 h (Fig. 2.2). Under aerobic/anaerobic cycling periods of 45 min and 1.5 h, *S. oneidensis* produced 2.3 μM and 6.7 μM H_2O_2, respectively (Fig. 2.2). During the first aerobic phase, H_2O_2 production rates under strictly aerobic conditions or with alternating aerobic/anaerobic periods of 3 h and 6 h were similar (4.6-5.6 μM). However, H_2O_2 production rates with alternating aerobic/anaerobic cycling periods of 45 min and 1.5 h were 4-fold lower (1.2 μM) compared to the strictly aerobic and 3 h and 6 h aerobic/anaerobic cycling conditions (Fig. 2.2). During the second aerobic phase, H_2O_2 production rates with the 3 h and 6 h aerobic/anaerobic cycling periods decreased 5-fold and were similar to H_2O_2 production rates with aerobic/anaerobic cycling periods of 45 min and 1.5 h (0.8-1.3 μM) (Fig. 2.2). During the third aerobic phase, H_2O_2 production rates with aerobic/anaerobic cycling periods of 45 min, 1.5 h, 3 h, and 6 h were similar (0.4-0.9 μM) (Fig. 2.2). H_2O_2 was not detected during abiotic Fe(II) oxidation experiments carried out under strictly aerobic conditions for 74 h (data not shown).

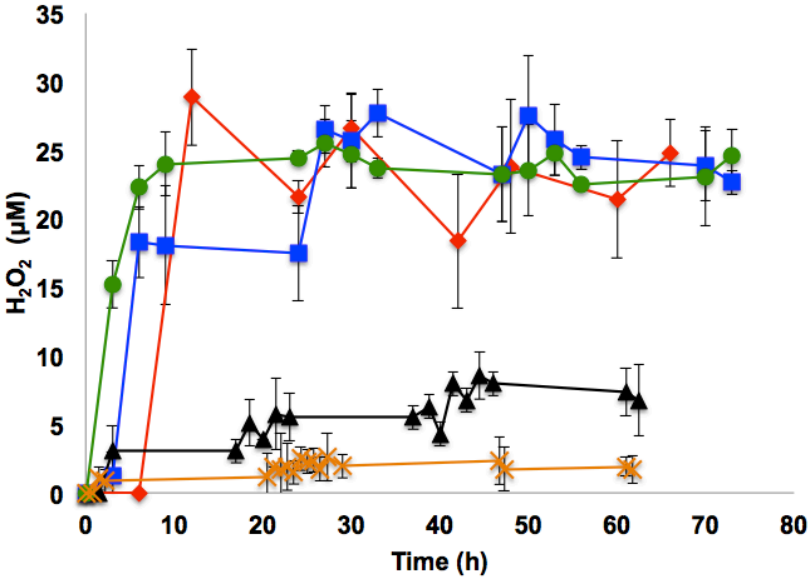

Figure 2.2. H_2O_2 production by *S. oneidensis* held under strictly aerobic conditions or with aerobic/anaerobic cycling periods of 45 min, 1.5 h, 3 h and 6 h: red ◆, 6 h cycling; blue ■, 3 h cycling; black ▲, 1.5 h cycling; green ●, strict aerobic; orange ×, 45 min cycling.

1,4-Dioxane Degradation by the Microbially-Driven Fenton Reaction. To initiate HO• radical production by the *S. oneidensis*-driven Fenton reaction (Fig. 2.1), Fe(III)-containing *S. oneidensis* cultures were exposed to alternating aerobic/anaerobic periods of 45 min, 1.5 h, 3 h, and 6 h (Fig. 2.3 and Supplementary Figs. 2.S3, 2.S4, and 2.S5). During the initial 3 h anaerobic and ensuing 3 h aerobic periods, 1,4-dioxane concentrations decreased 2.4 mM in the incubation under DD conditions (Fig. 2.3b). However, 1,4-dioxane concentrations also decreased 1.5 mM in control DD incubations lacking Fe(III) or *S. oneidensis* cells (Fig. 2.3b). The decrease in 1,4-dioxane concentrations in the control incubations was attributed to 1,4-dioxane volatilization during hydrated compressed air and nitrogen inputs. To address this possibility, a series of additional control experiments were carried out in which 1,4-dioxane concentrations were monitored under DD conditions with *S. oneidensis* cells omitted and subjected to a series of

five 3 h anaerobic/aerobic cycling periods for 74 h (Fig. 2.3b). 1,4-dioxane concentrations decreased 46% (from 12.0 to 6.5 mM) during the first 9 h of the 74 h incubations. On the other hand, in control incubations held under strict anaerobic conditions for 74 h without hydrated compressed air or nitrogen inputs, 1,4-dioxane concentrations remained constant at 10.0 mM (Fig. 2.3b). These results indicate that during the first 9 h of the 74 h control incubations (consisting of alternating 3 h aerobic/anaerobic cycling periods) 1,4-dioxane concentrations decreased approximately 46% (to 5.5 mM) due to 1,4-dioxane volatilization. In a similar manner, 1,4-dioxane volatilization in control reactions with alternating compressed air and nitrogen inputs during the 45 min, 1.5 h and 6 h aerobic/anaerobic cycling experiments resulted in decreases of approximately 35%, 37% and 50% of the initial 1,4-dioxane concentrations, respectively (Supplementary Figs. 2.S4-b, 2.S3-b and 2.S5-b respectively).

During the first 3 h anaerobic period under DD conditions, *S. oneidensis* reduced 10.0 mM Fe(III) to 1.1 mM Fe(II) (grey shaded area in Figs. 2.2a-b, 2.3a-c, 2.4a-b, 2.5a-c and Supplementary Figs. 2.S2, 2.S3a-f, 2.S4a-f, 2.S5a-f). At the 3-h mark, compressed nitrogen gas input was switched to compressed air, Fe(II) was oxidized for a 3 h incubation period (unshaded area in Figs. 2.2a-b, 2.3a-c, 2.4a-b, 2.5a-c and Supplementary Figs. 2.S2, 2.S3a-f, 2.S4a-f, 2.S5a-f), and Fe(II) levels dropped to below detection limits at the 6-h time point. During the ensuing 3 h anaerobic period, Fe(II) rebounded from below detection limits to 5.5 mM (microbial Fe(III) reduction rate of 0.3 mM/h). At the 9-h time point, 1,4-dioxane volatilization stopped (even though compressed nitrogen inputs were continued to ensure anaerobic conditions for the ensuing 18 h) and 1,4-dioxane concentrations remained constant at 7.0 mM (i.e., corresponding to the observed volatilization losses of 6.5 mM 1,4-dioxane during the initial 9 h period). After the ensuing 3 h aerobic period (24-h time point), Fe(II) levels decreased from 5.5 to 2.6 mM (O_2-

catalyzed Fe(II) oxidation rate of 1.0 mM/h). After the next 3 h anaerobic period (27-h time point), the Fe(II) concentrations again rebounded to 5.5 mM (microbial Fe(III) reduction rate of 1.1 mM/h). During the 9 h time period between the 24-h and 33-h time points, 1,4-dioxane concentrations decreased rapidly to 1 mM (0.6 mM/hr). However, in control incubations carried out under DD conditions but lacking *S. oneidensis* cells or Fe(III), 1,4-dioxane concentrations remained constant at 7.0 mM and remained at that concentration throughout the remainder of the 74 h incubation. At the 49-h time point, the incubations under DD conditions were subjected to two additional alternating 3 h anaerobic/aerobic cycling periods that resulted in production of 6.3 mM Fe(II) (71-h time point; microbial Fe(III) reduction rate of 0.2 mM/h) followed by a decrease in Fe(II) concentrations to 2.2 mM (74-h time point; O_2-catalyzed Fe(II) oxidation rate of 1.4 mM/h) (Fig 2.2a). 1-4 dioxane concentrations decreased to below detection limits at the 53-h time point and remained below detection limits (0.2 mM; Supplementary Table 2.S3) throughout the remainder of the 74 h incubation.

Similar patterns of microbial (*S. oneidensis*-catalyzed) Fe(III) reduction and chemical (O_2-catalyzed) Fe(II) oxidation were observed in analogous experiments carried out with 45 min, 1.5 h, 3h, and 6 h aerobic/anaerobic cycling periods (Supplementary Figs. 2.S4-A, 2.S3-A and 2.S5-A respectively). Compared to the 3 h aerobic/anaerobic cycling experiments, 1,4-dioxane degradation rates were 34% slower during the 1.5 h aerobic/anaerobic cycling experiment (Supplementary Fig. 2.S3-b). 1,4-Dioxane was not degraded (i.e., depletion was only due to volatilization) during the 45 min aerobic/anaerobic cycling experiment (Supplementary Fig. 2.S4-b). However, 1,4-dioxane degradation rates with 3 h and 6 h aerobic/anaerobic cycling periods were nearly identical (Fig. 2.3b and Supplementary Fig. 2.S5-b).

Cell viability analyses indicated that *S. oneidensis* cell densities decreased

approximately 70% during the 3 h anaerobic periods, yet rebounded to initial cell densities (10^9 cells/ml) during subsequent 3 h aerobic periods (Supplementary Figs. 2.S2, 2.S3-f and 2.S4-f). To test for 1,4-dioxane toxicity, *S. oneidensis* was grown aerobically in LS growth medium supplemented with 10 mM 1,4-dioxane. Aerobic growth rates in the presence or absence of 1,4-dioxane were nearly identical, an indication that 10 mM 1,4-dioxane was not toxic to *S. oneidensis* (Supplementary Fig. 2.S1). Although cell densities decreased approximately 70% during the 3 h anaerobic incubation periods, lactate was consumed at similar rates (0.21 mM/h) during the 3 h aerobic and anaerobic cycling periods. Lactate was not depleted in abiotic control incubations carried out with otherwise identical aerobic and anaerobic cycling periods (Fig. 2.4a).

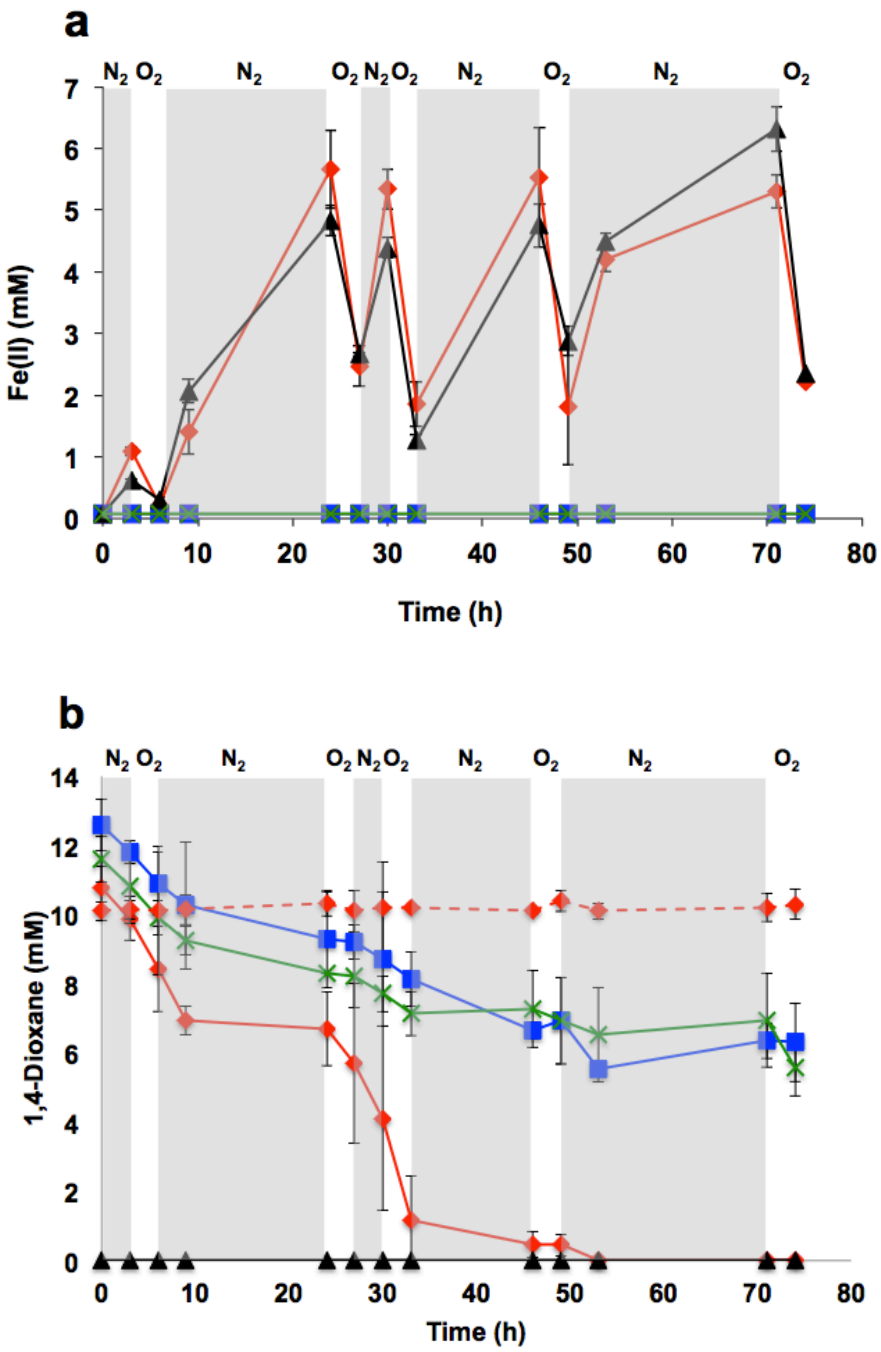

Figure 2.3. Fe(II) and 1,4-dioxane concentrations during microbially-driven Fenton degradation of 1,4-dioxane (10 mM initial concentration) with an aerobic/anaerobic cycling period of 3 h: (a) Fe(II); (b) 1,4-dioxane; red ◆, cells + 1,4-dioxane + Fe(III); blue ■, *S. oneidensis* cells omitted; black ▲, 1,4-dioxane omitted; green ×,Fe(III) omitted; dashed red ◆, No Gas control. Grey shaded areas correspond to anaerobic phases and unshaded areas correspond to aerobic phases. Incubations were carried out

in two parallel yet identical cultures and error bars indicate range of error between incubations.

Inhibition of the Microbially-Driven 1,4-Dioxane Degradation Process. To determine if $HO^{\bullet}$ radical scavenging compounds inhibited the microbially-driven Fenton reaction, a series of control incubations were carried out under DD conditions in the presence of the $HO^{\bullet}$ radical scavenging compounds mannitol (120 mM) or thiourea (40 mM) (Fig. 2.5b). 1,4-dioxane concentrations in all incubations decreased to 6.0 mM during the initial 9 h aerobic and anaerobic cycling periods (due to 1,4-dioxane volatility; as described above). 1,4-dioxane was degraded to below detection limits (0.2 mM; Supplementary Table 2.S3) after 53 h of alternating 3 h aerobic/anaerobic cycling periods in the absence of mannitol or thiourea (Fig. 2.5b), while 1,4-dioxane remained constant at 6.0 mM in the presence of mannitol or thiourea. To test for toxicity effects of mannitol and thiourea, *S. oneidensis* was grown aerobically in LS growth medium supplemented with mannitol (120 mM) or thiourea (40 mM). Aerobic growth rates in the presence or absence of mannitol or thiourea were nearly identical, an indication that these compounds were not toxic to *S. oneidensis* (Supplementary Fig. 2.S6). The ability of the $HO^{\bullet}$ radical scavenging compounds mannitol and thiourea to inhibit 1,4-dioxane degradation indicates that $HO^{\bullet}$ radicals are involved in the microbially-driven 1,4-dioxane degradation process.

The requirement for microbial Fe(III) reduction was tested by replacing Fe(III) with NO_3^- and carrying out an otherwise identical set of DD experiments with NO_3^--containing *S. oneidensis* cultures subjected to alternating 3 h aerobic/anaerobic cycling periods. 1,4-dioxane was not degraded with NO_3^- as electron acceptor (Fig. 2.5b), nor was 1,4-dioxane degraded in the absence of Fe(III) or *S. oneidensis* cells (Fig. 2.3b). These results indicate that microbial

Fe(III) reduction was required to drive the 1,4-dioxane degradation process. In all control incubations, lactate was consumed at similar rates (0.21 mM/h) under either strictly aerobic or anaerobic Fe(III)-reducing conditions. Lactate concentrations remained constant in 74 h abiotic control incubations held under strictly aerobic or anaerobic conditions (Fig. 2.6a). Apart from the 45% loss due to volatilization, 1,4-dioxane was not degraded under strictly aerobic conditions, which is identical to previously reported findings (Supplementary Fig. 2.S7) (30).

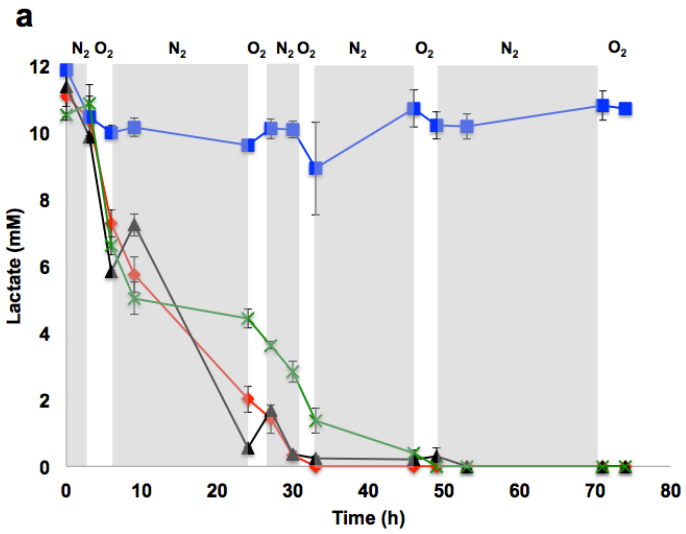

Figure 2.4. Lactate, acetate, and oxalate concentrations during microbially-driven Fenton degradation of 1,4-dioxane (10 mM) with an aerobic/anaerobic cycling period of 3 h: (a) lactate; (b) acetate; (c) oxalate; red ◆, cells + 1,4-dioxane + Fe(III); blue ■, *S. oneidensis* cells omitted; black ▲, 1,4-dioxane omitted; green ×,Fe(III) omitted. Grey shaded areas correspond to anaerobic phases and unshaded areas correspond to aerobic phases. Incubations were carried in two parallel yet identical cultures and error bars indicate range of error between incubations.

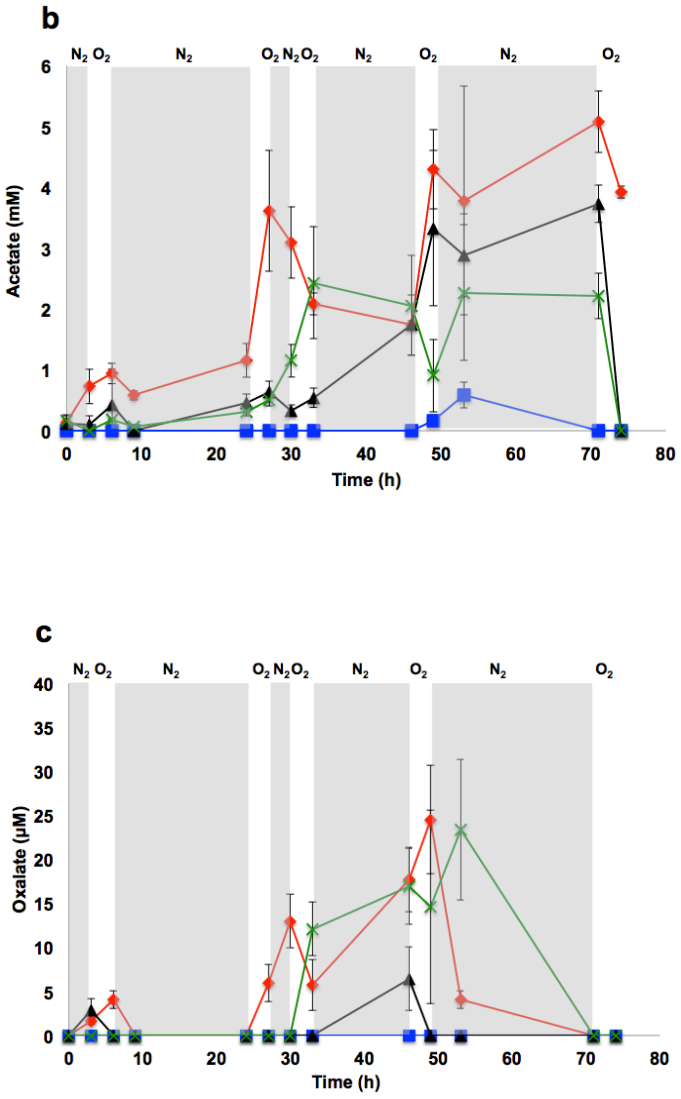

Figure 2.4 continued

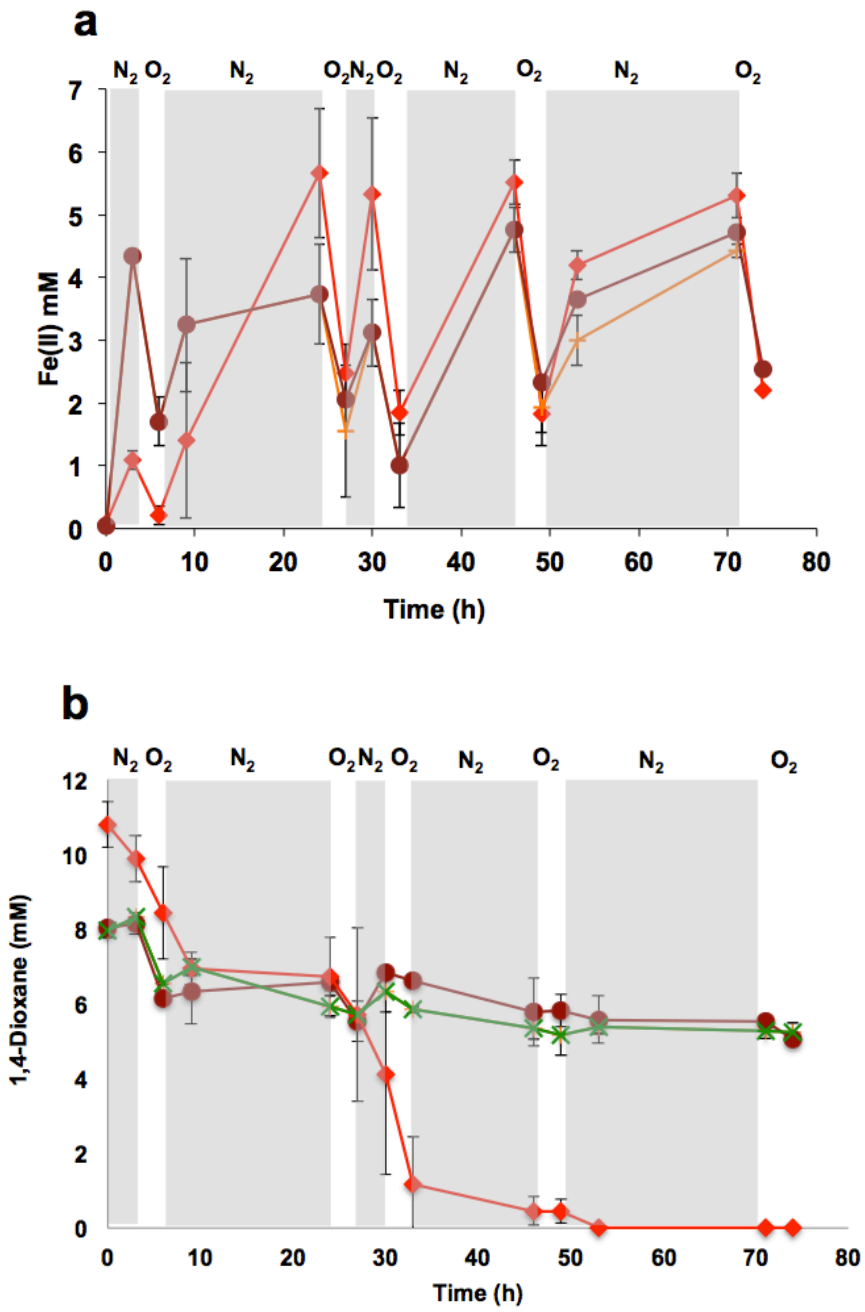

Figure 2.5. Fe(II) and 1,4-dioxane concentrations during the microbially-driven Fenton degradation of 1,4-dioxane (10 mM) with an aerobic/anaerobic cycling period of 3 h in the presence of inhibitors: (a) Fe(II); (b) 1,4-dioxane; red ◆, *S. oneidensis* cells + 1,4-dioxane + Fe(III); orange +, mannitol; brown •, thiourea; green ×, nitrate. Grey shaded areas correspond to anaerobic phases and unshaded areas correspond to aerobic phases. Incubations were carried out in two parallel yet identical cultures and error bars indicate range of error between incubations.

Identification of Transient 1,4-Dioxane Degradation Products During the Microbially-Driven Fenton Reaction. The major transient 1,4-dioxane degradation products detected during conventional (purely abiotic) Fenton reactions include formate, glycolate, glyoxylate, ethylene glycol diformate, acetate, and oxalate, which are produced by HO• radical attack of 1,4-dioxane with the α-oxy radical as key intermediate(36). With LC/UV-DA and IC detection methods, only acetate and oxalate were detected as transient 1,4-dioxane degradation products during the microbially-driven Fenton reaction. In the first 3 h anaerobic period, 0.7 mM acetate (at a rate of 0.24 mM/h) was produced under DD conditions, while acetate concentrations remained below detection limits (40.38 μM) in DD control incubations lacking *S. oneidensis* cells or Fe(III) or in the presence of HO• scavenging compounds (Fig. 2.4b). During the ensuing 3 h aerobic period of all biotic incubations, acetate concentrations increased at similar rates (0.08 mM/h) (Fig. 2.4b), presumably due to the microbially catalyzed aerobic oxidation of lactate. Acetate concentrations remained constant during the next 18 h anaerobic period. Upon introduction of compressed air at the 24-h time point under DD conditions, acetate concentrations increased rapidly at the rate of 0.81 mM/h (Fig. 2.4b). During this same time period, 1,4-dioxane concentrations decreased sharply (0.33 mM/h) as compared to decreases in 1,4-dioxane concentrations (0.07 mM/h) in DD control incubations lacking *S. oneidensis* cells or Fe(III) (Fig. 2.3b).

During the next set of aerobic/anaerobic cycling periods, acetate concentrations decreased sharply from 3.6 mM to 2.1 mM at the 33-h time point (0.25 mM/h). At the 49-h time point, acetate production rates (1.13 mM/h) under DD conditions increased approximately 45% compared to DD control incubations (0.80 mM/h) lacking *S. oneidensis* cells or Fe(III). Higher acetate production rates are most likely due to 1,4-dioxane (and not lactate) degradation since

lactate had been completely depleted by the 46-h time point (Figs. 2.3b and 2.5b). Since lactate was also completely depleted in all reactions containing *S. oneidensis* cells, microbial oxidation of lactate to acetate most likely contributed to acetate production (Figs. 2.3a and 2.5a). Acetate concentrations in the incubations containing the $HO^{\bullet}$ radical scavenging compounds mannitol or thiourea, however, remained constant at 1-2 mM throughout the 74 h incubation period (Fig. 2.6b). In addition, the total acetate produced under DD conditions with 3 h aerobic/anaerobic cycling periods was 7.7 mM (approximately 2-fold greater than that detected in the control incubations (2.5-4.9 mM) (Table 2.1). The 2-to-3-fold greater amount of acetate produced in the presence of 1,4-dioxane was reflected in the 2-to-4-fold greater amount of 1,4-dioxane degraded in the microbially-driven Fenton reaction compared to DD control incubations lacking *S. oneidensis* cells or Fe(III) or in the presence of mannitol or thiourea (Table 2.1). Similar results were obtained in DD incubations with aerobic/anaerobic cycling frequencies of 1.5 h, 45 min, and 6 h (Supplementary Table 2.S1).

Approximately 4 μM oxalate was produced during the initial set of 3 h aerobic/anaerobic cycling periods under DD conditions, while oxalate was not detected in DD control incubations lacking *S. oneidensis* cells or Fe(III) (Figs. 2.3c and 2.5c). At the 24-h time point, oxalate concentrations under DD conditions steadily increased to 13.0 μM at a rate of 2.2 μM/h. At the 33-h time point, strictly anaerobic conditions were held for the ensuing 18 h and oxalate concentrations increased to 17.7 μM at a rate of 0.9 μM/h (2-fold greater than control incubations lacking *S. oneidensis* cells or Fe(III)). At the 46-h time point, oxalate concentrations increased further to 24.5 μM during the 3 h aerobic incubation period (Figs. 2.3c and 2.5c). Approximately 0.04 mM oxalate was produced under DD conditions (2-to-4-fold greater than control incubations lacking *S. oneidensis* cells or Fe(III), Table 2.1). Results similar to those of

the 3 h aerobic/anaerobic cycling period experiments were obtained with aerobic/anaerobic cycling periods of 45 min, 1.5 h, and 6 h (Supplementary Figs. 2.S3e, 2.S4e, 2.S5e and Supplementary Table 2.S1).

A carbon mass balance was also carried out to account for total carbon input and output during the microbially-driven Fenton reaction. Total carbon input under DD conditions (except in controls where 1,4-dioxane was omitted) was 70 mmol. Total carbon output (acetate plus oxalate) under DD conditions was 15.4 mmol and the corresponding carbon input from 1,4-dioxane degradation was 43.2 mmol. The 2-to-4-fold greater amounts of 1,4-dioxane degraded under DD conditions were reflected in a 2-to-3-fold greater total carbon output (acetate plus oxalate) compared to the DD control incubations carried out in the absence of 1,4-dioxane or in the presence of 1,4-dioxane and the $HO^{\bullet}$ scavenging compounds mannitol or thiourea (Table 2.2). Similar observations were made under DD conditions with aerobic/anaerobic cycling frequencies of 1.5 h, 45 min and 6 h (Supplementary Table 2.S2). Total carbon input (lactate plus 1,4-dioxane) did not completely account for total carbon output (acetate plus oxalate), most likely due to further reaction of acetate and oxalate with $HO^{\bullet}$ radicals and the resulting unaccounted carbon loss, potentially as CO_2 (Table 2.2).

Table 2.1. Substrate degradation and transient intermediate production during the microbially-driven Fenton degradation of 1,4-dioxane [a]

	3 h cycling			
	Degraded (mM)		Produced (mM)	
	1,4-Dioxane	Lactate	Acetate	Oxalate
Cells + 1,4-dioxane+Fe(III)	10.8 ± 0.6	11.1 ± 0.6	7.7 ± 0.8	0.04 ± 0.002
Cells omitted	6.3 ± 0.4	1 ± 0.3	0	0
1,4-Dioxane omitted	0	11.4 ± 0.4	4.8 ± 0.4	0.01 ± 0.002
Fe(III) omitted	6 ± 0.2	10.5 ± 0.1	3.9 ± 0.4	0.03 ± 0.004
Mannitol	2.8 ± 0.5	9.3 ± 0.3	2.8 ± 0.3	0.01 ± 0.009
Thiourea	3 ± 0.01	9.5 ± 0.03	4.7 ± 0.6	0.01 ± 0.004
Nitrate	2.8 ± 2.4	9.5 ±0.1	2.5 ± 0.3	0.01 ± 0.006

[a] Incubations were carried in two parallel yet identical cultures and error bars indicate range of error between incubations.

Table 2.2. Total input and output carbon detected during the microbially-driven Fenton degradation of 1,4-dioxane [a]

	3 h cycling			
	Input Carbon (mmol)		Output Carbon (mmol)	
	Lactate + 1,4-Dioxane	1,4-Dioxane degraded	Acetate	Oxalate
Cells+1,4-dioxane+Fe(III)	70	43.2 ± 2.5	15.4 ± 1.6	0.08 ± 0.004
Cells omitted	70	25.2 ± 1.6	0	0
1,4-Dioxane omitted	30	0	9.6 ± 0.8	0.02 ± 0.004
Fe(III) omitted	70	24 ± 0.7	7.8 ± 0.8	0.06 ± 0.008
Mannitol	70	11 ± 2	5.6 ± 0.6	0.02 ± 0.018
Thiourea	70	12 ± 0.04	9.4 ± 1.2	0.02 ± 0.008
Nitrate	70	11.2 ± 9.6	5 ± 0.6	0.02 ± 0.012

[a] Incubations were carried in two parallel yet identical cultures and error bars indicate range of error between incubations. Carbon mmols per liter of reaction volume

2.4 Discussion

In the present study, a microbially-driven Fenton reaction was designed to degrade the widespread environmental contaminant 1,4-dioxane. The microbially-driven Fenton reaction autocatalytically generated $HO^{\bullet}$ radicals that degraded 1,4-dioxane at circumneutral pH without the need for continual addition of exogenous H_2O_2 or UV irradiation to regenerate Fe(II) as Fenton reagents. The 1,4-dioxane degradation process was driven by pure cultures of the Fe(III)-reducing facultative anaerobe *S. oneidensis* provided with lactate as carbon and energy source, Fe(III) as electron acceptor, and exposed to alternating aerobic and anaerobic conditions. H_2O_2 produced during the aerobic period was most likely the byproduct of microbial aerobic respiration since H_2O_2 was not detected during abiotic O_2-catalyzed Fe(II) oxidation experiments. Alternate aerobic/anaerobic cycling periods of 3 h and 6 h resulted in the maximum rate and extent of H_2O_2 production, both of which were nearly identical to the rate and extent of H_2O_2 production under strictly aerobic conditions. H_2O_2 production with 45 min and 1.5 h cycling periods resulted in lower rates and extents of H_2O_2 production (Fig. 2.2). During the transition from anaerobic-to-aerobic conditions, *S. oneidensis* batch cultures displayed lag times in H_2O_2 production. H_2O_2 production rates were maximal during the 3 h and 6 h aerobic/anaerobic cycling periods, but 3-to-10-fold lower during the 45 min and 1.5 h cycling periods (Fig. 2.2). In addition, the 3 h aerobic/anaerobic cycling period was sufficient to achieve the maximum rate and extent of H_2O_2 production, which was reflected in the results of the 1,4-dioxane degradation experiments described below.

Since 1,4-dioxane is a semi-volatile compound, approximately 46% of the decrease in 1,4-dioxane concentrations was attributed to volatilization during hydrated compressed gas inputs, while the remaining 54% decrease in 1,4-dioxane concentrations to below detection limits

(0.2 mM; Supplementary Table 2.S3) was due to degradation by HO• radicals produced by the microbially-driven Fenton reaction(47). Approximately 46% of the initial 1,4-dioxane concentration was removed by volatilization during the hydrated gas inputs due to continual diffusion of 1,4-dioxane to the vapor phase until vapor-liquid equilibrium was attained at 9 h. 1,4-dioxane was not further volatilized since the compressed gases were saturated with water prior to injection (Fig. 2.3b and Supplementary Fig. 2.S7). The inability of the microbially-driven Fenton reaction to degrade 1,4-dioxane in the presence of HO• radical scavenging compounds mannitol or thiourea or in the absence of either *S. oneidensis* cells or Fe(III) implicated HO• radicals as the main driver of the 1,4-dioxane degradation process. The absence of 1,4-dioxane degradation under strictly aerobic or strictly anaerobic Fe(III)-reducing conditions indicates that 1,4-dioxane degradation was not due to aerobic or anaerobic enzymatic 1,4-dioxane degradation reactions catalyzed by *S. oneidensis*.(2, 19)

Alternately, the microbially-driven Fenton reaction described in the present study may be initiated by H_2O_2-catalyzed Fe(III) reduction reactions(48, 49). In this scenario, H_2O_2 produced by *S. oneidensis* during the preceding aerobic cycling period catalyzes chemical (purely abiotic) Fe(III) reduction reactions. The H_2O_2-catalyzed Fe(III) reduction reactions, however, are Fe(III) speciation-dependent, and some soluble organic-Fe(III) complexes such as Fe(III)-oxalate are not reduced by H_2O_2 (50). Since *S. oneidensis* produces an yet unidentified Fe(III)-chelating organic ligand that enhances Fe(III) bioavailability(51-53), the results of the present study do not preclude the possibility that soluble organic-Fe(III) complexes produced by *S. oneidensis* are reduced by H_2O_2 produced during the preceding aerobic cycling period. However, the absence of 1,4-dioxane degradation in Fe(III)-amended DD control incubations held under strictly aerobic conditions for 74 h indicates that HO• radical production is most

likely not initiated by H_2O_2-catalyzed Fe(III) reduction reactions, but requires *S. oneidensis*-catalyzed Fe(III) reduction reactions during the anaerobic cycling periods.(48, 49)

Although the LC and IC methods used in the present study may have missed detection of other 1,4-dioxane degradation products (e.g., aldehydes) analyzed by other methods(36), acetate and oxalate were detected as 1,4-dioxane degradation products of the microbially driven Fenton reaction. In conventional (purely abiotic) Fenton reactions, acetate and oxalate are produced by $HO^{\bullet}$ radical attack of 1,4-dioxane with α-oxy radicals as the key intermediate for subsequent degradation reactions.(36) The α-oxy radicals follow two separate degradation pathways that depend on O_2 concentrations in the chemical Fenton reaction system. In O_2-limited systems, the α-oxy radicals are degraded to acetate, formate, formaldehyde, and oxalate, while in O_2-replete systems, the α-oxy radicals are degraded to ethylene glycol diformate(24, 36). In the present study, 1,4-dioxane degradation by the microbially driven Fenton reaction resulted in production of acetate and oxalate as the main 1,4-dioxane degradation products, while ethylene glycol diformate was not detected. In addition, formate, glycolate, and glyoxylate were not detected during the microbially-driven 1,4-dioxane degradation process, most likely due to the high reactivity of these intermediates with $HO^{\bullet}$ radical(36). Since only 40 μM oxalate was produced during degradation of 10 mM 1,4-dioxane, the majority of 1,4-dioxane may have been mineralized to CO_2 or stalled at another upstream intermediate such as hydroxyethoxyacetic acid (HEAA)(36, 54).

In previous applications of conventional (purely abiotic) Fenton reactions, 1,4-dioxane was degraded at rates approximately 20-fold greater than the microbially-driven Fenton reaction designed in the present study (rate constant of 0.0036 min^{-1} for 3 h aerobic/anaerobic cycling period at pH 7.0). Such differences may be due to the high concentrations (15 mM) of

exogenous H_2O_2 employed to drive the chemical Fenton reaction systems(24, 36). However, after normalization on a per mg protein basis, the reaction rates observed in the present study are 4-to-5-fold greater than the enzymatic rates of 1,4-dioxane degradation by *Pseudonocardia* species(2). In the present study, *S. oneidensis* produced micromolar levels of H_2O_2, presumably as a by-product of microbial aerobic respiration during the aerobic cycling periods. Addition of exogenous H_2O_2 was therefore not required to drive the microbially-driven Fenton reaction. The chemical Fenton reaction also requires re-reduction of Fe(III) produced during H_2O_2-catalyzed Fe(II) oxidation reactions. Fe(III) re-reduction processes such as those catalyzed by UV irradiation are possible during ex situ 1,4-dioxane degradation processes(39), yet UV light penetration represents a formidable obstacle for in situ 1,4-dioxane remediation technologies.

In the microbially-driven Fenton reaction designed in the present study, *S. oneidensis* respiratory processes catalyze both H_2O_2 production and Fe(III) re-reduction. Since microbial Fe(III) reduction has been detected in a variety of aquatic environments, including contaminated subsurface aquifers(55), the microbially-driven Fenton reaction may be induced by exposing Fe(III)-reducing facultative anaerobes in Fe(III)-containing contaminated environments to alternating aerobic and anaerobic conditions. Alternately, the microbially-driven Fenton reaction may be stimulated by injecting soluble Fe(III), nanoparticulate zero-valent iron (nZVI)(56) or electrolytic systems(57) in the flow path of 1,4-dioxane-contaminated subsurface aquifers and exposing endogenous (or injected) Fe(III)-reducing bacteria to alternating aerobic and anaerobic conditions. Microbially-driven Fenton reaction may also be initiated through bioaugmentation at plume fringes where heterogeneous aerobic/anaerobic redox zonation may occur(58). The microbially-driven Fenton reaction thus provides a foundation for development of alternative in situ remediation technologies that degrade 1,4-dioxane or other environmental contaminants

(e.g., PCP(29, 30), PCE(23), TCE(31) and TCA(32)) susceptible to attack by $HO^{\bullet}$ radicals generated by the Fenton reaction.

2.5 References

1. **Stickney JA, Sager SL, Clarkson JR, Smith LA, Locey BJ, Bock MJ, Hartung R, Olp SF.** 2003. An updated evaluation of the carcinogenic potential of 1,4-dioxane. Reg Tox Pharm **38:**183-195.

2. **Mahendra S, Alvarez-Cohen L.** 2006. Kinetics of 1,4-dioxane biodegradation by monooxygenase-expressing bacteria. Environmental Science & Technology **40:**5435-5442.

3. **DeRosa CT, Wilbur S, Holler J, Richter P, Stevens YW.** 1996. Health evaluation of 1,4-dioxane. Toxicol Ind Health **12:**1-43.

4. **Mohr TKG, Stickney JA, DiGuiseppi WH.** 2010. Environmental Investigation and Remediation: 1,4-Dioxane and other Solvent Stabilizers. CRC Press.

5. **Anonymous.** 1999. U.S. Environmental Protection Agency, Integrated Risk Information System (IRIS) on 1,4-Dioxane, National Center for Environmental Assessment, Washington, DC.

6. **Abe A.** 1999. Distribution of 1,4-dioxane in relation to possible sources in the water environment. The Science of the total environment **227:**41-47.

7. **Jackson RE, Dwarkanath V.** 1999. Chlorinated degreasing solvents:physical-chemical properties affecting aquifer contamiants and remediation. Ground Water Monit Rem **19:**102-110.

8. **Lanigan RS.** 2000. Addendum to the final report on the safety assessment of polysorbates. Int J Toxicol **19:**43-89.

9. **Zenker MJ, Borden RC, Barlaz MA.** 2003. Occurence and treatment of 1,4-dioxane in aqueous environments. Environ Eng Sci **20**.

10. **Sei K, Kakinoki T, Inoue D, Soda S, Fujita M, Ike M.** 2010. Evaluation of the biodegradation potential of 1,4-dioxane in river, soil and activated sludge samples. Biodegradation **21:**585-591.

11. **Adams CD, Scanian PA, Secrist ND.** 1998. Oxidation and biodegradability enhancement of 1,4-dioxane using hydroxide peroxide and ozone. Environ Sci Technol **28:**1812-1816.

12. **Hill RR, Jeffs GE, Roberts DR.** 1997. Photocatalytic degradation of 1,4-dioxane in aqueous solution. J Photochem Photobiol A **108:**55-58.

13. **Beckett MA, Hua I.** 2003. Enhanced sonochemical decomposition of 1,4-dioxane by ferrous iron. Water Research **37:**2372-2376.

14. **Roy D, Anagnostu G, Chaphalkar P.** 1994. Biodegradation of dioxane and diglyme in industrial waste. J Environ Sci Health Part A Environ Sci Eng **29:**129-147.

15. **Chidambara Raj CB, Ramkumar N, Haja jahabar siraj A, Chidambaram SP.** 1997. Biodegradation of acetic, benzoic, isophthalic, toluic and terephthalic acids using a mixed culture: effluents of PTA production. Process saf Environ Prot **75:**245-256.

16. **Vainberg S, McClay K, Masuda H, Root D, Condee C, Zylstra GJ, Steffan RJ.** 2006. Biodegradation of ether pollutants by Pseudonocardia sp. strain ENV478. Appl Environ Microbiol **72:**5218-5224.

17. **Nakamiya K, Hashimoto S, Ito H, Edmonds JS, Morita M.** 2005. Degradation of 1,4-dioxane and cyclic ethers by an isolated fungus. Appl Environ Microbiol **71:**1254-1258.

18. **Kim YM, Jeon JR, Murugesan K, Kim EJ, Chang YS.** 2009. Biodegradation of 1,4-dioxane and transformation of related cyclic compounds by a newly isolated Mycobacterium sp. PH-06. Biodegradation **20:**511-519.

19. **Mahendra S, Alvarez-Cohen L.** 2005. Pseudonocardia dioxanivorans sp. nov., a novel actinomycete that grows on 1,4-dioxane. Int J Syst Evol Microbiol **55:**593-598.

20. **Steffan R.** 2007. Biodegradation of 1,4-Dioxane. SERDP **August**.

21. **Richard J. Watts, Brett C. Bottenberg, Thomas F. Hess, Mark D. Jensen, Teel. AL.** 1999. Role of reductants in the enhanced desorption and transformation of chloroaliphatic compounds by modified Fenton's reactions. Environmental Science & Technology **33:**3432-3437.

22. **Kinne M, Poraj-Kobielska M, Ralph SA, Ullrich R, Hofrichter M, Hammel KE.** 2009. Oxidative cleavage of diverse ethers by an extracellular fungal peroxygenase. The Journal of biological chemistry **284:**29343-29349.

23. **Jho EH, Singhal N, Turner S.** 2010. Fenton degradation of tetrachloroethene and hexachloroethane in Fe(II) catalyzed systems. Journal of hazardous materials **184:**234-240.

24. **Vescovi T, Coleman HM, Amal R.** 2010. The effect of pH on UV-based advanced oxidation technologies--1,4-dioxane degradation. Journal of hazardous materials **182:**75-79.

25. **Kim YK, Huh IR.** 1997. Enhancing biological treatability of landfill leachate by chemical oxidation. Environmental Engineering Science **14:**73-79.

26. **Tyre BW, Watts RJ, Miller GC.** 1991. Treatment of 4 Biorefractory Contaminants in Soils Using Catalyzed Hydrogen-Peroxide. Journal of Environmental Quality **20:**832-838.

27. **Topudurti K, Keefe M, Wooliever P, Lewis N.** 1994. Field-Evaluation of Perox-Pure(Tm) Chemical Oxidation Technology. Water Science and Technology **30:**95-104.

28. **Andreozzi R, Campanella L, Fraysse B, Garric J, Gonnella A, Giudice RL, Marotta R, Pinto G, Pollio A.** 2004. Effects of advanced oxidation processes (AOPs) on the toxicity of a mixture of pharmaceuticals. Water science and technology : a journal of the International Association on Water Pollution Research **50:**23-28.

29. **Barbeni M, Minero C, Pelizzetti E, Borgarello E, Serpone N.** 1987. Chemical Degradation of Chlorophenols with Fenton Reagent (Fe-2++H2O2). Chemosphere **16:**2225-2237.

30. **McKinzi AM, Dichristina TJ.** 1999. Microbially driven Fenton reaction for transformation of pentachlorophenol. Environmental Science & Technology **33:**1886-1891.

31. **Tsai TT, Kao CM, Surampalli RY, Weng CH, Liang SH.** 2010. Treatment of TCE-Contaminated Groundwater Using Fenton-Like Oxidation Activated with Basic Oxygen Furnace Slag. Journal of Environmental Engineering-Asce **136:**288-294.

32. **Pignatello JJ, Liu D, Huston P.** 1999. Evidence for an Additional Oxidant in the Photoassisted Fenton Reaction. Environmental Science & Technology **33:**1832-1839.

33. **Yeh CKJ, Wu HM, Chen TC.** 2003. Chemical oxidation of chlorinated non-aqueous phase liquid by hydrogen peroxide in natural sand systems. Journal of hazardous materials **96:**29-51.

34. **Baciocchi R, Boni MR, D'Aprile L.** 2004. Application of H2O2 lifetime as an indicator of TCE Fenton-like oxidation in soils. Journal of hazardous materials **107:**97-102.

35. **Son HS, Im JK, Zoh KD.** 2009. A Fenton-like degradation mechanism for 1,4-dioxane using zero-valent iron (Fe0) and UV light. Water Research **43:**1457-1463.

36. **Stefan MI, Bolton JR.** 1998. Mechanism of the degradation of 1,4-dioxane in dilute aqueous solution using the UV hydrogen peroxide process. Environmental Science & Technology **32:**1588-1595.

37. **Kim SM, Vogelpohl A.** 1998. Degradation of organic pollutants by the photo-fenton-process. Chemical Engineering & Technology **21:**187-191.

38. **Coleman HM, Vimonses V, Leslie G, Amal R.** 2007. Degradation of 1,4-dioxane in water using TiO2 based photocatalytic and H2O2/UV processes. Journal of Hazardous Materials **146:**496-501.

39. **Kim CG, Seo HJ, Lee BR.** 2006. Decomposition of 1,4-dioxane by advanced oxidation and biochemical process. J Environ Sci Health A Tox Hazard Subst Environ Eng **41:**599-611.

40. **Dichristina TJ, Delong EF.** 1994. Isolation of Anaerobic Respiratory Mutants of Shewanella-Putrefaciens and Genetic-Analysis of Mutants Deficient in Anaerobic Growth on Fe3+. Journal of Bacteriology **176:**1468-1474.

41. **Dichristina TJ, Arnold RG, Lidstrom ME, Hoffmann MR.** 1988. Dissimilative Iron Reduction by the Marine Eubacterium Alteromonas putrefaciens Strain 200. Water Science & Technology **20:**69-79.

42. **DiChristina TJ, Moore CM, Haller CA.** 2002. Dissimilatory Fe(III) and Mn(IV) reduction by Shewanella putrefaciens requires ferE, a homolog of the pulE (gspE) type II protein secretion gene. J Bacteriol **184:**142-151.

43. **Sambrook J, Fritsh EF, Maniatis T.** 1989. Molecular Cloning: A Laboratory Manual. Cold Spring Harbor Laboratory Press; Cold Spring Harbor, NY.

44. **Obuekwe CO, Westlake DWS, Cook FD.** 1981. Effect of Nitrate on Reduction of Ferric Iron by a Bacterium Isolated from Crude-Oil. Canadian Journal of Microbiology **27:**692-697.

45. **Dichristina TJ.** 1992. Effects of Nitrate and Nitrite on Dissimilatory Iron Reduction by Shewanella-Putrefaciens-200. Journal of Bacteriology **174:**1891-1896.

46. **Kiassen NV, Marchington D, McGowan HCE.** 1994. H202 Determination by the I3- Method and by KMn04 Titration. Anal Chem **66:**2921-2925.

47. **Nakamura S, Daishima S.** 2005. Simultaneous determination of 22 volatile organic compounds, methyl-tert-butyl ether, 1,4-dioxane, 2-methylisoborneol and geosmin in water by headspace solid phase microextraction-gas chromatography-mass spectrometry. Analytica Chimica Acta **548:**79-85.

48. **Laat JD, Gallard H.** 1999. Catalytic Decomposition of Hydrogen Peroxide by Fe(III) in Homogeneous Aqueous Solution: Mechanism and Kinetic Modeling. Environ Sci Technol **33:**2726-2732.

49. **Halliwell B, Gutteridge JM.** 1986. Oxygen free radicals and iron in relation to biology and medicine: some problems and concepts. Arch Biochem Biophys **246:**501-514.

50. **Daneshvar N, Khataee AR.** 2006. Removal of azo dye C.I. acid red 14 from contaminated water using Fenton, UV/H(2)O(2), UV/H(2)O(2)/Fe(II), UV/H(2)O(2)/Fe(III) and UV/H(2)O(2)/Fe(III)/oxalate processes: a comparative study. J Environ Sci Health A Tox Hazard Subst Environ Eng **41:**315-328.

51. **Jones ME, Fennessey CM, DiChristina TJ, Taillefert M.** 2010. Shewanella oneidensis MR-1 mutants selected for their inability to produce soluble organic-Fe(III) complexes are unable to respire Fe(III) as anaerobic electron acceptor. Environ Microbiol **12:**938-950.

52. **Fennessey CM, Jones ME, Taillefert M, DiChristina TJ.** 2010. Siderophores Are Not Involved in Fe(III) Solubilization during Anaerobic Fe(III) Respiration by Shewanella oneidensis MR-1. Applied and Environmental Microbiology **76:**2425-2432.

53. **Taillefert M, Beckler JS, Carey E, Burns JL, Fennessey CM, DiChristina TJ.** 2007. Shewanella putrefaciens produces an Fe(III)-solubilizing organic ligand during anaerobic respiration on insoluble Fe(III) oxides. Journal of Inorganic Biochemistry **101:**1760-1767.

54. **Mahendra S, Petzold CJ, Baidoo EE, Keasling JD, Alvarez-Cohen L.** 2007. Identification of the intermediates of in vivo oxidation of 1 ,4-dioxane by monooxygenase-containing bacteria. Environ Sci Technol **41:**7330-7336.

55. **Lovley DR.** 1997. Microbial Fe(III) reduction in subsurface environments. FEMS Microbiology Reviews **20:**305-313.

56. **Joo SH, Feitz AJ, Sedlak DL, Waite TD.** 2005. Quantification of the oxidizing capacity of nanoparticulate zero-valent iron. Environ Sci Technol **39:**1263-1268.

57. **Gilbert DM, Sale TC.** 2005. Sequential Electrolytic Oxidation and Reduction of Aqueous Phase Energetic Compounds. Environ Sci Technol **39:**9270-9277.

58. **Haack SK, Bekins BA.** 2000. Microbial populations in contaminant plumes. Hydrogeology **8:**63-76.

2.6 Supplemental information

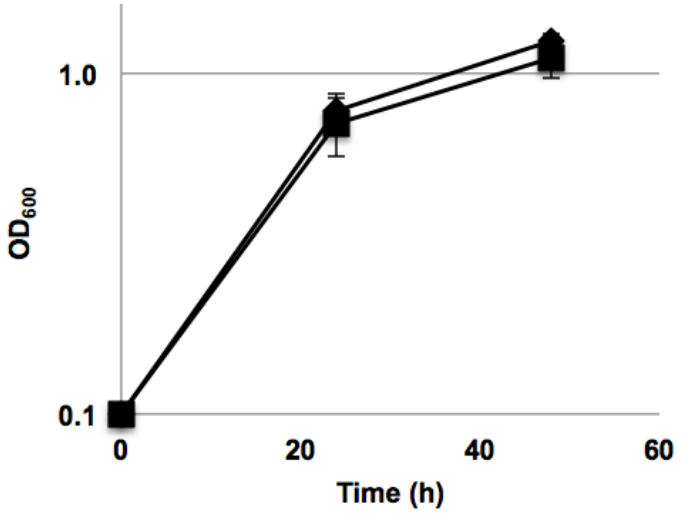

Figure 2.S1. Growth curve of *S. oneidensis* in the presence of 10 mM (■) and 0 mM (◆) 1,4-dioxane. Cell cultures were grown in LS media under aerobic conditions in the presence of 10 mM lactate as electron donor.

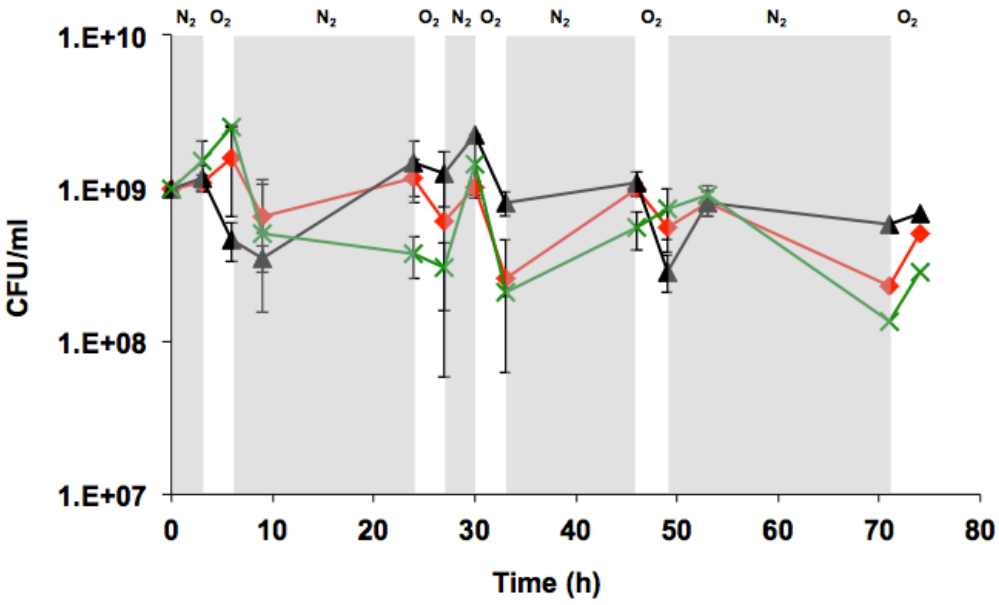

Figure 2.S2. Cell counts during microbially-driven Fenton degradation of 1,4-dioxane (10 mM) under aerobic/anaerobic cycling period of 3 h; red ◆, cells + 1,4-dioxane + Fe(III); black ▲, 1,4-dioxane omitted; green×,Fe(III) omitted. Grey shaded areas depict anaerobic phase and unshaded areas depict aerobic phase.

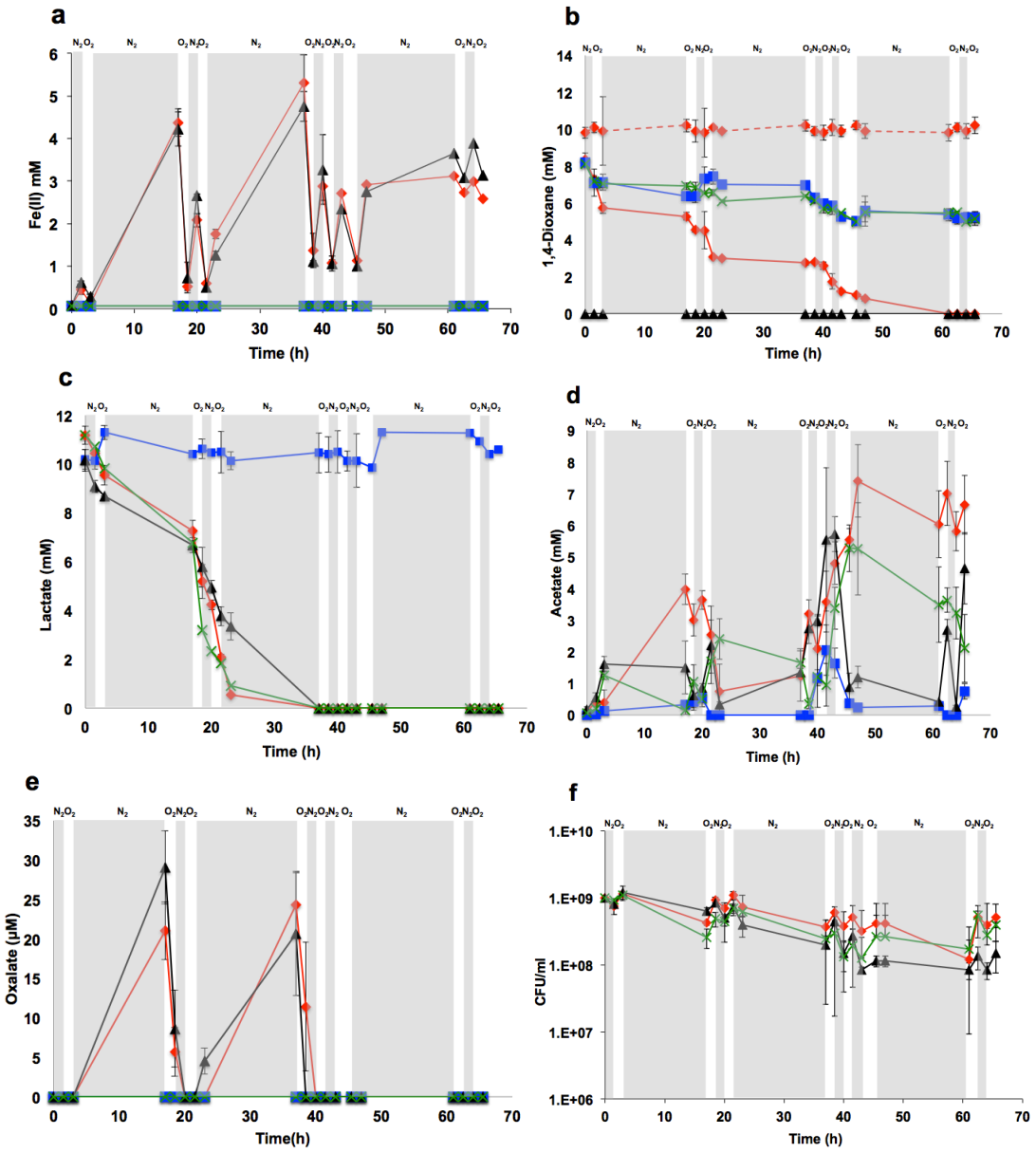

Figure 2.S3. Concentration profiles during microbial Fenton degradation of 1,4-dioxane (10 mM) under aerobic/anaerobic cycling period of 1.5 h: (a) Fe(II); (b) 1,4-dioxane; (c) lactate; (d) acetate; (e) oxalate; (f) cell count; red ◆, cells + 1,4-dioxane + Fe(III); blue ■, cells omitted; black ▲, 1,4-dioxane omitted; green ×,Fe(III) omitted; dashed red ◆, No Gas control. Grey shaded areas depict anaerobic phase and unshaded areas depict aerobic phase.

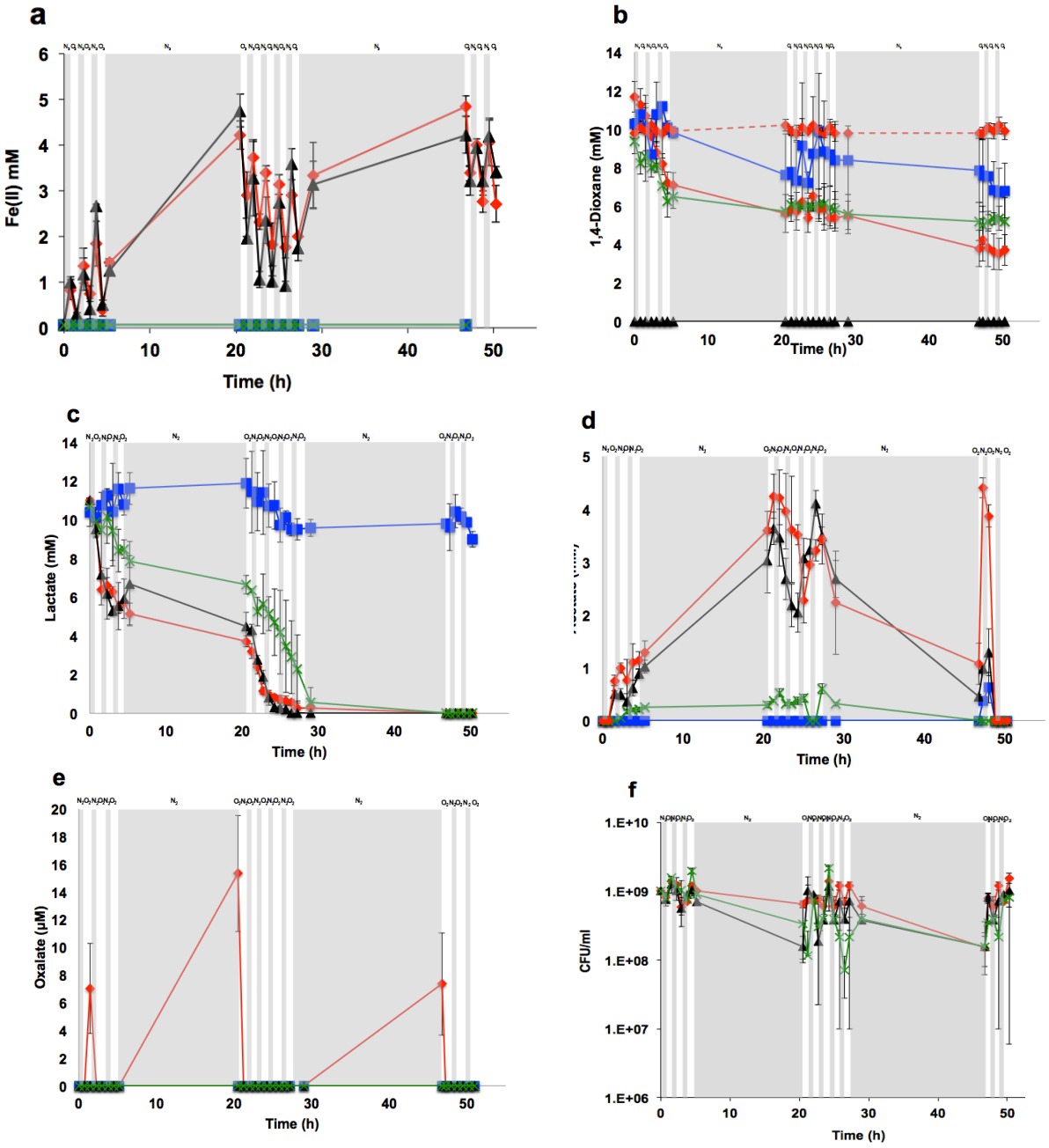

Figure 2.S4. Concentration profiles during microbial Fenton degradation of 1,4-dioxane (10 mM) under aerobic/anaerobic cycling period of 45 min: (a) Fe(II); (b) 1,4-dioxane; (c) lactate; (d) acetate; (e) oxalate; (f) cell count; red ◆, cells + 1,4-dioxane + Fe(III); blue ■, cells omitted; black ▲, 1,4-dioxane omitted; green ×,Fe(III) omitted; dashed red ◆, No Gas control. Grey shaded areas depict anaerobic phase and unshaded areas depict aerobic phase.

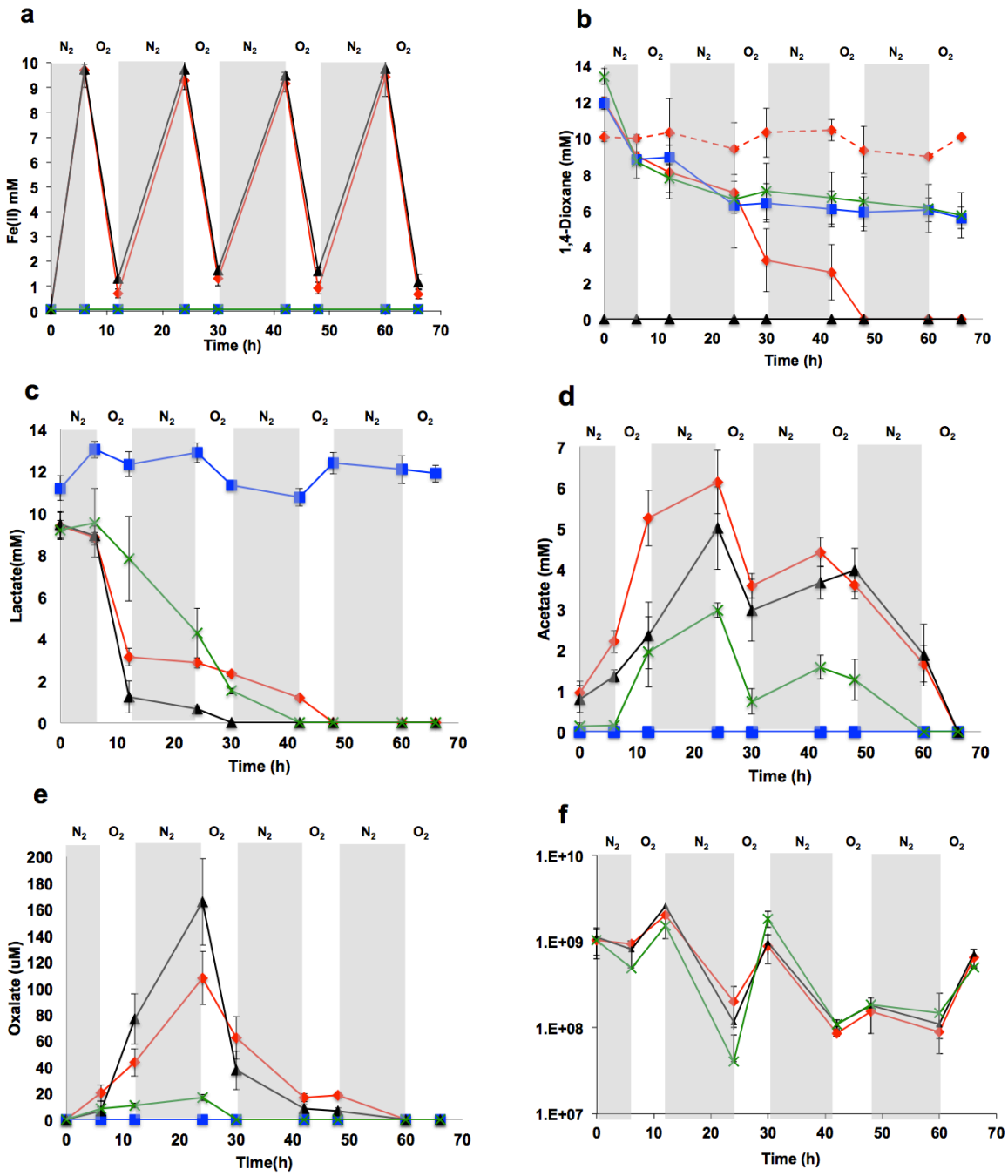

Figure 2.S5. Concentration profiles during microbial Fenton degradation of 1,4-dioxane (10 mM) under aerobic/anaerobic cycling period of 6 h: (a) Fe(II); (b) 1,4-dioxane; (c) lactate; (d) acetate; (e) oxalate; (f) cell count; red ◆, cells + 1,4-dioxane + Fe(III); blue ■, cells omitted; black ▲, 1,4-dioxane omitted; green ×,Fe(III) omitted; dashed red ◆, No Gas control. Grey shaded areas depict anaerobic phase and unshaded areas depict aerobic phase.

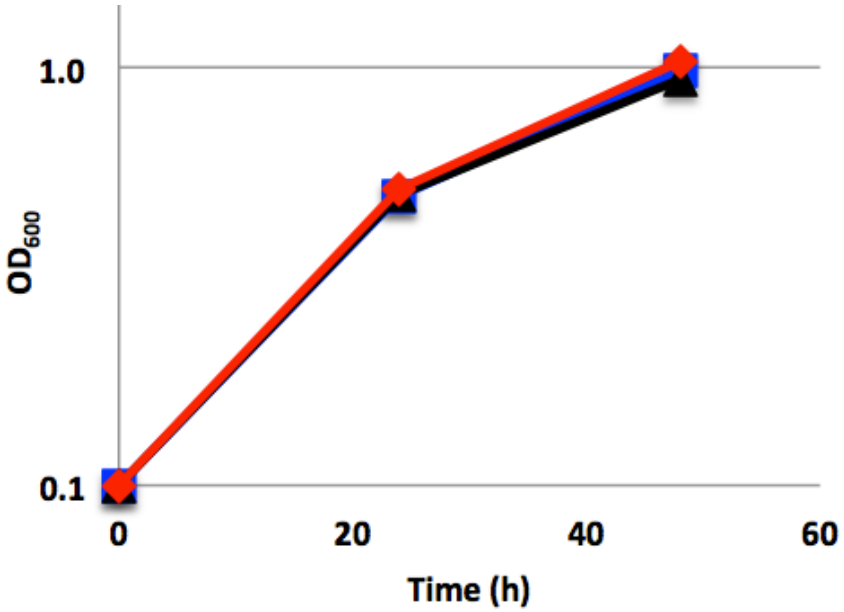

Figure 2.S6. *S. oneidensis* growth curves in the presence of radical scavengers. 120 mM mannitol (blue ■), 40 mM thiourea (black ▲) and no scavenger (red ◆). Cell cultures were grown in LS media under aerobic conditions in the presence of 10 mM lactate as electron donor.

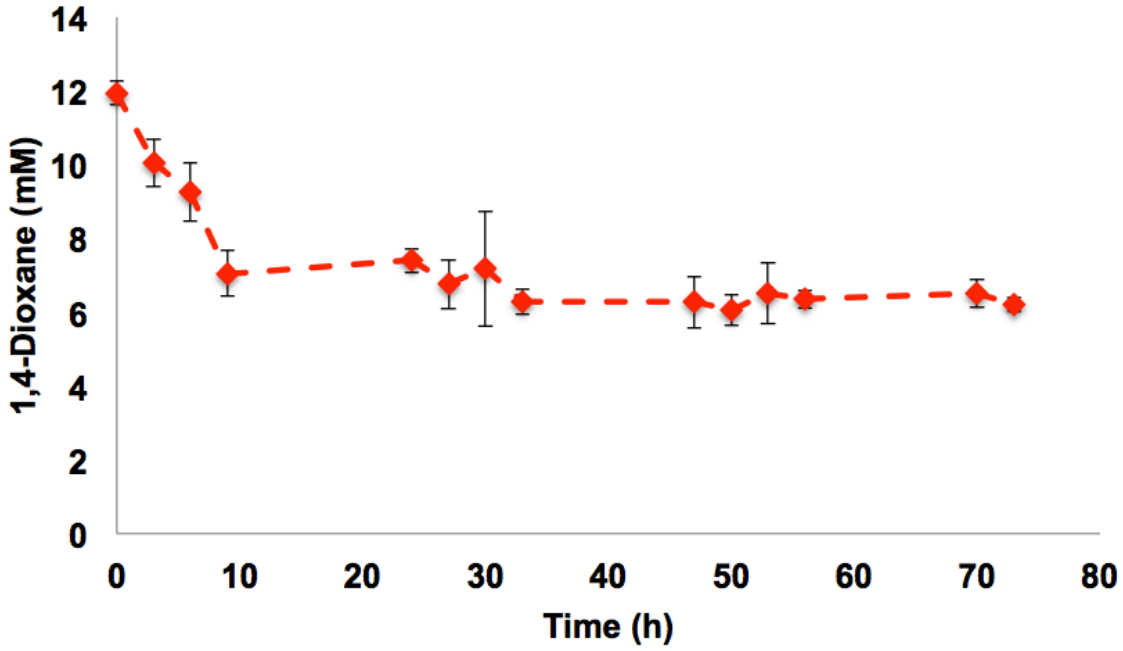

Figure 2.S7. 1,4-Dioxane profile (10 mM) under strict aerobic condition. Incubations were carried in two parallel yet identical cultures and error bars indicate standard deviations between cultures.

Table 2.S1. Total substrate degradation and intermediate production during the microbially-driven Fenton degradation of 1,4-dioxane with aerobic/anaerobic cycling periods of 1.5 h, 45 min, and 6 h [a]

	1.5 h cycling				45 min cycling			
	Degraded (mM)		Produced (mM)		Degraded (mM)		Produced (mM)	
	1,4-Dioxane	Lactate	Acetate	Oxalate	1,4-Dioxane	Lactate	Acetate	Oxalate
Cells + 1,4-dioxane+Fe(III)	8.4 ± 0.4	11.2 ± 0.4	14.1 ± 0.5	0.05 ± 0.003	8 ± 0.1	11 ± 0.1	9 ± 0.3	0.03 ± 0.003
Cells omitted	3 ± 0.2	0	3.4 ± 0.2	0	3.5 ± 1.7	1.4 ± 0.3	0.6 ± 0.2	0
1,4-Dioxane omitted	0	10.2 ± 0.4	10.6 ± 0.8	0.05 ± 0.005	0	10.4 ± 0.7	6.7 ± 0.3	0
Fe(III) omitted	3 ± 0.2	11.2 ± 0.4	9.3 ± 0.6	0	4.2 ± 1.9	10.7 ± 0.4	1.2 ± 0.04	0

	6 h cycling			
	Degraded (mM)		Produced (mM)	
	1,4-Dioxane	Lactate	Acetate	Oxalate
Cells + 1,4-dioxane+Fe(III)	12.02 ± 0.27	9.38 ± 0.64	6.97 ± 0.53	0.107 ± 0.01
Cells omitted	6.26 ± 0.62	0	0	0
1,4-Dioxane omitted	0	9.44 ± 0.62	5.27 ± 0.7	0.165 ± 0.01
Fe(III) omitted	7.68 ± 0.6	9.21 ± 0.43	3.82 ± 0.42	0.016 ± 0.003

[a] Incubations were carried in two parallel yet identical cultures and error bars indicate range of error between incubations.

Table 2.S2. Total input and output carbon during the microbially-driven Fenton degradation of 1,4-dioxane with aerobic/anaerobic cycling periods of 1.5 h, 45 min, and 6 h [a]

	1.5 h cycling				45 min cycling			
	Input Carbon (mmol)		Output Carbon (mmol)		Input Carbon (mmol)		Output Carbon (mmol)	
	Lactate + 1,4-Dioxane	1,4-Dioxane degraded	Acetate	Oxalate	Lactate + 1,4-Dioxane	1,4-Dioxane degraded	Acetate	Oxalate
Cells+1,4-dioxane+Fe(III)	70	33.5 ± 1.4	28.2 ± 1	0.1 ± 0.006	70	31.9 ± 0.3	18 ± 0.6	0.06 ± 0.006
Cells omitted	70	11.9 ± 0.8	6.8 ± 0.4	0	70	14 ± 6.9	1.2 ± 0.4	0
1,4-Dioxane omitted	30	0	21.2 ± 1.6	0.1 ± 0.01	30	0	13.4 ± 0.6	0
Fe(III) omitted	70	11.9 ± 0.9	18.6 ± 1.2	0	70	16.7 ± 7.7	2.4 ± 0.08	0

	6 h cycling			
	Input Carbon (mmol)		Output Carbon (mmol)	
	Lactate + 1,4-Dioxane	1,4-Dioxane degraded	Acetate	Oxalate
Cells+1,4-dioxane+Fe(III)	70	48.08 ± 1.08	13.94 ± 1.06	0.214 ± 0.02
Cells omitted	70	25.04 ± 2.48	0	0
1,4-Dioxane omitted	30	0	10.54 ± 1.4	0.33 ± 0.02
Fe(III) omitted	70	38.4 ± 0.24	7.64 ± 0.84	0.032 ± 0.006

Table 2.S3. Limit of detection (LOD) and the limit of quantitation (LOQ) of analytes in this study

Compound	Limit of detection (LOD)	Limit of quantitation (LOQ)
1,4-Dioxane	0.2 mM	0.69 mM
Acetate	40.38 uM	134.6 uM
Oxalate	1.1 uM	3.79 uM
Lactate	17.97 uM	59.9 uM
Glycolate	22.83 uM	76.1 uM
Glyoxylate	36.69 uM	122.3 uM
Formate	10.68 uM	35.6 uM
Ethylene glycol diformate	52.8 uM	176 uM

Table 2.S4: Composition of LS medium

Compound	Concentration (mM)
Sodium DL lactate	10
Potassium Phosphate	10
NH_4SO_4	15
$MgSO_4$. $7H_2O$	1
$CaCl_2.2H_2O$	0.48
EDTA, disodium salt	0.67
$FeSO_4.7H_2O$	0.1
$NaHCO_3$	0.2
$FeCl_3$	0.1
Na_2SeO_4	0.01
H_3BO_3	0.05
$ZnSO_4.7H_2O$	0.005
$Na_2MoO_4.2H_2O$	0.007
$CuSO_4.5H_2O$	0.001
$MnSO_4.H_2O$	0.001
$CoSO_4.7H_2O$	0.05
$NiCl_2.6H_2O$	0.08
NaCl	0.1

CHAPTER 3

SIMULTANEOUS DEGRADATION OF COMINGLED CONTAMINANTS TRICHLOROETHYLENE, TETRACHLOROETHYLENE, AND 1,4-DIOXANE BY A MICROBIALLY DRIVEN FENTON REACTION

Abstract

Improper disposal of 1,4-dioxane and the chlorinated organic solvents trichloroethylene (TCE) and tetrachloroethylene (PCE) has resulted in widespread contamination of soil and groundwater. In the present study, a new microbially-driven Fenton reaction system was designed and applied to generate hydroxyl ($HO^{\bullet}$) radicals for simultaneous degradation of source zone levels of single, binary, and ternary mixtures of TCE, PCE, and 1,4-dioxane. The new Fenton reaction system was driven by fed batch cultures of the Fe(III)-reducing facultative anaerobe *Shewanella oneidensis* amended with lactate, Fe(III), and contaminants and exposed to alternating anaerobic and aerobic conditions. To avoid contaminant loss due to volatility, the Fe(II)-generating, hydrogen peroxide-generating, and contaminant degradation phases of the microbially-driven Fenton reaction system were separated. The microbially-driven Fenton reaction system degraded TCE, PCE, and 1,4-dioxane either as single contaminants or as binary and ternary mixtures. In the presence of equimolar concentrations of TCE and PCE, the ratio of the experimentally derived rates of TCE and PCE degradation was nearly identical to the ratio of the corresponding $HO^{\bullet}$ radical reaction rate constants. The new microbially-driven Fenton reaction system may be applied as an *ex*

situ platform for simultaneous degradation of co-mingled TCE, PCE, and 1,4-dioxane and provides valuable information for future development of *in situ* remediation technologies.

3.1 Introduction

The chlorinated organic solvents trichloroethylene (TCE) and tetrachloroethylene (PCE) have been historically employed as solvents in a variety of industrial processes including vapor degreasing of metal surfaces, paint stripping, and dry cleaning (1, 2). TCE and PCE are carcinogenic and improper disposal practices at industrial sites have resulted in widespread contamination of soil and ground water (1-6). Due to their high density and low aqueous phase solubility, TCE and PCE are also highly persistent in contaminated environments (3, 4). The potential carcinogen 1,4-dioxane is generally employed as a stabilizer for TCE and PCE in industrial processes,(7-11) and thus TCE- and PCE-contaminated ground water is often comingled with 1,4-dioxane (9, 12-20).

Current TCE and PCE remediation technologies are based on photolysis, sonolysis, and reductive transformations by iron-bearing minerals or dechlorinating microorganisms (6, 21-26). Photolysis and sonolysis, however, are limited by UV light penetration and low energy transfer efficiency, respectively (27), while microbially-catalyzed reductive dehalogenation reactions are limited by microbial nutrient requirements, contaminant bioavailability, and incomplete dechlorination leading to the production of toxic intermediates (28). Current 1,4-dioxane remediation technologies such as carbon absorption, air stripping, and distillation are limited by problems associated with 1,4-dioxane solubility, boiling point, and vapor pressure, respectively (29). Other 1,4-dioxane remediation technologies such as photo-remediation by UV light (30) and ultrasound-aided degradation

are also limited by UV light penetration and low energy transfer efficiency, respectively (31, 32).

Chemical oxidation is also an attractive remediation technology for degradation of TCE, PCE, and 1,4-dioxane (2, 5, 12, 33). Currently deployed chemical oxidants include ozone, titanium oxide, persulfate, permanganate, peroxide, zero valent iron (ZVI), and hydroxyl ($HO^{\bullet}$) radicals (2, 5). $HO^{\bullet}$ radicals represent a powerful oxidant with oxidation potentials (+2.76 V) higher than ozone (+2.07 V), persulfate (+2.01 V), and permanganate (+1.68 V) (33). $HO^{\bullet}$ radicals may be produced by the conventional Fenton reaction (eq 1) in which ferrous iron (Fe(II)) catalyzes the decomposition of hydrogen peroxide (H_2O_2) to produce Fe(III), hydroxyl ion (OH^-) and $HO^{\bullet}$ radical:

$$Fe(II) + H_2O_2 \rightarrow Fe(III) + OH^- + HO^{\bullet} \quad (1)$$

Conventional Fenton reaction-generated $HO^{\bullet}$ radicals oxidatively degrade a number of hazardous compounds including chlorinated aliphatics and aromatics (34), pentachlorophenol (PCP) (35, 36), PCE (37), TCE (1, 5, 23, 26, 33), 1,1,2-trichloroethane (TCA) (38), 1,4-dioxane (29), and petroleum hydrocarbons (39). Conventional Fenton reaction-driven degradation of TCE, PCE, and 1,4-dioxane is limited, however, by the high concentrations of the Fenton reagents Fe(II) and H_2O_2 that must be continuously supplied to produce $HO^{\bullet}$ radicals and drive TCE, PCE, and 1,4-dioxane degradation (1, 24). At neutral pH, addition of Fe(III)-complexing ligands may improve conventional Fenton reaction efficiencies by preventing Fe(III) oxide precipitation (40). UV irradiation is often employed to induce Fe(III) re-reduction and photolytic radical production in photo-Fenton systems. The UV irradiation systems, however, are limited by UV light penetration, and H_2O_2 must still be continuously supplied to drive the conventional Fenton reaction (29).

Microbially-driven Fenton reactions that alternately produce the Fenton reagents H_2O_2 (via microbial O_2 respiration) and Fe(II) (via microbial Fe(III) reduction) alleviate the need for continual addition of H_2O_2 and Fe(II) to drive $HO^{\bullet}$ radical production (12, 17, 29, 41). The Fe(III)-reducing facultative anaerobe *Shewanella oneidensis* was recently employed to drive the Fenton reaction for oxidative degradation of PCP and 1,4-dioxane (29, 36). In the *S. oneidensis*-driven Fenton reaction, batch liquid cultures were amended with Fe(III) and 1,4-dioxane and subsequently exposed to alternating anaerobic and aerobic conditions. During the anaerobic period *S. oneidensis* produced Fe(II) via microbial Fe(III) reduction, while during the aerobic period, *S. oneidensis* produced H_2O_2 via microbial O_2 respiration. During the transition from anaerobic-to-aerobic conditions, Fe(II) and H_2O_2 interacted chemically via the Fenton reaction to produce $HO^{\bullet}$ radicals that completely degraded 1,4-dioxane at source zone concentrations (29).

Although TCE and PCE are often comingled with 1,4-dioxane in contaminated ground water, only a limited number of studies have examined simultaneous degradation of multiple contaminants, with emphasis on binary mixtures of TCE and 1,4-dioxane or TCE and PCE (26, 42-44). The main objectives of the present study were to (i) design a new fed batch, microbially-driven Fenton reaction system that minimizes contaminant loss due to volatility by separating the Fe(II)-generating, H_2O_2-generating, and contaminant degradation phases and ii) apply the new microbially-driven Fenton reaction system to simultaneously degrade single, binary, and ternary mixtures of TCE, PCE, and 1,4-dioxane.

3.2 Materials And Methods

Culture Medium and Chemical Reagents. *S. oneidensis* was routinely cultured aerobically on LB medium (10 g/L tryptone, 5 g/L yeast extract, and 10 g/L NaCl) (45).

TCE, PCE, and 1,4-dioxane degradation experiments were conducted in minimal salt solution (LS; pH 7.0, Supplementary Table 3.S2) amended with 50 mM lactate as carbon and energy source and 10 mM Fe(III)-citrate as anaerobic electron acceptor (36, 46). Fe(III)-citrate was prepared by previously described methods (47). TCE, PCE, 1,4-dioxane, acetonitrile, ferrozine, phosphoric acid, mannitol, sodium acetate, sodium nitrate, sodium lactate, and thiourea were obtained from Sigma-Aldrich. In the contaminant degradation experiments, contaminants were added to the fed batch reactor system at final concentrations that reflected source zone levels: TCE (100 μM), PCE (100 μM), and 1,4-dioxane (2 mM).

Design of Fed Batch Reactor System for Simultaneous Degradation of TCE, PCE, and 1,4-Dioxane by the Microbially-Driven Fenton Reaction. The toxicity of single, binary, and ternary mixtures of TCE, PCE, and 1,4-dioxane was tested in LS medium by comparing aerobic growth of *S. oneidensis* batch cultures in the presence and absence of the contaminant mixtures. To avoid inadvertent loss of contaminants due to volatility during injection of compressed nitrogen or compressed air (Henry's law constant for TCE: 0.11 mol kg^{-1} bar^{-1}, PCE: 0.05 mol kg^{-1} bar^{-1}, 1,4-dioxane: 220 mol kg^{-1} bar^{-1}) (29, 48-51), the batch reactor system previously employed for 1,4-dioxane degradation (29) was modified and the Fe(II)-generating, H_2O_2-generating, and contaminant degradation phases were separated (Supplementary Fig. 3.S14). In the Fe(II)-generating phase, contaminant-free *S. oneidensis* liquid cultures (10^9 cells mL^{-1} in LS medium amended with 10 mM Fe(III)) were incubated in 60-mL glass serum bottles under anaerobic conditions by injecting (hydrated) compressed nitrogen until the entire 10 mM pool of Fe(III) was reduced to approximately 10 mM Fe(II) (approximately 24 h of anaerobic incubation; Fe(II)-generating phase). The compressed nitrogen line was then replaced by a (hydrated) compressed air line and the 10 mM Fe(II)-

containing *S. oneidensis* liquid culture was incubated under aerobic conditions until the 10 mM pool of Fe(II) was oxidized to approximately 4 mM level (approximately 24 h of aerobic incubation; H_2O_2-generating phase). The 4 mM residual Fe(II) was carried into the contaminant degradation phase to interact with the pool of microbially-produced H_2O_2 and generate HO• radicals (similar to HO• radical production by the previously reported 1,4-dioxane-degrading batch reactor system) (29).

The contaminant degradation phase was initiated by adding single, binary, and ternary mixtures of TCE, PCE, and 1,4-dioxane with a sterile syringe. The contaminant degradation phase was carried out for approximately 5 days (without gas injection) and the contaminant concentrations were monitored via high pressure liquid chromatography (HPLC). Following completion of the first 5-day contaminant degradation phase (i.e., after contaminants were degraded to below detection limits), a second cycle of Fe(II)-generating and H_2O_2-generating phases was carried out during the 7-8 and 8-9 day time periods, respectively, followed by re-spiking of contaminant mixtures to initial concentrations and carrying out a second 5-day contaminant degradation phase during the 9-14 day time period. An identical third cycle of Fe(II)-generating, H_2O_2-generating, and contaminant degradation phases was carried during the 14-19 day time period. Reactor temperature (25°C) and pH (7.0) were held constant throughout all reactor phases.

Inhibition of the Microbially-Driven Fenton Reaction in Control Incubations. A series of four control incubations were carried out to confirm that the single, binary, and ternary mixtures of TCE, PCE, and 1,4-dioxane were degraded by HO• radicals generated by the *S. oneidensis*-driven Fenton reaction. The four control incubations were carried out in the fed batch reactor system described above with the following changes: In the first set of

control incubations, the H_2O_2-generating and contaminant degradation phases were carried out with 15 mM NO_3^- replacing 10 mM Fe(III) as electron acceptor. In the second set of control incubations, the $HO^{\bullet}$ radical-scavenging compounds mannitol (120 mM) and thiourea (20 mM) were added to the fed batch reactor system prior to initiating the H_2O_2-generating phase. The toxicities of mannitol and thiourea were tested in LS medium by comparing aerobic growth of *S. oneidensis* batch cultures in the presence and absence of mannitol or thiourea and single, binary, and ternary mixtures of TCE, PCE, and 1,4-dioxane. In the third set of control incubations, Fe(III) or *S. oneidensis* cells (abiotic control) were omitted from the H_2O_2-generating and contaminant degradation phases. In the fourth set of control incubations, contaminant concentrations were monitored in abiotic sealed serum bottles maintained under strict anaerobic conditions without injection of compressed nitrogen for a 20-day anaerobic incubation period.

Analytical Methods. Samples were withdrawn and centrifuged at 6000 x g for 10 min. HCl-extracted Fe(II) concentrations were determined with a previously described Ferrozine-based colorimetric technique (52). 1,4-dioxane concentrations were determined via HPLC using a ZORBAX SB-C18 column with 20% aqueous acetonitrile as the mobile phase and a constant flow rate of 1.0 ml/min (15). Chromatograms were generated at 190 nm for 1,4-dioxane with a retention time of 2.4 min. TCE and PCE samples were extracted with ethyl acetate (1:1 volume ratio) and the organic phase was directly injected into the HPLC system using ZORBAX SB-C18 column with 60% aqueous acetonitrile as the mobile phase and a constant flow rate of 1.0 ml/min. Chromatograms were generated at 214 nm for TCE and PCE with retention times of 4.5 and 7.5 min, respectively. Lactate and acetate were analyzed via HPLC using a SUPELCOGEL C-610H column with 0.1% H_3PO_4 as the mobile

phase and a constant flow rate of 0.3 ml/min. Chromatograms were generated at 210 nm for lactate and acetate with retention times of 29.41 and 35.06 respectively. Calibration curves were generated from standards to determine the concentrations of each compound.

3.3 Results

TCE Degradation in the Presence and Absence of PCE and 1,4-Dioxane. In the following results section, the single, binary, and ternary mixtures of TCE, PCE, and 1,4-dioxane were designated as follows: TCE alone = T, PCE alone = P, 1,4-dioxane alone = D, TCE + PCE = TP, TCE + 1,4-dioxane = TD, PCE + 1,4-dioxane = PD, and TCE + PCE + 1,4-dioxane = TPD. To test for TPD toxicity, *S. oneidensis* was grown aerobically in LS growth medium supplemented with a ternary mixture of T (100 μM), P (100 μM), and D (2 mM). Aerobic growth rates in the presence and absence of TPD were nearly identical, which indicated that the TPD concentrations did not inhibit *S. oneidensis* metabolic activity (Supplementary Fig 3.S1).

To initiate $HO^{\bullet}$ radical production by the *S. oneidensis*-driven Fenton reaction, Fe(III)-containing *S. oneidensis* cultures were incubated under anaerobic conditions for 24 h, the pool of 10 mM Fe(III) was microbially reduced at a rate of 416.8 μM h^{-1}, and Fe(II) concentrations increased to 10 mM (Fe(II)-generating phase; grey-shaded area in Fig. 3.1a and Supplementary Figs. 3.S5a, 3.S5d, 3.S5e, and 3.S5g). At the 24-h time point, compressed air was injected for the next 24 h into all incubations, Fe(II) was air-oxidized at rates of 192.0 - 321.0 μM h^{-1}, and Fe(II) concentrations decreased from 10.0 mM to 2.3 - 5.4 mM (first H_2O_2-generating phase; yellow-shaded area in Fig. 3.1a and Supplementary Figs. 3.S5a, S5d, S5e, and S5g). At the 2-d time point, the T, TP, TD, and TPD mixtures were added to initiate the first contaminant degradation phase (2-7 d time period). During the first contaminant degradation

phase, Fe(III) was microbially reduced at rates of 39.2 - 41.7 μM h^{-1} and Fe(II) concentrations increased to 7.0-10.4 mM (unshaded area in Fig. 3.1a and Supplementary Figs. 3.S5a, 3.S5d, 3.S5e, and 3.S5g). During the first contaminant degradation phase with T as sole contaminant, T was degraded at an initial rate of 1.1 μM h^{-1} (Figs. 3.1b, 3.4a, and Supplementary Table 3.S3). By comparison, T was degraded in TP, TD, and TPD mixtures at initial rates 71%, 82%, and 74%, respectively, of the T degradation rate with T as sole contaminant (i.e., % of T1 degradation rate; Figs. 3.1b, 3.4a, and Supplementary Table 3.S3). T was degraded to below detection limits by the end of the first degradation phase (7-d time point) with T as sole contaminant and in the TD, TP, and TPD mixtures (Fig. 3.1b).

At the 7-d time point, a second cycle of Fe(II)- and H_2O_2-generating phases was carried out. Fe(II) was air-oxidized at rates of 195.8 - 237.5 μM h^{-1} and Fe(II) concentrations decreased from 7.0 - 10.4 mM to 2.3 - 4.7 mM (second H_2O_2-generating phase; yellow-shaded area in Fig. 3.1a and Supplementary Figs. 3.S5a, 3.S5d, 3.S5e, and 3.S5g). At the 9-d time point, the T, TP, TD, and TPD mixtures were again added to initiate a second contaminant degradation phase (9-14 d time period). During the second contaminant degradation phase, Fe(III) was microbially reduced at rates of 36.7 - 50.0 μM h^{-1} and Fe(II) concentrations increased to 6.7 - 10.7 mM. During the second contaminant degradation phase with T as sole contaminant, T was degraded at an initial rate of 1.5 μM h^{-1} (Figs. 3.1b, 3.4a, and Supplementary Table 3.S3). By comparison, T was degraded in the TP, TD, and TPD mixtures at initial rates of 51%, 67%, and 55%, respectively, of the T degradation rate with T as sole contaminant (i.e., % of T2 degradation rate; Figs. 3.1b, 3.4a, and Supplementary Table 3.S3). T was degraded to below detection limits by the end of the

second degradation phase (14-d time point) with T as sole contaminant and in the TD, TP, and TPD mixtures (Fig. 3.1b).

At the 14-d time point, a third cycle of Fe(II)- and H_2O_2-generating phases was carried out. Fe(II) was air-oxidized at rates of 133.3 - 208.3 μM h^{-1} and Fe(II) concentrations decreased to 3.5 - 5.7 mM (third H_2O_2-generating phase; yellow-shaded area in Fig. 3.1a and Supplementary Figs. 3.S5a, 3.S5d, 3.S5e, and 3.S5g). At the 16-d time point, the T, TP, TD, and TPD mixtures were added to initiate a third contaminant degradation phase (16-19 d time period). During the third contaminant degradation phase, Fe(III) was microbially reduced at rates of 33.3 - 48.6 μM h^{-1} and Fe(II) concentrations increased to 5.9 - 9.2 mM. During the third contaminant degradation phase with T as sole contaminant, T was degraded in the TP, TD, and TPD mixtures at initial rates of 1.4 μM h^{-1} (Figs. 3.1b, 3.4a, and Supplementary Table 3.S3). By comparison, T was degraded at initial rates of 46%, 65%, and 74%, respectively, of the T degradation rate with T as sole contaminant (i.e., % of T3 degradation rate; Figs. 3.1b, 3.4a, and Supplementary Table 3.S3). T was degraded to below detection limits by the end of the third degradation phase (19-d time point) with T as sole contaminant. Due to early termination of the third contaminant degradation phase, T was degraded to 37, 56, and 28 μM levels in the TD, TP, and TPD mixtures, respectively; Fig. 3.1b).

T was degraded at nearly identical rates as sole contaminant in the three successive contaminant degradation phases (2-7, 9-14, and 16-19 d time periods; Fig. 3.2a and Supplementary Table 3.S3). T concentrations remained constant at 100 μM in parallel control incubations lacking Fe(III) or *S. oneidensis* cells (abiotic control; Supplementary Fig. 3.S2), but including three identical cycles of successive anaerobic (Fe(II)-generating), aerobic (H_2O_2-generating), and contaminant (T, TP, TD, and TPD) degradation phases.

Identical patterns of microbial (*S. oneidensis*-catalyzed) Fe(III) reduction and chemical (O_2-catalyzed) Fe(II) oxidation were observed in parallel control incubations with contaminants omitted (Fig. 3.1a), which indicated that rates of microbially-catalyzed Fe(III) reduction and O_2-catalyzed Fe(II) oxidation were not affected by the presence of the T, TP, TD, or TPD mixtures.

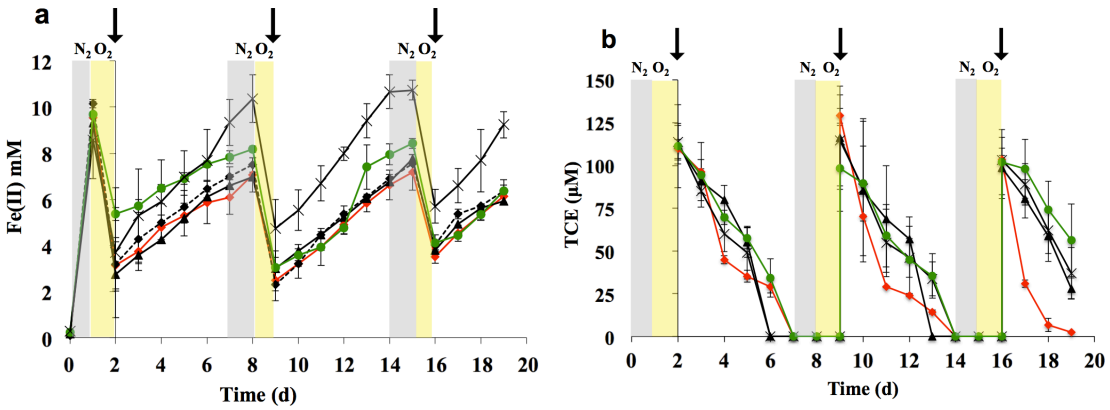

Figure 3.1. Concentration profiles during microbial Fenton degradation of TCE, PCE and 1,4-dioxane in fed batch liquid cultures of *S. oneidensis* amended with 10 mM Fe(III)-citrate, single, binary, and ternary mixtures of TPD (100 µM TCE, 100 µM PCE and 2 mM 1,4-dioxane) and subjected to : Anaerobic (0-1, 7-8, 14-15 day time periods), aerobic (1-2, 8-9, 15-16 day time periods) and TPD degradation (2-7, 9-14, 16-19 day time periods) phases: (a) Fe(II) (for TCE reactions); (b) TCE; (c) Fe(II) (for PCE reactions); (d) PCE; (e) Fe(II) (for 1,4-dioxane reactions); (f) 1,4-dioxane; solid red (◆), single contaminant only; solid black (x), TCE + 1,4-dioxane; solid green (●), TCE + PCE; solid blue (■), PCE + 1,4-dioxane; solid black (▲), TCE + PCE + 1,4-dioxane; dashed black (◆), no contaminant control. Grey shaded areas correspond to Fe(II)-generating phase, yellow shaded areas correspond to H_2O_2-generating phase, and unshaded areas correspond to contaminant degradation phase. Arrows indicate time of addition (day 2) and respiking (day 9 & 16) of contaminants. Error bars represent range of errors in duplicate batch reactors.

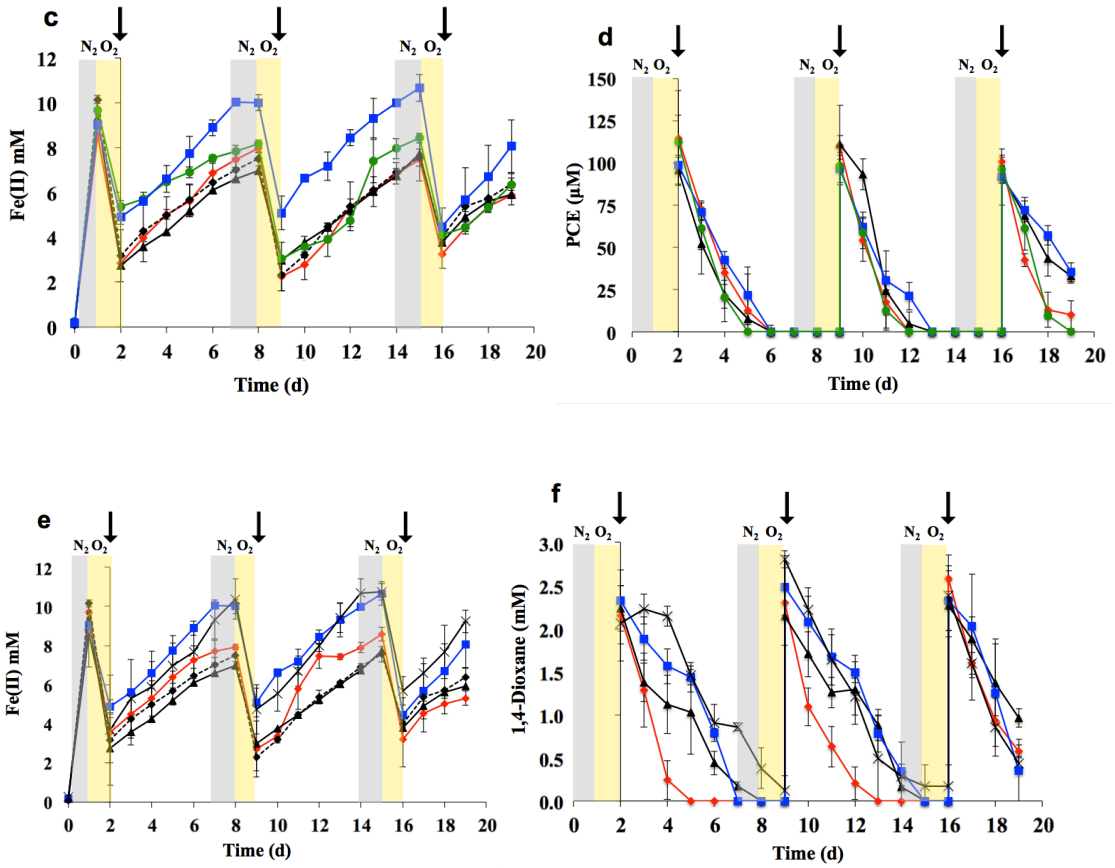

Figure 3.1 continued

PCE Degradation in the Presence and Absence of TCE and 1,4-Dioxane.

Nearly identical patterns of microbial (*S. oneidensis*-catalyzed) Fe(III) reduction and chemical (O_2-catalyzed) Fe(II) oxidation were observed in analogous P, TP, PD, and TPD contaminant degradation experiments (Fig. 3.1c and Supplementary Figs. 3.S5b, 3.S5d, 3.S5f, and 3.S5g). To initiate HO$^{\bullet}$ radical production by the *S. oneidensis*-driven Fenton reaction, Fe(III)-containing *S. oneidensis* cultures were incubated under anaerobic conditions for 24 h, the pool of 10.0 mM Fe(III) was microbially reduced at rates of 379.2 - 420.8 µM h^{-1} and Fe(II) concentrations increased to 9.1 - 10.1 mM (Fe(II)-generating phase; grey-shaded

area in Fig. 3.1c and Supplementary Figs. 3.S5b, 3.S5d, 3.S5f, and 3.S5g). At the 24-h time point, compressed air was injected for the next 24 h into all incubations and Fe(II) was air-oxidized at rates of 195.8 - 262.5 μM h^{-1} and Fe(II) concentrations decreased from 9.1 - 10.1 mM to 2.8 - 5.4 mM (first H_2O_2-generating phase; yellow-shaded area in Fig. 3.1c and Supplementary Figs. 3.S5b, 3.S5d, 3.S5f, and 3.S5g). At the 2-d time point, the P, PT, PD, and TPD mixtures were added to initiate the first contaminant degradation phase (2-7 d time period). P was degraded at an initial rate of 1.4 μM h^{-1} during the contaminant degradation phase with P as sole contaminant (Figs. 3.1d, 3.4b, and Supplementary Table 3.S4). By comparison, P was degraded in the PT, PD, and TPD mixtures at initial rates of 110%, 75%, and 62%, respectively, of the P degradation rate with P as sole contaminant (i.e., % of P1 degradation rate; Figs. 3.1d, 3.4b, and Supplementary Table 3.S4). P was degraded to below detection limits by the end of the first degradation phase (7-d time point) with P as sole contaminant and in the PT, PD, and TPD mixtures (Fig. 3.1d).

At the 7-d time point, a second cycle of Fe(II)- and H_2O_2-generating phases was carried out. At the 9-d time point, the P, PT, PD, and TPD mixtures were added to initiate a second contaminant degradation phase (9-14 day time period). During the second contaminant degradation phase with P as sole contaminant, P was degraded at an initial rate of 1.6 μM h^{-1} (Figs. 3.1d, 3.4b, and Supplementary Table 3.S4). By comparison, P was degraded at initial rates of 88%, 69%, and 96%, respectively, of the P degradation rate with P as sole contaminant (i.e., % of P2 degradation rate; Figs. 3.1d, 3.4b, and Supplementary Table 3.S4). P was degraded to below detection limits by the end of the second degradation phase (14-d time point) with P as sole contaminant and in the PT, PD, and TPD mixtures (Fig. 3.1d).

At the 14-day time point, a third cycle of Fe(II)- and H_2O_2-generating phases was carried out. At the 16-d time point, the P, PT, PD, and TPD mixtures were added to initiate a third contaminant degradation phase (16-19 d period). During the third contaminant degradation phase with P as sole contaminant, P was degraded at an initial rate of 1.2 μM h^{-1} (Figs. 3.1d, 3.4b, and Supplementary Table 3.S4). By comparison, P was degraded at initial rates of 98%, 69%, and 72%, respectively, of the P degradation rate with P as sole contaminant (i.e., % of P3 degradation rate; Figs. 3.1d, 3.4b, and Supplementary Table 3.S4). P was degraded to below detection limits by the end of the third degradation phase (19-d time point) with PT as contaminant mixture. Due to early termination of the third contaminant degradation phase (19-d time point), P was degraded to 10, 36, and 33 μM levels in the P, PD, and TPD mixtures, respectively; Fig. 3.1d).

P was degraded as sole contaminant at nearly identical rates in the three successive contaminant degradation phases (2-7, 9-14, and 16-19 day time periods; Fig. 3.2b and Supplementary Table 3.S4). P concentrations remained constant at 100 μM in parallel control incubations lacking Fe(III) or *S. oneidensis* cells (abiotic control; Supplementary Fig. 3.S3), but including three identical cycles of successive anaerobic (Fe(II)-generating), aerobic (H_2O_2-generating), and contaminant (P, PT, PD, and TPD) degradation phases. Identical patterns of microbial (*S. oneidensis*-catalyzed) Fe(III) reduction and chemical (O_2-catalyzed) Fe(II) oxidation were observed in parallel control incubations with contaminants omitted (Fig. 3.1c), which indicated that rates of microbially-catalyzed Fe(III) reduction and O_2-catalyzed Fe(II) oxidation were not affected by the presence of the P, PT, PD, or TPD mixtures.

1,4-Dioxane degradation in the presence and absence of TCE and PCE.

Nearly identical patterns of microbial (*S. oneidensis*-catalyzed) Fe(III) reduction and chemical (O_2-catalyzed Fe(II) oxidation were observed in analogous D, DT, DP, and TPD contaminant degradation experiments (Fig. 3.1e and Supplementary Figs. 3.S5c, 3.S5e, 3.S5f, and 3.S5g). To initiate $HO^{\bullet}$ radical production by the *S. oneidensis*-driven Fenton reaction, Fe(III)-containing *S. oneidensis* cultures were incubated under anaerobic conditions for 24 h, the pool of 10 mM Fe(III) was microbially reduced at rates of 358.3 - 441.7 μM h^{-1} and Fe(II) concentrations increased to 8.6 - 10.6 mM (Fe(II-generating phase; grey-shaded area in Fig. 3.1e and Supplementary Figs. 3.S5c, 3.S5e, 3.S5f, and 3.S5g). At the 24-h time point, compressed air was injected for the next 24 h into all incubations and Fe(II) was air-oxidized at rates of 237.5 - 241.7 μM h^{-1} and Fe(II) concentrations decreased from 8.6 - 10.6 mM to 2.8 - 4.9 mM (first H_2O_2-generating phase; yellow-shaded area in Fig. 3.1e and Supplementary Figs. 3.S5c, 3.S5e, 3.S5f, and 3.S5g). At the 2-d time point, the D, DT, DP and TPD mixtures were added to initiate the first contaminant degradation phase (2-7 d time period). D was degraded at an initial rate of 30.8 μM h^{-1} (Figs. 3.1f, 3.4c, and Supplementary Table 3.S5). By comparison, D was degraded in the DT, DP, and TPD mixtures at initial rates of 35%, 39%, and 54%, respectively, of the D degradation rate with D as sole contaminant (i.e., % of D1 degradation rate; Figs. 3.1f, 3.4c, and Supplementary Table 3.S5). D was degraded to below detection limits by the end of the first degradation phase (7-d time point) in the D and DP mixtures. However, D was only degraded to 0.17 mM and 0.85 mM levels in the DT and TPD mixtures, respectively (Fig. 3.1f).

At the 7-d time point, a second cycle of Fe(II)- and H_2O_2-generating phases was carried out. At the 9-d time point, the D, DT, DP, and TPD mixtures were added to initiate a

second contaminant degradation phase (9-14 d time period). During the second contaminant degradation phase with D as sole contaminant, D was degraded at an initial rate of 36.2 μM h^{-1} (Figs. 3.1f, 3.4c, and Supplementary Table 3.S5). By comparison, D was degraded at initial rates of 61%, 38%, and 36%, respectively, of the D degradation rate with D as sole contaminant (i.e., % of D2 degradation rate; Figs. 3.1f, 3.4c, and Supplementary Table 3.S5). D was degraded to below detection limits by the end of the second degradation phase (14-d time point) with D as sole contaminant. However, D was degraded only to 0.34, 0.30, and 0.16 mM levels in the DT, DP, and TDP mixtures, respectively (Fig. 3.1f).

At the 14-d time point, a third cycle of Fe(II)-generating, H_2O_2-generating, and contaminant degradation phases was carried out. At the 16-d time point, the D, DT, DP, and TPD mixtures were added to initiate a third contaminant degradation phase (16-19 d time period). During the third contaminant degradation phase with D as sole contaminant, D was degraded at an initial rate of 27.9 μM h^{-1} (Figs. 3.1f, 3.4c, and Supplementary Table 3.S5). By comparison, D was degraded at initial rates of 97%, 101%, and 70%, respectively, of the D degradation rate with D as sole contaminant (i.e., % of D3 degradation rate; Figs. 3.1f, 3.4c, and Supplementary Table 3.S5). Due to early termination of the third degradation phase (19-d time point), D was degraded to 0.6, 0.43, 0.48, and 0.96 mM levels in the D, DT, DP, and TPD mixtures, respectively (Fig. 3.1f).

D was degraded at nearly identical rates as sole contaminant in the three successive contaminant degradation phases (2-7, 9-14, and 16-19 d time periods; Fig. 3.2c and Supplementary Table 3.S5). D concentrations remained constant at 100 μM in parallel control incubations lacking Fe(III) or *S. oneidensis* cells (abiotic control; Supplementary Fig. 3.S4), but including three identical cycles of successive anaerobic (Fe(II)-generating),

aerobic (H_2O_2-generating), and contaminant (D, DT, DP, and TPD) degradation phases. Identical patterns of microbial (*S. oneidensis*-catalyzed) Fe(III) reduction and chemical (O_2-catalyzed) Fe(II) oxidation were observed in parallel control incubations with contaminants omitted (Fig. 3.1e), which indicated that rates of microbially-catalyzed Fe(III) reduction and O_2-catalyzed Fe(II) oxidation were not affected by the presence of the D, DT, DP, or TPD mixtures.

Inhibition of the Microbially-Driven Fenton Reaction in Control Incubations. To confirm that the single, binary, and ternary mixtures of TPD were degraded by $HO^{\bullet}$ radicals generated by the *S. oneidensis*-driven Fenton reaction, a series of control incubations were carried out in the presence of the $HO^{\bullet}$ radical-scavenging compounds mannitol or thiourea. The single, binary, or ternary mixtures of TPD were not degraded in the contaminant degradation phase in the presence of mannitol or thiourea (Supplementary Figs. 3.S2-4). To test for toxicity of mannitol and thiourea in the presence of TPD, *S. oneidensis* cultures were grown aerobically in LS growth medium supplemented with mannitol or thiourea and the ternary TPD mixture. Aerobic growth rates in the presence or absence of mannitol or thiourea were nearly identical, which indicates that a combination of mannitol or thiourea and TPD did not inhibit *S. oneidensis* metabolic activity (Supplementary Fig. 3.S1). The ability of the $HO^{\bullet}$ radical-scavenging compounds mannitol and thiourea to inhibit TPD degradation indicates that $HO^{\bullet}$ radicals derived from the microbially-driven Fenton reaction are involved in the degradation of single, binary, and ternary TPD mixtures.

The requirement for microbial Fe(III) reduction was tested by replacing Fe(III) with NO_3^- and carrying out an otherwise identical set of TPD degradation experiments with NO_3^--containing fed batch reactors. TPD was not degraded with NO_3^- as electron acceptor

(Supplementary Figs. 3.S2-4), or in the absence of *S. oneidensis* cells (Supplementary Figs. 3.S2-4). These results indicated that microbial Fe(III) reduction was required to drive the TPD degradation process. Furthermore, in all TPD degradation and control incubations, lactate was consumed at similar rates (87.5 - 100.0 μM h^{-1}), while lactate concentrations remained constant during the 17-day abiotic control incubations (Supplementary Figs. 3.S6-8 and 3.S12). Due to the microbially-catalyzed aerobic oxidation of lactate during the aerobic (H_2O_2-generating) phase, acetate was produced at rates of 50.0 - 66.7 μM h^{-1} (Supplementary Figs. 3.S9-11 and 3.S13).

3.4 Discussion

The high oxidation potential of HO• radicals derived from conventional Fenton reactions drives oxidative degradation of a variety of hazardous contaminants, including TCE, PCE, and 1,4-dioxane (23, 26, 29, 53). Conventional Fenton reactions are hampered, however, by the need for continuous supply of the Fenton reagents Fe(II) and H_2O_2 to sustain contaminant degradation (1, 17, 23, 25, 33, 41). Microbially-driven Fenton reactions, on the other hand, alternately regenerate Fe(II) (via microbial Fe(III) reduction under anaerobic conditions) and H_2O_2 (via microbial O_2 respiration under aerobic conditions), thus alleviating the need to continually supply the Fenton reagents to drive HO• radical production and contaminant degradation (29, 36). The Fe(III)-reducing facultative anaerobe *S. oneidensis* was recently employed to drive the Fenton reaction for HO• radical production and 1,4-dioxane degradation in a batch reactor system that included *S. oneidensis* cells, Fe(III), and alternate injections of compressed nitrogen (to facilitate microbial Fe(III) reduction) and compressed air (to facilitate microbial H_2O_2 production) (29). The Henry's Law constant for TCE (0.11 mol kg^{-1} bar^{-1}) and PCE (0.05 mol kg^{-1}), however, are over three orders of

magnitude lower than the Henry's law constant for 1,4-dioxane (220 mol kg^{-1} bar^{-1}) (29, 48-51). Thus, in initial batch reactor designs, the compressed gas injections quickly volatilized TCE and PCE to below detection levels (data not shown), while the concentrations of TCE and PCE remained constant in the absence of compressed gas injection (Supplementary Figs. 3.S2 and 3.S3). The batch reactor system was therefore modified to avoid TCE and PCE loss due to volatility. In the modified fed batch reactor system, the Fe(II)-generating (microbial Fe(III) reduction stimulated by injection of compressed nitrogen), H_2O_2-generating (microbial H_2O_2 production stimulated by injection of compressed air), and contaminant degradation phases (without injection of compressed gases) were separated and the fed batch reactor system was cycled three times through each of the three separate phases (Supplementary Fig. 3.S14).

Although TCE and PCE are often comingled with 1,4-dioxane in contaminated soil and ground water, only a limited number of studies have examined simultaneous degradation of multiple contaminants, with emphasis on binary mixtures of TCE and 1,4-dioxane or TCE and PCE (26, 42-44). The present study is the first report of simultaneous degradation of source zone levels of ternary mixtures of TCE, PCE, and 1,4-dioxane. In control incubations held under strictly anaerobic Fe(III)-reducing conditions, the TPD mixtures were not degraded, which demonstrated that *S. oneidensis* was unable to enzymatically degrade TCE, PCE, or 1,4-dioxane in the contaminant degradation phase. In addition, under a normal cycle of alternating anaerobic and aerobic conditions, the three contaminant mixtures were not degraded in the absence of Fe(III), in the absence of *S. oneidensis* cells, or in the presence of the $HO^{\bullet}$ radical-scavenging compounds mannitol or

thiourea. These findings indicate that the TPD mixtures were simultaneously degraded by $HO^{\bullet}$ radicals produced by the microbially-driven Fenton reaction (14).

The rates of TCE degradation (in single, binary, and ternary mixtures of contaminants) ranged from 84-137% between the first, second, and third TCE degradation phases (i.e., by comparing rates of TCE degradation in phases T1, T2, T3 or TP1, TP2, TP3 or TD1, TD2, TD3 or TPD1, TPD2, TPD3; Fig. 3.2a; and Supplementary Table 3.S3). In a similar fashion, the rates of PCE and 1,4-dioxane degradation (in single, binary, and ternary mixtures of contaminants) also ranged from 77-168%. However, during the second (DT mixture) and third (DT and DP mixtures) 1,4-dioxane degradation cycles, 1,4-dioxane degradation rates were 104%, 150%, and 133% higher, respectively. The higher 1,4-dioxane degradation rates were most likely due to the incomplete degradation of 1,4-dioxane during the preceding contaminant degradation phase, the resulting carry over of 1,4-dioxane to the next cycle, and the inadvertent higher ratios of D/T or D/P (second phase: D/T - 33% higher; third phase: D/T - 28% higher, D/P - 6% higher) compared to the respective D/T or D/P ratios of the first degradation phase (Figs. 3.1b, 3.1d, 3.1f, 3.2b, 3.2c, and Supplementary Tables 3.S4 and 3.S5). Furthermore, lactate was only depleted to approximately 15 - 20 mM levels after three successive cycles (i.e., 30 - 40% of the initial 50 mM lactate feed remained after the third cycle), and correspondingly, acetate was produced (from lactate oxidation) at similar rates in each of the three cycles (Supplementary Figs. 3.S6-13). These results indicate that the microbially-driven Fenton reaction was not limited by lactate depletion upon completion of the third cycle, and that the microbially-driven Fenton system can handle at least three repeated feeds of ternary mixtures of TCE, PCE, and 1,4-dioxane without compromising the efficiency of contaminant degradation.

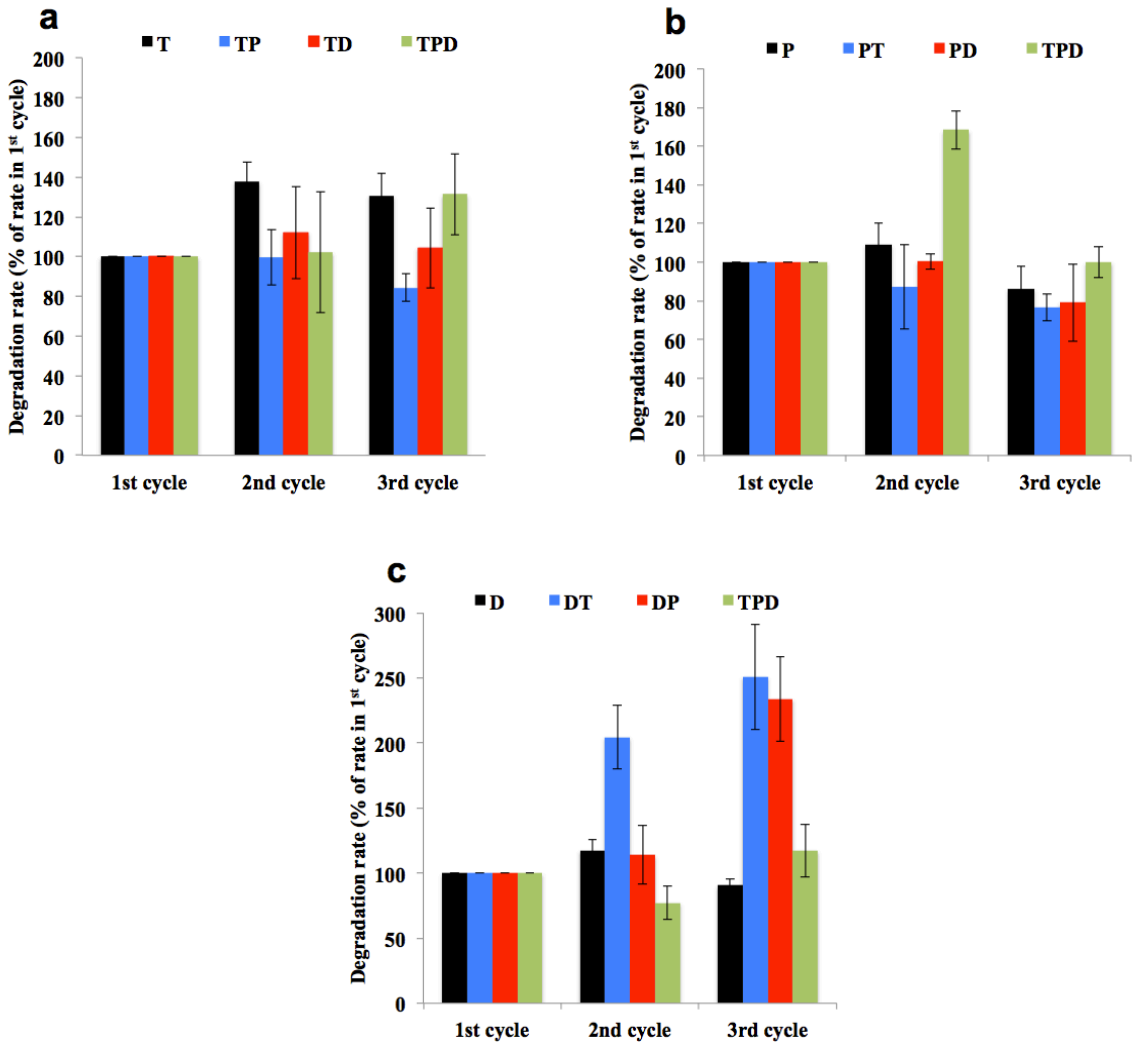

Figure 3.2. Comparison of rate of degradation of TCE, PCE and 1,4-dioxane between three contaminant degradation phase cycles. Rate of degradation during 2nd and 3rd cycles is calculated as % of rate of degradation during 1st cycle. (a) TCE, T1 = 1.1 µM h^{-1}, TP1 = 0.8 µM h^{-1}, TD1 = 0.9 µM h^{-1}, TPD1 = 0.8 µM h^{-1}; (b) PCE, P1 = 1.4 µM h^{-1}, PT1 = 1.6 µM h^{-1}, PD1 = 1.1 µM h^{-1}, TPD1 = 0.9 µM h^{-1}; (c) 1,4-Dioxane, D1 = 30.8 µM h^{-1}, DT1 = 10.9 µM h^{-1}, DP1 = 12.1 µM h^{-1}, TPD1 = 16.8 µM h^{-1}. Error bars represent range of errors in duplicate batch reactors.

Rates of contaminant degradation by HO$^{\bullet}$ radicals are a function of the contaminant-specific HO$^{\bullet}$ radical reaction rate constants ($k_{HO^{\bullet}}$) (TCE range: 0.85-1.59 X 10^{9}

M^{-1} s^{-1}, TCE average: 1.22 X 10^9 M^{-1} s^{-1}; PCE range: 1.62-2.33 X 10^9 M^{-1} s^{-1}, PCE average: 1.98 X 10^9 M^{-1} s^{-1}; 1,4-dioxane range: 1.1-2.4 X 10^9 M^{-1} s^{-1}, 1,4-dioxane average: 1.75 X 10^9 M^{-1} s^{-1}),(25, 54) the initial concentrations of contaminant, and the number of double bonds in the contaminant molecular structure.(26) Other factors impacting the Fenton degradation of TCE, PCE, and 1,4-dioxane include the myriad of unidentified $HO^{\bullet}$ radical-interacting intermediates produced during contaminant degradation (12, 38).

Despite these complicating factors, the predicted- and experimentally-derived contaminant degradation rates in the present study may be compared for the case of binary mixtures of TCE and PCE because both contaminants were added at identical concentrations and both contain an identical number of double bonds. Subsequently, the ratio of the experimentally-derived rates of PCE and TCE degradation in binary mixtures of PCE and TCE (designated P^{exp}/T^{exp}) is predicted to be equal to the ratio of PCE- and TCE-specific $k_{HO^{\bullet}}$ (designated $k_{HO^{\bullet}}(P)/k_{HO^{\bullet}}(T)$). P^{exp}/T^{exp} ratios (k_{obs}) ranged from 1.8 - 2.1 in the three degradation phases of the PCE and TCE binary mixture experiments (Fig. 3.3), which were comparable to $k_{HO^{\bullet}}(P)/k_{HO^{\bullet}}(T)$ ratios (1.5 - 1.9) previously reported for TCE and PCE degradation by purely chemical Fenton reactions (indicated by the dotted lines in Fig. 3.3) (25). Similar rate comparisons with binary mixtures of 1,4-dioxane and TCE or 1,4-dioxane and PCE were not possible because the source zone levels of 1,4-dioxane (2 mM) used in the present study were 20-fold greater than the source zone levels of TCE and PCE (100 μM) (55, 56). Correspondingly, the 20-fold higher 1,4-dioxane concentrations led to 1,4-dioxane degradation rates that were 9-to-34-fold higher than the TCE and PCE degradation rates in all contaminant mixtures (Tables 3.S6 and 3.S7). Regardless of the concentration-dependent differences in contaminant degradation rates, the microbially-driven Fenton reaction

degraded source zone levels of ternary mixtures of TCE, PCE, and 1,4-dioxane to below detection limits when contaminant degradation phases were extended to < 5-d time periods (first and second cycles; Figs. 3.1b, 3.1d, and 3.1f).

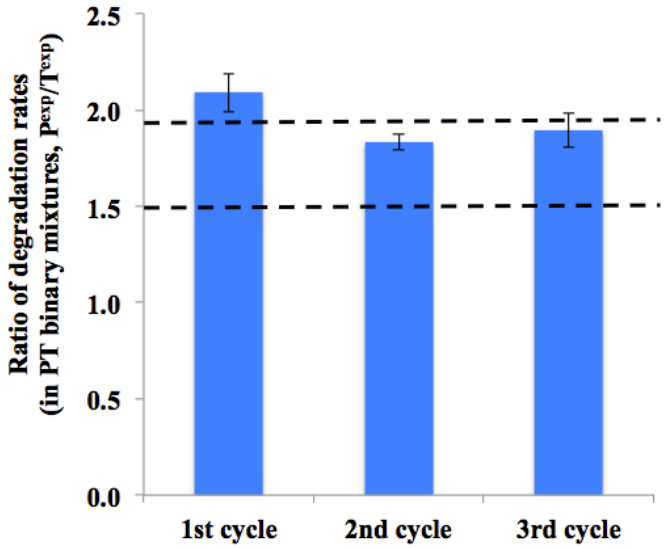

Figure 3.3. Ratio of the experimentally-derived rates of PCE and TCE degradation in binary mixtures of PCE and TCE (P^{exp}/T^{exp}) across three contaminant degradation phase cycles. Black dotted lines indicate reported range of ratio of $k_{HO^{\bullet}}(P)/k_{HO^{\bullet}}(T)$. Equal molar of TCE and PCE (100 µM) were added at the start of each cycle. Error bars represent range of errors in duplicate batch reactors.

Rates of degradation of TCE as sole contaminant (in first, second, and third TCE degradation phases) were 18-54% lower in binary and ternary mixtures of PCE and 1,4-dioxane (i.e., by comparing rates of TCE degradation in phases T1, TP1, TD1, TPD1 and T2, TP2, TD2, TPD2 and T3, TP3, TD3, TPD3; Fig. 3.4a and Supplementary Table 3.S3). Decreases in TCE degradation rates in the binary and ternary contaminant mixtures are most likely due to competition for $HO^{\bullet}$ radicals by PCE (with a $k_{HO^{\bullet}}$ 62% higher than TCE) or 1,4-dioxane (with a $k_{HO^{\bullet}}$ approximately 43% higher than TCE and amended at 20-fold higher concentrations than TCE) (25). Rates of degradation of PCE as sole contaminant (in first, second, and third PCE degradation phases) were not affected by TCE in binary mixtures of

TCE and PCE, but were 4-38 % lower in binary and ternary mixtures containing 1,4-dioxane (i.e., by comparing rates of PCE degradation in phases P1, TP1, PD1, TPD1, and P2, TP2, PD2, TPD2 and P3, TP3, PD3, TPD3; Fig 3.4b and Supplementary Table 3.S4). The inability of TCE to affect PCE degradation rates is most likely due to the 62% higher $k_{HO^{\bullet}}$ for PCE than TCE. Decreases in PCE degradation rates in the binary and ternary contaminant mixtures containing 1,4-dioxane are most likely due to competition for $HO^{\bullet}$ radicals by 1,4-dioxane, which was amended at 20-fold higher concentrations than PCE. Rates of degradation of 1,4-dioxane as sole contaminant (in first, second, and third TCE degradation phases) were 39-65% lower in binary and ternary mixtures of TCE and PCE (i.e., by comparing rates of 1,4-dioxane degradation in phases D1, TD1, PD1, TPD1 and D2, TD2, PD2, TPD2 and T3, TD3, PD3, TPD3; Fig 3.4c and Supplementary Table 3.S5). Decreases in 1,4-dioxane degradation rates in the binary and ternary contaminant mixtures are most likely due to competition for $HO^{\bullet}$ radicals by PCE (with a $k_{HO^{\bullet}}$ 13% higher than 1,4-dioxane; Fig. 3.4c). During the third 1,4-dioxane degradation cycle, however, 1,4-dioxane degradation rates rebounded to 70 – 101% of the degradation rates with 1,4-dioxane as sole contaminant, most likely due to decreases in PCE concentrations below threshold levels for PCE to compete effectively with 1,4-dioxane for $HO^{\bullet}$ radicals during the third contaminant degradation cycle (Fig. 3.4c).

Similar to previous results reported with purely chemical Fenton reactions, results of the present study indicate that contaminant degradation rates in the microbially-driven Fenton reaction depend on the $k_{HO^{\bullet}}$ of competing contaminants, the initial contaminant concentration, and the number of double bonds in the contaminant molecular structure. In binary and ternary mixtures, contaminants with greater $k_{HO^{\bullet}}$ suppress the degradation of other

contaminants with lower $k_{HO^{\bullet}}$ and the contaminant degradation phase must be extended for longer time periods to degrade contaminants below detection limits (26). The microbially-driven Fenton reaction may thus be applied as an effective *ex situ* platform for simultaneous degradation of at least three (and potentially more) co-mingled contaminants at source zone levels.

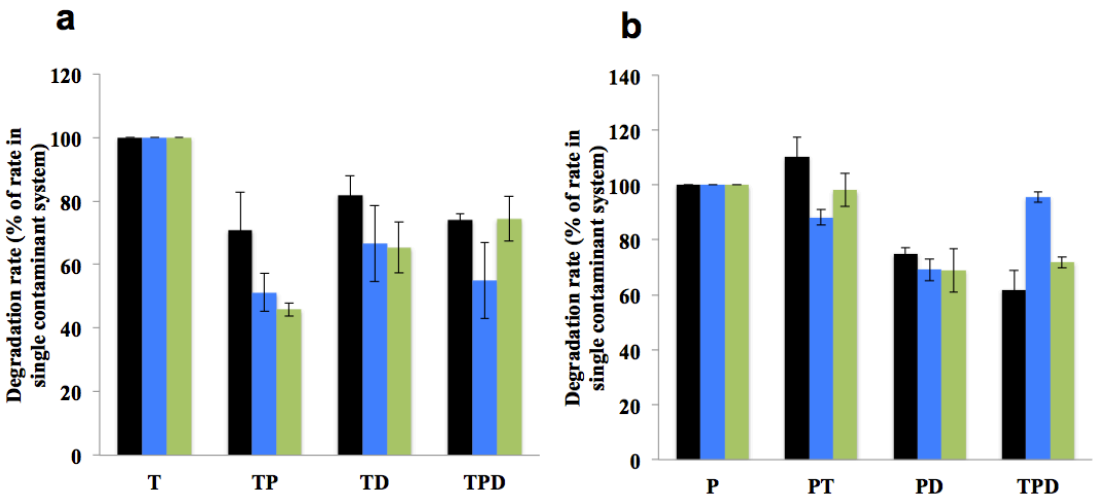

Figure 3.4. Comparison of rate of degradation of TCE, PCE and 1,4-dioxane between single, binary and ternary mixtures. Rate of degradation for binary and ternary mixtures is calculated as % of rate of single contaminant degradation. (a) TCE, T1 = 1.1 µM h^{-1}, T2 = 1.5 µM h^{-1}, T3 = 1.4 µM h^{-1}. (b) PCE, P1 = 1.4 µM h^{-1}, P2 = 1.6 µM h^{-1}, P3 = 1.2 µM h^{-1}. (c) 1,4-Dioxane, D1 = 30.8 µM h^{-1}, D2 = 36.2 µM h^{-1}, D3 = 27.9 µM h^{-1}. black, 1st cycle; blue, 2nd cycle; green, 3rd cycle. Error bars represent range of errors in duplicate batch reactors.

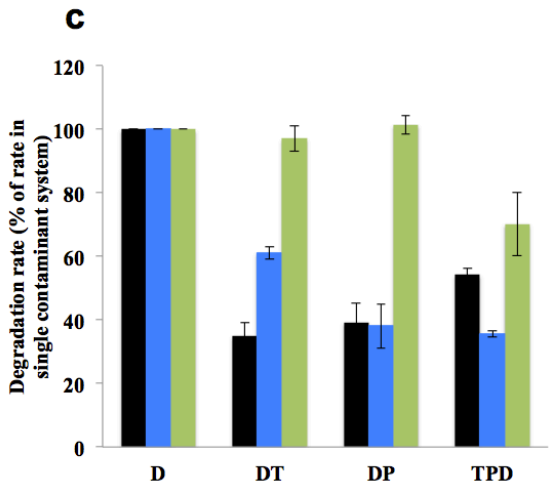

Figure 3.4 continued

Microbial respiratory processes catalyze both H_2O_2 production and Fe(III) re-reduction in the microbially-driven Fenton reaction designed in the present study. Microbial Fe(III) reduction is a dominant anaerobic respiratory process in many contaminated subsurface environments (57), which suggests that the microbially-driven Fenton reaction may be stimulated *in situ* by exposing Fe(III)-reducing facultative anaerobes in Fe(III)-containing contaminated environments to alternating anaerobic and aerobic conditions. Other in situ remediation strategies may include stimulation of the microbially-driven Fenton reaction by placing reactive iron barriers in the flow path of contaminated subsurface aquifers and exposing Fe(III)-reducing bacteria attached to the iron barriers to alternating anaerobic and aerobic conditions (58). In principal, targets for *ex situ* and *in situ* degradation by the microbially-driven Fenton reaction developed in the present study include multiple combinations of environmental contaminants susceptible to attack by Fenton reaction-generated $HO^{\bullet}$ radicals, including co-mingled plumes of 1,4-dioxane, PCP (35, 36), PCE (37), TCE (23), TCA (59) and PFAS (60).

3.5 References

1. **Teel AL, Warberg CR, Atkinson DA, Watts RJ.** 2001. Comparison of mineral and soluble iron Fenton's catalysts for the treatment of trichloroethylene. Water Res **35:**977-984.

2. **Wu X, Gu X, Lu S, Qiu Z, Sui Q, Zang X, Miao Z, Xu M, Danish M.** 2015. Accelerated degradation of tetrachloroethylene by Fe(II) activated persulfate process with hydroxylamine for enhancing Fe(II) regeneration Journal of Chemical Technology and Biotechnology doi:10.1002/jctb.4718.

3. **Chawla RC, Doura KF, McKay D.** 2001. Effect of Alcohol Cosolvents on the Aqueous Solubility of Trichloroethylene. Proceedings of the 2001 Conference on Environmental Research**:**52-66.

4. **Tsai TT, Kao CM, Hong A.** 2009. Treatment of tetrachloroethylene-contaminated groundwater by surfactant-enhanced persulfate/BOF slag oxidation--a laboratory feasibility study. J Hazard Mater **171:**571-576.

5. **Choi K, Lee W.** 2012. Enhanced degradation of trichloroethylene in nano-scale zero-valent iron Fenton system with Cu(II). J Hazard Mater **211-212:**146-153.

6. **Kang JW, Khan Z, Doty SL.** 2012. Biodegradation of trichloroethylene by an endophyte of hybrid poplar. Appl Environ Microbiol **78:**3504-3507.

7. **Lanigan RS.** 2000. Addendum to the final report on the safety assessment of polysorbates. Int J Toxicol **19:**43-89.

8. **Zenker MJ, Borden RC, Barlaz MA.** 2003. Occurence and treatment of 1,4-dioxane in aqueous environments. Environ Eng Sci **20:**423-432.

9. **Sei K, Kakinoki T, Inoue D, Soda S, Fujita M, Ike M.** 2010. Evaluation of the biodegradation potential of 1,4-dioxane in river, soil and activated sludge samples. Biodegradation **21:**585-591.

10. **Abe A.** 1999. Distribution of 1,4-dioxane in relation to possible sources in the water environment. Sci Total Environ **227:**41-47.

11. **Jackson RE, Dwarakanath V.** 1999. Chlorinated degreasing solvents: Physical-chemical properties affecting aquifer contamination and remediation. Ground Water Monitoring and Remediation **19:**102-110.

12. **Stefan MI, Bolton JR.** 1998. Mechanism of the degradation of 1,4-dioxane in dilute aqueous solution using the UV hydrogen peroxide process. Environmental Science & Technology **32:**1588-1595.

13. **Sun BZ, Ko K, Ramsay JA.** 2011. Biodegradation of 1,4-dioxane by a Flavobacterium. Biodegradation **22:**651-659.

14. **Mahendra S, Alvarez-Cohen L.** 2006. Kinetics of 1,4-dioxane biodegradation by monooxygenase-expressing bacteria. Environmental Science & Technology **40:**5435-5442.

15. **Kim YM, Jeon JR, Murugesan K, Kim EJ, Chang YS.** 2009. Biodegradation of 1,4-dioxane and transformation of related cyclic compounds by a newly isolated Mycobacterium sp. PH-06. Biodegradation **20:**511-519.

16. **Vescovi T, Coleman HM, Amal R.** 2010. The effect of pH on UV-based advanced oxidation technologies--1,4-dioxane degradation. Journal of hazardous materials **182:**75-79.

17. **Coleman HM, Vimonses V, Leslie G, Amal R.** 2007. Degradation of 1,4-dioxane in water using TiO2 based photocatalytic and H2O2/UV processes. Journal of Hazardous Materials **146:**496-501.

18. **Anderson RH, Anderson JK, Bower PA.** 2012. Co-occurrence of 1,4-dioxane with trichloroethylene in chlorinated solvent groundwater plumes at US Air Force installations: Fact or fiction. Integrated Environmental Assessment and Management **8:**731-737.

19. **Stickney JA, Sager SL, Clarkson JR, Smith LA, Locey BJ, Bock MJ, Hartung R, Olp SF.** 2003. An updated evaluation of the carcinogenic potential of 1,4-dioxane. Reg Tox Pharm **38:**183-195.

20. **USEPA.** 2014. Technical Fact Sheet - 1,4-Dioxane. Response OoSWaE,

21. **Cheng D, He J.** 2009. Isolation and characterization of "Dehalococcoides" sp. strain MB, which dechlorinates tetrachloroethene to trans-1,2-dichloroethene. Appl Environ Microbiol **75:**5910-5918.

22. **Liang SH, Wang SY, Chang YM, Kao CM.** 2015. Treatment of TCE-contaminated Groundwater using In Situ Potassium Permanganate Oxidation: Effects and Kinetics Evaluation. Research Journal of Biotechnology **10:**20-24.

23. **Tsai TT, Kao CM, Surampalli RY, Weng CH, Liang SH.** 2010. Treatment of TCE-Contaminated Groundwater Using Fenton-Like Oxidation Activated with Basic Oxygen Furnace Slag. Journal of Environmental Engineering-Asce **136:**288-294.

24. **Jho EH, Singhal N, Turner S.** 2010. Fenton degradation of tetrachloroethene and hexachloroethane in Fe(II) catalyzed systems. J Hazard Mater **184:**234-240.

25. **Yeh CK, Hsu CY, Chiu CH, Huang KL.** 2008. Reaction efficiencies and rate constants for the goethite-catalyzed Fenton-like reaction of NAPL-form aromatic hydrocarbons and chloroethylenes. J Hazard Mater **151:**562-569.

26. **Yeh KJ, Chen TC, Young WL.** 2013. Competitive Removal of Two Contaminants in a Goethite-Catalyzed Fenton Process at Neutral pH. Environmental Engineering Science **30:**47-52.

27. **Rashid MM, Sato C.** 2012. Degradation of Trichloroethylene and Tetrachloroethylene in Simulated Groundwater in a Flow-Through Photosono Reactor. Journal of Environmental Engineering-Asce **138:**1179-1185.

28. **Pavlostathis SP, Prytula MT, Yeh DH.** 2003. Potential and limitations of microbial reductive dechlorination for bioremediation applications. Water, Air and Soil Pollution: Focus **3:**117-129.

29. **Sekar R, DiChristina TJ.** 2014. Microbially driven fenton reaction for degradation of the widespread environmental contaminant 1,4-dioxane. Environ Sci Technol **48:**12858-12867.

30. **Klecka GM, Gonsior SJ.** 1986. Removal of 1,4-Dioxane from wastewater. Journal of Hazardous Materials **13:**161-168.

31. **Hill RR, Jeffs GE, Roberts DR.** 1997. Photocatalytic degradation of 1,4-dioxane in aqueous solution. J Photochem Photobiol A **108:**55-58.

32. **Beckett MA, Hua I.** 2003. Enhanced sonochemical decomposition of 1,4-dioxane by ferrous iron. Water Research **37:**2372-2376.

33. **Che H, Bae S, Lee W.** 2011. Degradation of trichloroethylene by Fenton reaction in pyrite suspension. J Hazard Mater **185:**1355-1361.

34. **Tyre BW, Watts RJ, Miller GC.** 1991. Treatment of 4 Biorefractory Contaminants in Soils Using Catalyzed Hydrogen-Peroxide. Journal of Environmental Quality **20:**832-838.

35. **Barbeni M, Minero C, Pelizzetti E, Borgarello E, Serpone N.** 1987. Chemical Degradation of Chlorophenols with Fenton Reagent (Fe-2++H2O2). Chemosphere **16:**2225-2237.

36. **McKinzi AM, Dichristina TJ.** 1999. Microbially driven Fenton reaction for transformation of pentachlorophenol. Environmental Science & Technology **33:**1886-1891.

37. **Jho EH, Singhal N, Turner S.** 2010. Fenton degradation of tetrachloroethene and hexachloroethane in Fe(II) catalyzed systems. Journal of hazardous materials **184:**234-240.

38. **Pignatello J, Liu D, Huston P.** 1999. Evidence for an Additional Oxidant in the Photoassisted Fenton Reaction. Environmental Science & Technology **33:**1832-1839.

39. **Ojinnaka C, Osuji L, Achugasim O.** 2012. Remediation of hydrocarbons in crude oil-contaminated soils using Fenton's reagent. Environ Monit Assess **184:**6527-6540.

40. **Lewis S, Lynch A, Bachas L, Hampson S, Ormsbee L, Bhattacharyya D.** 2009. Chelate-Modified Fenton Reaction for the Degradation of Trichloroethylene in Aqueous and Two-Phase Systems. Environ Eng Sci **26:**849-859.

41. **Kim CG, Seo HJ, Lee BR.** 2006. Decomposition of 1,4-dioxane by advanced oxidation and biochemical process. J Environ Sci Health A Tox Hazard Subst Environ Eng **41:**599-611.

42. **Hand S, Wang B, Chu KH.** 2015. Biodegradation of 1,4-dioxane: effects of enzyme inducers and trichloroethylene. Sci Total Environ **520:**154-159.

43. **Shim H, Ryoo D, Barbieri P, Wood TK.** 2001. Aerobic degradation of mixtures of tetrachloroethylene, trichloroethylene, dichloroethylenes, and vinyl chloride by toluene-o-xylene monooxygenase of Pseudomonas stutzeri OX1. Appl Microbiol Biotechnol **56:**265-269.

44. **Marco-Urrea E, Gabarrell X, Caminal G, Vicent T, Reddy CA.** 2008. Aerobic degradation by white-rot fungi of trichloroethylene (TCE) and mixtures of TCE and perchloroethylene (PCE). Journal of Chemical Technology and Biotechnology **83:**1190-1196.

45. **Sambrook J, Fritsh EF, Maniatis T.** 1989. Molecular Cloning: A Laboratory Manual. Cold Spring Harbor Laboratory Press; Cold Spring Harbor, NY.

46. **Obuekwe CO, Westlake DWS, Cook FD.** 1981. Effect of Nitrate on Reduction of Ferric Iron by a Bacterium Isolated from Crude-Oil. Canadian Journal of Microbiology **27:**692-697.

47. **Dichristina TJ, Delong EF.** 1994. Isolation of Anaerobic Respiratory Mutants of Shewanella-Putrefaciens and Genetic-Analysis of Mutants Deficient in Anaerobic Growth on Fe3+. Journal of Bacteriology **176:**1468-1474.

48. **Howard PH.** 1990. Handbook of Environmental Fate and Exposure Data for Organic Chemicals. Lewis Publishers, Inc, Chelsea, MI.

49. **ATSDR.** 1993. Agency for Toxic Substances and Disease Registry. Toxicological Profile for Tetrachloroethylene. Update. CDC, Atlanta, GA.

50. **Boulding RJ.** 1996. EPA Environmental Engineering Sourcebook. Ann Arbor Press, Chelsea, Mi.

51. **P.J. Linstrom PJ, Mallard WG.** NIST Chemistry WebBook, NIST Standard Reference Database Number 69, vol 20899. National Institute of Standards and Technology, Gaithersburg MD.

52. **Dichristina TJ.** 1992. Effects of Nitrate and Nitrite on Dissimilatory Iron Reduction by Shewanella-Putrefaciens-200. Journal of Bacteriology **174:**1891-1896.

53. **Andreozzi R, Campanella L, Fraysse B, Garric J, Gonnella A, Giudice RL, Marotta R, Pinto G, Pollio A.** 2004. Effects of advanced oxidation processes (AOPs) on the toxicity of a mixture of pharmaceuticals. Water Sci Technol **50:**23-28.

54. **Adams CD, Scanlan PA, Secrist ND.** 1994. Oxidation and biodegradability enhancement of 1,4-dioxane using hydrogen peroxide and ozone. Environ Sci Technol **28:**1812-1818.

55. **Steffan RJ.** 2007. Biodegradation of 1,4-Dioxane.

56. **Farm R.** 2001. Public Health Assessment. The New Jersey Department of Health and Senior Services, Dover Township, Ocean County, New Jersey.

57. **Lovley DR.** 1997. Microbial Fe(III) reduction in subsurface environments. FEMS Microbiology Reviews **20:**305-313.

58. **Cundya AB, Hopkinsona L, Whitby RLD.** 2008. Use of iron-based technologies in contaminated land and groundwater remediation: A review. Science of the Total Environment **400:**42-51.

59. **Joseph J. Pignatello, Di Liu, Huston. P.** 1999. Evidence for an Additional Oxidant in the Photoassisted Fenton Reaction. Environmental Science & Technology **33:**1832-1839.

60. **Cao MH, Wang BB, Yu HS, Wang LL, Yuan SH, Chen J.** 2010. Photochemical decomposition of perfluorooctanoic acid in aqueous periodate with VUV and UV light irradiation. J Hazard Mater **179:**1143-1146.

3.6 Supporting information

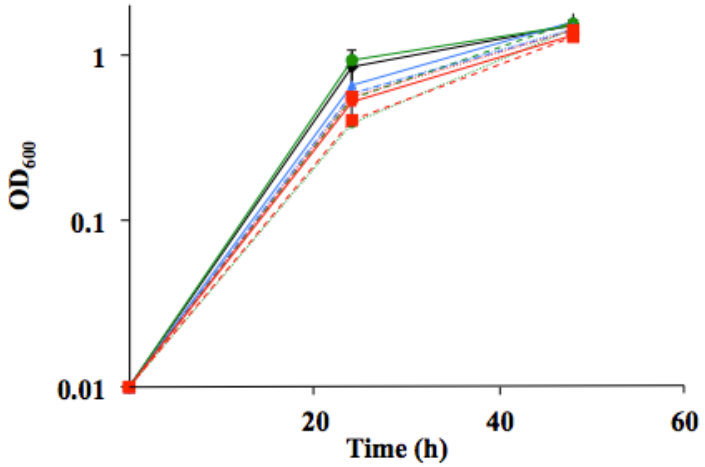

Figure 3.S1. Growth curve of *S. oneidensis* in the presence of 0 µM contaminants; solid black (◆), 100 µM TCE; solid blue (▲), 100 µM TCE + 120 mM mannitol; dashed blue (▲), 100 µM TCE + 20 mM thiourea; dotted blue (▲), 100 µM PCE; solid green (•), 100 µM PCE + 120 mM mannitol; dashed green (•), 100 µM PCE + 20 mM thiourea; dotted green (•), 100 µM TCE + 100 µM PCE + 2 mM 1,4-dioxane; solid red (■), 100 µM TCE + 100 µM PCE + 2 mM 1,4-dioxane + 120 mM mannitol; dashed red (■), 100 µM TCE + 100 µM PCE + 2 mM 1,4-dioxane + 20 mM thiourea dotted red (■). Cell cultures were grown in LS media under aerobic conditions in the presence of 50 mM lactate as electron donor.

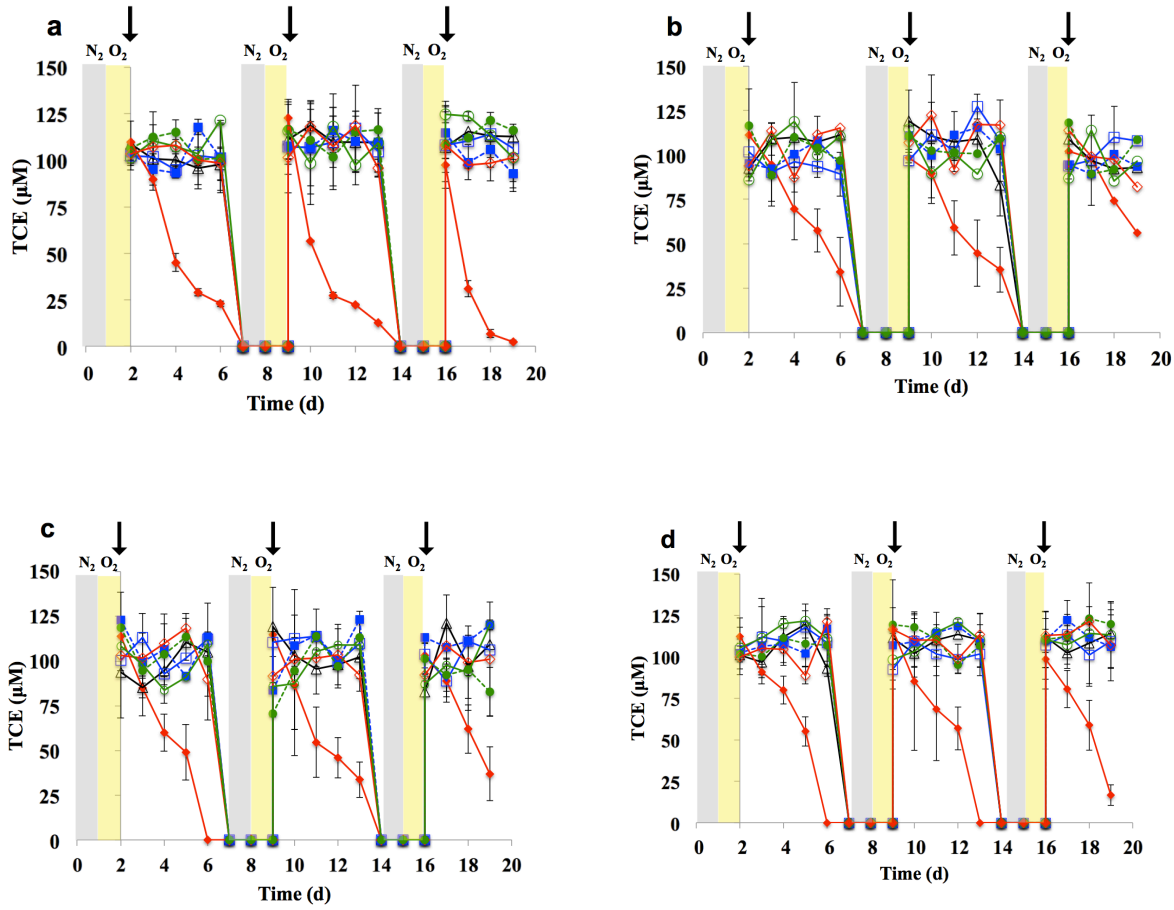

Figure 3.S2. TCE concentrations during microbial Fenton degradation of single, binary, and ternary mixtures of TPD in fed-batch liquid cultures of *S. oneidensis* amended with 10 mM Fe(III)-citrate, 100 µM TCE, 100 µM PCE and 2 mM 1,4-dioxane and subjected to : Anaerobic (0-1, 7-8, 14-15 day time periods), aerobic (1-2, 8-9, 15-16 day time periods) and TPD degradation (2-7, 9-14, 16-19 day time periods) phases: (a) TCE only; (b) TCE + PCE; (c) TCE + 1,4-dioxane; (d) TCE + PCE + 1,4-dioxane; solid filled red (◆), contaminant only; solid unfilled black (▲), contaminant + thiourea; solid unfilled blue (■), contaminant + mannitol; dashed filled blue (■), nitrate; dashed filled green (•), anaerobic only; solid unfilled green (•), Fe(III) omitted; solid unfilled red (◆), cells omitted. Grey shaded areas correspond to Fe(II)-generating phase, yellow shaded areas correspond to H_2O_2-generating phase, and unshaded areas correspond to contaminant degradation phase. Arrows indicate time of addition (day 2) and respiking (day 9 & 16) of contaminants. Error bars represent range of errors in duplicate batch reactors.

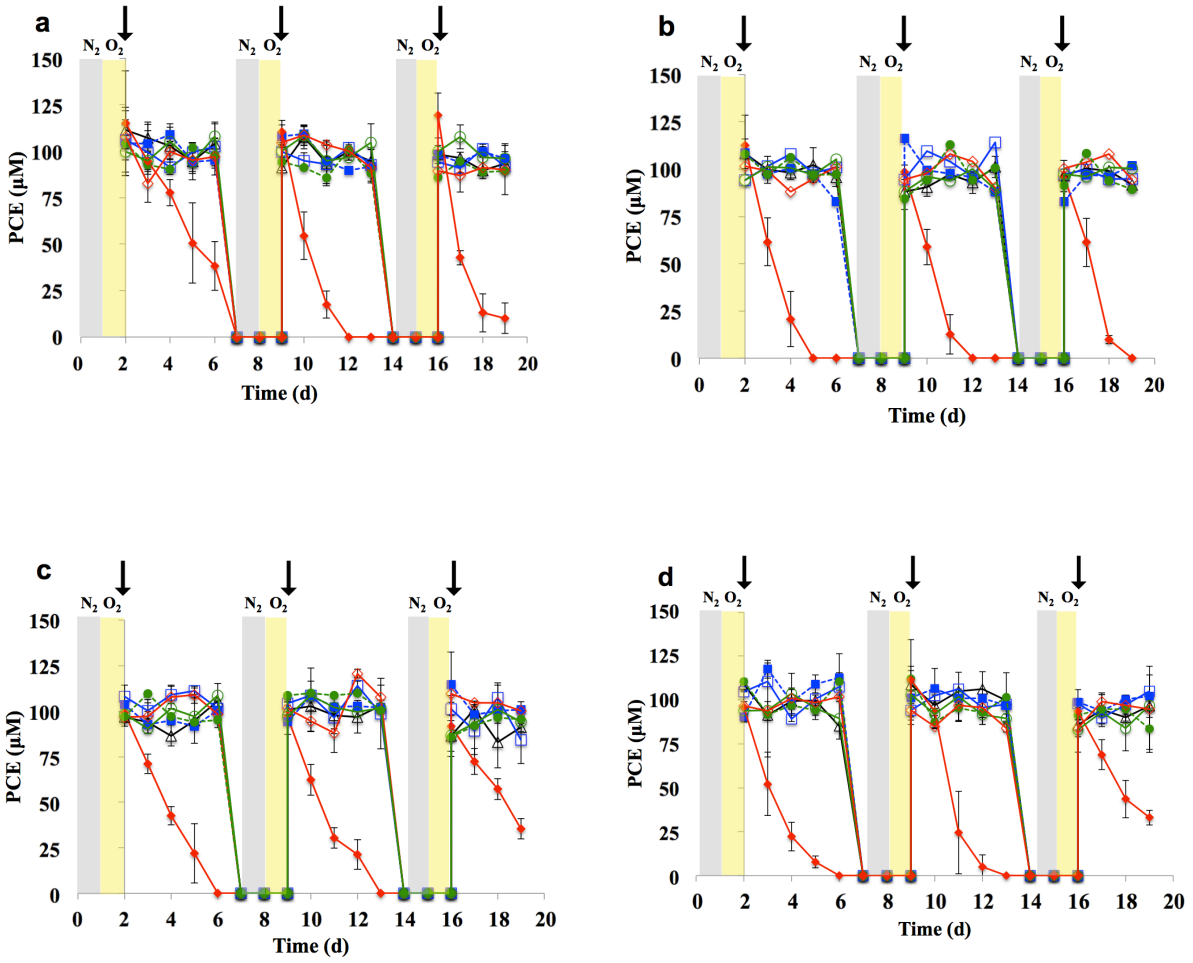

Figure 3.S3. PCE concentrations during microbial Fenton degradation of single, binary, and ternary mixtures of TPD in fed-batch liquid cultures of *S. oneidensis* amended with 10 mM Fe(III)-citrate, 100 µM TCE, 100 µM PCE and 2 mM 1,4-dioxane and subjected to : Anaerobic (0-1, 7-8, 14-15 day time periods), aerobic (1-2, 8-9, 15-16 day time periods) and TPD degradation (2-7, 9-14, 16-19 day time periods) phases: (a) PCE only; (b) PCE + TCE; (c) PCE + 1,4-dioxane; (d) PCE + TCE + 1,4-dioxane; solid filled red (◆), contaminant only; solid unfilled black (▲), contaminant + thiourea; solid unfilled blue (■), contaminant + mannitol; dashed filled blue (■), nitrate; dashed filled green (•), anaerobic only; solid unfilled green (•), Fe(III) omitted; solid unfilled red (◆), cells omitted. Grey shaded areas correspond to Fe(II)-generating phase, yellow shaded areas correspond to H_2O_2-generating phase, and unshaded areas correspond to contaminant degradation phase. Arrows indicate time of addition (day 2) and respiking (day 9 & 16) of contaminants. Error bars represent range of errors in duplicate batch reactors.

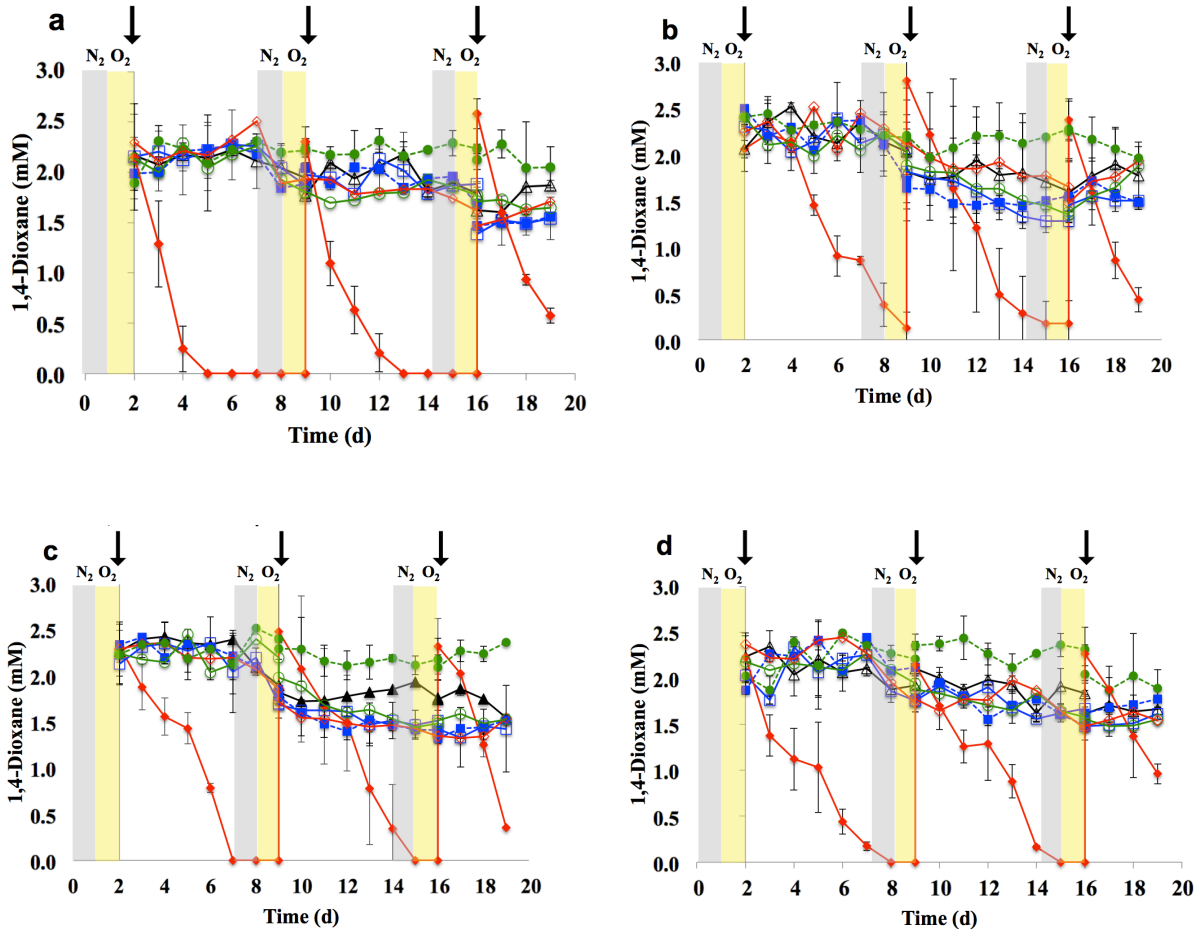

Figure 3.S4. 1,4-Dioxane concentrations during microbial Fenton degradation of single, binary, and ternary mixtures of TPD in fed-batch liquid cultures of *S. oneidensis* amended with 10 mM Fe(III)-citrate, 100 µM TCE, 100 µM PCE and 2 mM 1,4-dioxane and subjected to : Anaerobic (0-1, 7-8, 14-15 day time periods), aerobic (1-2, 8-9, 15-16 day time periods) and TPD degradation (2-7, 9-14, 16-19 day time periods) phases: (a) 1,4-dioxane only; (b) 1,4-dioxane + TCE; (c) 1,4-dioxane + PCE; (d) 1,4-dioxane + TCE + PCE; solid filled red (◆), contaminant only; solid unfilled black (▲), contaminant + thiourea; solid unfilled blue (■), contaminant + mannitol; dashed filled blue (■), nitrate; dashed filled green (•), anaerobic only; solid unfilled green (•), Fe(III) omitted; solid unfilled red (◆), cells omitted. Grey shaded areas correspond to Fe(II)-generating phase, yellow shaded areas correspond to H_2O_2-generating phase, and unshaded areas correspond to contaminant degradation phase. Arrows indicate time of addition (day 2) and respiking (day 9 & 16) of contaminants. Error bars represent range of errors in duplicate batch reactors.

Figure 3.S5

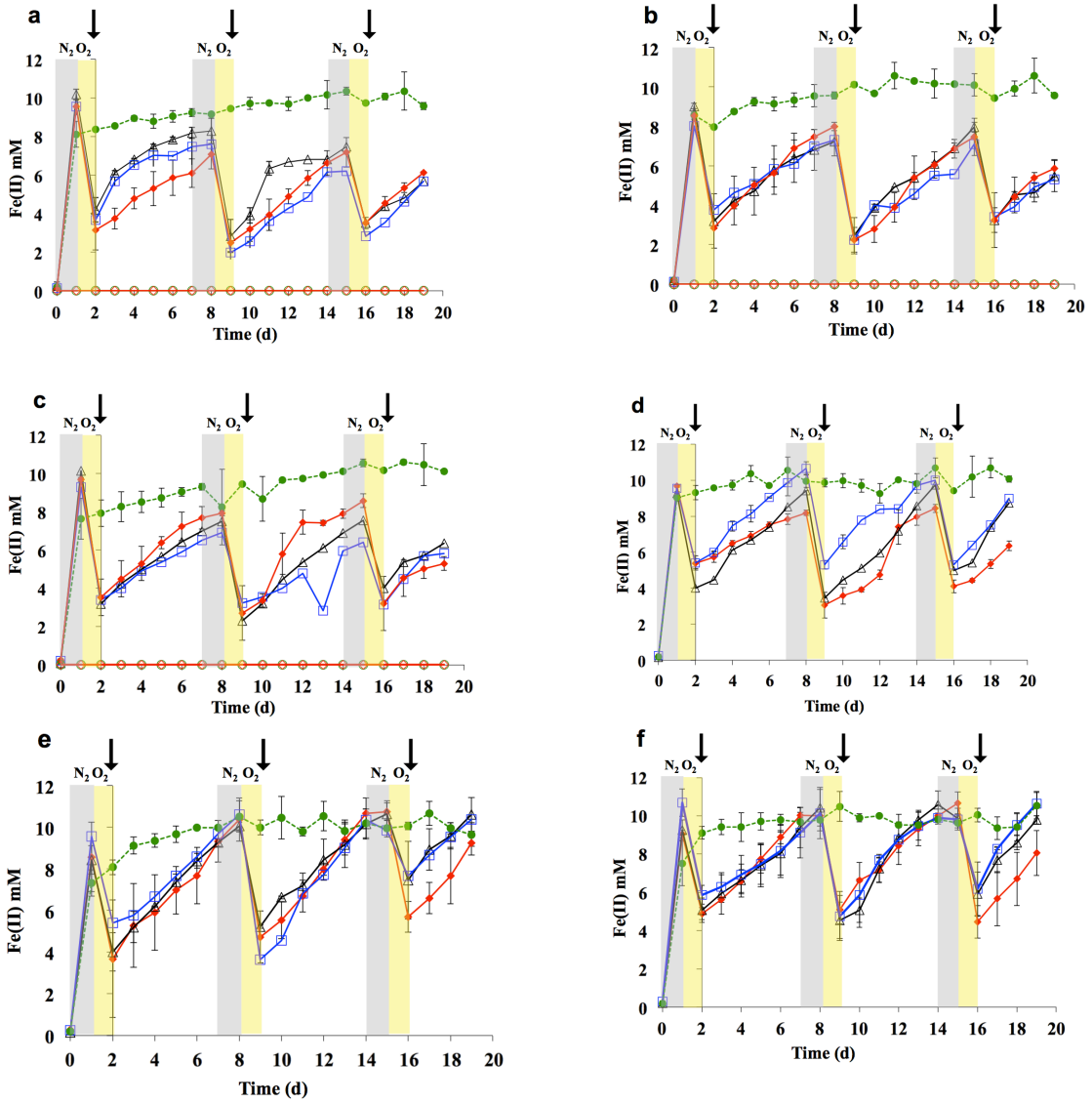

Figure 3.S5. Fe(II) concentrations during microbial Fenton degradation of single, binary, and ternary mixtures of TPD in fed-batch liquid cultures of *S. oneidensis* amended with 10 mM Fe(III)-citrate, 100 µM TCE, 100 µM PCE and 2 mM 1,4-dioxane and subjected to : Anaerobic (0-1, 7-8, 14-15 day time periods), aerobic (1-2, 8-9, 15-16 day time periods) and TPD degradation (2-7, 9-14, 16-19 day time periods) phases: (a) TCE only; (b) PCE only; (c) 1,4-dioxane only; (d) TCE + PCE; (e) TCE + 1,4-dioxane; (f) PCE + 1,4-dioxane; (g) TCE + PCE + 1,4-dioxane; solid filled red (◆), contaminant only; solid unfilled black (▲), contaminant + thiourea; ; solid unfilled blue (■), contaminant + mannitol; dashed filled green (•), anaerobic only; solid unfilled

green (•), Fe(III) omitted; solid unfilled red (◆), cells omitted. Grey shaded areas correspond to Fe(II)-generating phase, yellow shaded areas correspond to H_2O_2-generating phase, and unshaded areas correspond to contaminant degradation phase. Error bars represent range of errors in duplicate batch reactors.

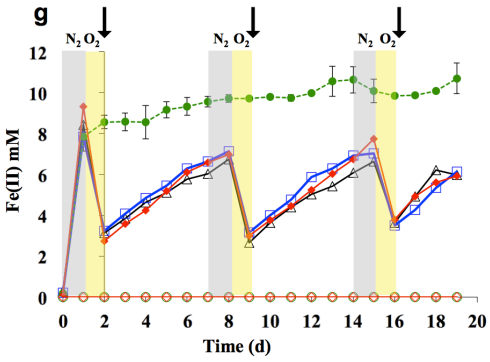

Figure 3.S5 continued

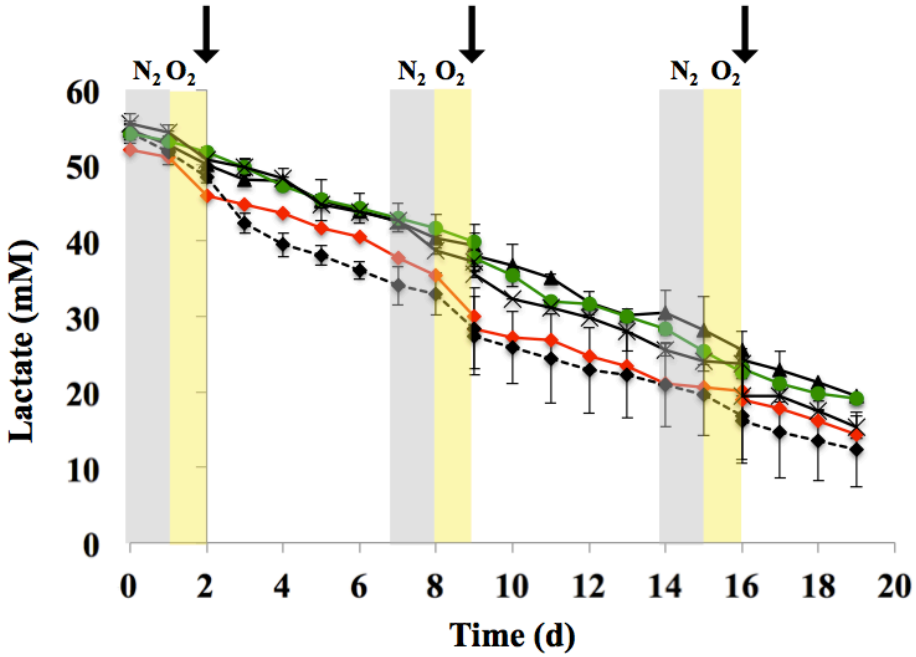

Figure 3.S6. Lactate concentrations profiles during microbial Fenton degradation of single, binary, and ternary mixtures of TPD in fed-batch liquid cultures of *S. oneidensis* amended with 10 mM Fe(III)-citrate, 100 µM TCE, 100 µM PCE and 2 mM 1,4-dioxane) and subjected to : Anaerobic (0-1, 7-8, 14-15 day time periods), aerobic (1-2, 8-9, 15-16 day time periods) and TPD degradation (2-7, 9-14, 16-19 day time periods) phases; solid red (◆), TCE only; solid black (x), TCE + 1,4-dioxane; solid green (•), TCE + PCE; solid black (▲), TCE + PCE + 1,4-dioxane; dashed black (◆), no contaminant control. Grey shaded areas correspond to Fe(II)-generating phase, yellow shaded areas correspond to H_2O_2-generating phase, and unshaded areas correspond to contaminant degradation phase. Arrows indicate time of addition (day 2) and respiking (day 9 & 16) of contaminants. Error bars represent range of errors in duplicate batch reactors.

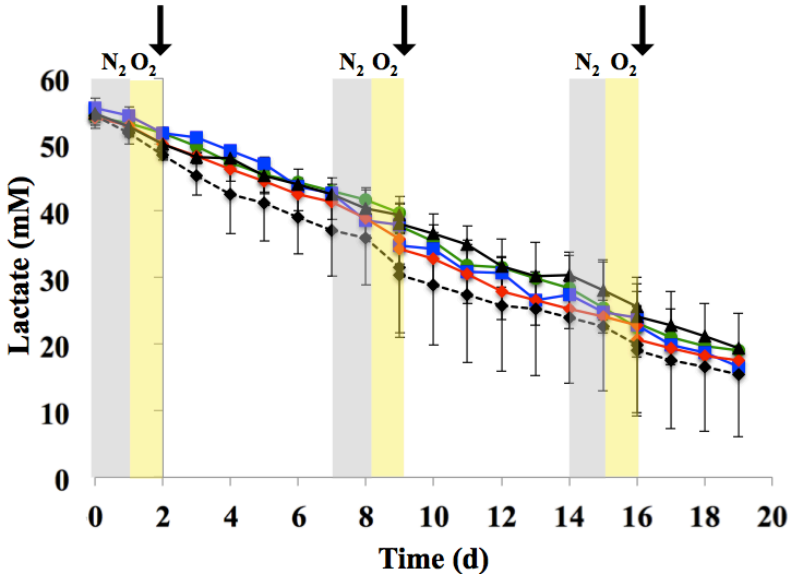

Figure 3.S7. Lactate concentrations profiles during microbial Fenton degradation of single, binary, and ternary mixtures of TPD in fed-batch liquid cultures of *S. oneidensis* amended with 10 mM Fe(III)-citrate, 100 µM TCE, 100 µM PCE and 2 mM 1,4-dioxane) and subjected to : Anaerobic (0-1, 7-8, 14-15 day time periods), aerobic (1-2, 8-9, 15-16 day time periods) and TPD degradation (2-7, 9-14, 16-19 day time periods) phases; solid red (◆), PCE only; solid blue (■), PCE + 1,4-dioxane; solid green (•), TCE + PCE; solid black (▲), TCE + PCE + 1,4-dioxane; dashed black (◆), no contaminant control. Grey shaded areas correspond to Fe(II)-generating phase, yellow shaded areas correspond to H_2O_2-generating phase, and unshaded areas correspond to contaminant degradation phase. Arrows indicate time of addition (day 2) and respiking (day 9 & 16) of contaminants. Error bars represent range of errors in duplicate batch reactors.

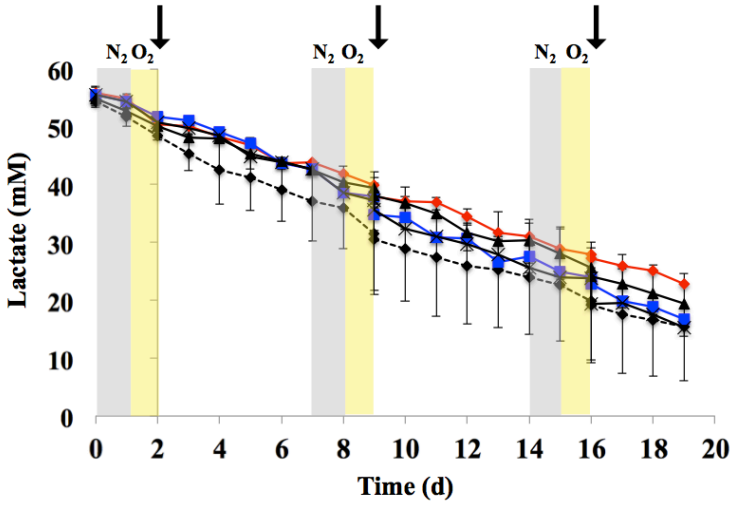

Figure 3.S8. Lactate concentrations profiles during microbial Fenton degradation of single, double and triple combinations of TPD in fed-batch liquid cultures of *S. oneidensis* amended with 10 mM Fe(III)-citrate, 100 µM TCE, 100 µM PCE and 2 mM 1,4-dioxane) and subjected to : Anaerobic (0-1, 7-8, 14-15 day time periods), aerobic (1-2, 8-9, 15-16 day time periods) and TPD degradation (2-7, 9-14, 16-19 day time periods) phases; solid red (◆), 1,4-dioxane only; solid blue (■), PCE + 1,4-dioxane; solid black (x), TCE + 1,4-dioxane; solid black (▲), TCE + PCE + 1,4-dioxane; dashed black (◆), no contaminant control. Grey shaded areas correspond to Fe(II)-generating phase, yellow shaded areas correspond to H_2O_2-generating phase, and unshaded areas correspond to contaminant degradation phase. Arrows indicate time of addition (day 2) and respiking (day 9 & 16) of contaminants. Error bars represent range of errors in duplicate batch reactors.

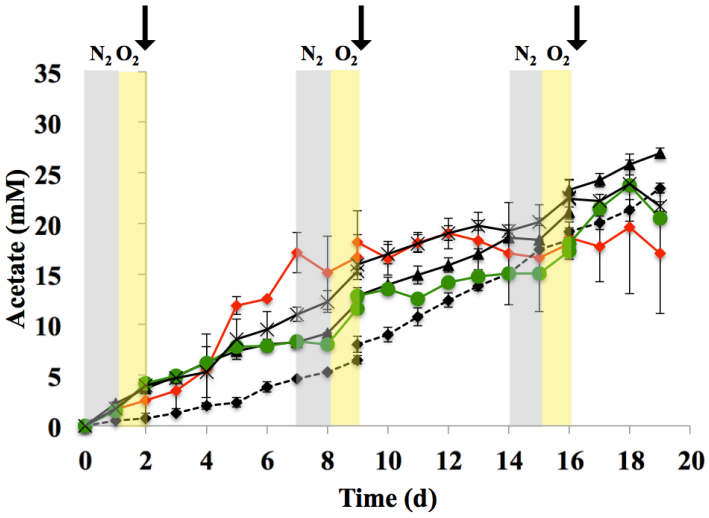

Figure 3.S9. Acetate concentrations profiles during microbial Fenton degradation of single, binary, and ternary mixtures of TPD in fed-batch liquid cultures of *S. oneidensis* amended with 10 mM Fe(III)-citrate, 100 µM TCE, 100 µM PCE and 2 mM 1,4-dioxane) and subjected to : Anaerobic (0-1, 7-8, 14-15 day time periods), aerobic (1-2, 8-9, 15-16 day time periods) and TPD degradation (2-7, 9-14, 16-19 day time periods) phases; solid red (◆), TCE only; solid black (x), TCE + 1,4-dioxane; solid green (●), TCE + PCE; solid black (▲), TCE + PCE + 1,4-dioxane; dashed black (◆), no contaminant control. Grey shaded areas correspond to Fe(II)-generating phase, yellow shaded areas correspond to H_2O_2-generating phase, and unshaded areas correspond to contaminant degradation phase. Arrows indicate time of addition (day 2) and respiking (day 9 & 16) of contaminants. Error bars represent range of errors in duplicate batch reactors.

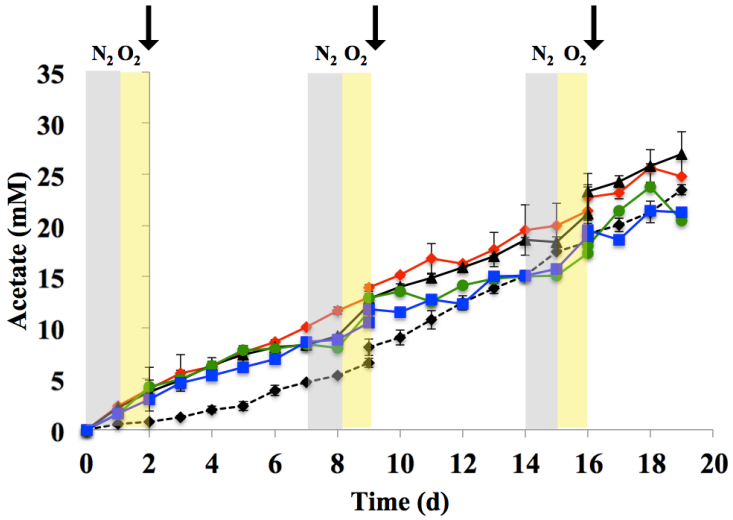

Figure 3.S10. Acetate concentrations profiles during microbial Fenton degradation of single, binary, and ternary mixtures of TPD in fed-batch liquid cultures of *S. oneidensis* amended with 10 mM Fe(III)-citrate, 100 µM TCE, 100 µM PCE and 2 mM 1,4-dioxane) and subjected to : Anaerobic (0-1, 7-8, 14-15 day time periods), aerobic (1-2, 8-9, 15-16 day time periods) and TPD degradation (2-7, 9-14, 16-19 day time periods) phases; solid red (◆), PCE only; solid blue (■), PCE + 1,4-dioxane; solid green (●), TCE + PCE; solid black (▲), TCE + PCE + 1,4-dioxane; dashed black (◆), no contaminant control. Grey shaded areas correspond to Fe(II)-generating phase, yellow shaded areas correspond to H_2O_2-generating phase, and unshaded areas correspond to contaminant degradation phase. Arrows indicate time of addition (day 2) and respiking (day 9 & 16) of contaminants. Error bars represent range of errors in duplicate batch reactors.

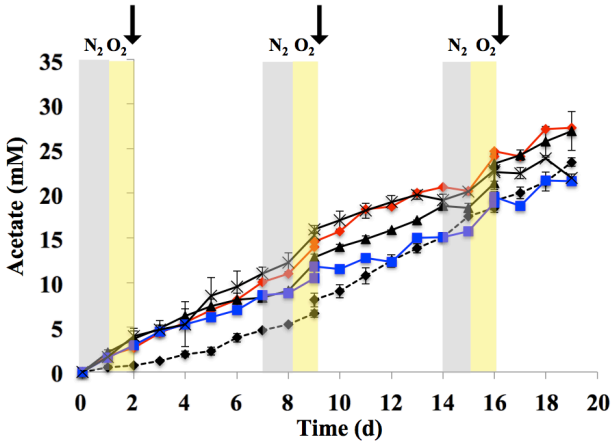

Figure 3.S11. Acetate concentrations profiles during microbial Fenton degradation of single, binary, and ternary mixtures of TPD in fed-batch liquid cultures of *S. oneidensis* amended with 10 mM Fe(III)-citrate, 100 µM TCE, 100 µM PCE and 2 mM 1,4-dioxane) and subjected to : Anaerobic (0-1, 7-8, 14-15 day time periods), aerobic (1-2, 8-9, 15-16 day time periods) and TPD degradation (2-7, 9-14, 16-19 day time periods) phases; solid red (◆), 1,4-dioxane only; solid blue (■), PCE + 1,4-dioxane; solid black (x), TCE + 1,4-dioxane; solid black (▲), TCE + PCE + 1,4-dioxane; dashed black (◆), no contaminant control. Grey shaded areas correspond to Fe(II)-generating phase, yellow shaded areas correspond to H_2O_2-generating phase, and unshaded areas correspond to contaminant degradation phase. Arrows indicate time of addition (day 2) and respiking (day 9 & 16) of contaminants. Error bars represent range of errors in duplicate batch reactors.

Figure 3.S12

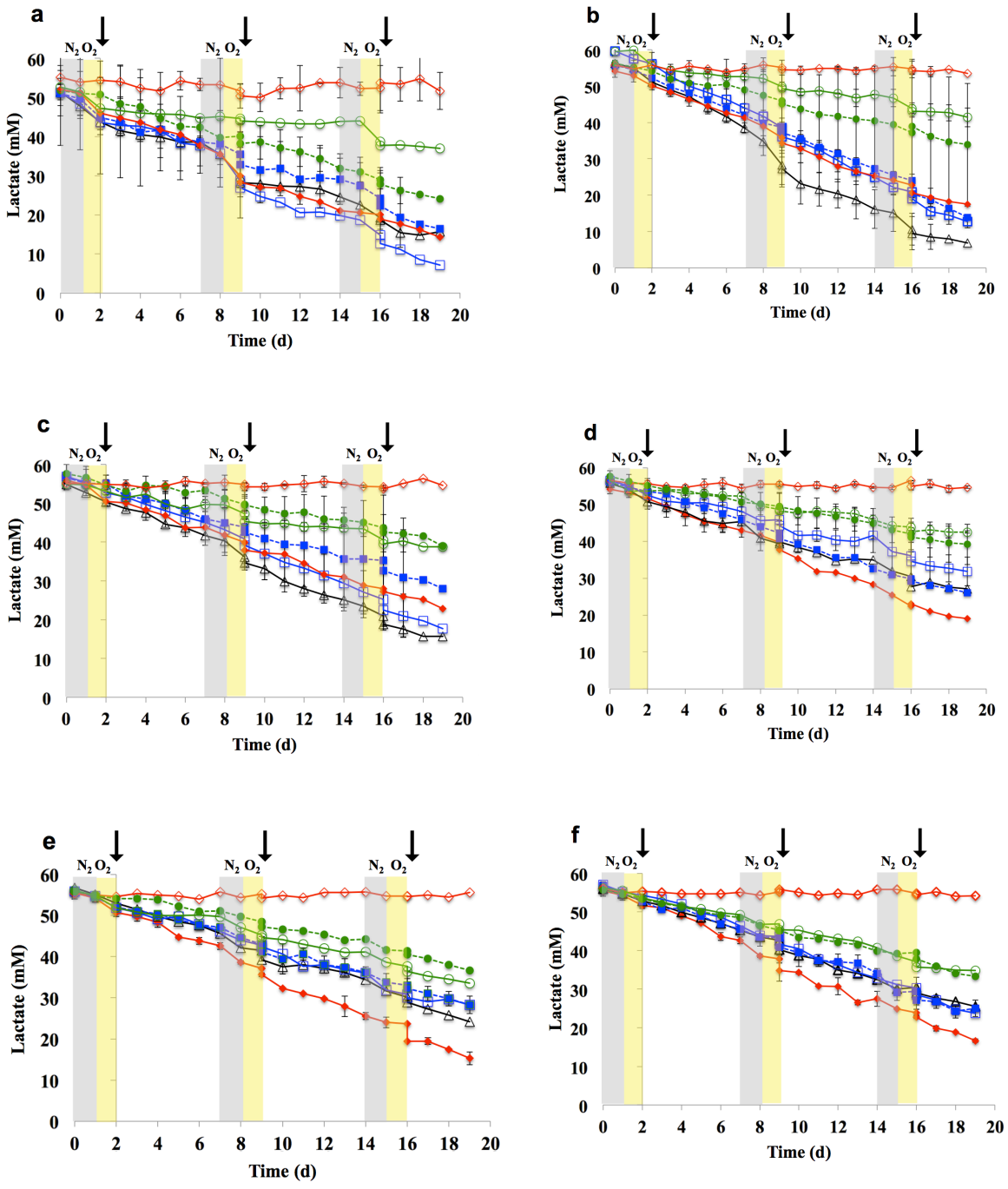

Figure 3.S12. Lactate concentrations during microbial Fenton degradation of single, binary, and ternary mixtures of TPD in fed-batch liquid cultures of *S. oneidensis* amended with 10 mM Fe(III)-citrate, 100 µM TCE, 100 µM PCE and 2 mM 1,4-dioxane and subjected to : Anaerobic (0-1, 7-8, 14-15 day time periods), aerobic (1-2, 8-9, 15-16 day time periods) and TPD degradation (2-7, 9-14, 16-19 day time

periods) phases: (a) TCE only; (b) PCE only; (c) 1,4-dioxane only; (d) TCE + PCE; (e) TCE + 1,4-dioxane; (f) PCE + 1,4-dioxane; (g) TCE + PCE + 1,4-dioxane; solid filled red (◆), contaminant only; solid unfilled black (▲), contaminant + thiourea; ; dashed filled blue (■), nitrate; solid unfilled blue (■), contaminant + mannitol; dashed filled green (●), anaerobic only; solid unfilled green (●), Fe(III) omitted; solid unfilled red (◆), cells omitted. Grey shaded areas correspond to Fe(II)-generating phase, yellow shaded areas correspond to H_2O_2-generating phase, and unshaded areas correspond to contaminant degradation phase. Arrows indicate time of addition (day 2) and respiking (day 9 & 16) of contaminants. Error bars represent range of errors in duplicate batch reactors.

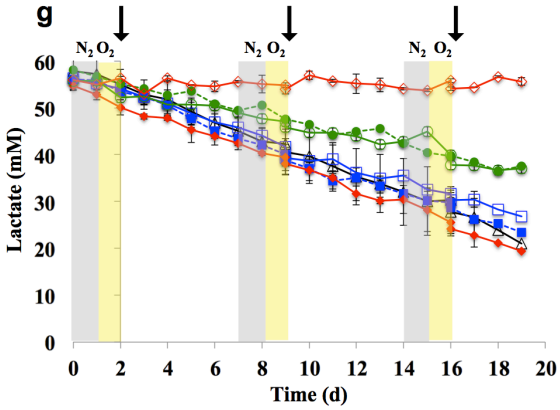

Figure 3.S12 continued

Figure 3.S13.

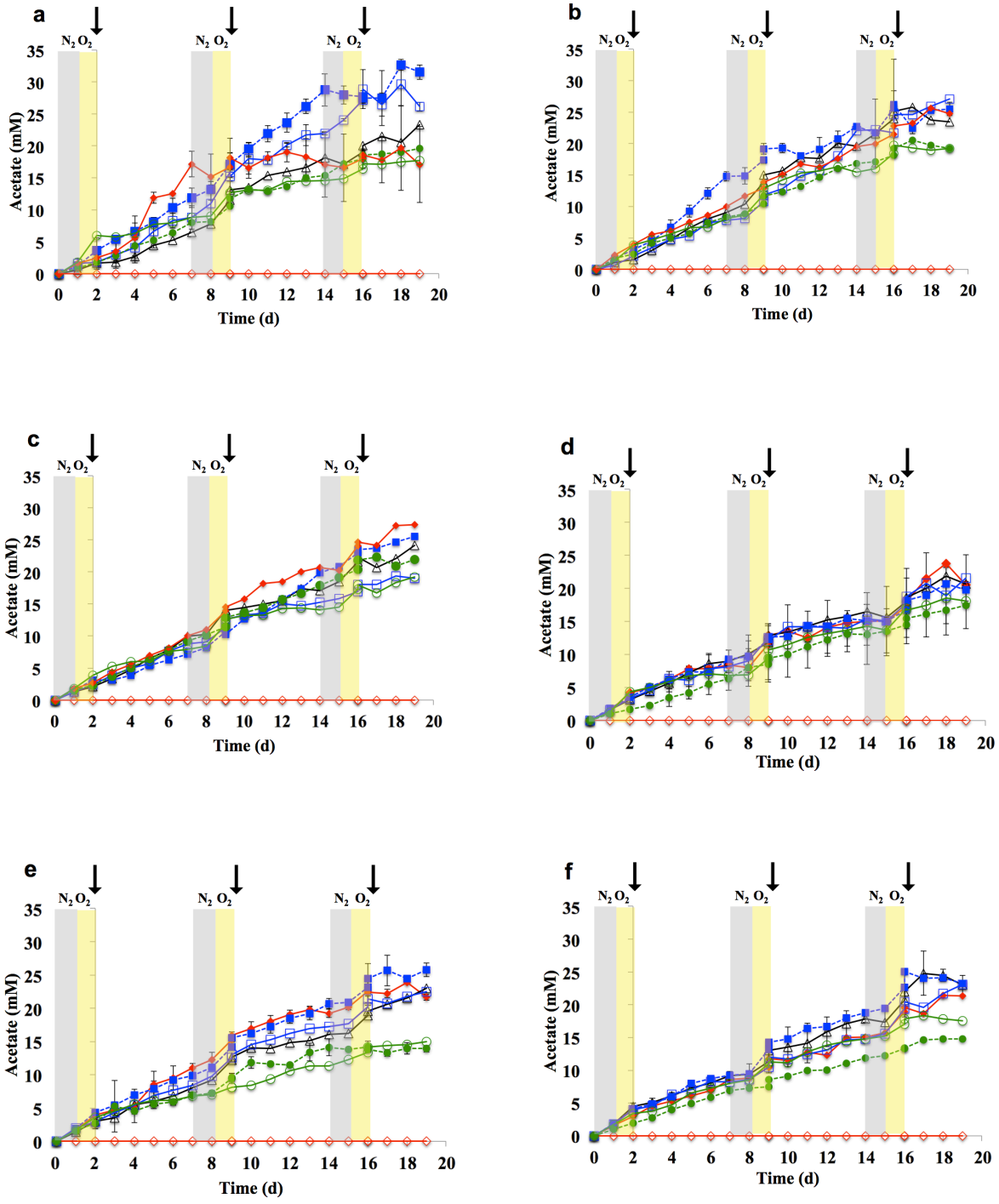

Figure 3.S13. Acetate concentrations during microbial Fenton degradation of single, binary, and ternary mixtures of TPD in fed-batch liquid cultures of *S. oneidensis* amended with 10 mM Fe(III)-citrate, 100 µM TCE, 100 µM PCE and 2 mM 1,4-dioxane and subjected to : Anaerobic (0-1, 7-8, 14-15 day time periods), aerobic (1-2,

8-9, 15-16 day time periods) and TPD degradation (2-7, 9-14, 16-19 day time periods) phases: (a) TCE only; (b) PCE only; (c) 1,4-dioxane only; (d) TCE + PCE; (e) TCE + 1,4-dioxane; (f) PCE + 1,4-dioxane; (g) TCE + PCE + 1,4-dioxane; solid filled red (◆), contaminant only; solid unfilled black (▲), contaminant + thiourea; dashed filled blue (■), nitrate; solid unfilled blue (■), contaminant + mannitol; dashed filled green (●), anaerobic only; solid unfilled green (●), Fe(III) omitted; solid unfilled red (◆), cells omitted. Grey shaded areas correspond to Fe(II)-generating phase, yellow shaded areas correspond to H_2O_2-generating phase, and unshaded areas correspond to contaminant degradation phase. Arrows indicate time of addition (day 2) and respiking (day 9 & 16) of contaminants. Error bars represent range of errors in duplicate batch reactors.

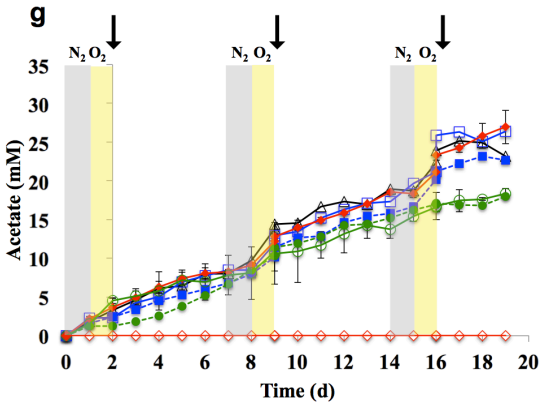

Figure 3.S13 continued

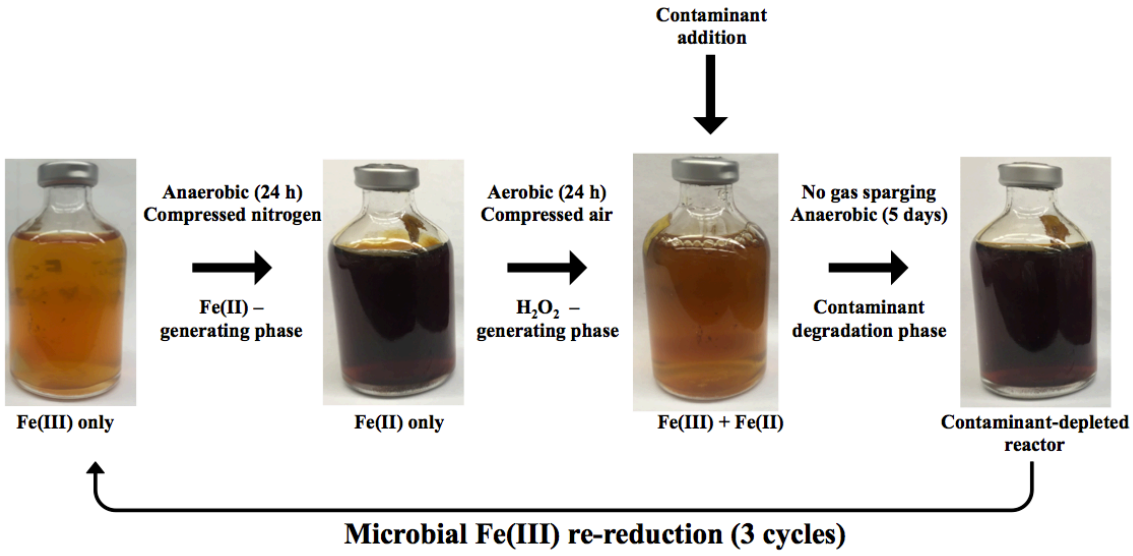

Figure 3.S14. Experimental setup of the new microbially-driven Fenton reaction system to simultaneously degrade single, binary, and ternary mixtures of TCE, PCE, and 1,4-dioxane

Table 3.S1. Limit of detection (LOD) and the limit of quantitation (LOQ) of analytes in this study

Compound	Limit of detection (LOD)	Limit of quantitation (LOQ)
1,4-Dioxane	0.2 mM	0.7 mM
Acetate	40.4 µM	134.6 µM
Lactate	18.0 µM	59.9 µM
Trichloroethylene	7.6 µM	23.0 µM
Tetrachloroethylene	8.9 µM	26.9 µM

Table 3.S2: Composition of LS medium

Compound	Concentration (mM)
Sodium DL lactate	10
Potassium Phosphate	10
NH_4SO_4	15
$MgSO_4.\ 7H_2O$	1
$CaCl_2.2H_2O$	0.48
EDTA, disodium salt	0.67
$FeSO_4.7H_2O$	0.1
$NaHCO_3$	0.2
$FeCl_3$	0.1
Na_2SeO_4	0.01
H_3BO_3	0.05
$ZnSO_4.7H_2O$	0.005
$Na_2MoO_4.2H_2O$	0.007
$CuSO_4.5H_2O$	0.001
$MnSO_4.H_2O$	0.001
$CoSO_4.7H_2O$	0.05
$NiCl_2.6H_2O$	0.08
NaCl	0.1

Table 3.S3. Initial rates of TCE degradation in the presence and absence of PCE and 1,4-dioxane during the microbially-driven Fenton reaction in a fed-batch reactor (% of T1, T2 and T3 for cycles 1, 2 and 3 respectively in parenthesis)

Cycle	T ($\mu M\ h^{-1}$)	TP ($\mu M\ h^{-1}$)	TD ($\mu M\ h^{-1}$)	TPD ($\mu M\ h^{-1}$)
1	1.1 ± 0.07	0.8 ± 0.19 (71%)	0.9 ± 0.12 (82%)	0.8 ± 0.05 (74%)
2	1.5 ± 0.01	0.8 ± 0.14 (51%)	1.0 ± 0.23 (67%)	0.8 ± 0.30 (55%)
3	1.4 ± 0.11	0.6 ± 0.07 (46%)	0.9 ± 0.02 (65%)	1.0 ± 0.20 (74%)

Table 3.S4. Initial rates of PCE degradation in the presence and absence of TCE and 1,4-dioxane during the microbially-driven Fenton reaction in a fed-batch reactor (% of P1, P2 and P3 for cycles 1, 2 and 3 respectively in parenthesis)

Cycle	P ($\mu M\ h^{-1}$)	PT ($\mu M\ h^{-1}$)	PD ($\mu M\ h^{-1}$)	TPD ($\mu M\ h^{-1}$)
1	1.4 ± 0.32	1.6 ± 0.28 (110%)	1.1 ± 0.28(75%)	0.9 ± 0.04 (62%)
2	1.6 ± 0.11	1.4 ± 0.22 (88%)	1.1 ± 0.04 (69%)	1.5 ± 0.10 (96%)
3	1.2 ± 0.12	1.2 ± 0.07 (98%)	0.8 ± 0.20 (69%)	0.9 ± 0.08 (72%)

Table 3.S5. Initial rates of 1,4-Dioxane degradation in the presence and absence of TCE and PCE during the microbially-driven Fenton reaction in a fed-batch reactor (% of D1, D2 and D3 for cycles 1, 2 and 3 respectively in parenthesis)

Cycle	D ($\mu M\ h^{-1}$)	DT ($\mu M\ h^{-1}$)	DP ($\mu M\ h^{-1}$)	TPD ($\mu M\ h^{-1}$)
1	30.8 ± 8.25	10.9 ± 4.14 (35%)	12.1 ± 1.12 (39%)	16.8 ± 5.55 (54%)
2	36.2 ± 4.13	22.2 ± 3.46 (61%)	13.9 ± 4.14 (38%)	13.0 ± 1.47 (35%)
3	27.9 ± 3.37	27.2 ± 6.74 (97%)	28.3 ± 4.44 (101%)	19.7 ± 5.45 (70%)

Table 3.S6. Ratio between rate of degradation of 1,4-dioxane and TCE across three contaminant degradation phase cycles.

Cycle	Single contaminant	Binary mixture	Ternary mixture
1	29.1 ± 6.31	14.4 ± 2.24	21.3 ± 5.11
2	24.8 ± 2.60	29.6 ± 4.25	16.1 ± 3.34
3	20.3 ± 1.29	29.9 ± 2.03	19.0 ± 1.84

Table 3.S7. Ratio between rate of degradation of 1,4-dioxane and PCE across three contaminant degradation phase cycles.

Cycle	Single contaminant	Binary mixture	Ternary mixture
1	21.7 ± 3.61	11.3 ± 1.31	19.1 ± 3.49
2	23.5 ± 0.61	12.9 ± 3.21	8.8 ± 1.17
3	22.8 ± 0.87	33.5 ± 1.57	22.4 ± 5.49

CHAPTER 4

NON-ENZYMATIC MICROBIALLY-DRIVEN PRODUCTION OF FERMENTABLE SUGARS FROM LIGNOCELLULOSE

Abstract

Pretreatment of recalcitrant lignocellulosic biomass is one of the most expensive steps in commercialization of lignocellulose bioprocessing. Efficient hydrolysis of pretreated cellulose and hemicellulose to fermentable sugars is also challenging since a multitude of lignocellulose-hydrolyzing enzymes are required. In the present study, we have developed a new method for lignocellulose degradation that combines both pretreatment and saccharification of cellulose and xylan in a single-step by a microbially-driven Fenton reaction system. The reaction produced a mixture of short oligosaccharides dominated by monomer sugars. Wild type Fe(III)-respiring *S. oneidensis* is unable to utilize cellodextrin and xylodextrin sugars as carbon and energy source, thus facilitating accumulation of large concentrations of fermentable sugars. The combined pretreatment and saccharification method for cellulose and xylan developed did not require the addition of acidic or alkali compounds or the use of hydrolyzing enzymes thus providing an economically feasible process to directly produce simple fermentable sugars from cellulose and xylan. The utility of the fermentable sugars produced from the microbially-driven Fenton degradation of lignocellulose was demonstrated by production of the biodegradable plastic polyhydroxybutyrate from Fenton-degraded xylan.

4.1 Introduction

Lignocellulosic biomass is the most abundant renewable resource for the biofuel and biorefinery industries and is a major global reservoir of organic carbon (1, 2). Complex carbohydrate (cellulose and hemicellulose) and aromatic (lignin) polymers are the main components of lignocellulosic biomass. The carbohydrate polymers are composed of different sugar monomers (mainly glucose and xylose) that are tightly bound to lignin via ester and ether linkages (3). The crystalline structure of cellulose fibrils along with the tight bonding with lignin render lignocellulose highly recalcitrant to degradation by microbial enzymes (4). Lignocellulose degradation in terrestrial environments is mediated by enzymes produced by lignocellulolytic fungi or bacteria, including carbohydrate hydrolases (e.g., cellulases and hemicellulases) and oxidative lignin-degrading enzymes (e.g., laccase and peroxidases)(2, 5, 6). More than 50% of the terrestrially-derived lignocellulosic flux from the continents to the ocean is remineralized in coastal marine environments by marine cellulolytic bacteria (2).

Conventional bioprocesses for production of biofuel or biorefinery products consists of polymer size reduction, pretreatment, enzymatic hydrolysis (saccharification), fermentation, and downstream product recovery. Pretreatment is required to breakdown the rigid lignocellulosic structure, rendering the structure more accessible to hydrolyzing enzymes (7). Enzymatic hydrolysis of pretreated lignocellulose produces simple sugars such as glucose and xylose that are subsequently metabolized to useful secondary chemicals. Simultaneous saccharification and co-fermentation (SSCF) and consolidated bioprocessing (i.e., combined enzyme production, hydrolysis and fermentation) have been

developed to reduce the costs of converting lignocellulosic biomass to useful secondary chemicals (6, 8). However, due to the recalcitrance of lignocellulosic biomass, pretreatment processes remain the main bottleneck and one of the most expensive steps in commercialization of lignocellulose bioprocessing (9-11). Current physical and chemical pretreatment technologies (e.g., milling, ammonia fiber explosion, CO_2 explosion, steam explosion, ozonolysis, acid hydrolysis, alkaline hydrolysis, ionic liquids) are problematic due to costs, pollution, safety, high energy demand, and the requirement for detoxification of phenolic inhibitory byproducts after pretreatment (10, 12). Biological pretreatment of lignocellulosic biomass, on the other hand, requires a unique synergistic consortia of bacteria and fungi for lignocellulose degradation activity (5). Efficient hydrolysis of pretreated cellulose and hemicellulose to fermentable sugars is also challenging since complete hydrolysis often requires a multitude of lignocellulose-hydrolyzing enzymes (6, 13).

Chemical oxidation is an attractive method to degrade lignocellulosic biomass (14-16). Lignocellulose depolymerization is driven by fungal lignolytic enzymes (e.g., peroxidases, laccases) that hydrolyze cellulose and partially degrade lignin via Fenton reaction-based chemistry (17-19). Recently, a new class of enzymes called lytic polysaccharide monooxygenases was identified from the fungus *Neurospora crassa* that employ an oxidative mechanism to degrade cellulose and hemicellulose (20, 21). Lignocellulose pretreatment via chemical (purely abiotic) Fenton reactions have also improved subsequent enzymatic saccharification of biomass and increase overall sugar yields (22). In the abiotic Fenton reaction (eq 1), hydrogen peroxide (H_2O_2) reacts with

ferrous iron (Fe(II)) to produce Fe(III), hydroxyl ion (OH-), and lignocellulose-depolymerizing $HO^{\bullet}$ radical:

$$Fe(II) + H_2O_2 \rightarrow Fe(III) + OH^- + HO^{\bullet} \quad (1)$$

In addition to lignocellulose, $HO^{\bullet}$ radicals oxidatively degrade a wide variety of environmental contaminants, including pentachlorophenol (PCP)(23, 24) and 1,4-dioxane (25). Conventional Fenton reaction-driven pretreatment of lignocellulose is limited, however, by the high concentrations of Fenton reagents Fe(II) and H_2O_2 that must be continuously supplied to produce $HO^{\bullet}$ radicals that drive lignocellulose degradation (16, 22). UV irradiation is often employed to induce Fe(III) re-reduction and photolytic radical production in photo-Fenton systems. The UV irradiation systems, however, are limited by UV light penetration, and H_2O_2 must still be continuously supplied to drive the conventional Fenton reaction (25). Although pretreatment of cellulose and hemicellulose by the Fenton reaction produce reducing sugars (26), the identity of the oligosaccharides produced from $HO^{\bullet}$ radical-based lignocellulosic degradation remain unknown.

Microbially-driven Fenton reactions that alternately produce the Fenton reagents H_2O_2 (via microbial O_2 respiration) and Fe(II) (via microbial Fe(III) reduction) at neutral pH alleviate the need for continual addition of H_2O_2 and Fe(II) to drive $HO^{\bullet}$ radical production (25, 27-29). The Fe(III)-reducing facultative anaerobe *Shewanella oneidensis* was recently employed to drive the Fenton reaction for oxidative degradation of PCP and 1,4-dioxane (24, 25). In the *S. oneidensis*-driven Fenton reaction, batch liquid cultures were amended with Fe(III) and contaminants and subsequently exposed to alternating aerobic and anaerobic conditions. During the aerobic period, *S. oneidensis*

produced H_2O_2 via microbial O_2 respiration, while during the anaerobic period *S. oneidensis* produced Fe(II) via microbial Fe(III) reduction. During the transition from aerobic-to-anaerobic conditions, H_2O_2 and Fe(II) interacted chemically via the Fenton reaction to produce HO• radicals that degraded PCP (24) and 1,4-dioxane (25). An identical microbially driven Fenton reaction was employed in the present study to generate HO• radicals for pretreatment of cellulose and hemicellulose, degradation of cellodextrins and xylodextrins, and production of short-chain sugar oligosaccharides in a single reactor system that did not require addition of conventional lignocellulose-hydrolyzing enzymes.

4.2 Materials and methods

Culture Medium and Chemical Reagents. *S. oneidensis* was routinely cultured aerobically on LB medium (10 g/L tryptone, 5 g/L yeast extract, and 10 g/L NaCl) at 30°C.(30) Cellulose, hemicellulose, cellodextrin and xylodextrin degradation experiments were conducted in minimal salt solution (LS; pH 7.0, Supplementary Table 4.S3) amended with 50 mM lactate as carbon and energy source and 10 mM Fe(III)-citrate as anaerobic electron acceptor. Fe(III) citrate was prepared by previously described methods (31). All chemicals unless otherwise specified were obtained from Sigma-Aldrich. Cellotriose, cellotetraose, cellopentaose, cellohexaose, xylobiose, xylotriose, xylotetraose, xylopentaose, and xylohexaose were obtained from Megazyme Inc. In the microbially-driven Fenton degradation experiments, sugar compounds were added to the fed batch reactor at the following concentrations: Carboxymethyl cellulose (CMC; 1% w/v), xylan (1% w/v), each cellodextrin (100 μM), and each xylodextrin (100 μM). The sugar compounds were designated as follows: Glucose = G1, Cellobiose = G2,

Cellotriose = G3, Cellotetraose = G4, Cellopentaose = G5, Cellohexaose = G6, Xylose = X1, Xylobiose = X2, Xylotriose = X3, Xylotetraose = X4, Xylopentaose = X5, Xylohexaose = X6.

Microbially Driven Fenton Degradation of CMC and Xylan on Solid Agar Medium. The degradation of CMC and xylan by the *S. oneidensis*-driven Fenton reaction was tested during colony growth on solid agar growth medium. *S. oneidensis* cells were serially-diluted on LS agar medium supplemented with CMC or xylan (1% w/v), Congo red dye (0.04% w/v), 10 mM Fe(III) and incubated at 30°C for 48 h. Congo red dye specifically binds to beta-glucans to form red-colored dye-polysaccharide complexes (32). A series of three controls incubations were carried out on solid agar growth medium with the following changes: CMC or xylan omitted, Fe(III) omitted, and incubations in the presence of $HO^{\bullet}$ scavenging compound thiourea (40 mM). The resulting colonies were visually scored for the presence of clear halos around the aerobically grown colonies that indicated degradation of CMC and xylan (32, 33).

Design of a Microbially Driven Fenton Reaction for Degradation of CMC, Xylan, Cellodextrin, and Xylodextrin Compounds. The experimental conditions for the microbially-driven Fenton degradation of cellulose, xylan, cellodextrin and xylodextrin compounds (designated as CXcx) were similar to the batch reactor system previously employed for 1,4-dioxane degradation with a few modifications (25). *S. oneidensis* was grown aerobically pregrown in LB, harvested and resuspended in LS medium (amended with 10 mM Fe(III), 50 mM lactate) to a final cell density of 10^9 cells mL^{-1} in 60-mL glass serum bottles. Anaerobic stock solutions of CXcx compounds were added and the cell cultures were incubated under anaerobic conditions by injecting

(hydrated) compressed nitrogen until 10 mM Fe(III) was reduced to 8.6-9.7 mM Fe(II) (6 h of anaerobic incubation; Fe(II) generating phase). The compressed nitrogen line was replaced by a (hydrated) compressed air line to initiate aerobic conditions and 8.6-9.7 mM Fe(II) was oxidized to 0.7-1.6 mM (6 h of aerobic incubation; $HO^{\bullet}$ production phase). During the aerobic phase, the Fenton reagents Fe(II) (produced by microbial Fe(III) reduction) and H_2O_2 (produced by microbial O_2 reduction) reacted to generate $HO^{\bullet}$ radicals. Sugar concentrations were monitored throughout the experiments via high pressure liquid chromatography (HPLC). Following the first aerobic phase, the anaerobic and aerobic phases were alternated for 12 h and 6 h respectively for 156 h and the reactor temperature (25'C) and pH (7.0) were held constant throughout the experiment.

Inhibition of the Microbially-Driven Fenton Reaction in Control Incubations. A series of four control incubations were carried out to confirm that CXcx were degraded by $HO^{\bullet}$ radicals generated by the *S. oneidensis*-driven Fenton reaction. The four control incubations were carried out in the batch reactor system described above with the following changes: In the first set of control incubations, sugar concentrations were monitored under alternating anaerobic and aerobic conditions with 15 mM NO_3^- replacing 10 mM Fe(III) as electron acceptor. In the second set of control incubations, the sugar degradation process was carried out in the presence of the $HO^{\bullet}$ radical scavenging compound thiourea (20 mM) added to the batch reactor system. In the third set of control incubations, sugar degradation was monitored in the absence of either Fe(III) or *S. oneidensis* cells (abiotic control). In the fourth set of control incubations, sugar concentrations were monitored in abiotic sealed serum bottles maintained under strict

anaerobic conditions without compressed nitrogen sparging for the entire incubation period.

Polyhydroxybutyrate (PHB) Production Derived From Fenton Degradation of Xylan by D-Xylose-Adapted *S. oneidensis* Mutant XM1. To produce PHB from Fenton-degraded xylan, *S. oneidensis* strain XM1 (a previously developed strain capable of metabolizing D-xylose (See Chapter 5) and harboring the PHB biosynthetic genes *phaCAB* in pBBR1MCS plasmid was cultured in LB with 0.5 mM arabinose for 24 h. Following expression of PHB biosynthetic genes *phaCAB*, the cells were resuspended in spent media resulting from Fenton degraded xylan (consisting of xylan degradation products including D-xylose). Lactate was completely consumed after 138 h of Fenton reaction (Fig. 4.S3). The spent media was incubated at 30˚C for 96 h and samples were periodically drawn to determine the concentration of D-xylose and PHB.

Analytical Techniques. Samples were withdrawn and centrifuged at 6000 x g for 10 min. HCl-extracted Fe(II) concentrations were determined with a previously described Ferrozine-based detection technique (34). Soluble sugar compounds were measured via HPLC according to a previously described protocol (35). 300 μL of an aqueous solution of sugar sample was mixed with 116 mM sodium cyanoborohydride solution in water, 350 mM aminobenzoic butyl ester (ABBE) and 0.83% acetic acid in a total volume of 1.2 mL. The solution was mixed and heated at 80°C for 60 min. Cyanoborohydride is the reductant of the ABBE bound-sugars after they dehydrate during the addition of ABBE. Subsequently, the aqueous phase was extracted three times with 0.5 mL chloroform and directly injected into the HPLC system. The sugar compounds were detected using a SUPELCOSIL LC-18-DB column (reverse phase) with mobile phase comprised of 0.1 M

ammonium acetate, pH 4.5, and acetonitrile (75:25, v/v) at a flow rate of 0.5 mL/min (Table 4.S1). Chromatograms were generated at 260 nm for the sugar compounds with retention times as shown in Supplementary Table 4.S2. Calibration curves were generated from standards to determine the concentrations of each compound. Lactate was analyzed via anion exchange HPLC using a SUPELCOGEL C-610H column with 0.1% H_3PO_4 as the mobile phase and a constant flow rate of 0.3 ml/min. Chromatograms were generated at 210 nm for lactate with retention times of 29.4 min. Calibration curves were generated from standards to determine the concentrations.

To determine the concentration of the reducing end of insoluble sugars, 50 mL of spent culture was washed with 3X volume of cold acetone and ethanol. The mixture was centrifuged at 15,000 x g for 5 min and the sugar pellet was weighed and resolubilized in 2 mL of 3 M NaOH solution. The mixture was centrifuged at 15,000 x g for 5 min. The concentration of reducing ends of the supernatant was determined by the dinitrosalicylic acid (DNS) assay. 100 μL of the supernatant was added to 900 μL of DNS solution. DNS solution was prepared as follows: 0.75% 3,5-dinitrosalycylic acid, 1.4% sodium hydroxide, 21.6% potassium sodium tartrate, 0.55% phenol and 0.55% sodium metabisulfate dissolved in water. The mixture was then boiled for 5 min, centrifuged at 15,000 x g for 5 min and the optical density of the supernatant was measured at 545 nm. Reducing sugar concentrations were calculated using glucose as standard (36).

PHB was analyzed as described previously (37, 38). Cell pellets were boiled in 0.5 mL of concentrated sulfuric acid for 60 min and then diluted with 1 mL of 14 mM H_2SO_4. Samples were centrifuged for 15 min at 16,000g cell debris and the supernatant was analyzed via liquid chromatography (LC) using a ZORBAX SB-C18 column with

5% aqueous acetonitrile at pH 2.8 as the mobile phase and a constant flow rate of 0.3 ml/min. Chromatograms were generated at 210 nm at a retention time of 7 min.

4.3. Results and Discussion

The microbially driven Fenton degradation of carboxymethyl cellulose (CMC) and xylan was first tested on solid agar media. Following 48 h of aerobic incubation, *S. oneidensis* colonies displayed distinct halos in the presence of Fe(III) and congo red indicating depolymerization activity (Fig. 1). HO• radical-mediated degradation of the polymers was confirmed by the addition of thiourea, a HO• radical-scavenging compound that inhibited degradation of CMC and xylan (Fig. 4.1). The degradation of CMC and xylan was subsequently demonstrated in a liquid batch reactor similar to a system previously employed for 1,4-dioxane degradation (Fig. 4.2) (25). Strikingly, during the initial 78 h period of the microbially-driven Fenton reaction with CMC and xylan, cellodextrins and xylodextrins accumulated at only low levels (Fig. 4.3).

To further investigate this initial period, the concentration of total reducing ends of the insoluble polymers was quantified by the DNS assay. The glucose-equivalent reducing end concentration for insoluble CMC and xylan increased sharply during the initial 78 h period (at rates of 0.56 and 1.42 μM mg^{-1} for CMC and xylan, respectively) indicating that the polymers underwent a fragmentation phase during this initial 78 h period (Fig. 4.3 and 4.S30). Following this fragmentation phase (i.e., 78 h – 156 h time

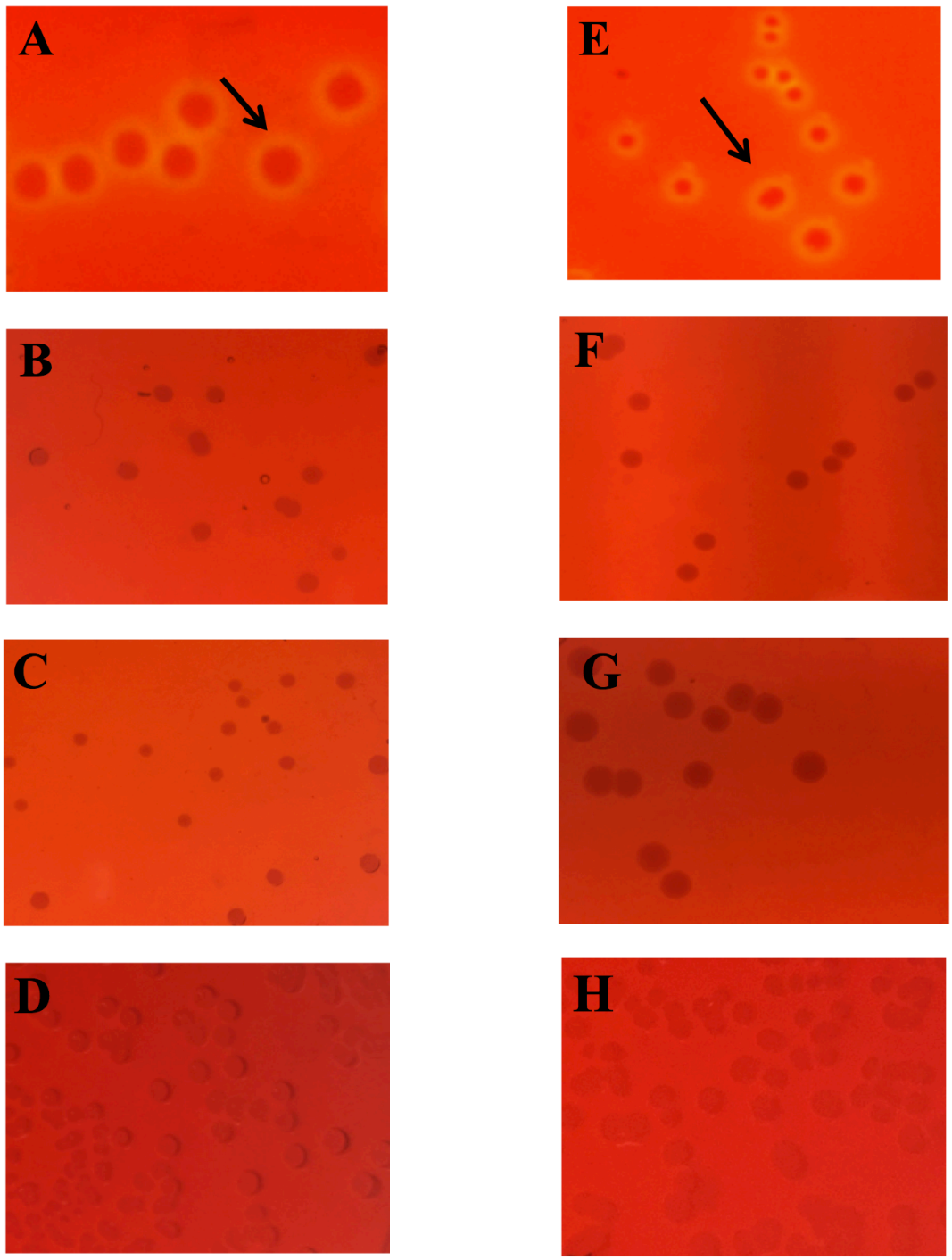

Figure 4.1. Microbially-driven Fenton degradation of cellulose (1% w/v) and xylan (1% w/v) by *S. oneidensis* on solid agar medium supplemented with Congo red dye (0.04% w/v) and 10 mM Fe(III). Black arrows indicate halos around colony: (A) CMC Fenton; (B) CMC Fenton – Fe(III) omitted; (C) CMC Fenton – thiourea; (D) Sugar omitted (CMC); (E) xylan Fenton; (F) xylan Fenton - Fe(III) omitted; (G) xylan Fenton – thiourea; (H) Sugar omitted (xylan)

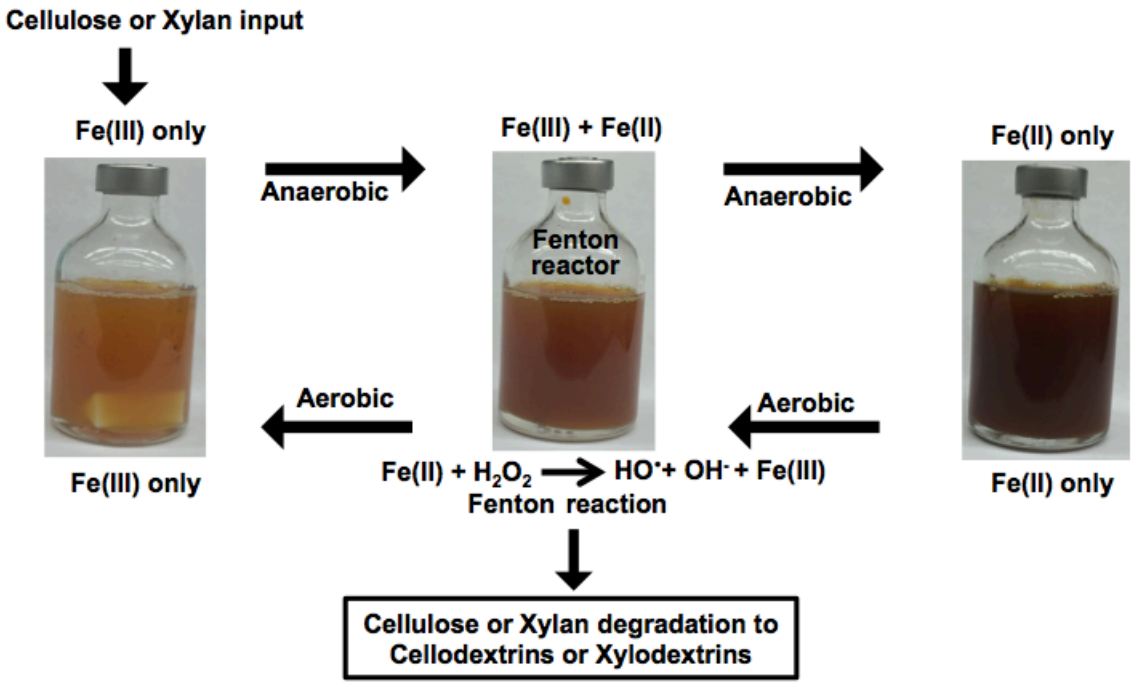

Figure 4.2. Experimental setup for the microbially driven Fenton reaction system to degrade cellulose and xylan in a batch reactor. Fe(II) produced during anaerobic phases interacts chemically via the Fenton reaction with H_2O_2 produced during aerobic phases to yield $HO^{\bullet}$ radicals that oxidatively degrade cellulose and xylan

period), the cellodextrin and xylodextrin compounds G1-6 and X1-6 began to accumulate, indicating that shorter oligosaccharides began to peel off the partially fragmented polymers (Figs. 4.3 and 4.S26-4.S29). Also during this period, the total reducing ends of the insoluble polymers began to plateau (Fig. 4.3B) or even decrease (Fig. 4.3C) correlating with the accumulation of soluble sugars (cellodextrins and xylodextrins respectively). This result indicates that following the fragmentation phase, the insoluble polymers further degraded producing soluble shorter oligosaccharides (G1-6 & X1-6). The total glucose-equivalent reducing end and total short oligosaccharide concentrations (degree of polymerization, DP 1-6) from xylan degradation was 2- (Figs.

4.3C and 4.S30B) and 8-fold (Figs. 4.3 and 4.S26-27) greater than that from CMC degradation, most likely because xylan is more

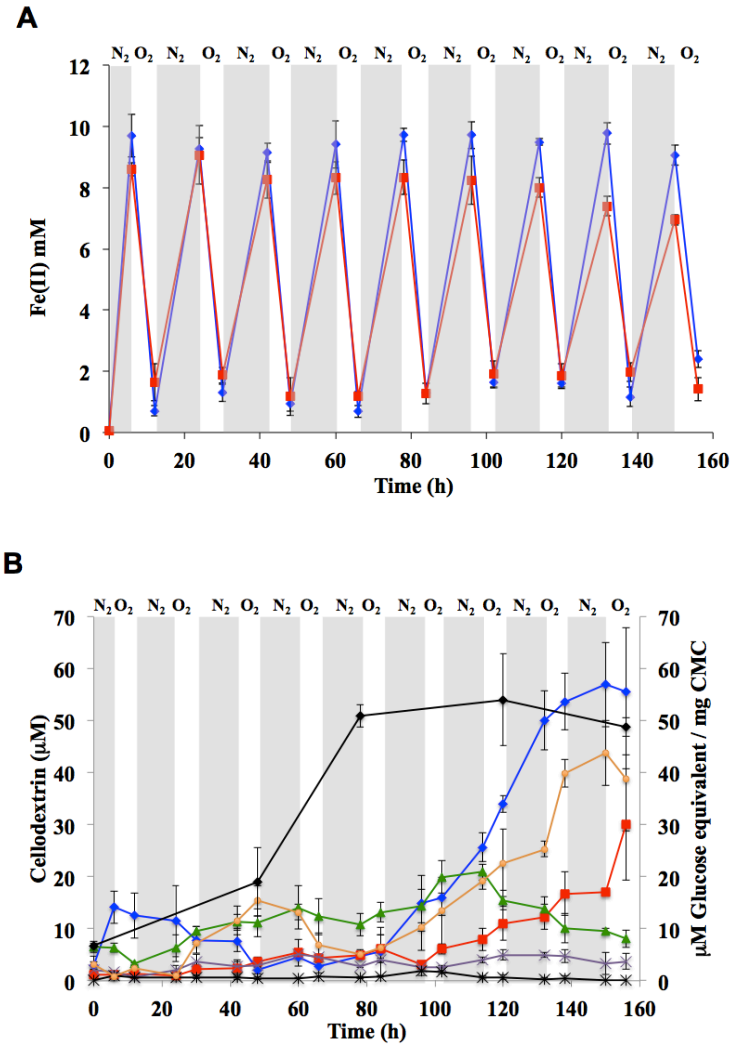

Figure 4.3. Microbial Fenton degradation of CMC and xylan in batch liquid cultures of *S. oneidensis* amended with 10 mM Fe(III) and 1% w/v CMC/xylan with an aerobic and anaerobic cycling period of 6 and 12 h respectively. (A) Fe(II) concentration profiles: blue (◆), CMC; red (■), xylan. (B) & (C) Concentration profiles during microbial Fenton degradation of polymer in batch liquid cultures of *S. oneidensis* amended with 10 mM Fe(III) and 1% w/v polymer with an aerobic and anaerobic cycling period of 6 and 12 h respectively: (B) CMC; (C) Xylan; blue (◆), G1 (or X1); red (■), G2 (or X2); green (▲), G3 (or X3); violet (X), G4 (or X4); black (*), G5 (or X5); orange (•), G6 (or X6); black (◆), reducing end concentration of insoluble CMC (or xylan). Grey shaded areas correspond to anaerobic phases, and unshaded areas correspond to aerobic phases. Error bars represent range of errors in duplicate batch reactors.

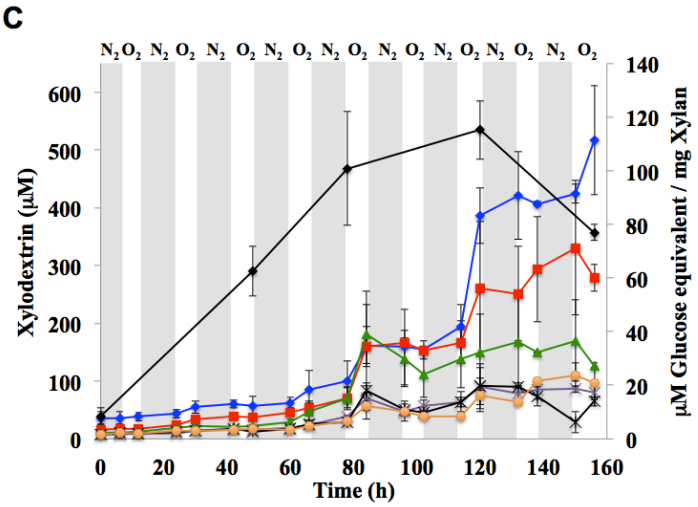

Figure 4.3 continued

easily degraded due to a more amorphous structure (39). This finding is also reflected in the larger size of halos in xylan compared to CMC-congo red plates (Figs. 4.1a and 4.1e). To test if xylose produced from Fenton degraded xylan was fermentable (Fig. 4.3C), the accumulation of xylose from Fenton degradation of xylan was coupled to production of polyhydroxybutyrate (PHB), a biodegradable plastic by xylose-adapted *S. oneidensis* strain XM1. XM1 produced 0.8 mg PHB gm^{-1} cell at a PHB production yield of 0.08% mg mg^{-1} DCW (comparable to previous reports with initial xylose concentration of 0.5 mM (See Chapter 5) (Fig. 4.4).

In the absence of cells, replacement of Fe with nitrate, and in the presence of the $HO^{\bullet}$ radical scavenging compound thiourea, there was no accumulation of the short oligosaccharides indicating that CMC and xylan were degraded by the $HO^{\bullet}$ radicals. However, periodic decreases in concentrations of cellodextrin and xylodextrin compounds during the Fenton reaction suggested that the $HO^{\bullet}$ radicals may also be degrading the short oligosaccharides (Figs. 4.S1-S2).

To investigate this finding more closely, the degradation of individual cellodextrin and xylodextrins was tested in the microbially driven Fenton reaction

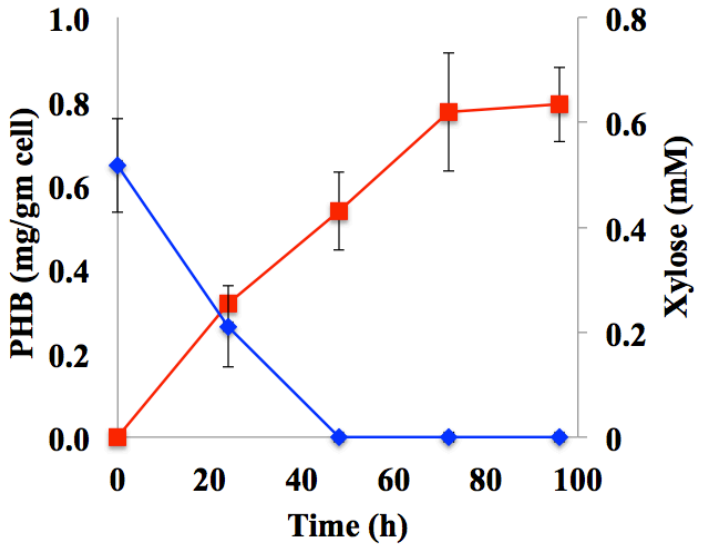

Figure 4.4. Xylose and PHB concentration profiles during PHB production by XM1 harboring the PHB biosynthetic genes *phaCAB*. Cells were cultured in LB and gene expression was induced by the addition of 0.5 mM arabinose. Cells were then resuspended in spent media from Fenton-degraded xylan as sole carbon and electron source. xylose; blue (◆), PHB; red (■). Error bars represent range of errors in duplicate batch reactors.

system. Cello- and xylodextrins with DP 1-6 were degraded giving rise to the smaller corresponding DP compounds as products (Figs. 4.S4, 4.S12, 4S22-23 and Tables 1, 2). The degradation rates of the monomer sugars G1 and X1 were the slowest (120 and 110 nM h^{-1} respectively), correlating with their highest accumulation rates (0.68 and 5.3 μM h^{-1} respectively) during CMC and xylan degradation, respectively (Fig 4.S24-25 and 4.S28). G5 degraded at the fastest rate among cellodextrins G1-6 (407 nM h^{-1}; 86.9 – 253.8% higher than G1-4 & G6), which explains the reason why G5 did not accumulate during the Fenton degradation of CMC (Fig. 4.S4, 4.S22-23 and 4.S26-27). The average

degradation rate of xylodextrins with even-numbered DP (262 nM/h) was 198 ± 13 % higher than xylodextrins with odd-numbered DP, most likely due to the inhibitory effects of alternating side chains (arabinose, glucuronic acid, and acetyl) (Figs. 4.S24-25) (32) in the xylodextrin structure on degradation activity of the HO• radicals (40). A carbon balance was also carried out to account for the total carbon input and output during the microbially driven Fenton reaction of cello- and xylodextrins. The total carbon accumulation from the degradation of each cello- and xylodextrin was lower by 47 ± 17 and 56 ± 26 % respectively compared to the carbon input (Tables 1B and 2B) most likely due to the production of aldonic acids of the respective sugars such as gluconic and cellobionic acids as oxidation byproducts that were not accounted for in the analyses (41, 42). Similar control experiments including cells omitted, replacement of Fe(III) with nitrate, and addition of the HO• radical scavenging compound thiourea inhibited the degradation of cello- and xylodextrins, indicating that cellodextrins and xylodextrins were degraded by the HO• radicals (Fig. 4.S5-10 and 4.S13-18).

In the present study, we have developed a new method for lignocellulose degradation that combines both pretreatment and saccharification of cellulose and xylan in a single-step, microbially driven Fenton reaction system (Fig. 4.5). The reaction produced a mixture of short oligosaccharides dominated by monomer sugars. Wild type Fe(III)-respiring *S. oneidensis* is unable to utilize cellodextrin and xylodextrin sugars as carbon and energy source, thus enabling the use of this bacteria to accumulate large concentrations of fermentable sugars (43). The combined pretreatment and saccharification method for cellulose and xylan developed did not require the addition of acid, alkali compounds or the use of hydrolyzing enzymes thus providing an

economically feasible process to directly produce simple fermentable sugars from cellulose and xylan (10). Microbial Fe(III) reduction is a dominant anaerobic respiratory process in soil and sediments, which suggests that the microbially driven Fenton reaction may play an important role in the degradation of decaying plant and woody materials in natural environments exposed to fluctuating redox conditions.

Table 4.1A. Degradation and accumulation of cellodextrin compounds during microbial Fenton degradation in batch liquid cultures of *S. oneidensis* amended with 10 mM Fe(III) and 100 μM of individual cellodextrin compounds with an aerobic and anaerobic cycling period of 6 and 12 h respectively. Error bars represent range of errors in duplicate batch reactors.

Fenton substrates		G1 (μM)	G2 (μM)	G3 (μM)	G4 (μM)	G5 (μM)	G6 (μM)
G6	Degradation						22.2 ± 0.3
	Accumulation	6.9 ± 0.8	5.3 ± 0.1	5.5 ± 0.8	6.7 ± 0.3	3.8 ± 0.6	
G5	Degradation					41.5 ± 4.1	
	Accumulation	6.9 ± 1.0	3.3 ± 1.0	7.3 ± 0.6	3.1 ± 0.3		
G4	Degradation				17.9 ± 1.0		
	Accumulation	7.1 ± 0.5	3.4 ± 1.0	11.0 ± 0.8			
G3	Degradation			17.3 ± 6.1			
	Accumulation	13.6 ± 1.7	7.2 ± 1.1				
G2	Degradation		11.7 ± 6.6				
	Accumulation	13.9 ± 0.2					
G1	Degradation	12.2 ± 1.0					

Table 4.1B. Degradation and accumulation of cellodextrin compounds (concentrations are calculated in terms of G1 units for all compounds) during microbial Fenton degradation in batch liquid cultures of *S. oneidensis* amended with 10 mM Fe(III) and 100 μM of individual cellodextrin compounds with an aerobic and anaerobic cycling period of 6 and 12 h respectively. Error bars represent range of errors in duplicate batch reactors. Numbers in brackets indicate total accumulation from degradation of respective compounds

Fenton substrates		G1 (μM)	G2 (μM)	G3 (μM)	G4 (μM)	G5 (μM)	G6 (μM)
G6	Degradation						133.2 ± 12.2
	Accumulation	6.9 ± 0.8	10.6 ± 0.2	16.5 ± 2.5	26.9 ± 1.2	18.9 ± 3.1	(79.8 ± 7.8)
G5	Degradation					207.5 ± 20.4	
	Accumulation	6.9 ± 1.0	6.5 ± 2.0	22.0 ± 1.8	12.2 ± 1.2	(47.7 ± 6.1)	
G4	Degradation				71.4 ± 4.1		
	Accumulation	7.1 ± 0.5	6.7 ± 2.1	33.1 ± 2.4	(46.9 ± 4.9)		
G3	Degradation			52.0 ± 18.4			
	Accumulation	13.6 ± 1.7	14.5 ± 2.2	(28.1 ± 3.9)			
G2	Degradation		23.5 ± 13.3				
	Accumulation	(13.9 ± 0.2)					
G1	Degradation	12.2 ± 1.0					

Table 4.2A. Degradation and accumulation of xylodextrin compounds during microbial Fenton degradation in batch liquid cultures of *S. oneidensis* amended with 10 mM Fe(III) and 100 μM of individual xylodextrin compounds with an aerobic and anaerobic cycling period of 6 and 12 h respectively. Error bars represent range of errors in duplicate batch reactors.

Fenton substrates			X1 (μM)	X2 (μM)	X3 (μM)	X4 (μM)	X5 (μM)	X6 (μM)
	X6	Degradation						21.2 ± 1.9
		Accumulation	24.1 ± 3.1	8.9 ± 0.4	6.8 ± 1.3	4.5 ± 0.3	13.8 ± 0.7	
	X5	Degradation					14.1 ± 0.7	
		Accumulation	12.8 ± 4.0	2.7 ± 0.3	2.7 ± 0.3	7.9 ± 0.9		
	X4	Degradation				31.6 ± 4.1		
		Accumulation	10.4 ± 1.1	3.8 ± 1.7	3.6 ± 1.3			
	X3	Degradation			15.1 ± 0.5			
		Accumulation	1.2 ± 0.3	3.9 ± 0.3				
	X2	Degradation		27.3 ± 1.1				
		Accumulation	26.6 ± 4.9					
	X1	Degradation	11.2 ± 2.5					

Table 4.2B. Degradation and accumulation of xylodextrin compounds (concentrations are calculated in terms of X1 units for all compounds) during microbial Fenton degradation in batch liquid cultures of *S. oneidensis* amended with 10 mM Fe(III) and 100 μM of individual xylodextrin compounds with an aerobic and anaerobic cycling period of 6 and 12 h respectively Error bars represent range of errors in duplicate batch reactors. Concentrations are calculated in terms of X1 units for all compounds. Numbers in brackets indicate total accumulation from degradation of respective compounds

Fenton substrates			X1 (μM)	X2 (μM)	X3 (μM)	X4 (μM)	X5 (μM)	X6 (μM)
X6	Degradation							127.3 ± 11.2
	Accumulation	24.2 ± 3.1	17.7 ± 0.8	20.5 ± 3.1	17.9 ± 1.2	68.9 ± 3.5	(149.2 ± 11.7)
X5	Degradation						70.4 ± 3.5	
	Accumulation	12.8 ± 4.0	5.3 ± 0.6	7.9 ± 0.9	31.4 ± 3.6	(57.4 ± 8.2)	
X4	Degradation					126.5 ± 16.3		
	Accumulation	10.4 ± 1.1	7.5 ± 3.3	10.7 ± 3.8	(28.6 ± 8.2)			
X3	Degradation				45.3 ± 1.5			
	Accumulation	1.2 ± 0.3	7.9 ± 0.6	(9.2 ± 0.9)				
X2	Degradation		54.7 ± 2.0					
	Accumulation	(26.6 ± 9.8)						
X1	Degradation	11.2 ± 2.5						

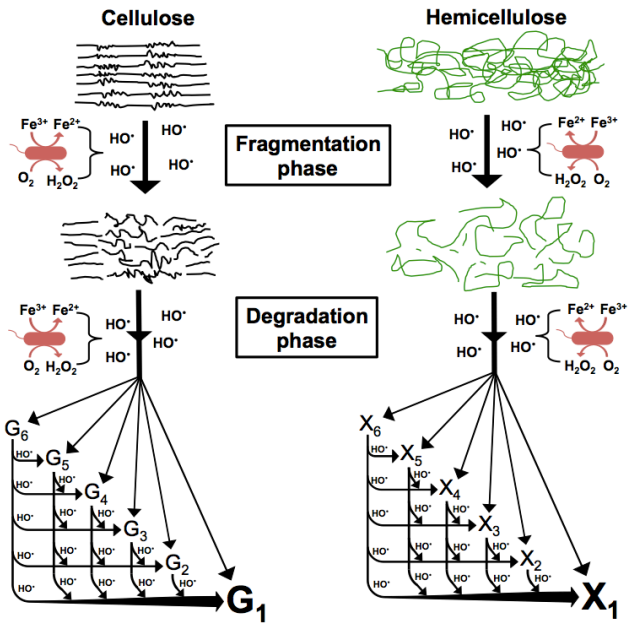

Figure 4.5. Model of microbially-driven fenton degradation of cellulose and xylan to fermentable sugars

4.4. References

1. **Vanholme B, Desmet T, Ronsse F, Rabaey K, Van Breusegem F, De Mey M, Soetaert W, Boerjan W.** 2013. Towards a carbon-negative sustainable bio-based economy. Front Plant Sci **4:**174.

2. **Gontikaki E, Thornton B, Cornulier T, Witte U.** 2015. Occurrence of Priming in the Degradation of Lignocellulose in Marine Sediments. PLoS One **10:**e0143917.

3. **Lange JP.** 2007. Lignocellulose conversion: an introduction to chemistry. Wiley-VCH, New York, NY, USA.

4. **Lee HV, Hamid SB, Zain SK.** 2014. Conversion of lignocellulosic biomass to nanocellulose: structure and chemical process. ScientificWorldJournal **2014:**631013.

5. **Sindhu R, Binod P, Pandey A.** 2016. Biological pretreatment of lignocellulosic biomass - An overview. Bioresource Technology **199:**76-82.

6. **Lynd LR, Weimer PJ, van Zyl WH, Pretorius IS.** 2002. Microbial cellulose utilization: fundamentals and biotechnology. Microbiol Mol Biol Rev **66:**506-577, table of contents.

7. **Sun S, Sun S, Cao X, Sun R.** 2016. The role of pretreatment in improving the enzymatic hydrolysis of lignocellulosic materials. Bioresour Technol **199:**49-58.

8. **Olson DG, McBride JE, Shaw AJ, Lynd LR.** 2012. Recent progress in consolidated bioprocessing. Curr Opin Biotechnol **23:**396-405.

9. **Jonsson LJ, Alriksson B, Nilvebrant NO.** 2013. Bioconversion of lignocellulose: inhibitors and detoxification. Biotechnol Biofuels **6:**16.

10. **Rabemanolontsoa H, Saka S.** 2016. Various pretreatments of lignocellulosics. Bioresource Technology **199:**83-91.

11. **Peng XW, Qiao WB, Mi SF, Jia XJ, Su H, Han YJ.** 2015. Characterization of hemicellulase and cellulase from the extremely thermophilic bacterium Caldicellulosiruptor owensensis and their potential application for bioconversion of lignocellulosic biomass without pretreatment. Biotechnology for Biofuels **8**.

12. **Jonsson LJ, Martin C.** 2016. Pretreatment of lignocellulose: Formation of inhibitory by-products and strategies for minimizing their effects. Bioresour Technol **199:**103-112.

13. **Zhang YH.** 2008. Reviving the carbohydrate economy via multi-product lignocellulose biorefineries. J Ind Microbiol Biotechnol **35:**367-375.

14. **Ratto M, Ritschkoff AC, Viikari L.** 1997. The effect of oxidative pretreatment on cellulose degradation by Poria placenta and Trichoderma reesei cellulases. Applied Microbiology and Biotechnology **48:**53-57.

15. **Koenings.** 1972. Effects of hydrogen peroxide on cellulose and its susceptibility on cellulase. Mater Org (Berl) **7:**133-147.

16. **Arantes V, Milagres AMF.** 2006. Degradation of cellulosic and hemicellulosic substrates using a chelator-mediated Fenton reaction. Journal of Chemical Technology and Biotechnology **81:**413-419.

17. **Kirk TK, Ibach R, Mozuch MD, Conner AH, Highley TL.** 1991. Characteristics of Cotton Cellulose Depolymerized by a Brown-Rot Fungus, by Acid, or by Chemical Oxidants. Holzforschung **45:**239-244.

18. **Kerem Z, Bao WL, Hammel KE.** 1998. Rapid polyether cleavage via extracellular one-electron oxidation by a brown-rot basidiomycete. Proceedings of the National Academy of Sciences of the United States of America **95:**10373-10377.

19. **Kerem Z, Jensen KA, Hammel KE.** 1999. Biodegradative mechanism of the brown rot basidiomycete Gloeophyllum trabeum: evidence for an extracellular hydroquinone-driven fenton reaction. Febs Letters **446:**49-54.

20. **Vaaje-Kolstad G, Westereng B, Horn SJ, Liu Z, Zhai H, Sorlie M, Eijsink VG.** 2010. An oxidative enzyme boosting the enzymatic conversion of recalcitrant polysaccharides. Science **330:**219-222.

21. **Agger JW, Isaksen T, Varnai A, Vidal-Melgosa S, Willats WGT, Ludwig R, Horn SJ, Eijsink VGH, Westereng B.** 2014. Discovery of LPMO activity on hemicelluloses shows the importance of oxidative processes in plant cell wall degradation. Proceedings of the National Academy of Sciences of the United States of America **111:**6287-6292.

22. **Kato DM, Elia N, Flythe M, Lynn BC.** 2014. Pretreatment of lignocellulosic biomass using Fenton chemistry. Bioresource Technology **162:**273-278.

23. **Barbeni M, Minero C, Pelizzetti E, Borgarello E, Serpone N.** 1987. Chemical Degradation of Chlorophenols with Fenton Reagent (Fe-2++H2O2). Chemosphere **16:**2225-2237.

24. **McKinzi AM, Dichristina TJ.** 1999. Microbially driven Fenton reaction for transformation of pentachlorophenol. Environmental Science & Technology **33:**1886-1891.

25. **Sekar R, DiChristina TJ.** 2014. Microbially driven fenton reaction for degradation of the widespread environmental contaminant 1,4-dioxane. Environ Sci Technol **48:**12858-12867.

26. **Silva JP, Carneiro LM, Roberto IC.** 2013. Treatment of rice straw hemicellulosic hydrolysates with advanced oxidative processes: a new and promising detoxification method to improve the bioconversion process. Biotechnol Biofuels **6:**23.

27. **Stefan MI, Bolton JR.** 1998. Mechanism of the degradation of 1,4-dioxane in dilute aqueous solution using the UV hydrogen peroxide process. Environmental Science & Technology **32:**1588-1595.

28. **Coleman HM, Vimonses V, Leslie G, Amal R.** 2007. Degradation of 1,4-dioxane in water using TiO2 based photocatalytic and H2O2/UV processes. Journal of Hazardous Materials **146:**496-501.

29. **Kim CG, Seo HJ, Lee BR.** 2006. Decomposition of 1,4-dioxane by advanced oxidation and biochemical process. J Environ Sci Health A Tox Hazard Subst Environ Eng **41:**599-611.

30. **Sambrook J, Fritsh EF, Maniatis T.** 1989. Molecular Cloning: A Laboratory Manual. Cold Spring Harbor Laboratory Press; Cold Spring Harbor, NY.

31. **Dichristina TJ, Delong EF.** 1994. Isolation of Anaerobic Respiratory Mutants of Shewanella-Putrefaciens and Genetic-Analysis of Mutants Deficient in Anaerobic Growth on Fe3+. Journal of Bacteriology **176:**1468-1474.

32. **Shin HD, McClendon S, Vo T, Chen RR.** 2010. Escherichia coli Binary Culture Engineered for Direct Fermentation of Hemicellulose to a Biofuel. Applied and Environmental Microbiology **76:**8150-8159.

33. **Jung HC, Park JH, Park SH, Lebeault JM, Pan JG.** 1998. Expression of carboxymethylcellulase on the surface of Escherichia coli using Pseudomonas syringae ice nucleation protein. Enzyme and Microbial Technology **22:**348-354.

34. **Dichristina TJ.** 1992. Effects of Nitrate and Nitrite on Dissimilatory Iron Reduction by Shewanella-Putrefaciens-200. Journal of Bacteriology **174:**1891-1896.

35. **Kratschmar D, Wallner S, Florenski S, Schmid D, Kuhn R.** 1999. Analysis of Oligosaccharides by MEKC with Aminobenzoic Alkyl Esters as Derivatization Agents. Chromatographia **50:**596-600.

36. **Miller GL.** 1959. Use of dinitrosalicylic acid reagent for determination of reducing sugar. Analytical Chemistry **31:**426-428.

37. **Kocharin K, Chen Y, Siewers V, Nielsen J.** 2012. Engineering of acetyl-CoA metabolism for the improved production of polyhydroxybutyrate in Saccharomyces cerevisiae. AMB Express **2:**52.

38. **Li LL, Gao J, Jiang H.** 2013. Production of 3-Hydroxybutyrate Monomers by Pseudomonas mendocina DS04-T Biodegraded Polyhydroxybutyrate. J Polym Environ **21:**826-832.

39. **Dimarogona M, Topakas E, Christakopoulos P.** 2012. Cellulose degradation by oxidative enzymes. Comput Struct Biotechnol J **2:**e201209015.

40. **Shekiro J, Kuhn EM, Selig MJ, Nagle NJ, Decker SR, Elander RT.** 2012. Enzymatic conversion of xylan residues from dilute acid-pretreated corn stover. Appl Biochem Biotechnol **168:**421-433.

41. **Li X, Chomvong K, Yu VY, Liang JM, Lin Y, Cate JH.** 2015. Cellobionic acid utilization: from Neurospora crassa to Saccharomyces cerevisiae. Biotechnol Biofuels **8:**120.

42. **Bey M, Zhou S, Poidevin L, Henrissat B, Coutinho PM, Berrin JG, Sigoillot JC.** 2013. Cello-oligosaccharide oxidation reveals differences between two lytic polysaccharide monooxygenases (family GH61) from Podospora anserina. Appl Environ Microbiol **79:**488-496.

43. **Rodionov DA, Yang C, Li X, Rodionova IA, Wang Y, Obraztsova AY, Zagnitko OP, Overbeek R, Romine MF, Reed S, Fredrickson JK, Nealson KH, Osterman AL.** 2010. Genomic encyclopedia of sugar utilization pathways in the Shewanella genus. BMC Genomics **11:**494.

4.5 Supporting information

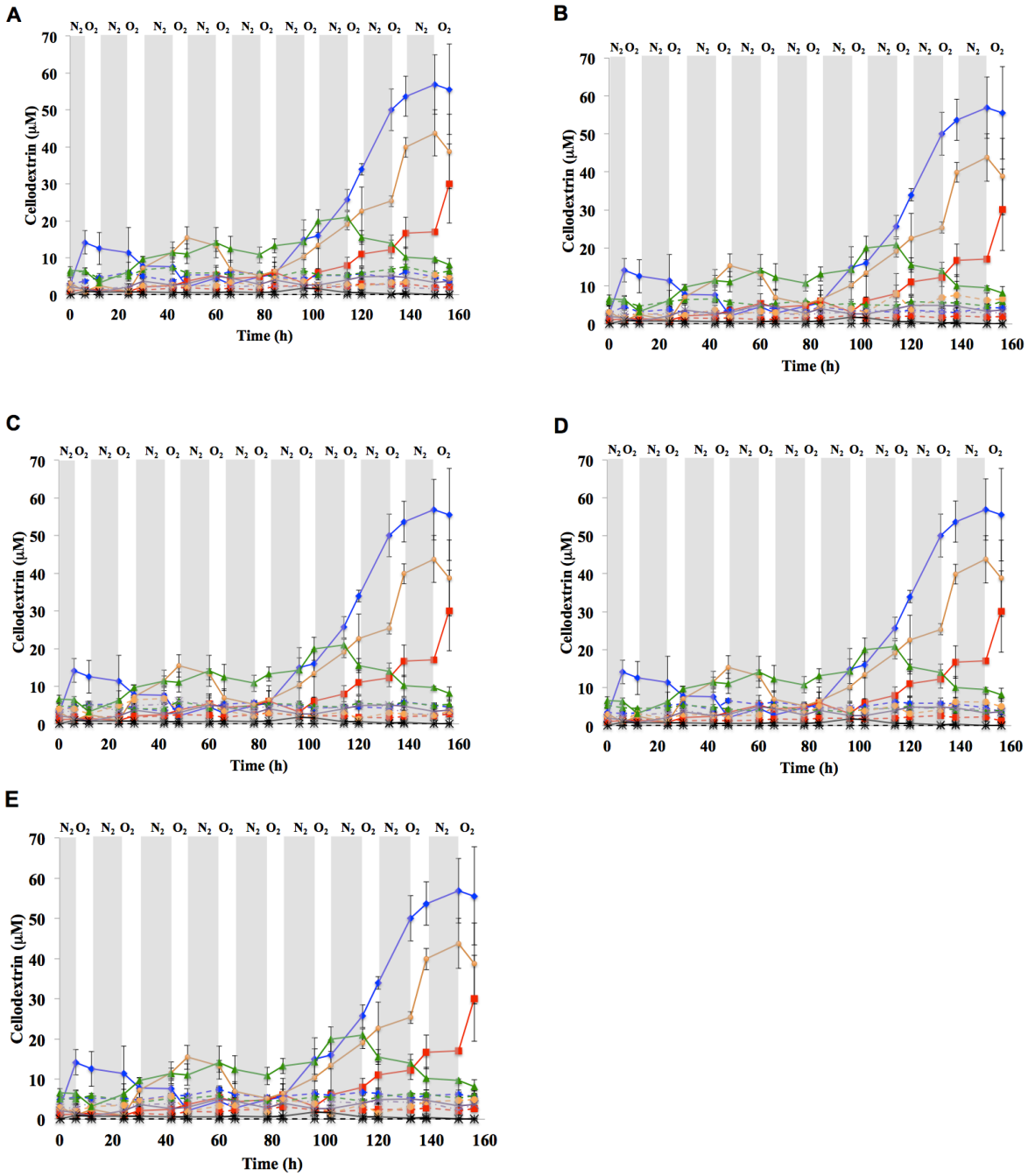

Figure 4.S1. Concentration profiles during microbial Fenton degradation of CMC in batch liquid cultures of *S. oneidensis* amended with 10 mM Fe(III) and 1% w/v CMC with an aerobic/anaerobic cycling period of 6 h: (A) cells omitted; (B) Fe(III) omitted; (C) nitrate; (D) thiourea; (E) anaerobic only; solid, fenton reaction; dashed, control; blue (◆), G1; red (■), G2; green (▲), G3; violet (x), G4; black (*), G5; orange (•), G6.

Grey shaded areas correspond to anaerobic phases, and unshaded areas correspond to aerobic phases. Error bars represent range of errors in duplicate batch reactors.

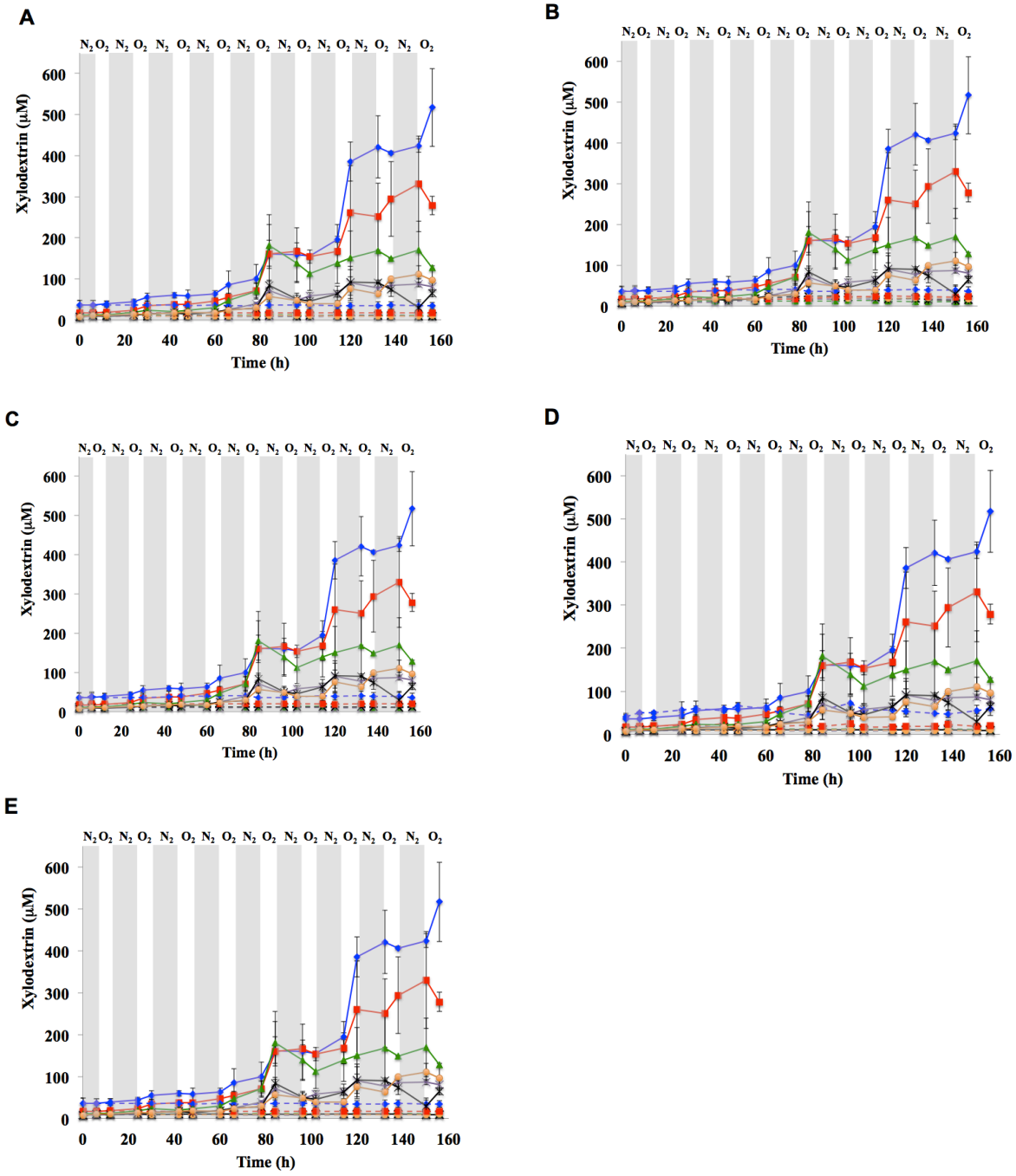

Figure 4.S2. Concentration profiles during microbial Fenton degradation of xylan in batch liquid cultures of *S. oneidensis* amended with 10 mM Fe(III) and 1% w/v xylan with an aerobic/anaerobic cycling period of 6 h: (A) cells omitted; (B) Fe(III)

omitted; (C) nitrate; (D) thiourea; (E) anaerobic only; solid, fenton reaction; dashed, control; blue (◆), X1; red (■), X2; green (▲), X3; violet (x), X4; black (*), X5; orange (•), X6. Grey shaded areas correspond to anaerobic phases, and unshaded areas correspond to aerobic phases. Error bars represent range of errors in duplicate batch reactors.

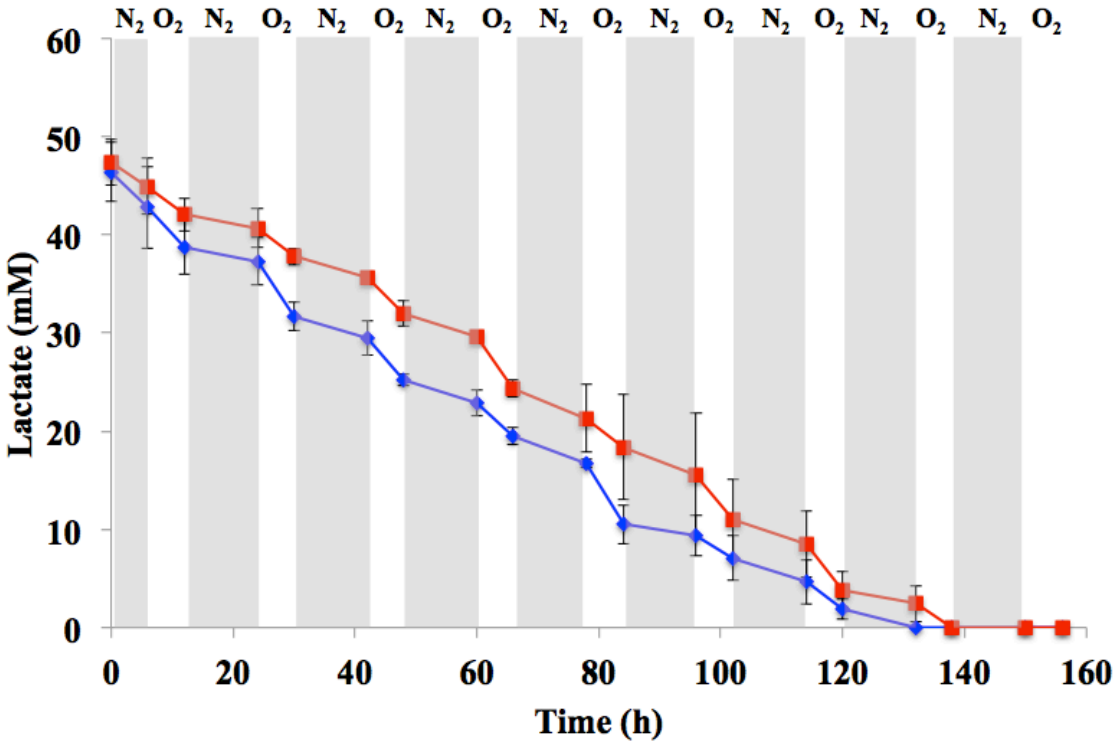

Figure 4.S3. Lactate concentration profiles during microbial Fenton degradation of CMC and xylan in batch liquid cultures of *S. oneidensis* amended with 10 mM Fe(III) and 1% w/v CMC/xylan with an aerobic/anaerobic cycling period of 6 h: blue (◆), CMC; red (■), xylan. Grey shaded areas correspond to anaerobic phases, and unshaded areas correspond to aerobic phases. Error bars represent range of errors in duplicate batch reactors.

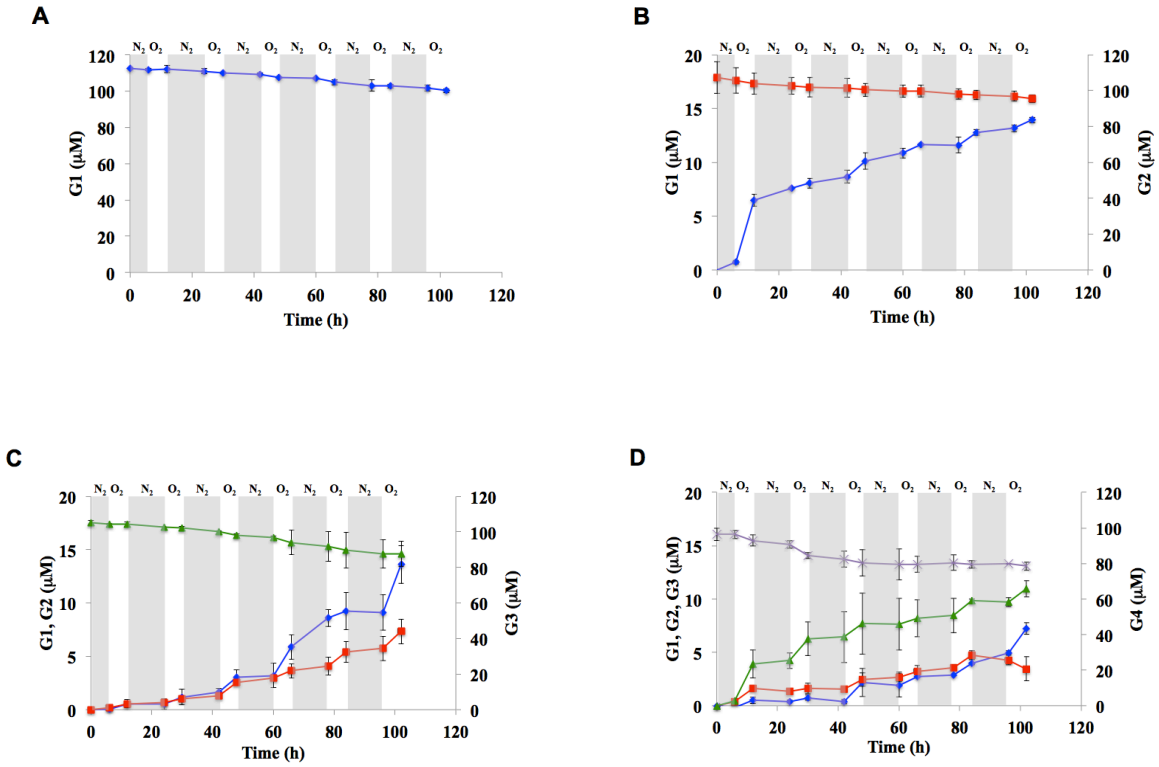

Figure. 4.S4. Concentration profiles during microbial Fenton degradation of cellodextrins in batch liquid cultures of *S. oneidensis* amended with 10 mM Fe(III) and 100 µM cellodextrins with an aerobic/anaerobic cycling period of 6 h: (A) G1 degradation; (B) G2 degradation; (C) G3 degradation; (D) G4 degradation; (E) G5 degradation; (F) G6 degradation; solid blue (◆), G1; solid red (■), G2; solid green (▲), G3; solid violet (x), G4; solid black (*), G5; solid orange (•), G6. Grey shaded areas correspond to anaerobic phases, and unshaded areas correspond to aerobic phases. Error bars represent range of errors in duplicate batch reactors.

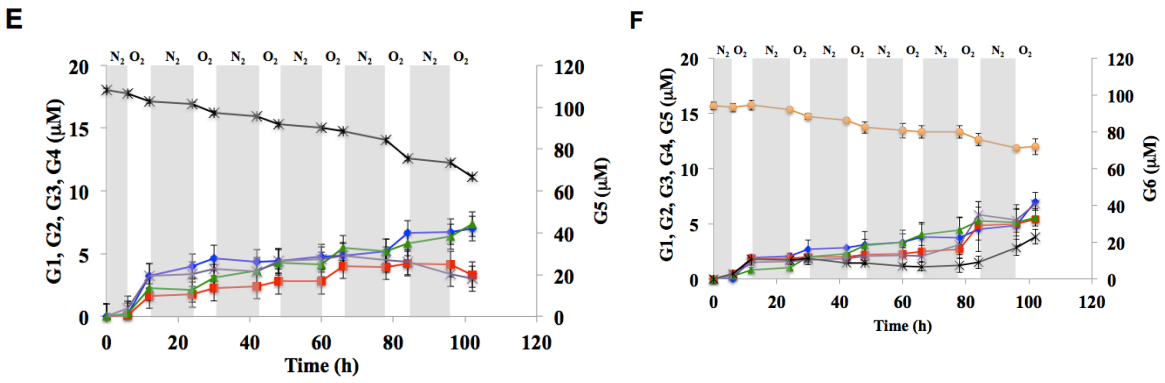

Figure 4.S4 continued

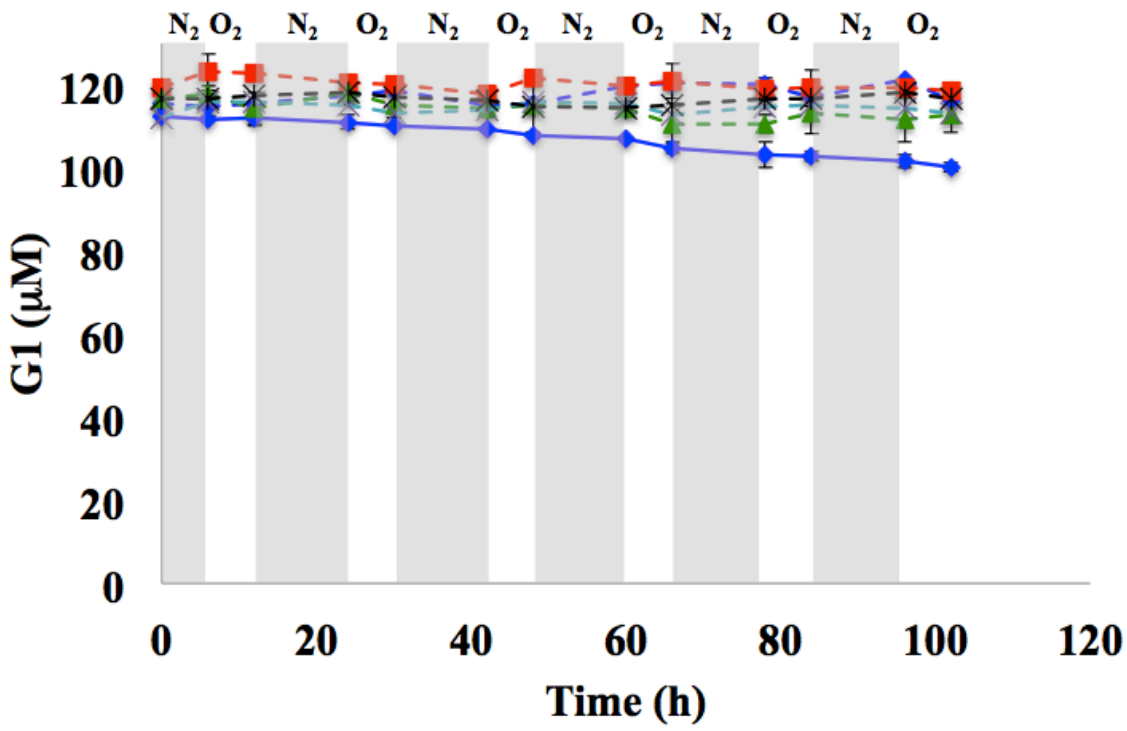

Figure 4.S5. Concentration profiles during microbial Fenton degradation of G1 in batch liquid cultures of *S. oneidensis* amended with 10 mM Fe(III) and 100 µM G1 with an aerobic/anaerobic cycling period of 6 h: solid, fenton reaction; dashed, control; blue (◆), cells omitted; red (■), Fe(III) omitted; green (▲), nitrate; violet (x), thiourea; black (*), anaerobic only; solid blue (◆), G1 fenton. Grey shaded areas correspond to anaerobic phases, and unshaded areas correspond to aerobic phases. Error bars represent range of errors in duplicate batch reactors.

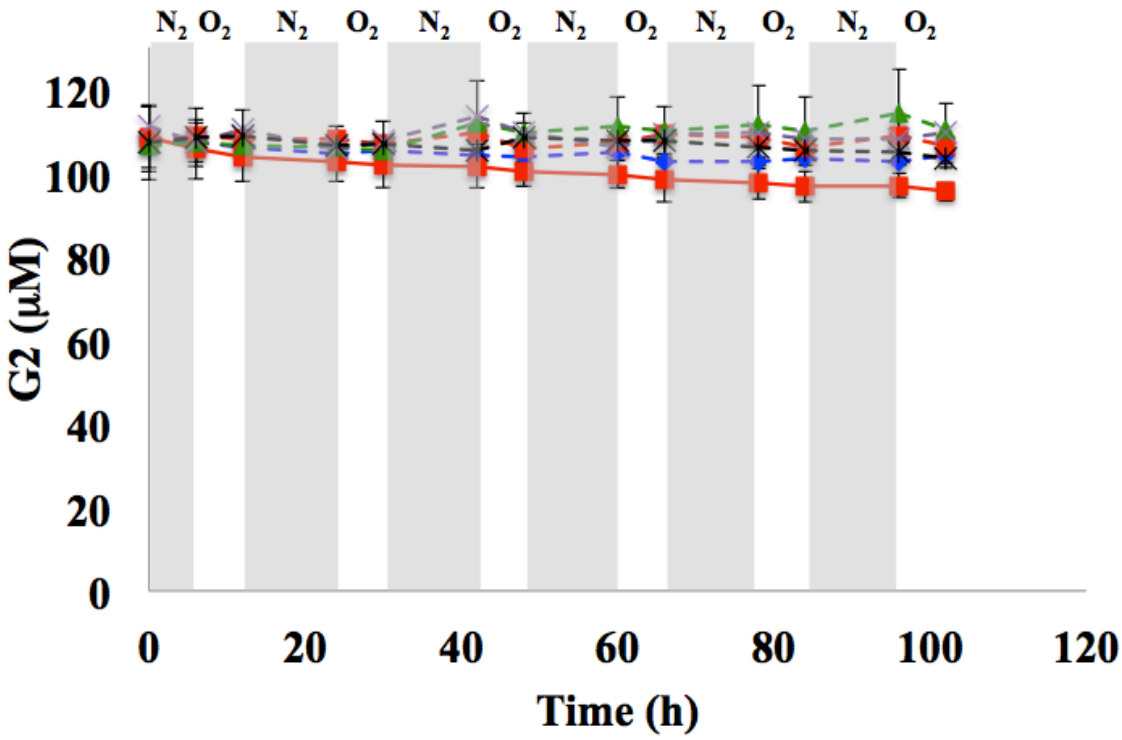

Figure 4.S6. Concentration profiles during microbial Fenton degradation of G2 in batch liquid cultures of *S. oneidensis* amended with 10 mM Fe(III) and 100 µM G2 with an aerobic/anaerobic cycling period of 6 h: solid, fenton reaction; dashed, control; blue (◆), cells omitted; red (■), Fe(III) omitted; green (▲), nitrate; violet (x), thiourea; black (*), anaerobic only; solid red (■), G2 fenton. Grey shaded areas correspond to anaerobic phases, and unshaded areas correspond to aerobic phases. Error bars represent range of errors in duplicate batch reactors.

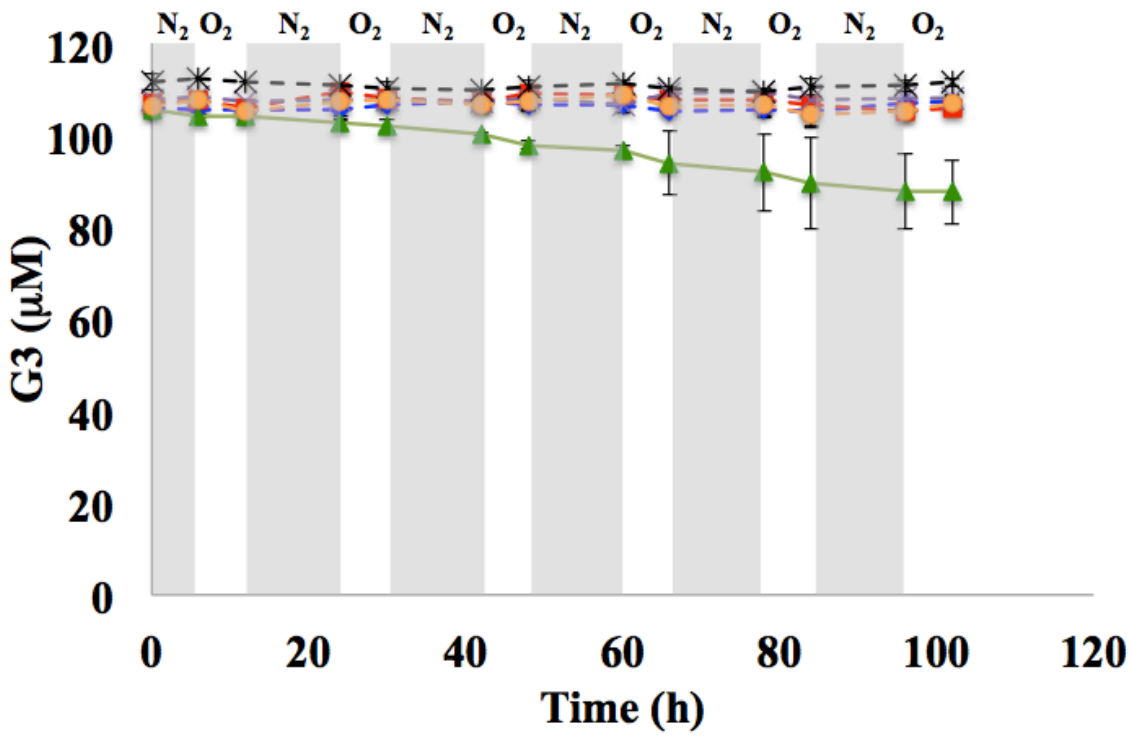

Figure 4.S7. Concentration profiles during microbial Fenton degradation of G3 in batch liquid cultures of *S. oneidensis* amended with 10 mM Fe(III) and 100 µM G3 with an aerobic/anaerobic cycling period of 6 h: solid, fenton reaction; dashed, control; blue (◆), cells omitted; red (■), Fe(III) omitted; green (▲), nitrate; violet (x), thiourea; black (*), anaerobic only; solid green (▲), G3 fenton. Grey shaded areas correspond to anaerobic phases, and unshaded areas correspond to aerobic phases. Error bars represent range of errors in duplicate batch reactors.

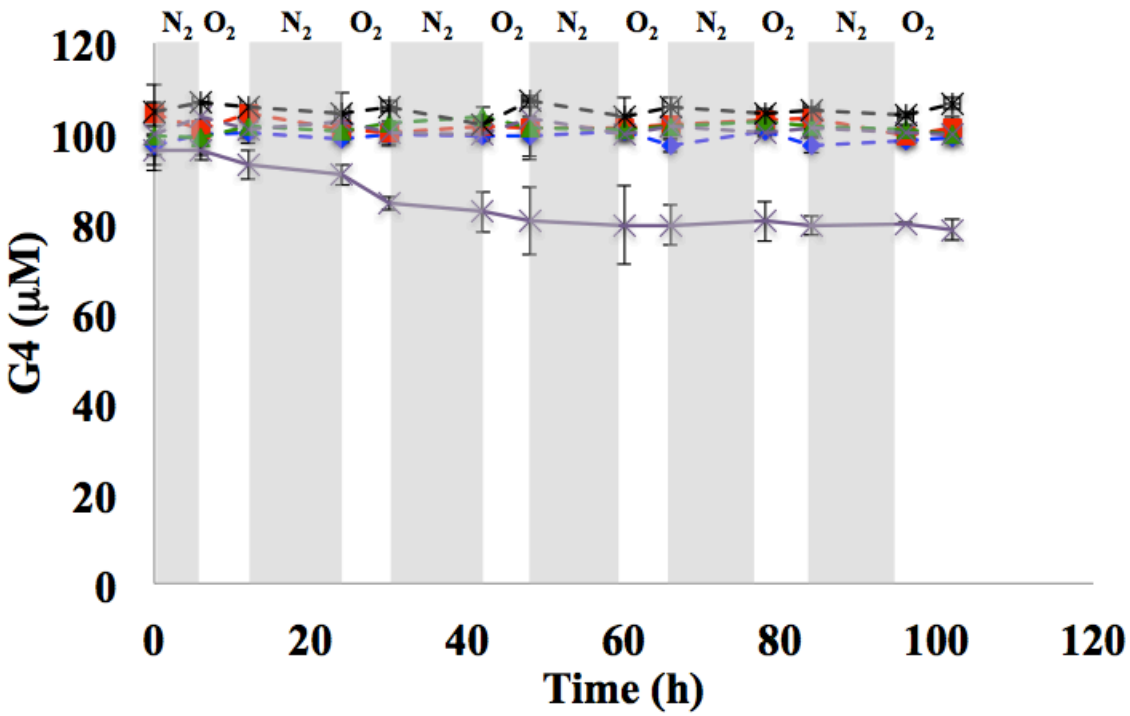

Figure 4.S8. Concentration profiles during microbial Fenton degradation of G4 in batch liquid cultures of *S. oneidensis* amended with 10 mM Fe(III) and 100 μM G4 with an aerobic/anaerobic cycling period of 6 h: solid, fenton reaction; dashed, control; blue (◆), cells omitted; red (■), Fe(III) omitted; green (▲), nitrate; violet (x), thiourea; black (*), anaerobic only; solid violet (x), G4 fenton. Grey shaded areas correspond to anaerobic phases, and unshaded areas correspond to aerobic phases. Error bars represent range of errors in duplicate batch reactors.

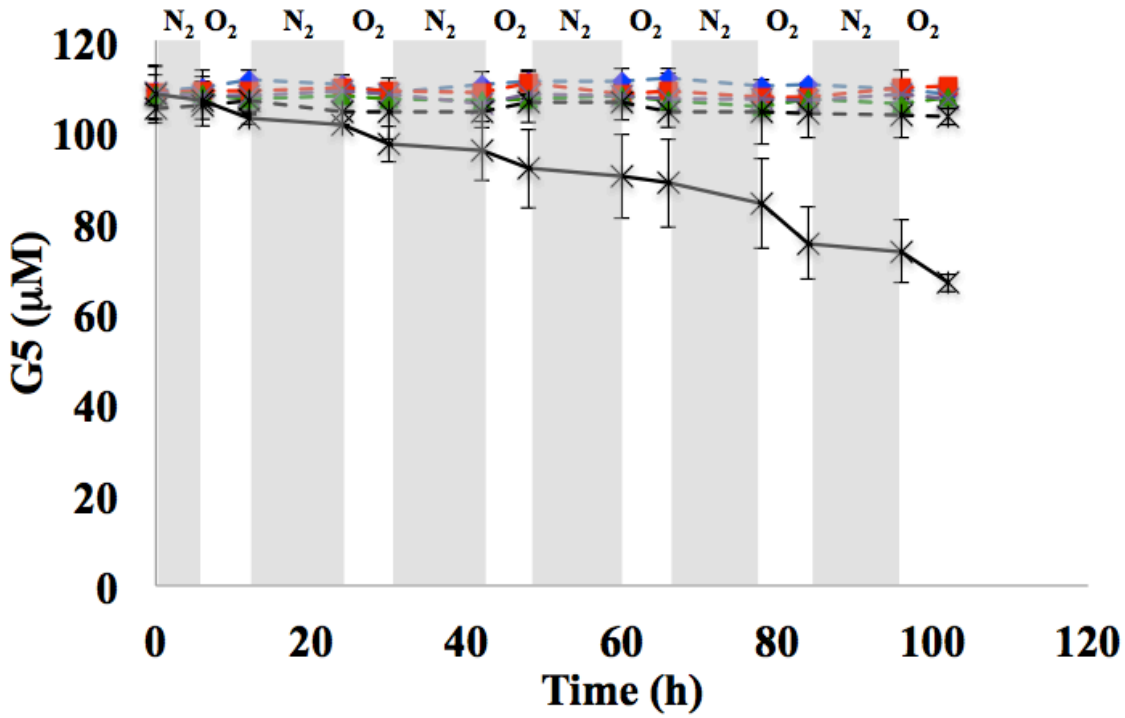

Figure 4.S9. Concentration profiles during microbial Fenton degradation of G5 in batch liquid cultures of *S. oneidensis* amended with 10 mM Fe(III) and 100 µM G5 with an aerobic/anaerobic cycling period of 6 h: solid, fenton reaction; dashed, control; blue (◆), cells omitted; red (■), Fe(III) omitted; green (▲), nitrate; violet (X), thiourea; black (*), anaerobic only; solid violet (x), G4 fenton. Grey shaded areas correspond to anaerobic phases, and unshaded areas correspond to aerobic phases. Error bars represent range of errors in duplicate batch reactors.

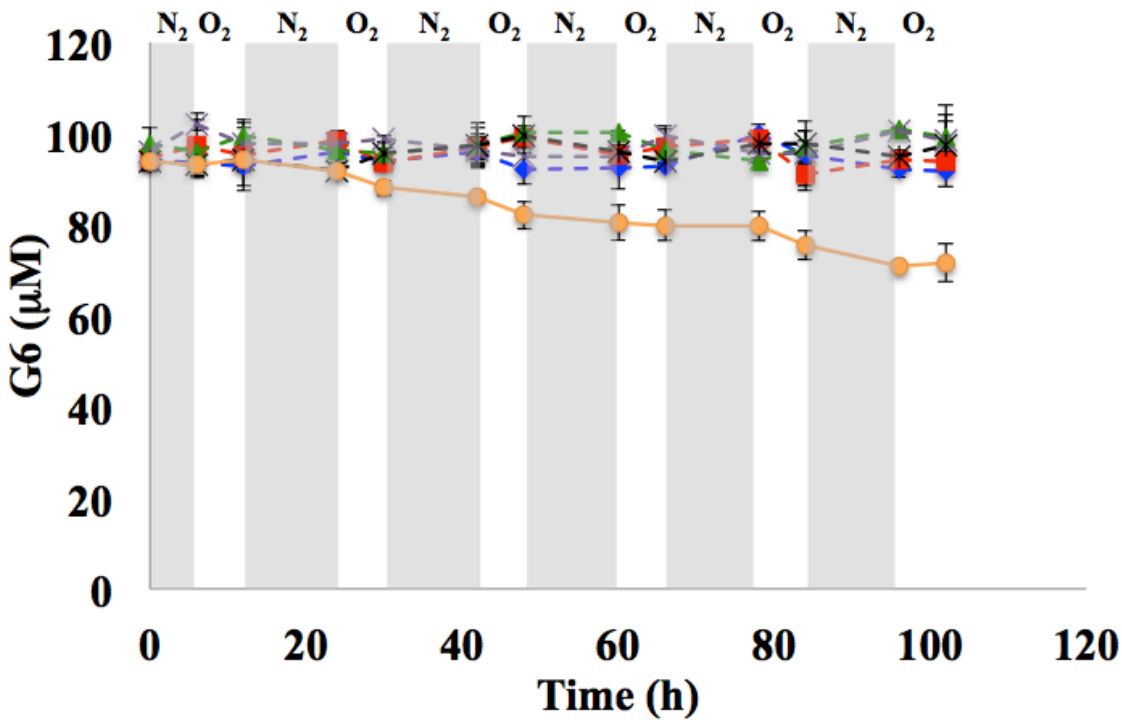

Figure 4.S10. Concentration profiles during microbial Fenton degradation of G6 in batch liquid cultures of *S. oneidensis* amended with 10 mM Fe(III) and 100 µM G6 with an aerobic/anaerobic cycling period of 6 h: solid, fenton reaction; dashed, control; blue (◆), cells omitted; red (■), Fe(III) omitted; green (▲), nitrate; violet (X), thiourea; black (*), anaerobic only; orange (•), G6 fenton. Grey shaded areas correspond to anaerobic phases, and unshaded areas correspond to aerobic phases. Error bars represent range of errors in duplicate batch reactors.

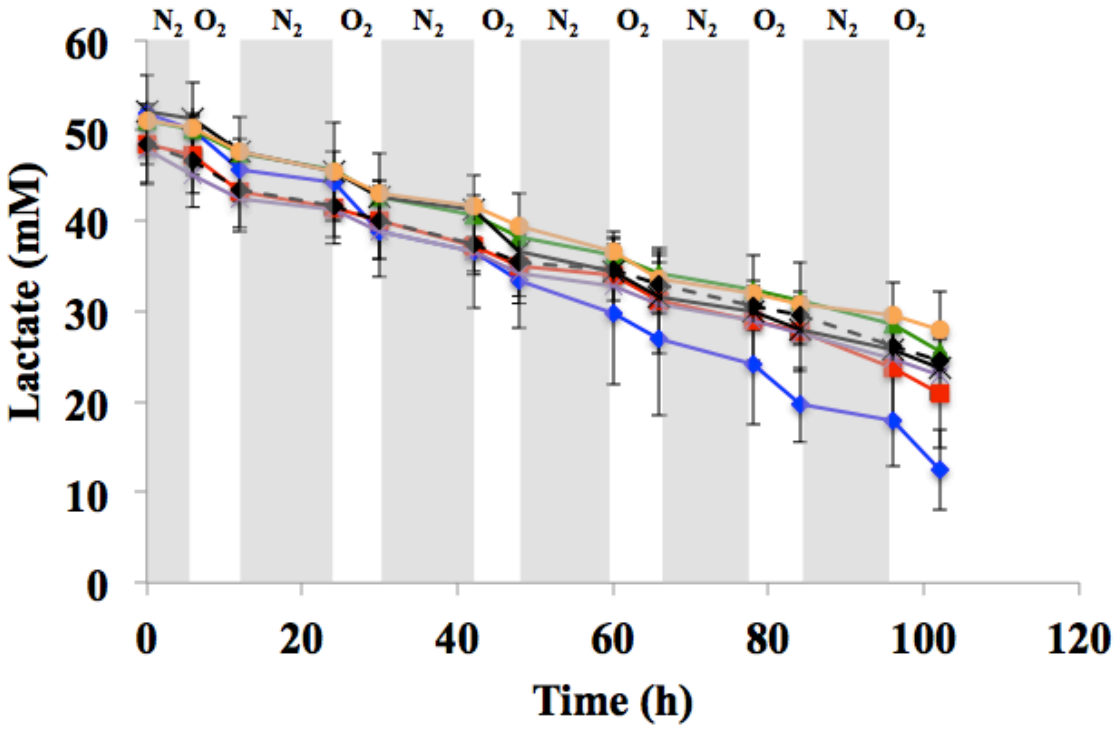

Figure 4.S11. Lactate concentration profiles during microbial Fenton degradation of cellodextrins in batch liquid cultures of *S. oneidensis* amended with 10 mM Fe(III) and 100 μM cellodextrins with an aerobic/anaerobic cycling period of 6 h: blue (◆), G1; red (■), G2; green (▲), G3; violet (x), G4; black (*), G5; orange (•), G6; dashed black (◆), no sugar . Grey shaded areas correspond to anaerobic phases, and unshaded areas correspond to aerobic phases. Error bars represent range of errors in duplicate batch reactors.

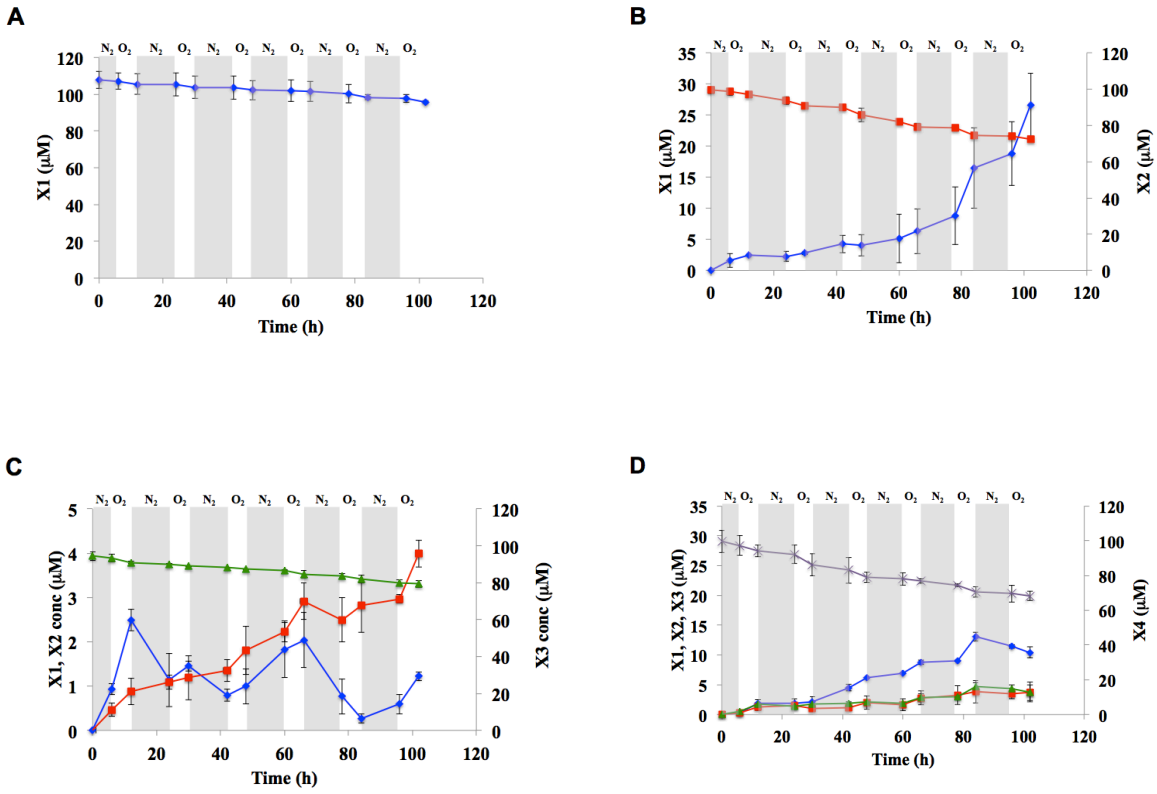

Figure. 4.S12. Concentration profiles during microbial Fenton degradation of xylodextrins in batch liquid cultures of *S. oneidensis* amended with 10 mM Fe(III) and 100 µM xylodextrins with an aerobic/anaerobic cycling period of 6 h: (A) X1 degradation; (B) X2 degradation; (C) X3 degradation; (D) X4 degradation; (E) X5 degradation; (F) X6 degradation; solid blue (◆), X1; solid red (■), X2; solid green (▲), X3; solid violet (x), X4; solid black (*), X5; solid orange (●), X6. Grey shaded areas correspond to anaerobic phases, and unshaded areas correspond to aerobic phases. Error bars represent range of errors in duplicate batch reactors.

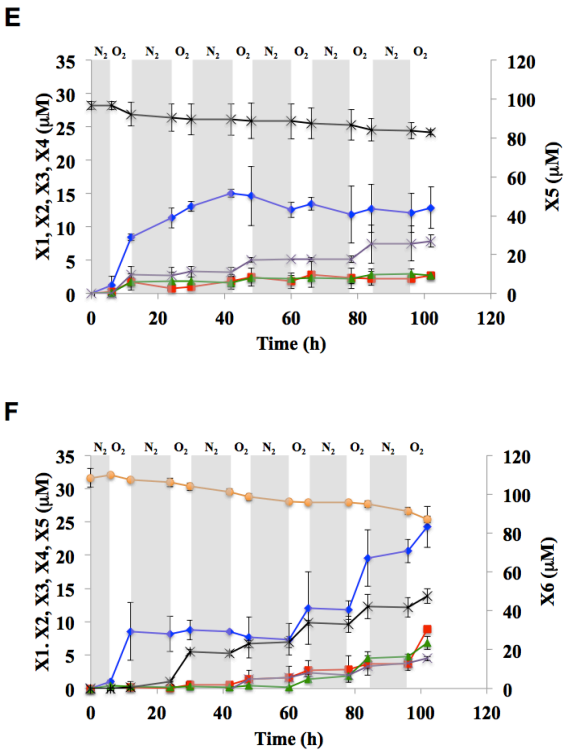

Figure 4.S12 continued

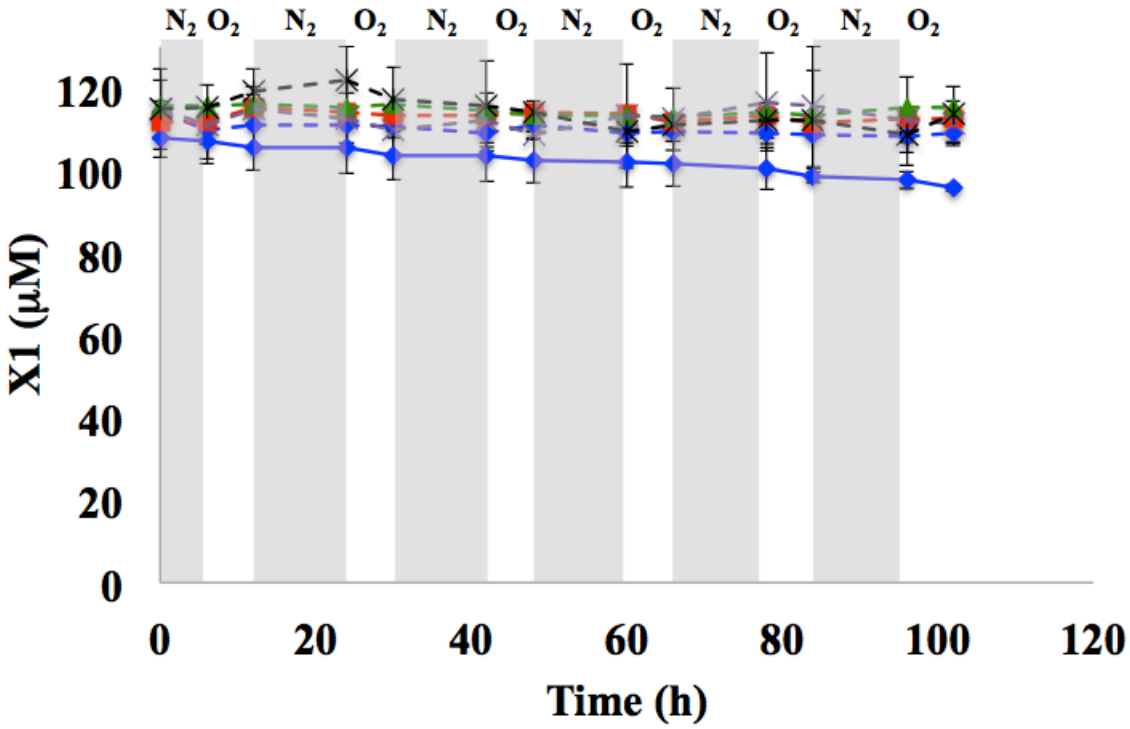

Figure 4.S13. Concentration profiles during microbial Fenton degradation of X1 in batch liquid cultures of *S. oneidensis* amended with 10 mM Fe(III) and 100 µM X1 with an aerobic/anaerobic cycling period of 6 h: solid, fenton reaction; dashed, control; blue (◆), cells omitted; red (■), Fe(III) omitted; green (▲), nitrate; violet (x), thiourea; black (*), anaerobic only; solid blue (◆), X1 fenton. Grey shaded areas correspond to anaerobic phases, and unshaded areas correspond to aerobic phases. Error bars represent range of errors in duplicate batch reactors.

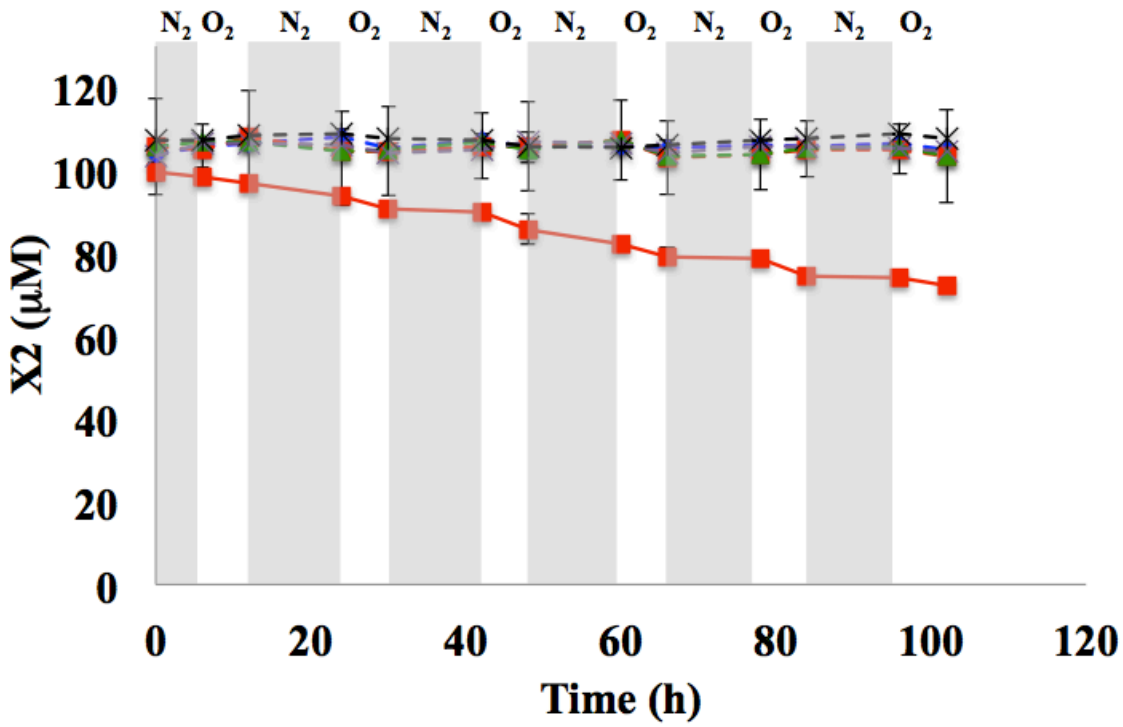

Figure 4.S14. Concentration profiles during microbial Fenton degradation of X2 in batch liquid cultures of *S. oneidensis* amended with 10 mM Fe(III) and 100 µM X2 with an aerobic/anaerobic cycling period of 6 h: solid, fenton reaction; dashed, control; blue (◆), cells omitted; red (■), Fe(III) omitted; green (▲), nitrate; violet (x), thiourea; black (*), anaerobic only; solid red (■), X2 fenton. Grey shaded areas correspond to anaerobic phases, and unshaded areas correspond to aerobic phases. Error bars represent range of errors in duplicate batch reactors.

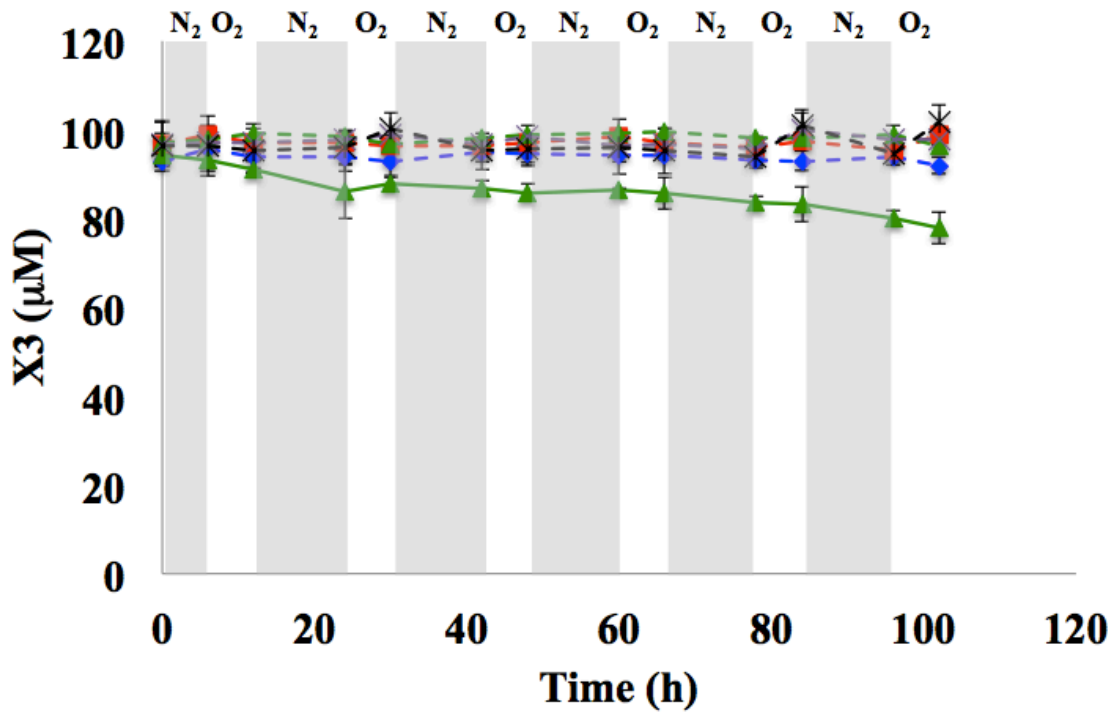

Figure 4.S15. Concentration profiles during microbial Fenton degradation of X3 in batch liquid cultures of *S. oneidensis* amended with 10 mM Fe(III) and 100 µM X3 with an aerobic/anaerobic cycling period of 6 h: solid, fenton reaction; dashed, control; blue (◆), cells omitted; red (■), Fe(III) omitted; green (▲), nitrate; violet (x), thiourea; black (*), anaerobic only; solid green (▲), X3 fenton. Grey shaded areas correspond to anaerobic phases, and unshaded areas correspond to aerobic phases. Error bars represent range of errors in duplicate batch reactors.

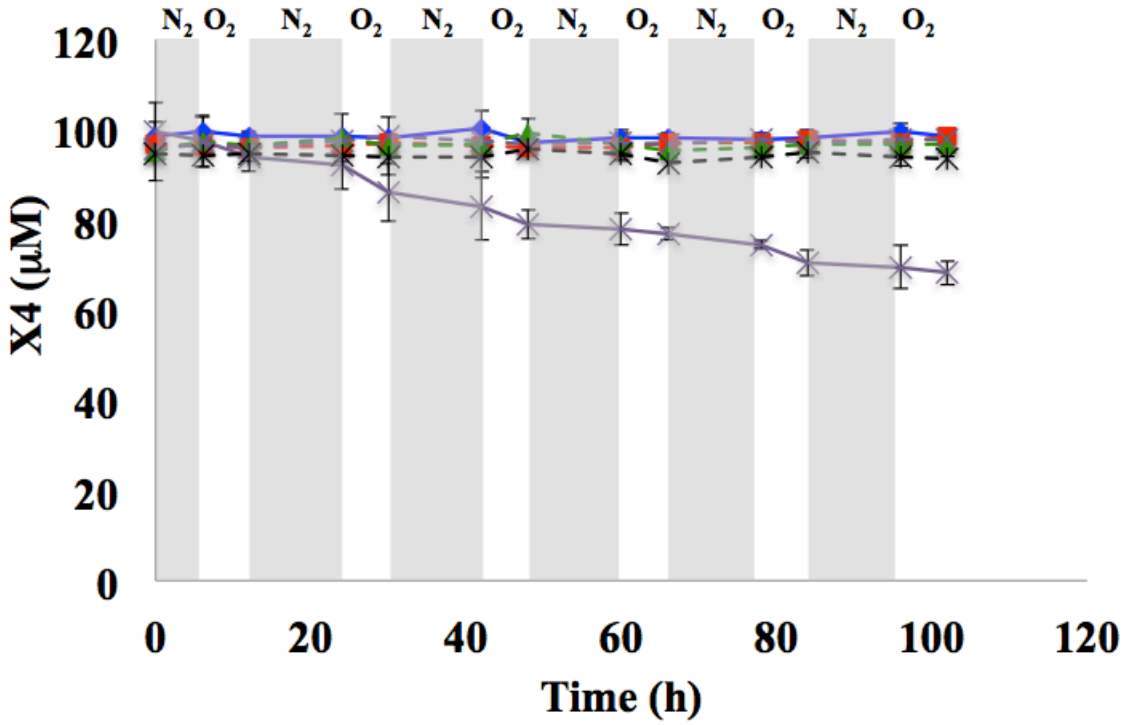

Figure 4.S16. Concentration profiles during microbial Fenton degradation of X4 in batch liquid cultures of *S. oneidensis* amended with 10 mM Fe(III) and 100 µM X4 with an aerobic/anaerobic cycling period of 6 h: solid, fenton reaction; dashed, control; blue (◆), cells omitted; red (■), Fe(III) omitted; green (▲), nitrate; violet (x), thiourea; black (*), anaerobic only; solid violet (x), X4 fenton. Grey shaded areas correspond to anaerobic phases, and unshaded areas correspond to aerobic phases. Error bars represent range of errors in duplicate batch reactors.

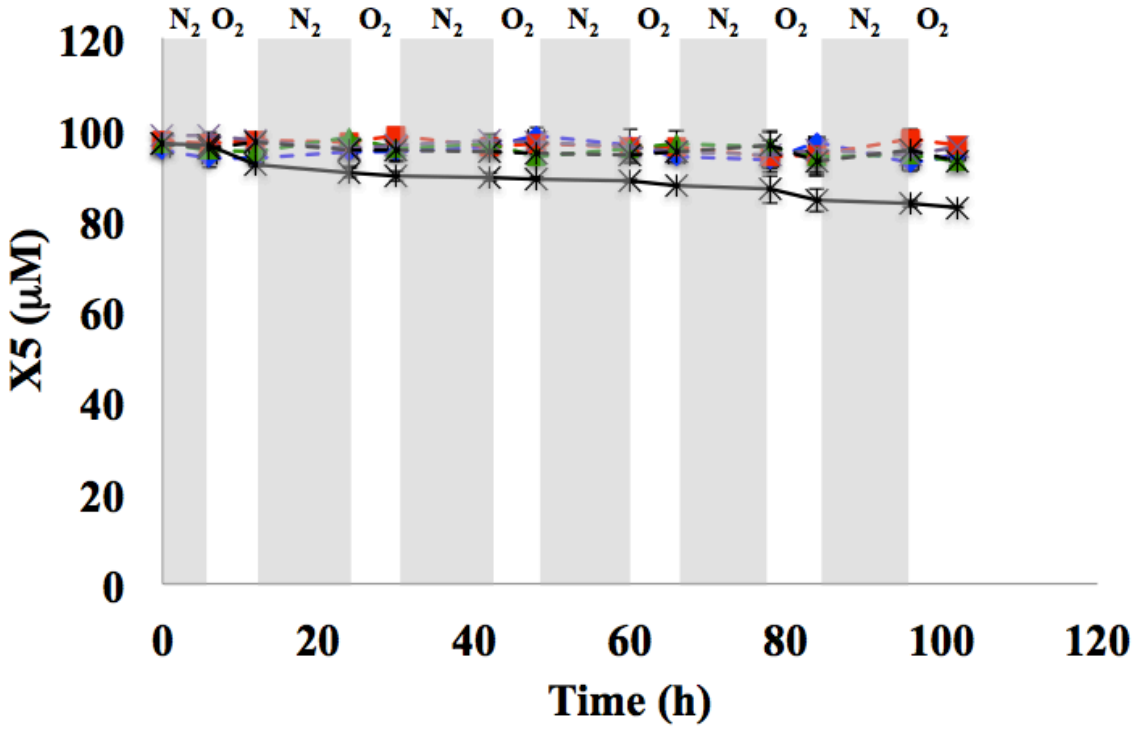

Figure 4.S17. Concentration profiles during microbial Fenton degradation of X5 in batch liquid cultures of *S. oneidensis* amended with 10 mM Fe(III) and 100 µM X5 with an aerobic/anaerobic cycling period of 6 h: solid, fenton reaction; dashed, control; blue (◆), cells omitted; red (■), Fe(III) omitted; green (▲), nitrate; violet (x), thiourea; black (*), anaerobic only; solid black (*), X5 fenton. Grey shaded areas correspond to anaerobic phases, and unshaded areas correspond to aerobic phases. Error bars represent range of errors in duplicate batch reactors.

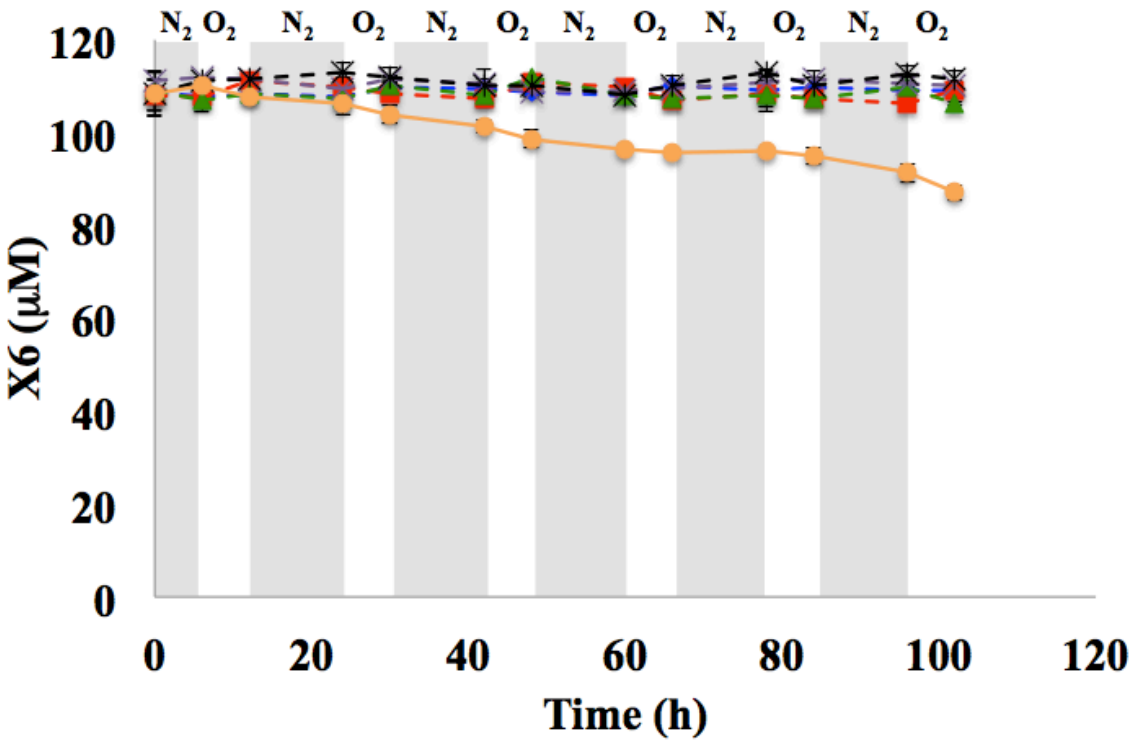

Figure 4.S18. Concentration profiles during microbial Fenton degradation of X6 in batch liquid cultures of *S. oneidensis* amended with 10 mM Fe(III) and 100 μM X6 with an aerobic/anaerobic cycling period of 6 h: solid, fenton reaction; dashed, control; blue (◆), cells omitted; red (■), Fe(III) omitted; green (▲), nitrate; violet (X), thiourea; black (*), anaerobic only; orange (•), X6 fenton. Grey shaded areas correspond to anaerobic phases, and unshaded areas correspond to aerobic phases. Error bars represent range of errors in duplicate batch reactors.

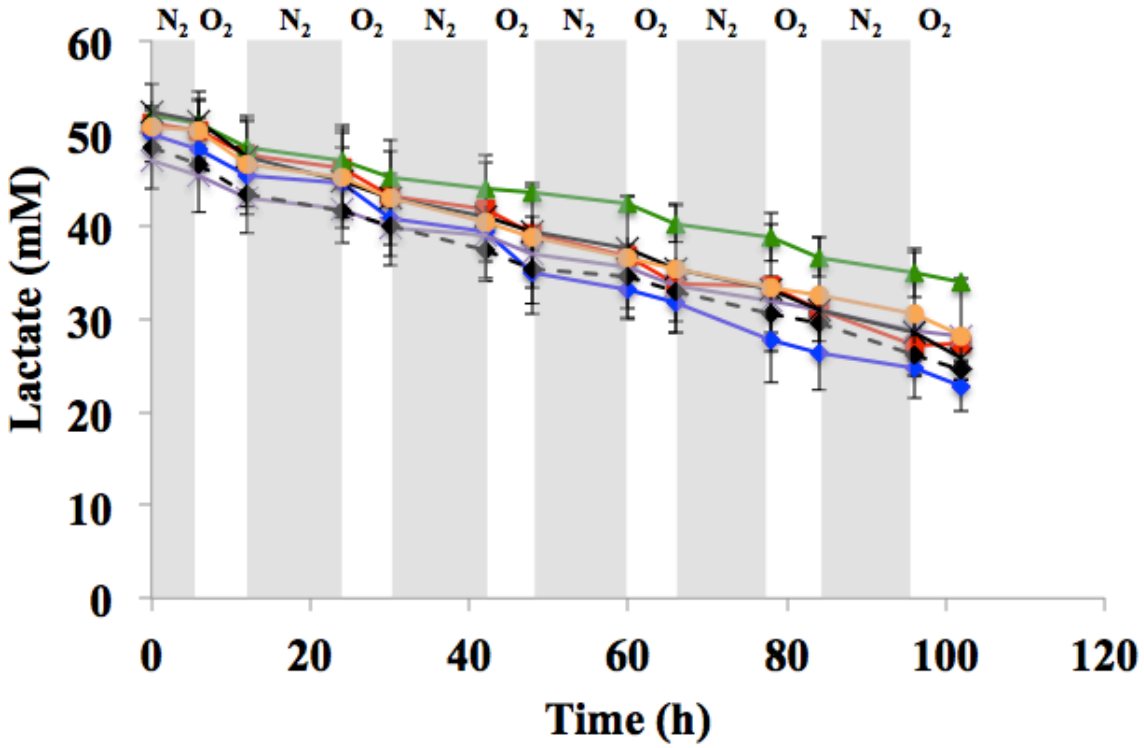

Figure 4.S19. Lactate concentration profiles during microbial Fenton degradation of xylodextrins in batch liquid cultures of *S. oneidensis* amended with 10 mM Fe(III) and 100 µM xylodextrins with an aerobic/anaerobic cycling period of 6 h: blue (◆), X1; red (■), X2; green (▲), X3; violet (x), X4; black (*), X5; orange (•), X6; dashed black (◆), no sugar . Grey shaded areas correspond to anaerobic phases, and unshaded areas correspond to aerobic phases. Error bars represent range of errors in duplicate batch reactors.

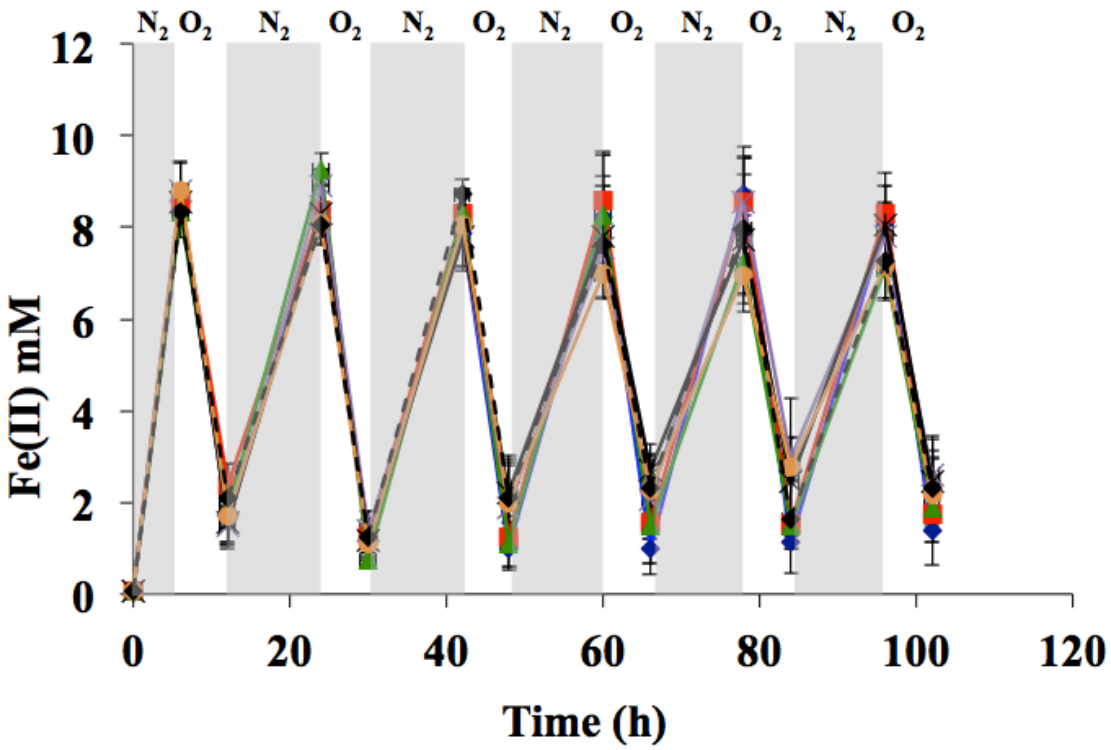

Figure 4.S20. Fe(II) concentration profiles during microbial Fenton degradation of cellodextrins in batch liquid cultures of *S. oneidensis* amended with 10 mM Fe(III) and 100 μM cellodextrins with an aerobic/anaerobic cycling period of 6 h: blue (◆), G1; red (■), G2; green (▲), G3; violet (x), G4; black (*), G5; orange (•), G6; dashed black (◆), no sugar. Grey shaded areas correspond to anaerobic phases, and unshaded areas correspond to aerobic phases. Error bars represent range of errors in duplicate batch reactors.

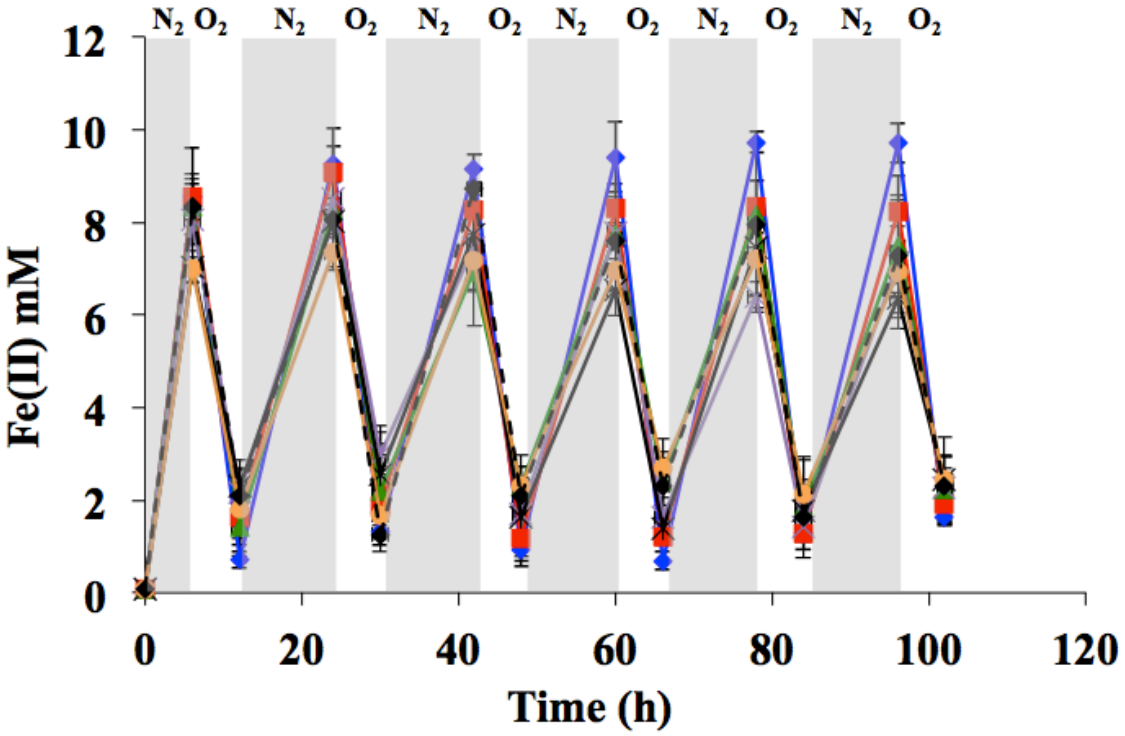

Figure 4.S21. Fe(II) concentration profiles during microbial Fenton degradation of xylodextrins in batch liquid cultures of *S. oneidensis* amended with 10 mM Fe(III) and 100 µM xylodextrins with an aerobic/anaerobic cycling period of 6 h: blue (◆), X1; red (■), X2; green (▲), X3; violet (x), X4; black (*), X5; orange (•), X6; dashed black (◆), no sugar . Grey shaded areas correspond to anaerobic phases, and unshaded areas correspond to aerobic phases. Error bars represent range of errors in duplicate batch reactors.

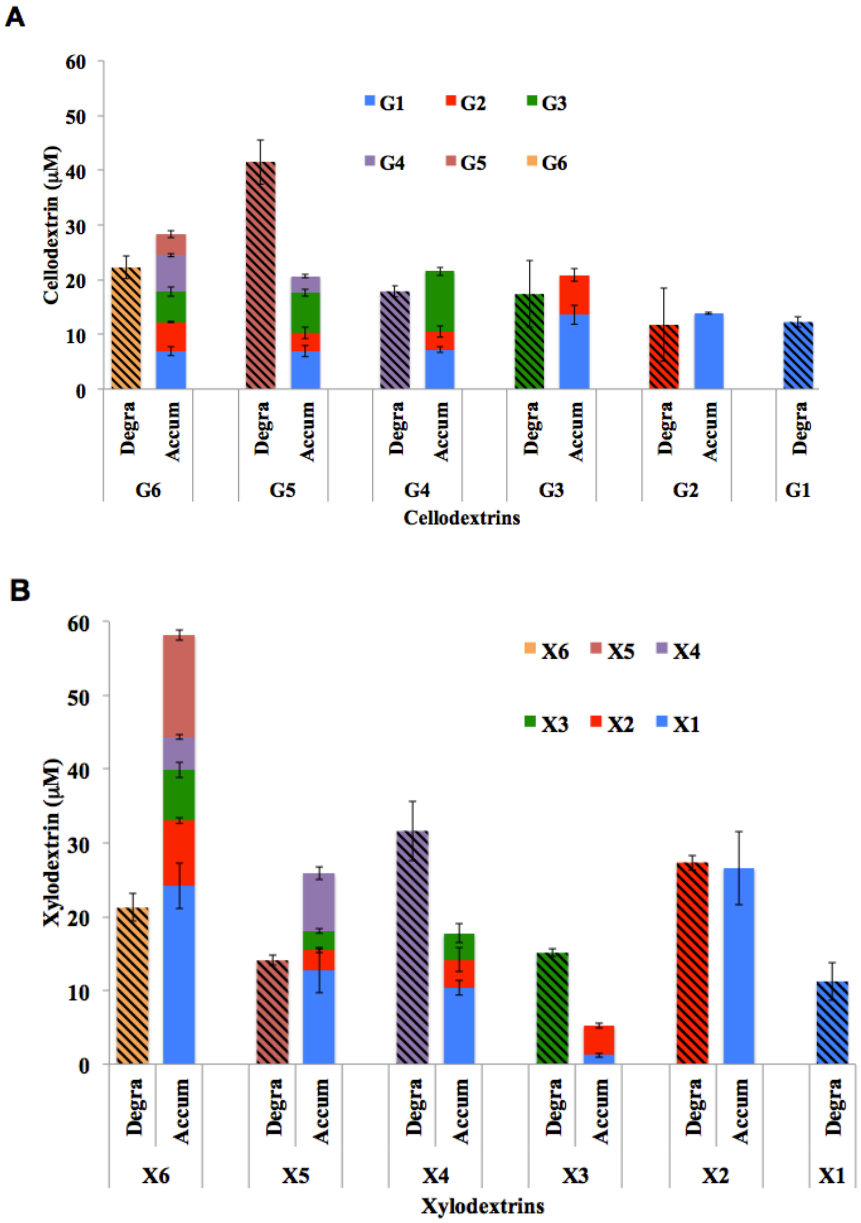

Figure 4.S22. Degradation and accumulation of cellodextrin and xylodextrin compounds during microbial Fenton degradation in batch liquid cultures of *S. oneidensis* amended with 10 mM Fe(III) and 100 μM of individual cellodextrin (or xylodextrin) compounds with an aerobic and anaerobic cycling period of 6 and 12 h respectively. (A) cellodextrins; (B) xylodextrins. stripped fill; degradation, solid fill; accumulation. Stacked columns depict individual cellodextrin (or xylodetrin) compounds. Error bars represent range of errors in duplicate batch reactors.

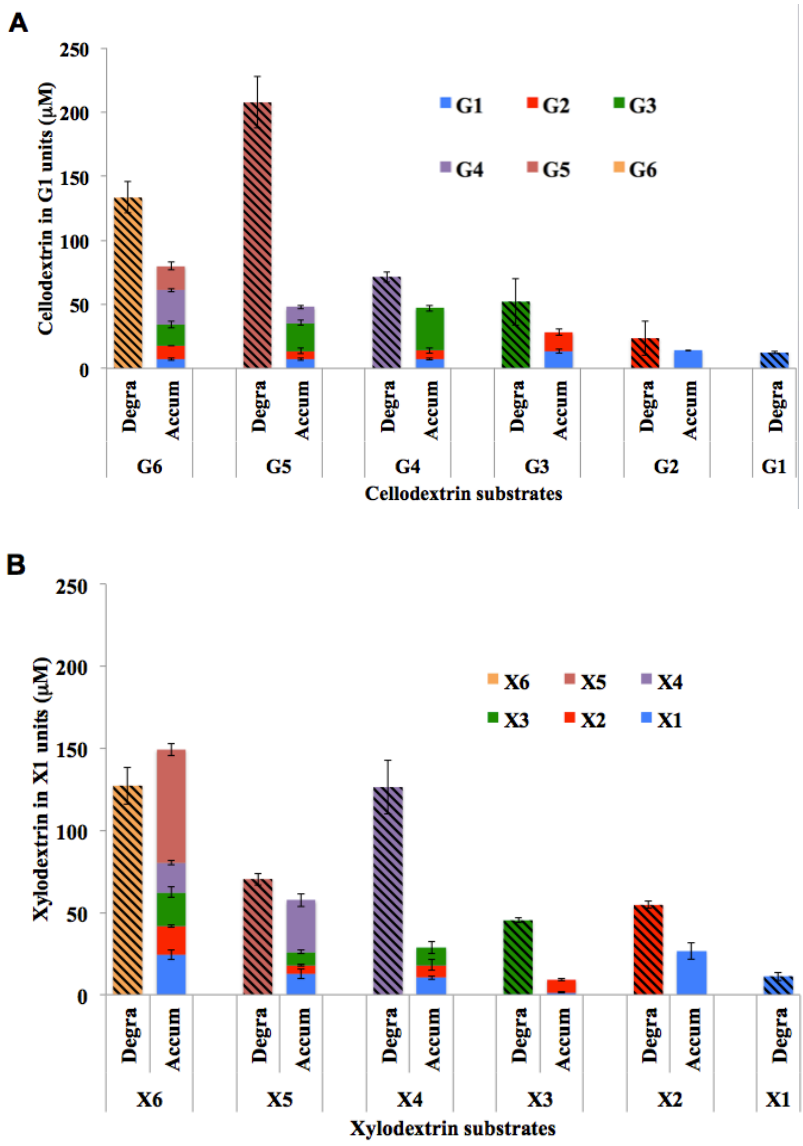

Figure. 4.S23. Degradation and accumulation of cellodextrin and xylodextrin compounds (concentrations are calculated in terms of G1 or X1 units for all compounds) during microbial Fenton degradation in batch liquid cultures of *S. oneidensis* amended with 10 mM Fe(III) and 100 µM of individual cellodextrin (or xylodextrin) compounds with an aerobic and anaerobic cycling period of 6 and 12 h respectively. (A) cellodextrins; (B) xylodextrins. stripped fill; degradation, solid fill; accumulation. Stacked columns depict individual cellodextrin (or xylodetrin) compounds. Error bars represent range of errors in duplicate batch reactors.

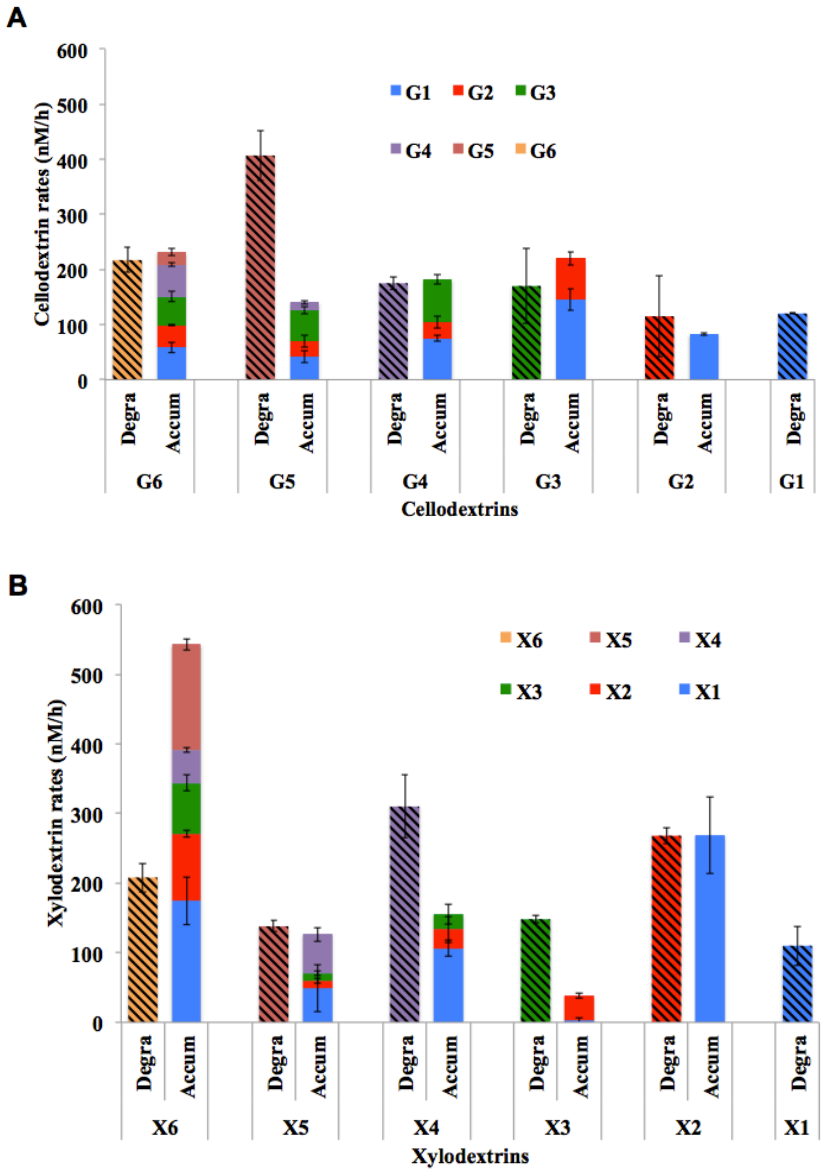

Figure. 4.S24. Degradation and accumulation rates of cellodextrin and xylodextrin compounds during microbial Fenton degradation in batch liquid cultures of *S. oneidensis* amended with 10 mM Fe(III) and 100 µM of individual cellodextrin (or xylodextrin) compounds with an aerobic and anaerobic cycling period of 6 and 12 h respectively. (A) cellodextrins; (B) xylodextrins. stripped fill; degradation, solid fill; accumulation. Stacked columns depict contribution of individual cellodextrin (or xylodetrin) compounds accumulation. Error bars represent range of errors in duplicate batch reactors.

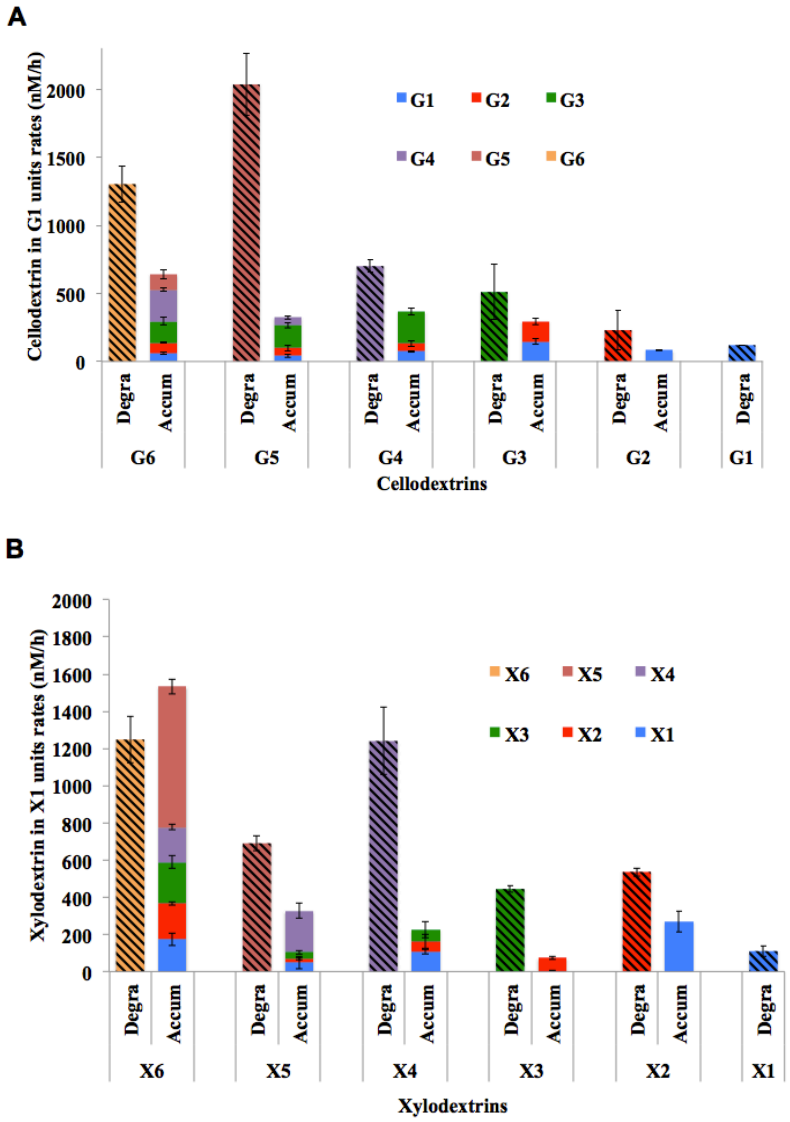

Figure. 4.S25. Degradation and accumulation rates of cellodextrin and xylodextrin (rates are calculated in terms of G1 or X1 units for all compounds) compounds during microbial Fenton degradation in batch liquid cultures of *S. oneidensis* amended with 10 mM Fe(III) and 100 µM of individual cellodextrin (or xylodextrin) compounds with an aerobic and anaerobic cycling period of 6 and 12 h respectively. (A) cellodextrins; (B) xylodextrins. stripped fill; degradation, solid fill; accumulation. Stacked columns depict contribution of individual cellodextrin (or xylodetrin) compounds accumulation. Error bars represent range of errors in duplicate batch reactors.

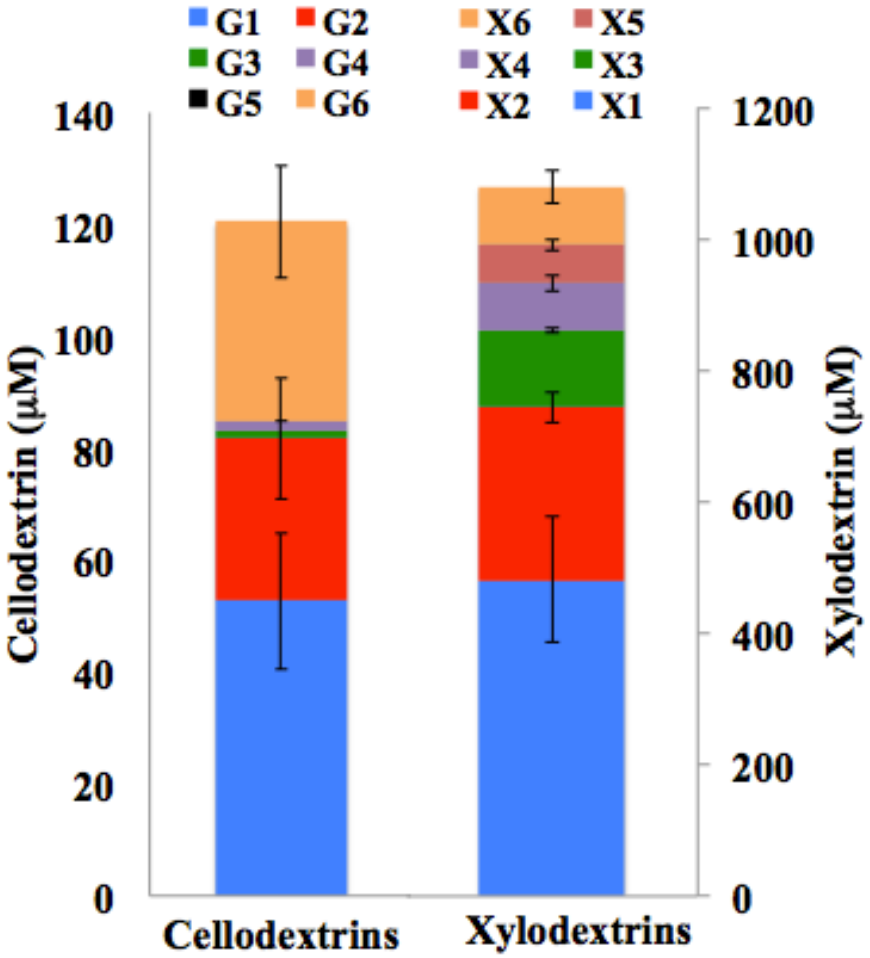

Figure. 4.S26. Accumulation of cellodextrin and xylodextrin compounds during microbial Fenton degradation in batch liquid cultures of *S. oneidensis* amended with 10 mM Fe(III) and 1% w/v of CMC (or xylan) with an aerobic and anaerobic cycling period of 6 and 12 h respectively. Stacked columns depict contribution of individual cellodextrin (or xylodetrin) compounds accumulation. Error bars represent range of errors in duplicate batch reactors.

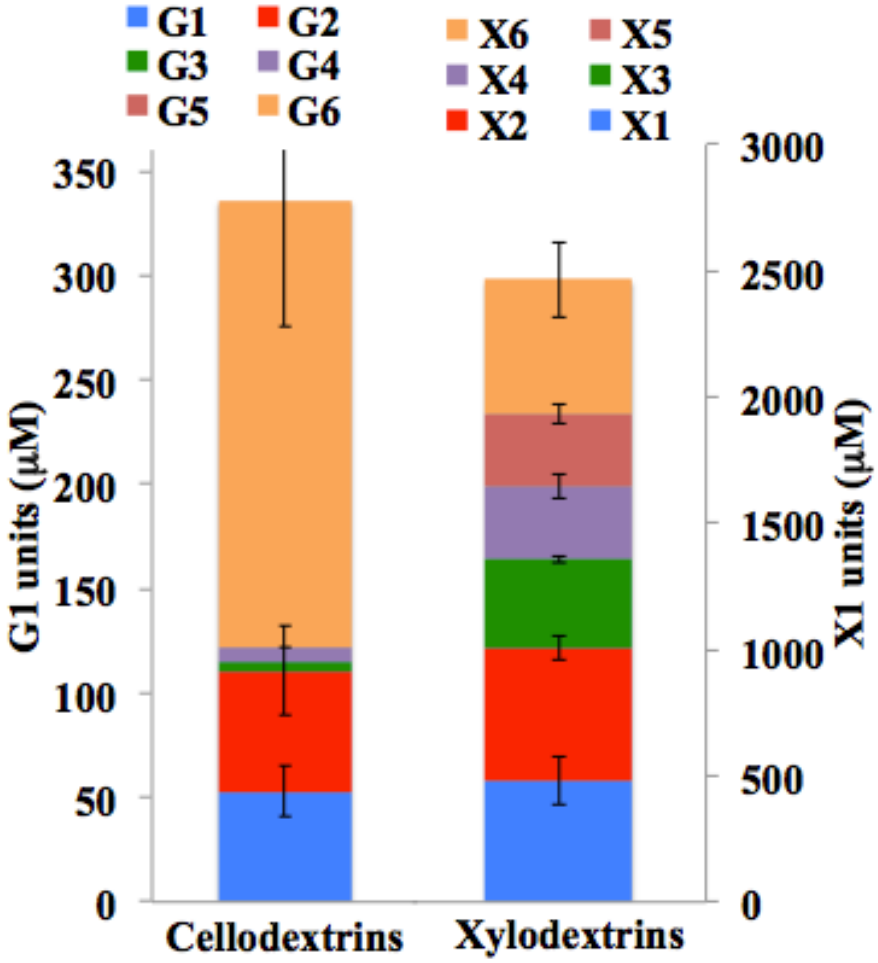

Figure. 4.S27. Accumulation of cellodextrin and xylodextrin compounds during microbial Fenton degradation in batch liquid cultures of *S. oneidensis* amended with 10 mM Fe(III) and 1% w/v of CMC (or xylan) with an aerobic and anaerobic cycling period of 6 and 12 h respectively. Stacked columns depict contribution of individual cellodextrin (or xylodetrin) compounds accumulation. Error bars represent range of errors in duplicate batch reactors. Concentrations are calculated in terms of G1 (or X1) units for all compounds

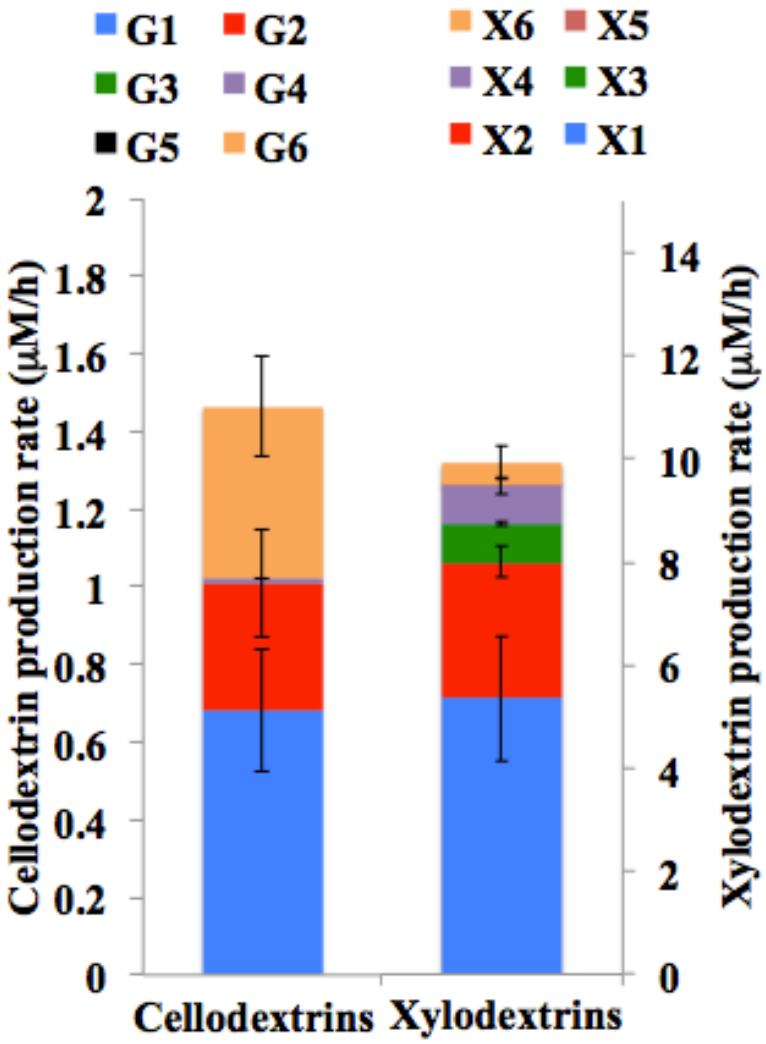

Figure. 4.S28. Accumulation rates of cellodextrin and xylodextrin compounds during microbial Fenton degradation in batch liquid cultures of *S. oneidensis* amended with 10 mM Fe(III) and 1% w/v CMC (or xylan) with an aerobic and anaerobic cycling period of 6 and 12 h respectively. Stacked columns depict contribution of individual cellodextrin (or xylodetrin) compounds produced. Error bars represent range of errors in duplicate batch reactors.

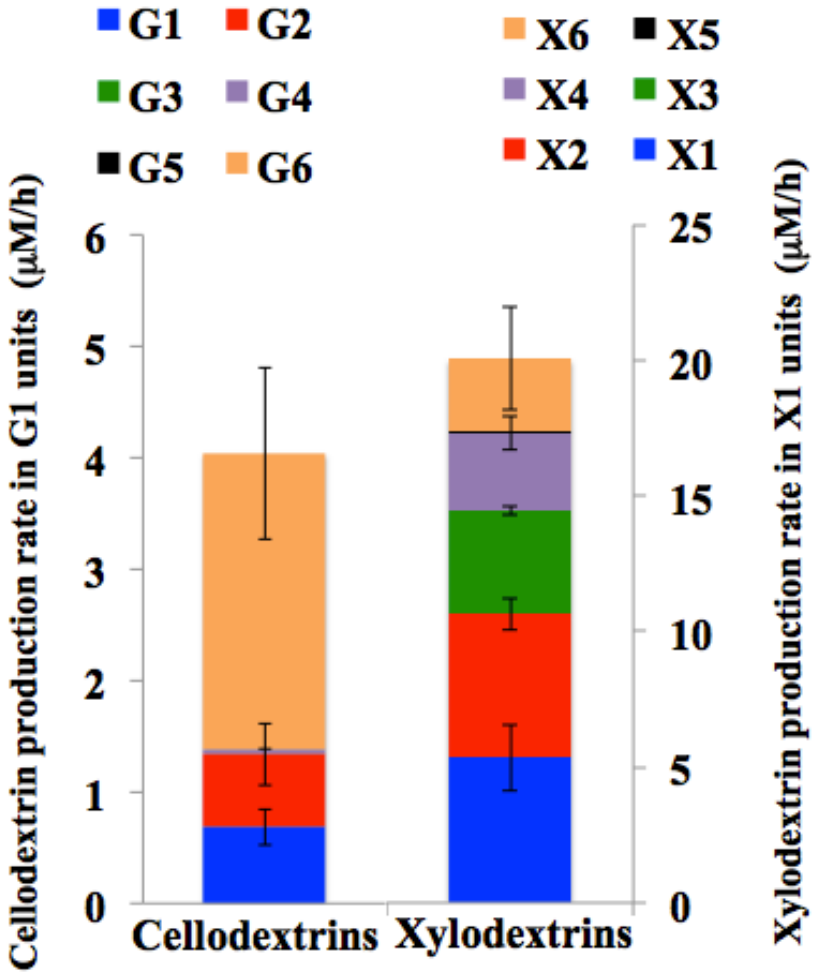

Figure. 4.S29. Accumulation rates of cellodextrin and xylodextrin compounds during microbial Fenton degradation in batch liquid cultures of *S. oneidensis* amended with 10 mM Fe(III) and 1% w/v CMC (or xylan) with an aerobic and anaerobic cycling period of 6 and 12 h respectively. Stacked columns depict contribution of individual cellodextrin (or xylodetrin) compounds produced. Error bars represent range of errors in duplicate batch reactors. Concentrations are calculated in terms of G1 (or X1) units for all compounds

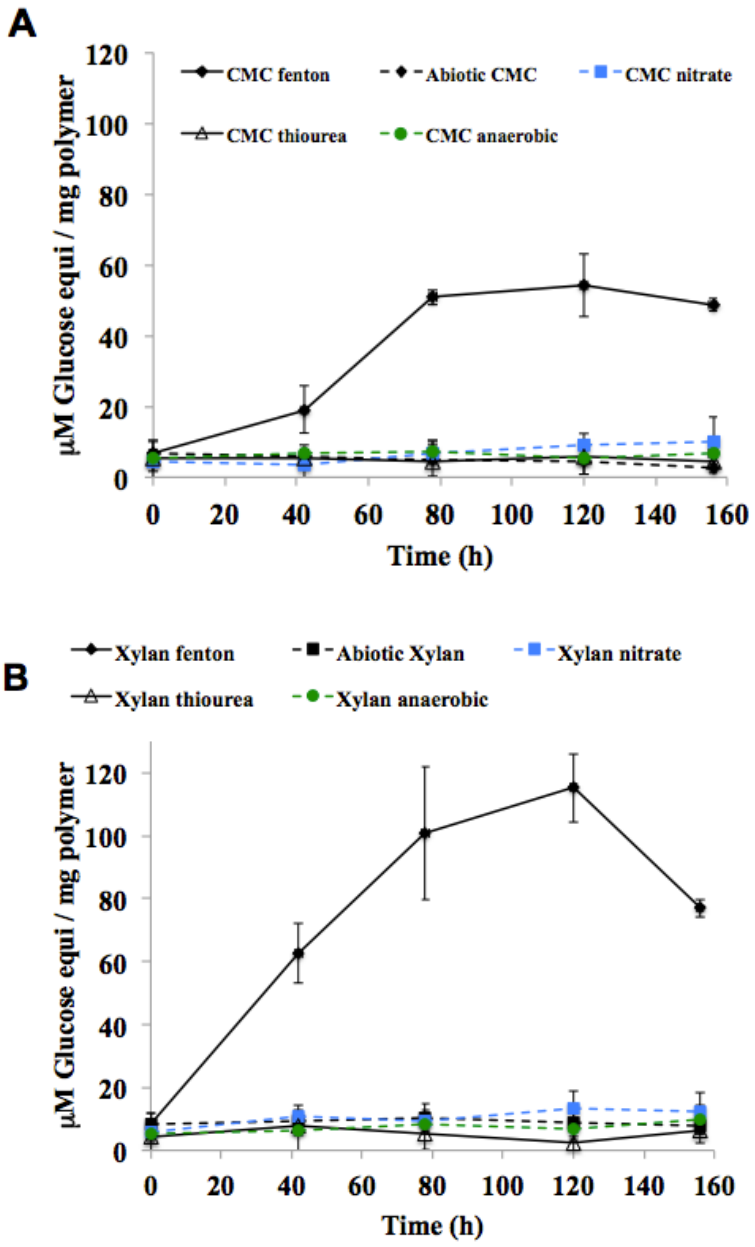

Figure. 4.S30. Concentration profile of reducing end concentration of insoluble polymer during microbial Fenton degradation of CMC (or xylan) in batch liquid cultures of *S. oneidensis* amended with 10 mM Fe(III) and 1% w/v CMC with an aerobic and anaerobic cycling period of 6 and 12 h respectively: **(A)** CMC; **(B)** xylan; solid black (◆), fenton reaction; dashed blue (■), nitrate; dashed green (•), anaerobic; dashed black (◆), abiotic; unfilled solid black (▲), thiourea. Error bars represent range of errors in duplicate batch reactors.

Table 4.S1. Limit of detection (LOD) and the limit of quantitation (LOQ) of analytes in this study

Compound	Limit of detection (LOD) (μM)	Limit of quantitation (LOQ) (μM)
Lactate	17.9	59.9
Glucose	1.3	3.9
Cellobiose	1.2	5.1
Cellotriose	0.9	2.9
Cellotetraose	0.9	2.7
Cellopentaose	1.0	3.2
Cellohexaose	0.64	2.0
Xylose	0.9	2.9
Xylobiose	2.5	7.6
Xylotriose	2.0	5.8
Xylotetraose	1.0	3.1
Xylopentaose	1.9	5.7
Xylohexaose	2.8	8.6

Table 4.S2. Retention time of standard sugar compounds in this study

Compound	Retention time (min)
Glucose	21.8
Cellobiose	15.1
Cellotriose	11.7
Cellotetraose	10.7
Cellopentaose	9.95
Cellohexaose	9.43
Xylose	26.2
Xylobiose	22.6
Xylotriose	16.43
Xylotetraose	13.84
Xylopentaose	12.9
Xylohexaose	12.14

Table 4.S3: Composition of LS medium

Compound	Concentration (mM)
Sodium DL lactate	10
Potassium Phosphate	10
NH_4SO_4	15
$MgSO_4.\ 7H_2O$	1
$CaCl_2.2H_2O$	0.48
EDTA, disodium salt	0.67
$FeSO_4.7H_2O$	0.1
$NaHCO_3$	0.2
$FeCl_3$	0.1
Na_2SeO_4	0.01
H_3BO_3	0.05
$ZnSO_4.7H_2O$	0.005
$Na_2MoO_4.2H_2O$	0.007
$CuSO_4.5H_2O$	0.001
$MnSO_4.H_2O$	0.001
$CoSO_4.7H_2O$	0.05
$NiCl_2.6H_2O$	0.08
NaCl	0.1

CHAPTER 5

ACTIVATION OF AN OTHERWISE SILENT XYLOSE METABOLIC PATHWAY IN *SHEWANELLA ONEIDENSIS* BY ADAPTIVE EVOLUTION

Abstract

Shewanella oneidensis is unable to metabolize the sugar xylose as carbon and energy source. In the present study, an otherwise silent xylose catabolic pathway was activated in *S. oneidensis* by following an adaptive evolution strategy. Genome-wide scans indicated that the *S. oneidensis* genome encoded two proteins with similarity to the xylose oxido-reductase pathway enzymes xylose reductase (SO_0900) and xylulokinase (SO_4230), and purified SO_0900 and SO_4230 displayed xylose reductase and xylulokinase activities, respectively. The *S. oneidensis* genome was missing, however, an *E. coli* XylE-like xylose transporter. After 12 monthly transfers in minimal growth medium containing successively higher xylose concentrations, a *S. oneidensis* mutant (termed strain XM1) was isolated for the acquired ability to grow aerobically on xylose as carbon and energy source. Whole genome sequencing indicated that strain XM1 contained a mutation in an unknown membrane protein (SO_1396) resulting in a glutamine to histidine conversion at amino acid position 207. Homology modeling demonstrated that the Q207H mutation in SO_1396 was located at the homologous xylose-docking site in XylE. The ability to uptake and metabolize xylose to a useful secondary chemical was demonstrated in strain XM1 genetically engineered to contain the *Ralstonia eutropha phb*ABC gene cluster and produce the biodegradable plastic polyhydroxybutyrate.

5.1 Introduction

Xylose is one of the primary products of lignocellulose degradation and, after glucose, is the second most abundant carbohydrate in nature. The xylose polymer xylan is the primary constituent of hemicellulose that comprises approximately 17% of dry weight of hardwoods and up to 31% of plants (1). Xylose catabolism is a key component of sustainable processes that produce useful secondary products from lignocellulosic biomass (2-4). Xylose catabolism is also of commercial interest because xylose conversion to useful secondary chemicals such as bioethanol and biodegradable plastics can reduce losses associated with lignocellulose bioprocessing (5, 6). Industrially important byproducts of xylose metabolism include xylitol, which is used as a natural sweetener in the food and confectionary industries (7).

Xylose metabolic pathways include the oxido-reductase, isomerase, and Weimberg-Dahms pathways (Fig. 1) (1, 8). Extracellular xylose is transported inside the cell via the ATP-binding cassette (ABC) or major facilitator superfamily (MFS) xylose transporters XylFGH and XylE, respectively (9, 10). In the oxido-reductase pathway of yeast (11), NAD(P)H dependent D-xylose (referred to below as xylose) reductase converts intracellular xylose to xylitol, which is then oxidized to xylulose by D-xylitol dehydrogenase. Xylulose is then phosphorylated by xylulokinase to xylulose 5-phosphate, which enters the pentose phosphate pathway. In the xylose isomerase pathway of *Escherichia coli* (11), xylose isomerase converts xylose to xylulose, which enters the pentose phosphate pathway similar to the oxidoreductase pathway (1, 12). In the Weimberg-Dahms pathway of *Caulobacter crescentus*, xylose dehydrogenase catalyzes the conversion of xylose to xylonolactone, which is then converted to

either α-ketoglutaric semialdehyde via the Weimburg pathway or to glucoaldehyde and pyruvate via the Dahms pathway (8).

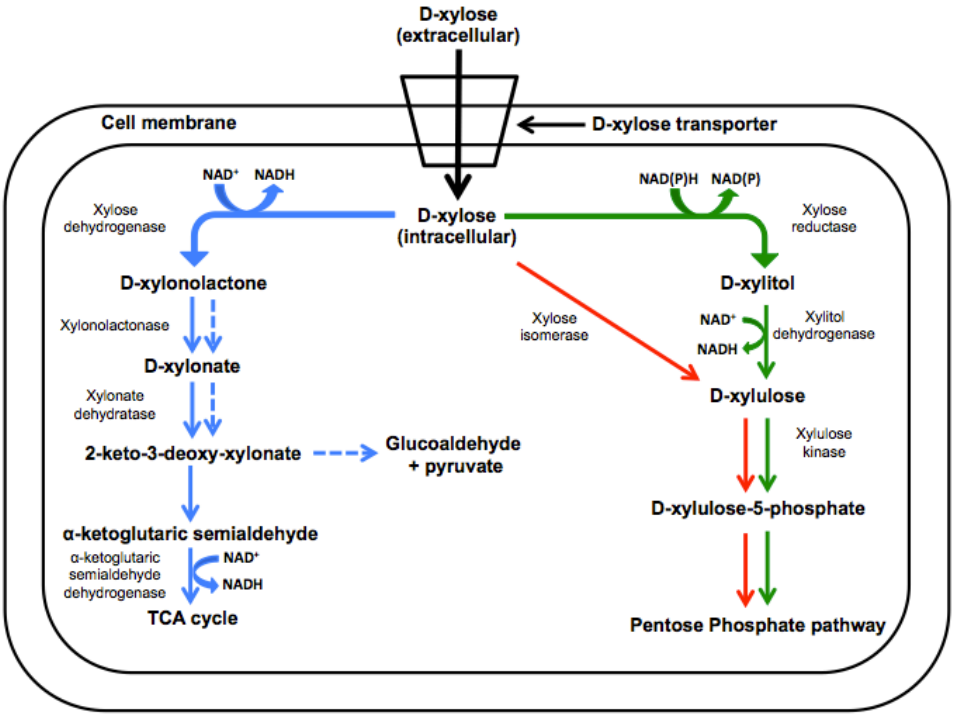

Figure 5.1. Xylose metabolic pathways in microorganisms. Weinberg pathway; solid blue, Dahms pathway; dashed blue, isomerase pathway; solid red, oxidoreductase pathway; solid green.

The metal-reducing facultative anaerobe *Shewanella oneidensis* displays a variety of diverse metabolic systems that couple the oxidation of a wide variety of electron donors (13) to the reduction of a set of electron acceptors whose redox potentials span nearly the entire continuum of potentials encountered in nature (14). Recently, the list of electron donors has been expanded to include glucose and glycerol through adaptive evolution and metabolic

engineering (15-17). Genes encoding canonical xylose metabolic pathways, however, are missing from the *S. oneidensis* genome (18).

In the present study, an adaptive evolution approach was followed to generate *S. oneidensis* mutants that metabolize xylose as sole carbon and energy source. In adaptive evolution, mutations arise under selective pressure and a subset of the cell population acquires a mutation that facilitates growth under a new set of environmental conditions (19). Mutator cells include 'growth advantage in stationary phase' (GASP) mutants in which genetic alterations in small cell populations display a higher competitive advantage over weaker cells (20). Adaptive evolution is a useful strategy for strain improvement in metabolic engineering (21-23) since apriori knowledge of the targeted metabolic process is not required (6). The remarkable metabolic flexibility displayed by *S. oneidensis* (24) led us to hypothesize that under selective growth conditions *S. oneidensis* mutator cells may acquire xylose metabolic capability.

Environmental concern over conventional non-biodegradable plastic has stimulated development of alternative clean technologies for production of biodegradable plastic (25). Alternative clean technologies include biosynthesis of biodegradable polymers by recombinant microorganisms genetically engineered to produce biodegradable plastic from renewable resources (25). The plastic industry primarily produces polymers from petroleum-based sources. Second generation biodegradable plastics include polyhydroxybutyrate (PHB) produced from renewable sugar sources such as lignocellulosic biomass (25, 26).

The chemical properties of biorenewable polymers such as polyhydroxybutyrate (PHB) are comparable to that of conventional plastics. PHB is a linear polyester of the monomer (R)-3-hydroxybutyric acid that belongs to the group of short chain length PHAs consisting of C3-

C5 hydroxyacid monomers (27). PHB is accumulated intracellularly by microorganisms to store carbon and energy in response to conditions of physiological stress (25, 28-33). The PHB biosynthetic pathway of *Ralstonia eutropha* consists of three enzymes that carry out three sequential reactions (34) producing acetyl-CoA as intermediate by-product (5, 35). The first enzyme of the PHB pathway is acetyl-CoA-acetyltransferase (encoded by *phaA*), which catalyzes the condensation of two acetyl-CoA molecules to form acetoacetyl-CoA. This step is followed by reduction of acetoacetyl-CoA to (R)-3-hydroxybutyryl-CoA by NADPH-dependent acetoacetyl-CoA reductase (encoded by *phaB*). Finally, PHA synthase (encoded by *phaC*) catalyzes the polymerization of (R)-3-hydroxybutyryl-CoA monomers to PHB (36). Some microorganisms also produce intracellular PHB depolymerases that breakdown PHB and utilize the monomeric 3-hydroxybutyrate as nutrient source (37). Sequence analysis revealed that *S. oneidensis* genome does not contain PHB-depolymerizing enzymes, thus permitting accumulation of intracellular PHB (38).

The main objectives of the present study were to (i) adaptively evolve *S. oneidensis* to metabolize xylose as carbon and energy source, (ii) identify the enzymes mutated in the adaptively evolved xylose catabolic pathway in *S. oneidensis*, (iii) determine the ability of the xylose-adapted strain to grow aerobic and anaerobically with xylose as sole electron donor, and (iv) genetically engineer xylose-adapted *S. oneidensis* mutants to express the PHB biosynthesis genes (*phaCAB*) of *R. eutropha* and produce PHB with xylose as carbon and energy source.

5.2 Materials and methods

Bacterial Strains and Growth Conditions. Bacterial strains and plasmids used in this study are listed in Table S2. *S. oneidensis* and *E. coli* were routinely cultured aerobically on LB medium (10 g/L tryptone, 5 g/L yeast extract, and 10 g/L NaCl) at 30°C and 37°C respectively (39). *Ralstonia eutropha* was grown aerobically in nutrient broth media at 30°C. When required for selection, chloramphenicol (25 μg ml^{-1}), amphicillin (100 μg ml^{-1}), and gentamicin (15 μg ml^{-1}) were amended to basal growth medium. Fe(III) citrate was prepared by previously described procedures (40, 41) and added at a final concentration of 10 mM. All chemical reagents were obtained from Sigma-Aldrich.

Adaptive Evolution of S. oneidensis to Metabolize Xylose as Sole Carbon and Energy Source. Wild-type *S. oneidensis* cells were initially grown in SM minimal medium for 48 h with 18 mM lactate as sole carbon and energy source (Table S1) (42). The cell culture was subsequently serially transferred each month over a 12-month period to fresh SM medium with increasing ratios of xylose-to-lactate concentrations. The final mutant mix was plated on LB agar and single colonies were screened for xylose utilization via the dinitrosalicylic (DNS) assay that facilitates visual detection of reducing sugars. After 12 months, xylose-adapted *S. oneidensis* strain XM1 was isolated and grew aerobically with 65 mM xylose as sole carbon and energy source. To facilitate identification of the xylose metabolic pathway in *S. oneidensis* strain XM1, the genome was sequenced with 300X coverage on an Illumina sequencing platform, assembled and analyzed with the CLC Workbench software (CLC BioQiagen, Aarhus, Denmark) together with NCBI database (38) and modeling software I-TASSER (43).

Overall Respiratory Activity of Xylose-Adapted S. oneidensis XM1. The *S. oneidensis* wild-type and xylose-adapted mutant strain XM1 were tested for aerobic and anaerobic growth with 5 mM xylose, glucose, arabinose, galactose, lactose, sucrose, cellobiose, fructose, maltose, mannose, mannitol, trehalose, D-xylitol, or gluconate as electron donor and either O_2, 5 mM nitrate (NO_3^-), 10 mM fumarate or 10 mM Fe(III)-citrate as terminal electron acceptor. The cell cultures were incubated at 30˚C for 68 h and samples were withdrawn periodically for determination of cell density (OD_{600}), nitrite, and Fe(II) concentrations.

Cloning and Expression of S. oneidensis Xylose-Metabolizing Genes in *E. coli*. The primers used for cloning genes SO_0900, SO_4673, SO_4230, and SO_2452 are listed in Table S3. These primers were used to PCR-amplify the full length genes from the *S. oneidensis* genome. The amplified genes were ligated into plasmid pQE80L (containing a His-tag at the N-terminus to facilitate protein purification) and transformed into *E. coli* JM109. The resulting recombinant strains were cultured in LB media with 100 μg mL^{-1} ampicillin at 37˚C and induced with 1 mM IPTG at 25˚C for 24 hours for expression of SO_0900, SO_4673, SO_4230 and SO_2452. Cells were collected by centrifugation and re-suspended in a buffer containing 50 mM sodium phosphate, 0.3 M NaCl (pH 8.0), and 10 mM imidazole. Subsequently, the cells were sonicated and the soluble and insoluble fractions were separated by centrifugation. The recombinant protein was purified using immobilized metal (nickel) affinity chromatography (HIS-Select™ Resin, Sigma-Aldrich).

Preparation of Cell-free Extract and Protein Purification. *E. coli* cells were prepared according to previously described procedures (44). *E. coli* cells were grown on LB medium and harvested by centrifugation at 5,000xg at 4°C for 30 min. Cells were washed once with extraction buffer (10 mM Tris/HCl, pH 7.5). Washed cell pellets were stored at -20°C until use. Cell pellets were resuspended to an OD_{600} of 50 in the equilibration buffer (50 mM Na_2HPO4, 300 mM NaCl and 10 mM imidazole at pH 8) and sonicated (8 cycles of 10 s with 30 s cooling period). Cell debris was discarded after centrifugation at 16,000xg for 20 min at 4°C. Supernatant was used as cell-free extract and Bradford assay was used for estimation of protein concentration in the extract.

His-tagged protein in the cell-free extract was purified at 4°C using HIS-Select HF nickel affinity gel (Sigma-Aldrich) which employs immobilized metal-ion affinity chromatography (IMAC) according to the manufacturer's small-scale purification protocol. 600 μL aliquots of the cell-free extract were added to 150 μL affinity gel in equilibration buffer. After overnight incubation, the gel was washed five times with equilibration buffer. The bound his-tagged protein was then eluted using 100 μL elution buffer (50 mM Na_2HPO4, 300 mM NaCl, and 250 mM imidazole at pH 8). Imidazole was removed by overnight dialysis at 4°C using extraction buffer as the dialysis solution. The purified protein product was used for SDS-PAGE analysis, determination of protein concentration and activity assays.

Activity Assays for Protein Expression. Xylose reductase activity was determined in McIlvaine buffer at pH 7.2 (prepared by adding 16.5 ml 0.2 M Na_2HPO4 to 3.5 ml 0.1 M citric acid) containing 0.35 mM NADPH and 200 mM xylose and purified protein

SO_0900 (44). For measuring the catalytic activity of xylose reductase on xylose, k_m and V_{max} were determined by varying the xylose concentrations (0.01–0.25 M) under constant concentrations of NADPH (0.35 mM) and purified protein (10 μL) in the assay mixture and fitting the data to Lineweaver-Burk equation: $1/v = (k_m/V_{max})[S] + 1/V_{max}$. The extinction coefficient (e) for NADPH at 340 nm is 6.22 x 10^{-3} M^{-1} cm^{-1}. One unit of xylose reductase activity is the amount of enzyme which converts 1 μmol of NADPH to $NADP^+$ per min. Xylulokinase was assayed by previously described methods (45). Reactions were carried out at 30˚C and pH 7.5 in 96-well microtiter plates in a final volume of 200 μL. The reaction mixture consisted of the following (final concentrations indicated): 71 mM Tris–HCl pH 7.5, 7.1 mM $MgCl_2$, 1 mM EDTA, 50 mM KCl, 7.1 mM KF, 5 mM KCN, 1.4 mM ATP, 1 mM PEP, 0.3 mM NADH, 0.7 U mL^{-1} pyruvate kinase, 1 U mL^{-1} lactate dehydrogenase, and 5 mM xylulose. NADH consumption was monitored continuously at 340 nm for 10 min. One unit of xylulokinase activity is the amount of enzyme that converts 1 μmol of NADH to NAD^+ per min. For measuring the catalytic activity of xylulokinase on xylulose, k_m and V_{max} were determined by varying the xylulose concentrations (1–20 mM) under constant concentrations of NADH (0.3 mM) and purified protein (10 μL) in the assay mixture. Xylitol dehydrogenase was assayed by a previously described method (46): the reaction mixture consisted of (final concentrations indicated): 77 mM glycine, 6.3 mM NAD^+, 1 mM 2-mercaptoethanol, and 200 mM xylitol. The disappearance of NADH was monitored continuously at 340 nm for 10 min. One unit of xylitol dehydrogenase activity is the amount of enzyme that converts 1 μmol of NAD^+ to NADH per min. For measuring the catalytic activity of xylitol dehydrogenase on xylitol, k_m and V_{max} were determined by

varying the xylitol concentrations (1–200 mM) under constant concentrations of NAD^+ (6.3 mM) and purified protein (10 μL) in the assay mixture.

In-Frame Deletion Mutagenesis of S. oneidensis Genes SO_1396, SO_0900, and SO_4230 Genes encoding SO_1396, SO_0900, and SO_4230 were deleted in-frame from the XM1 genome as described previously (47). Regions corresponding to ~750 bp upstream and downstream of each open reading frame (ORF) were PCR-amplified with iProof ultrahigh-fidelity polymerase (Bio-Rad, Hercules, CA), generating fragments F1 and F2, which were fused by overlap extension PCR to generate fragment F3. The primers used for construction of ΔSO1396, ΔSO0900, ΔSO4230 are listed in Table S3. Fragment F3 was cloned into pKO2.0 with BamHI and SalI restriction endonucleases and electroporated into *E. coli* strain β2155 λ *pir*. pKO2.0-F3 was mobilized into recipient *S. oneidensis* wild-type via biparental mating procedures. A plasmid integrant was identified via PCR analysis, and the mutation was resolved on LB agar containing sucrose (10%). Following counter selection on LB agar containing sucrose (10% [wt/vol]), the corresponding in-frame deletion mutant strains (designated ΔSO1396, ΔSO0900, ΔSO4230, respectively) were isolated and confirmed via PCR. The *S. oneidensis* wild-type, XM1, ΔSO1396, ΔSO0900, ΔSO4230 strains were tested for aerobic growth with 5 mM xylose as electron donor and O_2 as terminal electron acceptor. The cells were incubated at 30˚C for 144 h and samples were withdrawn periodically for determination of cell density (OD_{600}).

Homology modeling of $SO1396^{Q207H.}$ The secondary structure of SO_1396^{Q207H} was predicted using I-TASSER server and a model structure was constructed based on

secondary structure similarity to known protein structures in the protein data base. The membrane domain of the respiratory complex I from *E. coli* (PDB ID:3rkoC) was used as the template to construct SO1396$^{\mathbf{Q207H}}$ models based on the best Z-scores with known protein structures by I-TASSER (43).

Cloning and Expression of SO1396$^{\mathbf{Q207H}}$ in *S. oneidensis*. The primers used for cloning SO1396^{Q207H} on pBBR1MCS are listed in Table S3. The cloned plasmid was transformed into strain XM1-ΔSO1396^{Q207H} strain. The resulting recombinant strain was cultured in LB media with 25 μg mL^{-1} chloramphenicol. Strain XM1-ΔSO1396^{Q207H} pBBR1MCS + SO1396 ^{Q207H} was tested for aerobic growth with 5 mM xylose as electron donor 30˚C for 144 h and samples were withdrawn periodically for determination of cell density (OD_{600}).

Analytical Methods. The concentration of reducing ends of the supernatant was determined by the dinitrosalicylic acid (DNS) assay (48). 100 μL of the supernatant was added to 900 μL of DNS solution prepared by dissolving in water a mixture of 0.75% 3,5-dinitrosalycylic acid, 1.4% sodium hydroxide, 21.6% potassium sodium tartrate, 0.55% phenol and 0.55% sodium metabisulfate. The mixture was then boiled for 5 min, centrifuged at 15,000xg for 5 min and the optical density of the supernatant was measured at 545 nm. Reducing sugar concentrations were calculated using glucose as standard.

Xylose concentrations were measured via high pressure liquid chromatography (HPLC) following a modified version of a previously described protocol (49). 300 μL of xylose solution was mixed with 100 μL of 1.4 M sodium cyanoborohydride solution in

water, 700 μL of a methanolic solution of 0.6 M aminobenzoic butyl ester (ABBE) and 100 μL of 10% acetic acid. The solution was heated at 80°C for 60 min and then extracted three times with 0.5 mL dichloromethane prior to injection directly into the HPLC system equipped with a SUPELCOSIL LC-18-DB column. The mobile phase was comprised of 0.1 M ammonium acetate, pH 4.5 (solvent A) and acetonitrile (solvent B). Separation was carried out with a mixture of mobile phase A-acetonitrile (75:25, V/V) at a flow rate of 0.5 mL/min. Chromatograms were generated at 260 nm and a calibration curve was generated from standard. Nitrite (NO_2^-) concentrations were measured by diluting samples 250-fold in a solution consisting of 9.6 mM sulfanilic acid, 96 mM potassium bisulfate, and 3.2 mM *N*, *N*-ethylenediamine (50). Samples were held in the dark for 15 min prior to measuring absorbance at 510 nm. PHB was analyzed as described previously (35, 51). Cells from 1 mL culture were harvested by centrifugation at 5,000xg for 10 min. The cell pellet was boiled in 50 μL of concentrated sulfuric acid for 60 min and then diluted with 150 μL of 14 mM H_2SO_4. Samples were centrifuged for 15 min at 16,000xg cell debris and the supernatant was analyzed via liquid chromatography (LC) using a ZORBAX SB-C18 column with 5% aqueous acetonitrile at pH 2.8 as the mobile phase and a constant flow rate of 0.3 ml/min. Chromatograms were generated at 210 nm at a retention time of 7 min.

Protein concentrations were measured by the Bradford assay using a protein reagent dye (Bio-Rad, Hercules, CA, USA) with bovine serine albumin as the standard. SDS-PAGE was performed using a Mini-protean TGX electrophoresis kit (Bio-Rad, Hercules, CA, USA) and stained with Bio-safe Comassie Blue (Bio-Rad, Hercules, CA, USA). A 100-KDa precision plus protein standard ladder was used as a standard mass protein marker. Cell

density (OD_{600}) was measured on a UV/visible light spectrophotometer (Beckman Coulter, CA, USA)

Cloning and Expression of R. eutropha phaCAB in *Shewanella oneidensis.* The primers used for cloning *phaCAB* are listed in Table S3. The PHB biosynthetic gene cluster *phaCAB* from *R. eutropha* was cloned into a pBBR1MCS expression vector and expression controlled by a pBAD promoter induced by arabinose. The plasmid was transformed into the *S. oneidensis* XM1 strain. The resulting recombinant *S. oneidensis* strain was cultured in LB media with 25 μg mL^{-1} chloramphenicol at 30˚C for 24 hours for *phaCAB* expression. Arabinose concentration of 0.5 mM was used to induce *phaCAB* expression at OD = 0.2.

PHB Production from Xylose as Sole Carbon and Energy Source by Xylose-Adapted *S. oneidensis* Strain XM1. The *S. oneidensis* XM1 strain harboring the PHB biosynthetic gene cluster *phaCAB* of *R. eutropha* was cultured aerobically in LB medium with 0.5 mM arabinose. Cells were harvested, washed, and resuspended in SM minimal media with varying xylose concentrations (0, 0.1, 0.5, 5, 50, and 100 mM) and incubated at 30˚C for 96 h. Samples were periodically drawn to determine the concentration of xylose and PHB as described above.

5.3 Results

Isolation of Xylose-Adapted *S. oneidensis* Strain XM1. Wild-type *S. oneidensis* is unable to grow with xylose as carbon and energy source. The wild type strain was

therefore subjected to an adaptive evolution strategy to generate *S. oneidensis* mutants with the acquired ability to metabolize xylose as carbon and energy source. Wild-type *S. oneidensis* cells were initially grown in SM minimal growth medium with 18 mM lactate as carbon source and energy source and subsequently serially transferred over a 12-month period to SM medium amended with increasing ratios of xylose-to-lactate concentrations. *S. oneidensis* strain XM1 was isolated from the adaptively evolved mutant mix after the 12th successive transfer. Strain XM1 grew aerobically with 65 mM xylose as sole carbon and energy source. However, strain XM1 was unable to grow aerobically on a variety of other sugars, including glucose, arabinose, galactose, lactose, sucrose, cellobiose, fructose, maltose, mannose, mannitol, trehalose, D-xylitol, and gluconate (data not shown). This finding suggests that strain XM1 may have developed a GASP phenotype specific to xylose. Similar findings were previously reported with *S. oneidensis* mutants adapted to grow in the presence of glucose as carbon and energy source (15).

Xylose consumption rates by Xylose-Adapted *S. oneidensis* Strain XM1.

Strain XM1 was further tested for xylose consumption in SM minimal medium amended 5 mM xylose as carbon and energy source. Under aerobic conditions, strain XM1 grew at a rate of 0.063 h^{-1}, (Fig 2A), while the wild-type strain grew at a rate of 0.003 h^{-1} (i.e., at rates 5% of strain XM1). Strain XM1 consumed xylose at a rate of 27 μM h^{-1}, while the wild-type strain consumed xylose at a rate of 1.2 μM h^{-1} (i.e., 5% of strain XM1) (Fig. 2A). Strain XM1 was also able to utilize lactate as sole carbon source at rates similar to the wild-type strain, thus indicating that lactate metabolism was not altered during the adaptation process (data not shown). The anaerobic respiratory capabilities of *S. oneidensis* wild-type and strain

XM1 were also determined under anaerobic conditions with xylose as electron donor and NO_3^-, fumarate or Fe(III) as electron acceptor.

With NO_3^- as electron acceptor, strain XM1 grew at the rate of 0.027 h^{-1} (Fig 2C), while the wild-type strain grew at a much lower rate of 0.002 h^{-1} (i.e., 7% of strain XM1). Strain XM1 consumed xylose at a rate of 6.32 μM h^{-1}, while the wild-type strain consumed xylose at 1.9 μM h^{-1} (i.e., at rates 30% of strain XM1) (Fig. 2C). Strain XM1 produced nitrite (product of microbially-catalyzed nitrate reduction) at the rate of 38.2 μM h^{-1} (Fig. 2D), while the wild type strain produced nitrite at a much lower rate of 1.5 μM h^{-1} (i.e., at rates 4% of strain XM1). With fumarate as electron acceptor, strain XM1 grew at the rate of 0.034 h^{-1} (Fig 2B), while the wild-type strain grew at a rate of 0.002 h^{-1} (i.e., at rates 6% of strain XM1). Strain XM1 consumed xylose at a rate of 10.6 μM h^{-1}, while the wild type strain consumed xylose at 0.73 μM h^{-1} (i.e., at rates 7% of strain XM1) (Fig. 2B). With Fe(III) as electron acceptor, strain XM1 produced Fe(II) (product of microbially-catalyzed Fe(III) reduction) at the rate of 20.9 μM h^{-1}) (Fig 2E), while the wild-type strain produced Fe(II) at a much lower rate of 3.0 μM h^{-1} (i.e., at rates 14% of strain XM1). During the 68 h growth period, strain XM1 consumed xylose at a rate of 6.8 μM h^{-1}, while the wild-type strain consumed xylose at 2.2 μM h^{-1} (i.e., at rates 32% of strain XM1) (Fig. 2E). These results indicate that strain XM1 consumed xylose under aerobic and anaerobic nitrate-, fumarate- and Fe(III)-reducing conditions.

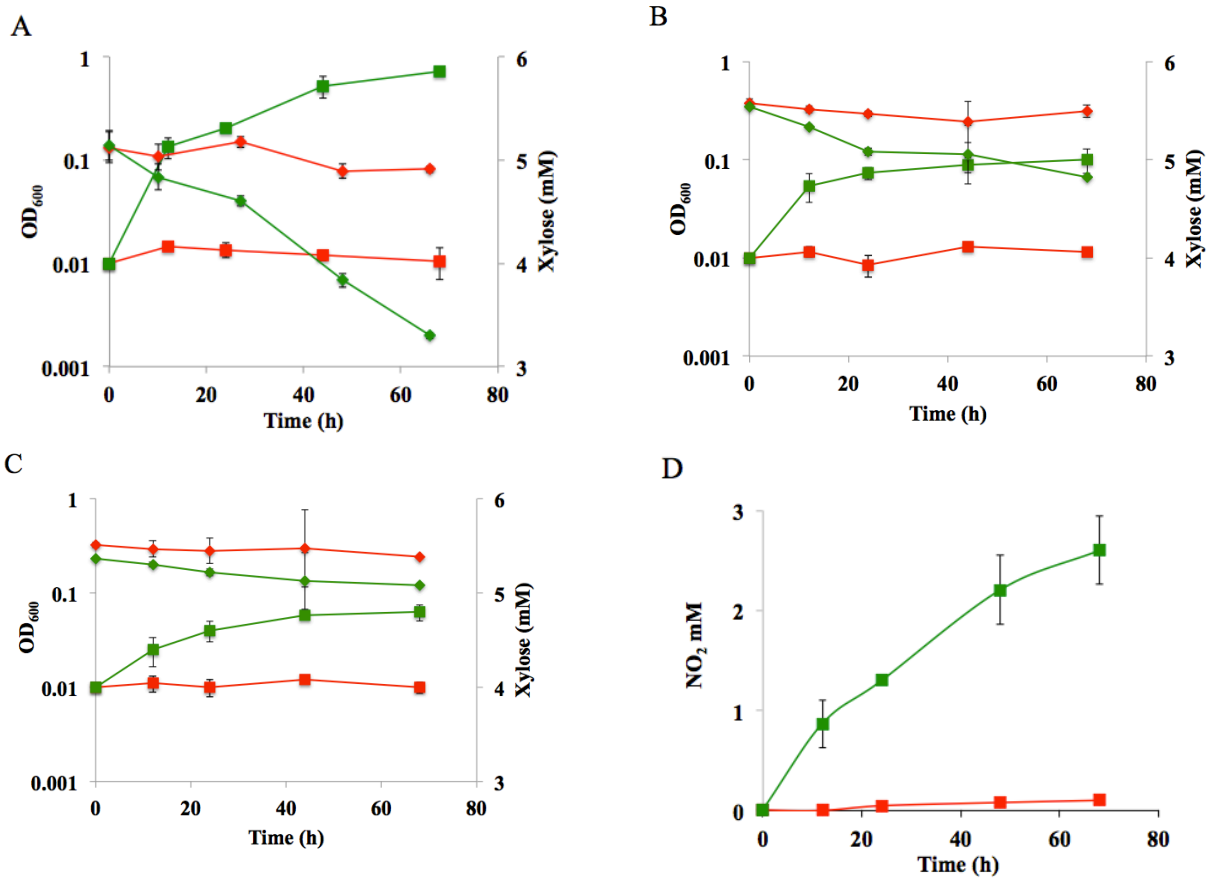

Figure 5.2. Aerobic and anaerobic respiratory activities of strain XM1 with xylose as sole carbon and energy source. (A) Growth and xylose concentration profiles of *S. oneidensis* and strain XM1 in the presence of O_2 as electron acceptor in minimal media. Xylose concentration of 5 mM was used in this experiment. Wild type; red, XM1; green, OD_{600}; (■), xylose concentration; (◆). (B) Growth and xylose concentration profiles of *S. oneidensis* and strain XM1 in the presence of fumarate as electron acceptor in minimal media. 5 mM xylose and 10 mM fumarate were used in this experiment. Wild type; red, XM1; green, OD_{600}; (■), xylose concentration; (◆). (C) Growth and xylose concentration profiles of *S. oneidensis* and strain XM1 in the presence of nitrate (NO_3) as electron acceptor in minimal media. 5 mM xylose and 5 mM nitrate were used in this experiment. Wild type; red, XM1; green, OD_{600}; (■), xylose concentration; (◆). (D) Nitrite concentration profiles during growth curve of *S. oneidensis* and strain XM1 in the presence of NO_3 as electron acceptor in minimal media. 5 mM xylose and 5 mM nitrate were used in this experiment. Wild type; red (■), XM1; green (■). (E) Fe(II) and xylose concentration profiles during growth curve of *S. oneidensis* and strain XM1 in the presence of Fe(III) as electron acceptor in minimal media. 5 mM xylose and 10 mM Fe(III) were used in this experiment. Wild type; red, XM1; green, Fe(II); (■), xylose concentration; (◆). Error bars represent range of errors in duplicate batch reactors.

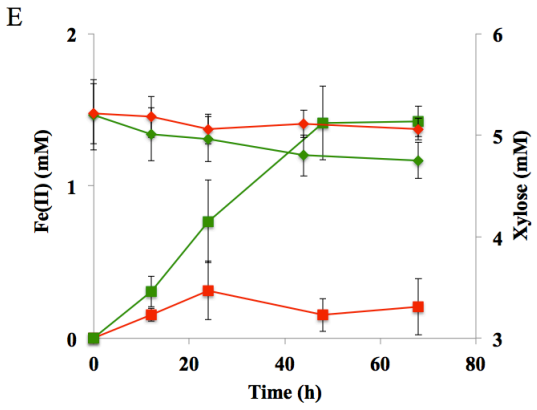

Figure 5.2 continued

Identification of the Xylose Transporter in *S. oneidensis*. The single nucleotide mutation that enabled strain XM1 to grow on xylose as the carbon and energy source was identified by whole genome sequencing. A single nucleotide mutation was identified in SO_1396 that converted glutamine (Q) to histidine (H) at amino acid position 207. SO_1396 is annotated as a membrane protein of unknown function (38). To investigate the function of SO_1396, in frame gene deletion mutant XM1-ΔSO1396^{Q207H} was tested for the ability to metabolize xylose as the sole carbon and energy source under aerobic conditions. Strain XM1 grew at the rate of 0.035 h^{-1}, while strain XM1- Δ SO1396^{Q207H} was unable to grow in the presence of xylose as the sole carbon and energy source (Fig. 3). Expression of SO_1396^{Q207H} on plasmid pBBR1MCS in XM1 ΔSO1396^{Q207H} strain rescued the growth on xylose by approximately 84% (with a growth rate of 0.029 h^{-1}; Fig. 3). These results suggest that the mutant membrane protein SO_1396^{Q207H} functions as a xylose transporter. Homology modeling of SO_1396^{Q207H} (Fig. 4A) predicted that the secondary structure of SO_1396^{Q207H} is partly outward occluded with a top width of 62 Å and a bottom width of 53 Å. Only minor secondary structural changes were observed in overlapping structures of SO_1396^{Q207} and SO_1396^{Q207H} (Fig. 4B and C).

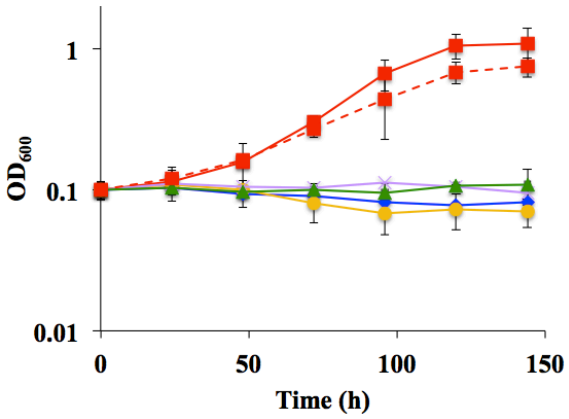

Figure 5.3. Aerobic growth profiles of *S. oneidensis* and strain XM1 strains in the presence of xylose as sole carbon and electron source in minimal media. 5 mM xylose was used in this experiment. Wild type; blue (◆), XM1; red (■), XM1-ΔSO1396^{Q207H}; orange (•), XM1-ΔSO1396^{Q207H} + pBBR_SO1396^{Q207H}; dashed red (■), XM1-ΔSO0900; violet (x), XM1-ΔSO4230; green (▲). Error bars represent range of errors in duplicate batch reactors.

Identification of Genes Encoding the Xylose Metabolic Pathway of Strain XM1.

Strain XM1 containing mutated membrane protein SO_1396^{Q207H} consumed xylose as carbon and energy source under both aerobic and anaerobic conditions. To identify the genes encoding the xylose metabolic pathway, proteins with similarity to known xylose metabolic proteins in other organisms were identified in the XM1 genome sequence via Blast sequence analysis (38). Xylose isomerase and all proteins involved in the Weimberg-Dahms pathway were absent from the strain XM1 genome (data not shown). For the oxido-reductase pathway, the aldo/keto reductase SO_0900 in the strain XM1 genome displayed similarity to known xylose reductases in *E. coli* (51% similar to ECs0473) and *Z. mobilis* (32% similar to ZMO0976) (Table S5) (44). SO_0900 was therefore hypothesized to function as the xylose reductase in strain XM1.

D-Xylitol dehydrogenase (XDH) is the next protein following xylose reductase in the oxidoreductase pathway. XDH is a member of the alcohol and threonine dehydrogenase protein superfamily, containing NAD(P) and catalytic zinc binding domains for conversion of xylitol to xylulose (52). L-threonine dehydrogenase SO_4673 displayed similarity to xylitol dehydrogenase (40-46%; Table S6) and also contains NAD(P) and catalytic zinc binding domains (38). Alcohol dehydrogenase SO_2452 displayed 36-40% similarity to known D-xylitol dehydrogenases (Table S7). In addition, *S. halifaxis* and *S. pealeana* metabolize xylitol and contain an alcohol dehydrogenase that functions as xylitol dehydrogenase (18). SO_4673 and SO_2452 were therefore targeted as candidates for xylitol dehydrogenase in strain XM1.

Xylulokinase (XK) is the next protein following D-xylitol dehydrogenase in the oxido-reductase pathway. XK displayed highest similarity (42%; Table S8) to SO_4230, a glycerol kinase (GlpK) . Based on secondary structure alignment, *E. coli* GlpK is highly similar to xylulokinase in *E.coli* (53). Since GlpK from strain XM1 and *E.coli* display 84% similarity (Table S8), SO_4230 was predicted to function as the xylulokinase in strain XM1. The proteins following xylulokinase in the known xylose metabolic pathway are present in the XM1 genome (54).

Purification and Activity of Xylose Metabolic Pathway Proteins in Strain XM1. Based on Blast similarities, strain XM1 proteins SO_0900, SO_4673, SO_2452, and SO_4230 were predicted to be involved in the xylose metabolic pathway. The corresponding genes were cloned into expression vector pQE80L and transformed into *E. coli* JM109. The enzymes were expressed as fusion proteins with a His-tag at their N-terminus, and one-step affinity purification was based on the interaction of the N-terminal

His-tag and Nickel affinity gel. The purified proteins SO_0900, SO_4673, SO_2452, and SO_4230 displayed the expected molecular weights of ~ 41, 41, 38, and 60 kDa on SDS-PAGE gels (Fig. S1 and S2). Purified SO_0900 displayed XR specific activity of 2.93 U/mg with a V_{max} of 3.41 U/mg and k_m of 93 mM with 250 mM xylose as substrate (Table 1). Purified SO_4230 displayed XK specific activity of 0.2 U/mg with a V_{max} of 0.52 U/mg and k_m of 1.7 mM with 5 mM xylulose as substrate (Table 1). However, purified proteins SO_4673 and SO_2452 did not display XDH activity with varying levels of xylitol (1-200 mM) as substrate. These results indicate that SO_0900 and SO_4230 may function as the xylose reductase and xylulokinase, respectively. However, the identity of XDH in strain XM1 remains unknown. To confirm the role of SO_0900 and SO_4230 in the xylose metabolism in strain XM1, SO_0900 and SO_4230 were deleted in-frame and the resulting single gene knockout mutants (XM1-Δ0900 and XM1-Δ4230 strains) were tested for the ability to utilize xylose as carbon and energy source under aerobic conditions. Strain XM1 grew at the rate of 0.035 h^{-1}, while strains XM1- Δ 0900 and XM1- Δ 4230 were unable to grow in the presence of xylose as carbon and energy source (Fig. 3). These results suggest that SO_0900 and SO_4230 function as the xylose reductase and xylulokinase, respectively, in strain XM1.

Table 5.1. Kinetic parameters of purified proteins in this study

Protein	Substrate	Specific activity (U/mg)	V_{max} (U/mg)	k_m (mM)
SO_0900	Xylose	2.93 ± 0.17 (250 mM)	3.41 ± 0.21	93 ± 7
SO_4230	Xylulose	0.2 ± 0.013 (5 mM)	0.52 ± 0.02	1.7 ± 0.12
SO_4673	Xylitol	ND*	ND*	ND*
SO_2452	Xylitol	ND*	ND*	ND*

PHB production by Strain XM1 With Xylose as Carbon and Energy Source.

The PHB biosynthetic gene cluster *phaCAB* of *R. eutropha* was cloned into expression vector pBBR1MCS under control of the pBAD promoter. After arabinose induction, strain XM1-*phaCAB* produced PHB with xylose as carbon and energy source at rates that were proportional to initial xylose concentrations (up to 50 mM) and xylose consumption rates (Figs. 5A, 5B, and S4). PHB was produced maximally at 1.79 mg per gm dry weight cell with 50 mM initial xylose concentrations and xylose consumption rates of 78.0 μM h^{-1} (Fig. 5A, 5B and S4).

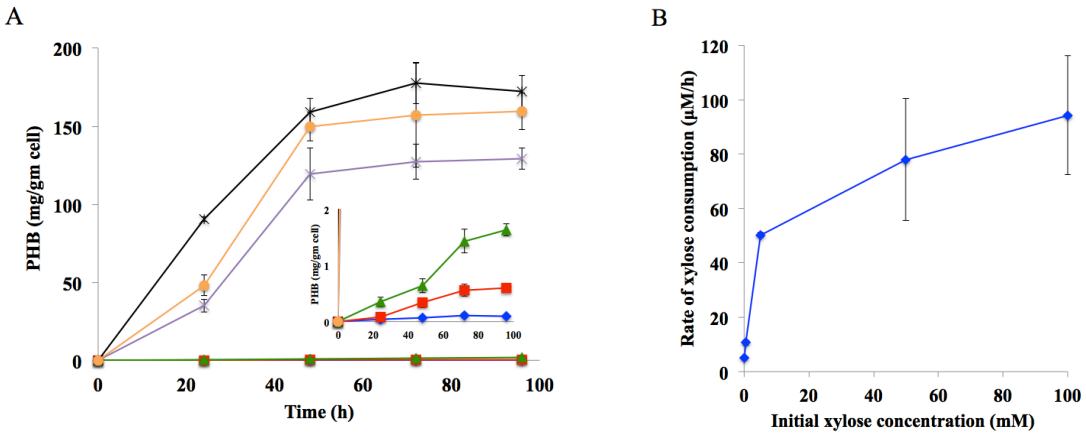

Figure 5.4. Production of polyhydrohybutyrate by strain XM1 with xylose as sole carbon and energy source. (A) PHB concentration profiles of XM1 harboring the PHB biosynthetic genes *phaCAB*. Cells were cultured in LB and gene expression was induced by the addition of 0.5 mM arabinose. Cells were then resuspended in minimal media with 0 - 100 mM initial xylose concentrations. 5 mM; violet (x), 50 mM; black (*), 100 mM; orange (●). Inset - 0 mM; blue (◆), 0.1 mM; red (■), 0.5 mM; green (▲). Error bars represent range of errors in duplicate batch reactors. (B) Rate of xylose consumption profiles by strain XM1 harboring the PHB biosynthetic genes *phaCAB*. Cells were cultured in LB and gene expression was induced by the addition of 0.5 mM arabinose. Cells were then resuspended in minimal media with 0 - 100 mM initial

xylose concentrations. (C) % PHB produced/xylose consumed (mg/mg) and % PHB yield (% PHB/DCW in mg/mg) by strain XM1 across different initial xylose concentrations (0.1 – 100 mM). XM1 dry cell weight (DCW) = 0.43 mg/mL/OD_{600}. % PHB produced/xylose consumed; blue (◆), % PHB yield; red (■). Black dotted lines indicate optimal initial concentration of xylose (5 mM) and optimal % PHB/xylose (or) % PHB yield by XM1. Error bars represent range of errors in duplicate batch reactors.

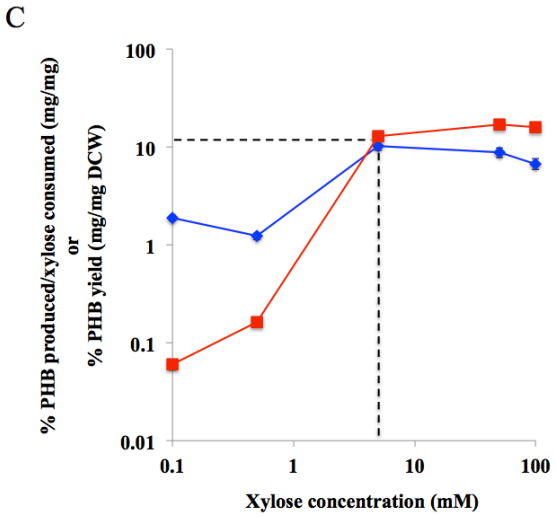

Figure 5.4 continued

5.4 Discussion

The facultative anaerobe *S. oneidensis* respires a diverse spectrum of electron acceptors under both aerobic and anaerobic conditions (14, 55, 56). *S. oneidensis* is employed to drive electricity production in microbial fuel cells and to produce the biofuels ethanol and isobutanol from substrates such as glycerol and glucose through metabolic engineering (16, 17, 57). However, *S. oneidensis* displays a more limited range of electron donor utilization (13, 57). Electron rich carbon sources such as glucose and xylose are the primary products derived from the saccharification of lignocellulosic biomass (58).

Recently, *S. oneidensis* was adaptively evolved and metabolically engineered to metabolize glucose as carbon and energy source (15-17). Although the complete glucose metabolic pathway has been identified in *S. oneidensis*, xylose metabolism remains elusive (18). The present study is the first report to identify a previously unknown xylose catabolic pathway in *S. oneidensis*.

Xylose catabolic pathways were not previously detected in the *S. oneidensis* genome (18), and correspondingly, wild type *S. oneidensis* was unable to consume xylose. The newly isolated, xylose-adapted strain XM1, on the other had, consumed xylose and grew under aerobic and anaerobic nitrate-, fumarate-, and Fe(III)-reducing conditions (Fig. 2). Whole genome sequencing indicated that strain XM1 contained a mutation in an unknown membrane protein, SO_1396 resulting in a glutamine to histidine conversion at amino acid position 207. Only minor structural differences were noted between the predicted structure of SO_1396 wild-type and Q207H mutant forms (Fig. 4B and C). Histidine is weakly charged at neutral pH with pK_a of a bulky (imidazole) R-group at 6.04, while glutamine is polar and neutral at pH 7.0. This minor structural change may have enabled xylose to be transported into strain XM1 by SO_1396^{Q207H} via interaction with predicted active site residues. Similar observations of point mutations affecting substrate specificities in sugar transporters have been previously reported (59-61). SO_1396^{Q207H} structure is predicted to contain 8 transmembrane domains (TM) and the structure is outward occluded with the top width wider (62 Å) compared to bottom width (53 Å) similar to *E. coli* xylose transporter XylE (Fig. 4A). Xylose transport by XylE is coordinated through hydrogen bonding by glutamine and asparagine and interaction with several aromatic amino acid residues (tyrosine, tryptophan and phenylalanine) (62). Similar polar residues found in SO_1396^{Q207H}

included Q202 (TM5), Q277 (TM6), Q290 (TM6), Q325 (TM7), N278 (TM6) and aromatic residues included W187 (TM5), W312 (TM7), W345 (TM8), Y287 (TM6), Y314 (TM7), F188 (TM5), F284 (TM6), and F350 (TM8), These residues may play a similar role in aiding xylose binding and uptake by SO_1396^{Q207H} (Fig. 4D).

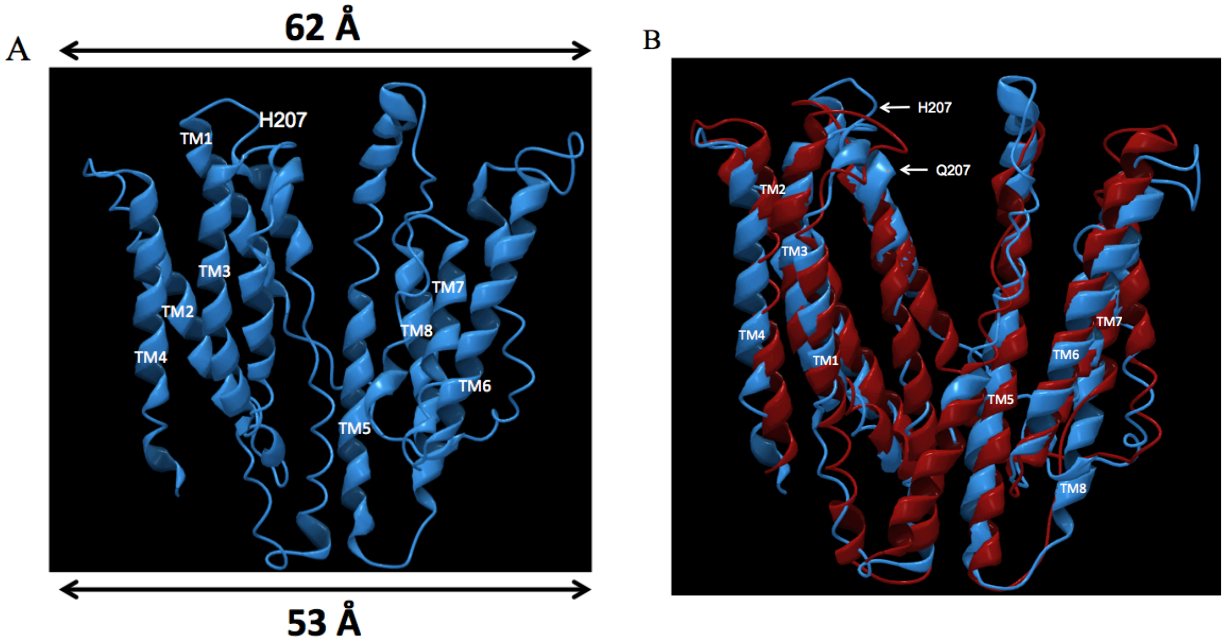

Figure 5.5. Predicted secondary structure of SO1396^{Q207H}. (A) The homology model based on membrane domain of the respiratory complex I from *E.coli* as template (PDB ID: 3rkoC) contains 8 transmembrane domains (labeled as TM). Single point mutation in xylose adapted XM1 was found in SO1396 at 207th amino acid residue (Q207H). (B) Front view of secondary structure alignment between WT SO_1396 and SO_1396^{Q207H}. WT SO_1396; red, SO_1396^{Q207H}; blue, (C) Top view of secondary structure alignment between WT SO_1396 and SO_1396^{Q207H}. WT SO_1396; red, SO_1396^{Q207H}; blue. (D) Top view of homology model of SO1396^{Q207H} illustrating the residues predicted to aid in xylose binding and uptake.

C

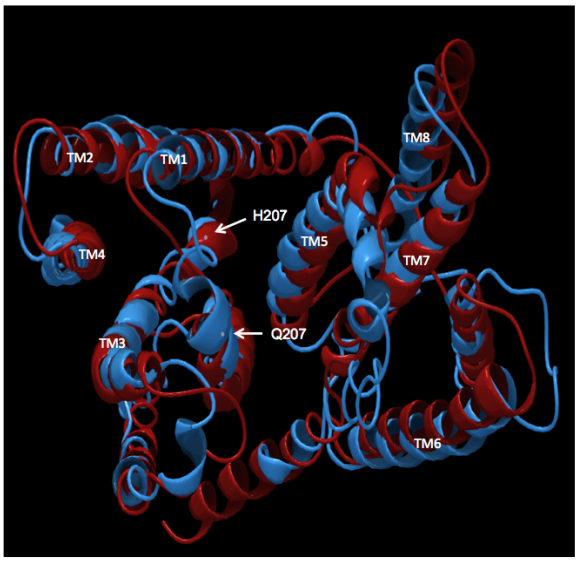

D

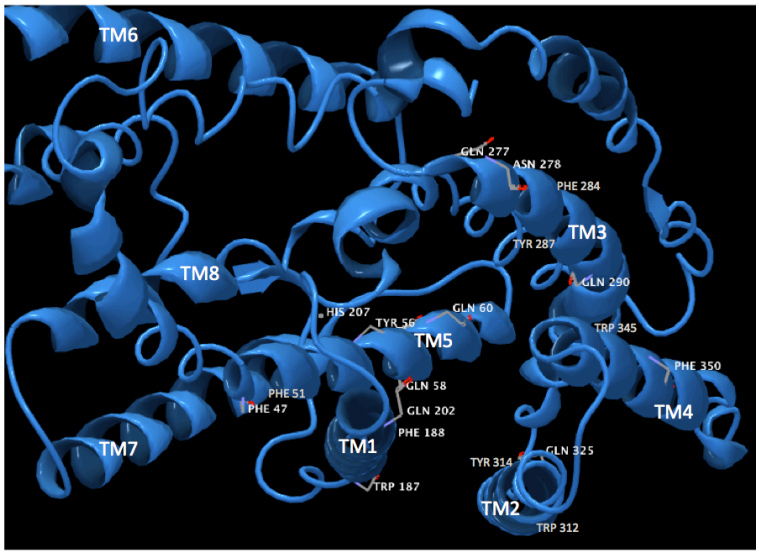

Figure 5.5 continued

Strain XM1 is predicted to contain the xylose oxido-reductase pathway (Fig. 1). Although the XM1 genome does not contain a putative xylose reductase, the aldo/keto reductase SO_0900 displayed similarity to the *E. coli* and *Z. mobilis* xylose reductases

(Table. S5) (44). The kinetic parameters of XR activity of purified SO_0900 with xylose as substrate were comparable to that of ZMO0976 from *Z. mobilis* (Table S9). Moreover, deletion mutant XM1-SO_0900 was unable to metabolize xylose as carbon and energy source, thus indicating that SO_0900 may function as a xylose reductase (Fig. 3).

The secondary structure of *E. coli* GlpK is homologous to *E. coli* XK, and the kinetic and structural properties of *E. coli* XK are derived from *E. coli* GlpK (53). Interestingly, XM1 GlpK (SO_4230) was also highly similar (84%; Table. S8) to *E. coli* GlpK, and the secondary structure of SO_4230 was highly homologous to *E. coli* XK (Fig. S3). Moreover, residues Asp10 and Asp244 (required for XK catalytic activity in *E. coli*) of SO_4230 were homologous to Asp6 and Asp233 of *E. coli* XK, respectively (Highlighted in green in Fig. S3) (53). SO_4230 displayed XR activity with D-xylulose as substrate, however, unlike SO_0900, the kinetic parameters of SO_4230 differed from other known XKs (Table. S9). The specific activity and V_{max} of known XKs were up to 100-fold higher then that of SO_4230. The k_m of SO_4230 was 3-5-fold higher than that of known XKs (Table. S9). Deletion mutant strain XM1- ΔSO_4230 was unable to metabolize xylose as carbon and energy source, thus indicating that SO_4230 may function as a xylulokinase (Fig. 3).

Although SO_4673 and SO_2452 displayed high similarities to known XDH proteins (Table. S6 and S7), purified forms of SO_4673 and SO_2452 did not display XDH activity with D-xylitol as substrate (Table 1). However, SO_4673 and SO_2452 displayed dehydrogenase activity with threonine and ethanol as substrates, respectively (data not shown) thus confirming that the purified proteins were active. The current working model of the xylose catabolic pathway in strain XM1 includes putative xylose transporter

SO_1396^{Q207H}, xylose reductase SO_0900, and xylulose reductase SO_4230 identified in the present study (Fig. S5). The identity of *S. oneidensis* XDH, however, remains unknown.

Xylose metabolism in strain XM1 was coupled to PHB production by growing recombinant strain XM1 harboring the PHB biosynthetic genes *phaCAB* in the presence of varying initial concentrations of xylose. Although PHB production increased 68-fold when initial xylose concentrations were increased 10-fold (0.5 - 5 mM), a further 10-fold increase in initial xylose concentrations (5 - 50 mM) led to only a 1.3-fold increase in PHB production (Fig. 5A). To further investigate, initial xylose concentrations were increased to 100 mM that led to a 7% decrease in PHB production (Fig. 5A). This result indicated that the efficiency of PHB production and xylose consumption were limited in strain XM1 (Fig. 5B and C). To achieve maximal %PHB produced per mg xylose consumed, 5 mM initial xylose concentration was the most optimal with a PHB production yield of 10% mg mg^{-1} DCW by strain XM1 (Fig. 5C).

An otherwise silent xylose catabolic pathway was activated in *S. oneidensis* by application of adaptive evolution strategy. Xylose catabolism was subsequently coupled to PHB production. The expansion of *S. oneidensis* to convert the lignocellulose component xylose to a useful chemical product such as PHB may be beneficial in diverse biotechnological applications. Metabolism of multiple carbon sources such as glucose, glycerol and xylose by *S.oneidensis* will improve efficiency of electricity generation, biofuel production and bioremediation of toxic contaminants (16, 17, 63).

5.5 References

1. **Jackson S, Nicolson SW.** 2002. Xylose as a nectar sugar: from biochemistry to ecology. Comparative Biochemistry and Physiology Part B: Biochemistry and Molecular Biology **131:**613-620.

2. **Lia X, Parka A, Estrelaa R, Kimb S, Jin Y, Cate J.** 2016. Comparison of xylose fermentation by two high-performance engineered strains of Saccharomyces cerevisiae. Biotechnology Reports **9:**53-56.

3. **Li P, Sun H, Chen Z, Li Y, Zhu T.** 2015. Construction of efficient xylose utilizing Pichia pastoris for industrial enzyme production. Microb Cell Fact **14:**22.

4. **Lee SJ, Lee SJ, Lee DW.** 2013. Design and development of synthetic microbial platform cells for bioenergy. Front Microbiol **4:**92.

5. **Sandstrom AG, Munoz de Las Heras A, Portugal-Nunes D, Gorwa-Grauslund MF.** 2015. Engineering of Saccharomyces cerevisiae for the production of poly-3-d-hydroxybutyrate from xylose. AMB Express **5:**14.

6. **Agrawal M, Mao ZC, Chen RR.** 2011. Adaptation Yields a Highly Efficient Xylose-Fermenting Zymomonas mobilis Strain. Biotechnology and Bioengineering **108:**777-785.

7. **Ko BS, Kim J, Kim JH.** 2006. Production of xylitol from D-xylose by a xylitol dehydrogenase gene-disrupted mutant of Candida tropicalis. Appl Environ Microbiol **72:**4207-4213.

8. **Stephens C, Christen B, Fuchs T, Sundaram V, Watanabe K, Jenal U.** 2007. Genetic analysis of a novel pathway for D-xylose metabolism in Caulobacter crescentus. J Bacteriol **189:**2181-2185.

9. **Young E, Poucher A, Comer A, Bailey A, Alper H.** 2011. Functional Survey for Heterologous Sugar Transport Proteins, Using Saccharomyces cerevisiae as a Host. Applied and Environmental Microbiology **77:**3311-3319.

10. **Gu Y, Ding Y, Ren C, Sun Z, Rodionov DA, Zhang W, Yang S, Yang C, Jiang W.** 2010. Reconstruction of xylose utilization pathway and regulons in Firmicutes. BMC Genomics **11:**255.

11. **Ceroni F, Carbonell P, Francois JM, Haynes KA.** 2015. Editorial - Synthetic Biology: Engineering Complexity and Refactoring Cell Capabilities. Front Bioeng Biotechnol **3:**120.

12. **Lee SM, Jellison T, Alper HS.** 2012. Directed evolution of xylose isomerase for improved xylose catabolism and fermentation in the yeast Saccharomyces cerevisiae. Appl Environ Microbiol **78:**5708-5716.

13. **Szeinbaum N, Burns JL, DiChristina TJ.** 2014. Electron transport and protein secretion pathways involved in Mn(III) reduction by Shewanella oneidensis. Environ Microbiol Rep **6:**490-500.

14. **Wee SK, Burns JL, DiChristina TJ.** 2014. Identification of a molecular signature unique to metal-reducing Gammaproteobacteria. FEMS Microbiol Lett **350:**90-99.

15. **Howard EC, Hamdan LJ, Lizewski SE, Ringeisen BR.** 2012. High frequency of glucose-utilizing mutants in Shewanella oneidensis MR-1. FEMS Microbiol Lett **327:**9-14.

16. **Choi D, Lee SB, Kim S, Min B, Choi IG, Chang IS.** 2014. Metabolically engineered glucose-utilizing Shewanella strains under anaerobic conditions. Bioresour Technol **154:**59-66.

17. **Flynn JM, Ross DE, Hunt KA, Bond DR, Gralnick JA.** 2010. Enabling unbalanced fermentations by using engineered electrode-interfaced bacteria. MBio **1**.

18. **Rodionov DA, Yang C, Li X, Rodionova IA, Wang Y, Obraztsova AY, Zagnitko OP, Overbeek R, Romine MF, Reed S, Fredrickson JK, Nealson KH, Osterman AL.** 2010. Genomic encyclopedia of sugar utilization pathways in the Shewanella genus. BMC Genomics **11:**494.

19. **Roth JR, Kugelberg E, Reams AB, Kofoid E, Andersson DI.** 2006. Origin of mutations under selection: the adaptive mutation controversy. Annu Rev Microbiol **60:**477-501.

20. **Finkel SE.** 2006. Long-term survival during stationary phase: evolution and the GASP phenotype. Nat Rev Microbiol **4:**113-120.

21. **Fong SS, Marciniak JY, Palsson BO.** 2003. Description and interpretation of adaptive evolution of Escherichia coli K-12 MG1655 by using a genome-scale in silico metabolic model. J Bacteriol **185:**6400-6408.

22. **Kuyper M, Toirkens MJ, Diderich JA, Winkler AA, van Dijken JP, Pronk JT.** 2005. Evolutionary engineering of mixed-sugar utilization by a xylose-fermenting Saccharomyces cerevisiae strain. FEMS Yeast Res **5:**925-934.

23. **Rosenberg SM.** 2001. Evolving responsively: adaptive mutation. Nat Rev Genet **2:**504-515.

24. **Tang YJ, Martin HG, Dehal PS, Deutschbauer A, Llora X, Meadows A, Arkin A, Keasling JD.** 2009. Metabolic flux analysis of Shewanella spp. reveals evolutionary robustness in central carbon metabolism. Biotechnol Bioeng **102:**1161-1169.

25. **Akaraonye E, Keshavarz T, Roy I.** 2010. Production of polyhydroxyalkanoates: the future green materials of choice. J Chem Technol Biotechnol **85:**732-743.

26. **Keshavarz T, Roy I.** 2010. Polyhydroxyalkanoates: bioplastics with a green agenda. Curr Opin Microbiol **13:**321-326.

27. **Hankermeyer CR, RS T.** 1999. Polyhydroxybutyrate: Plastic made and degraded by microorganisms, vol 159. Springer, New York.

28. **Green R.** 2010. Current strategies for optimizing polyhydroxyalkanoate production in bacteria systems. MMG 445 Basic Biotechnol eJournal **6:**1-6.

29. **Khanna S, Srivastava A.** 2005. Recent advances in microbial polyhydroxyalkanoates. Process Biochem **40:**607-619.

30. **Steinbuchel A, Hustede E, Liebergesell M, Pieper U, Timm A, Valentin H.** 1993. Molecular basis for biosynthesis and accumulation of polyhydroxyalkanoic acids in bacteria. FEMS Microbiol Rev **10:**347-350.

31. **Doi Y, Kawaguchi Y, Koyama N, Nakamura S, Hiramitsu M, Yoshida Y, Kimura H.** 1992. Synthesis and degradation of polyhydroxyalkanoates in Alcaligenes eutrophus. FEMS Microbiol Lett **103:**103-108.

32. **Pham TH, Webb JS, Rehm BHA.** 2004. The role of polyhydroxyalkanoate biosynthesis by Pseudomonas aeruginosa in rhamnolipid and alginate production as well as stress tolerance and biofilm formation. Microbiological Research **150:**3405-3413.

33. **Singh M, Patel S, Kalia V.** 2009. Bacillus subtilis as potential producer for polyhydroxyalkanoates. Microb Cell Fact **8:**38.

34. **Steinbüchel A.** 2001. Perspectives for biotechnological production and utilization of biopolymers: Metabolic engineering of polyhydroxyalkanoate biosynthesis pathways as a successful example. Macromol Biosci **1:**1-24.

35. **Kocharin K, Chen Y, Siewers V, Nielsen J.** 2012. Engineering of acetyl-CoA metabolism for the improved production of polyhydroxybutyrate in Saccharomyces cerevisiae. AMB Express **2:**52.

36. **Peoples OP, Sinskey AJ.** 1989. Poly-beta-hydroxybutyrate (PHB) biosynthesis in Alcaligenes eutrophus H16. Identification and characterization of the PHB polymerase gene (phbC). J Biol Chem **264:**15298-15303.

37. **Handrick R, Reinhardt S, Kimmig P, Jendrossek D.** 2004. The "intracellular" poly(3-hydroxybutyrate) (PHB) depolymerase of Rhodospirillum rubrum is a periplasm-located protein with specificity for native PHB and with structural similarity to extracellular PHB depolymerases. J Bacteriol **186:**7243-7253.

38. **Geer LY, Marchler-Bauer A, Geer RC, Han L, He J, He S, Liu C, Shi W, Bryant SH.** 2010. The NCBI BioSystems database. Nucleic Acids Res **38:**D492-496.

39. **Sambrook J, Fritsh EF, Maniatis T.** 1989. Molecular Cloning: A Laboratory Manual. Cold Spring Harbor Laboratory Press; Cold Spring Harbor, NY.

40. **Dichristina TJ, Delong EF.** 1994. Isolation of Anaerobic Respiratory Mutants of Shewanella-Putrefaciens and Genetic-Analysis of Mutants Deficient in Anaerobic Growth on Fe3+. Journal of Bacteriology **176:**1468-1474.

41. **Taratus EM, Eubanks SG, DiChristina TJ.** 2000. Design and application of a rapid screening technique for isolation of selenite reduction-deficient mutants of Shewanella putrefaciens. Microbiol Res **155:**79-85.

42. **Payne AN, Dichristina TJ.** 2006. A rapid mutant screening technique for detection of technetium [Tc(VII)] reduction-deficient mutants of Shewanella oneidensis MR-1. FEMS Microbiol Lett **259:**282-287.

43. **Roy A, Kucukural A, Zhang Y.** 2010. I-TASSER: a unified platform for automated protein structure and function prediction. Nat Protoc **5:**725-738.

44. **Agrawal M, Chen RR.** 2011. Discovery and characterization of a xylose reductase from Zymomonas mobilis ZM4. Biotechnol Lett **33:**2127-2133.

45. **Akinterinwa O, Cirino PC.** 2009. Heterologous expression of D-xylulokinase from Pichia stipitis enables high levels of xylitol production by engineered Escherichia coli growing on xylose. Metab Eng **11:**48-55.

46. **McCorkindale J, Edson NL.** 1954. Polyol dehydrogenases. I. The specificity of rat-liver polyol dehydrogenase. Biochem J **57:**518-523.

47. **Burns JL, Ginn BR, Bates DJ, Dublin SN, Taylor JV, Apkarian RP, Amaro-Garcia S, Neal AL, Dichristina TJ.** 2010. Outer Membrane-Associated Serine Protease Involved in Adhesion of Shewanella oneidensis to Fe(III) Oxides. Environmental Science & Technology **44:**68-73.

48. **Miller GL.** 1959. Use of dinitrosalicylic acid reagent for determination of reducing sugar. Analytical Chemistry **31:**426-428.

49. **Kratschmar D, Wallner S, Florenski S, Schmid D, Kuhn R.** 1999. Analysis of Oligosaccharides by MEKC with Aminobenzoic Alkyl Esters as Derivatization Agents. Chromatographia **50:**596-600.

50. **Montgomery H, Dymock JF.** 1962. The rapid determination of nitrite in fresh and saline waters. Analyst **87:**374-378.

51. **Li LL, Gao J, Jiang H.** 2013. Production of 3-Hydroxybutyrate Monomers by Pseudomonas mendocina DS04-T Biodegraded Polyhydroxybutyrate. J Polym Environ **21:**826-832.

52. **Metzger MH, Hollenberg CP.** 1995. Amino acid substitutions in the yeast Pichia stipitis xylitol dehydrogenase coenzyme-binding domain affect the coenzyme specificity. Eur J Biochem **228:**50-54.

53. **Di Luccio E, Petschacher B, Voegtli J, Chou HT, Stahlberg H, Nidetzky B, Wilson DK.** 2007. Structural and kinetic studies of induced fit in xylulose kinase from Escherichia coli. J Mol Biol **365:**783-798.

54. **Kanehisa M, Goto S.** 2000. KEGG: kyoto encyclopedia of genes and genomes. Nucleic Acids Res **28:**27-30.

55. **Myers CR, Nealson KH.** 1988. Bacterial manganese reduction and growth with manganese oxide as the sole electron acceptor. Science **240:**1319-1321.

56. **Cooper R, Goff J, Reed B, Sekar R, DiChristina TJ.** 2015. Breathing Iron: Molecular Mechanism of Microbial Iron Reduction by Shewanella oneidensis, p 5.2.1-1-5.2.1-13. *In* Yates M, Nakatsu C, Miller R, Pillai S (ed), Manual of Environmental Microbiology, Fourth Edition doi:10.1128/9781555818821.ch5.2.1. ASM Press, Washington DC.

57. **Jeon JM, Park H, Seo HM, Kim JH, Bhatia SK, Sathiyanarayanan G, Song HS, Park SH, Choi KY, Sang BI, Yang YH.** 2015. Isobutanol production from an engineered Shewanella oneidensis MR-1. Bioprocess Biosyst Eng **38:**2147-2154.

58. **Visser EM, Leal TF, de Almeida MN, Guimaraes VM.** 2015. Increased enzymatic hydrolysis of sugarcane bagasse from enzyme recycling. Biotechnol Biofuels **8:**5.

59. **Shinnick SG, Perez SA, Varela MF.** 2003. Altered substrate selection of the melibiose transporter (MelY) of Enterobacter cloacae involving point mutations in Leu-88, Leu-91, and Ala-182 that confer enhanced center dot maltose transport. Journal of Bacteriology **185:**3672-3677.

60. **King SC, Wilson TH.** 1990. Identification of Valine 177 as a Mutation Altering Specificity for Transport of Sugars by the Escherichia-Coli Lactose Carrier - Enhanced Specificity for Sucrose and Maltose. Journal of Biological Chemistry **265:**9638-9644.

61. **Van Camp BM, Crow RR, Peng Y, Varela MF.** 2007. Amino acids that confer transport of Raffinose and Maltose Sugars in the Raffinose Permease (RafB) of Escherichia coli as implicated by spontaneous mutations at Val-35, Ser-138, Ser-139, Gly-389 and Ile-391. Journal of Membrane Biology **220:**87-95.

62. **Sun L, Zeng X, Yan C, Sun X, Gong X, Rao Y, Yan N.** 2012. Crystal structure of a bacterial homologue of glucose transporters GLUT1-4. Nature **490:**361-366.

63. **Sekar R, DiChristina TJ.** 2014. Microbially driven fenton reaction for degradation of the widespread environmental contaminant 1,4-dioxane. Environ Sci Technol **48:**12858-12867.

5.6 Supplementary Information

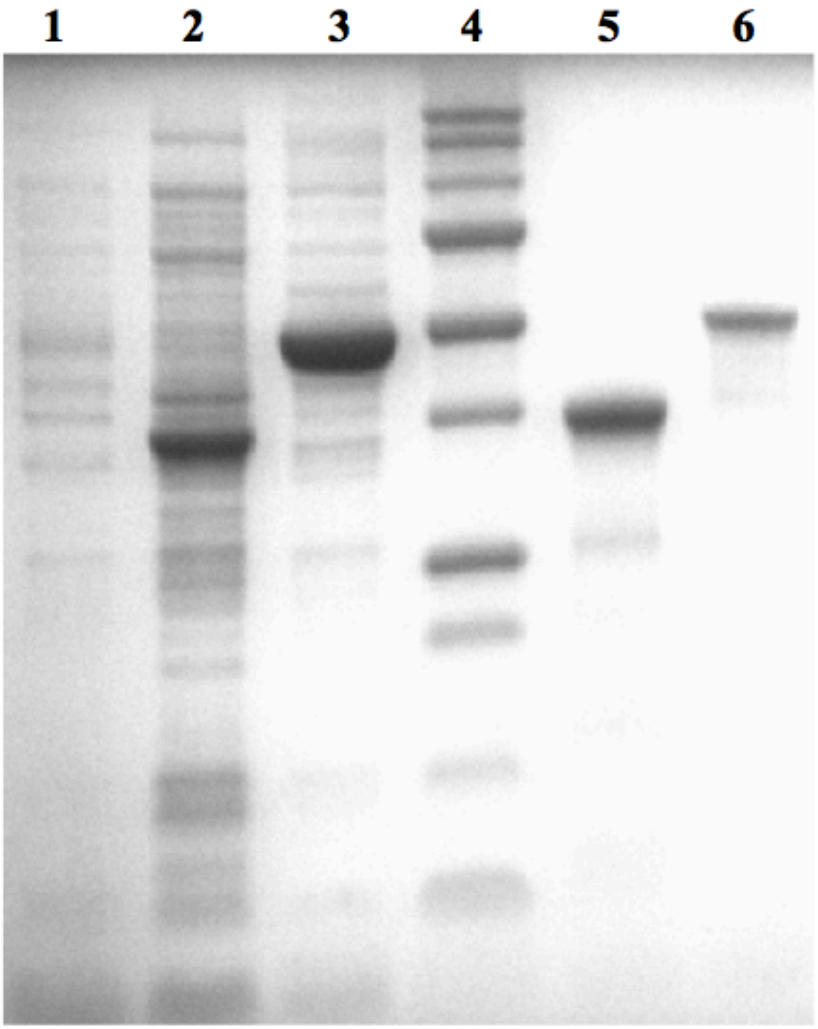

Figure. 5.S1. SDS-PAGE for expression of recombinant SO_0900 & SO_4230 from *E. coli* JM109. Each lane was loaded with 20 g protein. Lanes: 1, Empty pQE80L plasmid crude; 2, SO_0900 crude; 3, SO_4230 crude; 4, MW marker; 5, SO_0900 pure; 6, SO_4230 pure.

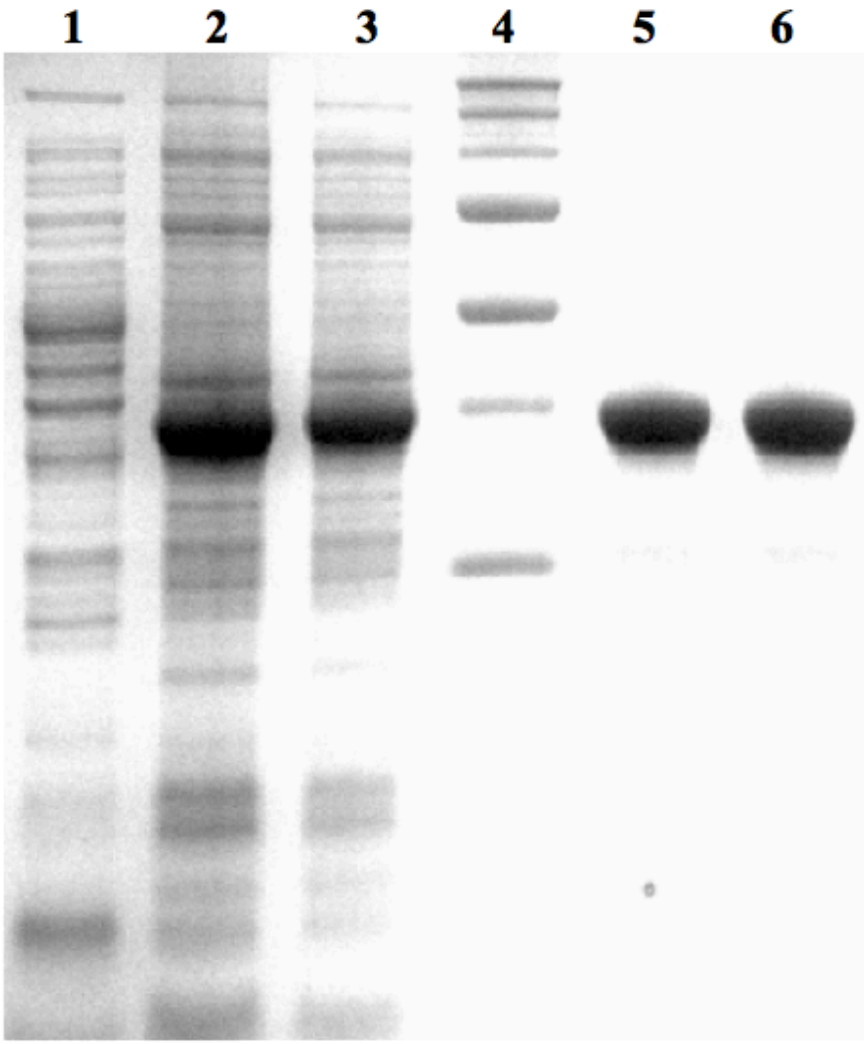

Figure. 5.S2. SDS-PAGE for expression of recombinant SO_4673 & SO_2452 from *E. coli* JM109. Each lane was loaded with 20 g protein. Lanes: 1, Empty pQE80L plasmid crude; 2, SO_4673 crude; 3, SO_2452 crude; 4, MW marker; 5, SO_4673 pure; 6, SO_2452 pure.

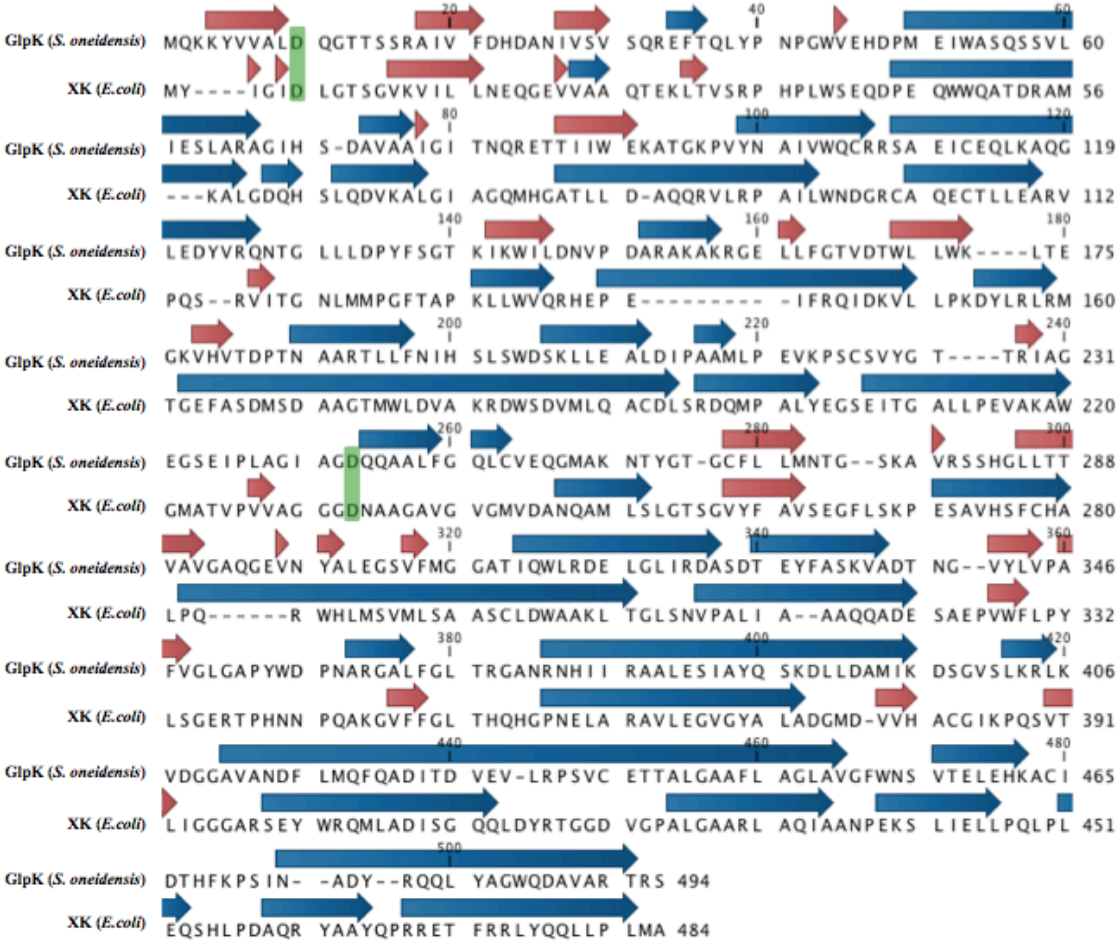

Figure. 5.S3. Pairwise sequence alignment of glycerol kinase (from *S. oneidensis*) and xylulokinase (from *E.coli*). Blue arrows indicate alpha helix and red arrows indicate beta strands. Green shades indicate homologous residues Asp10, Asp244 (GlpK - *S. oneidensis*) and Asp6, Asp233 (XK - *E.coli*).

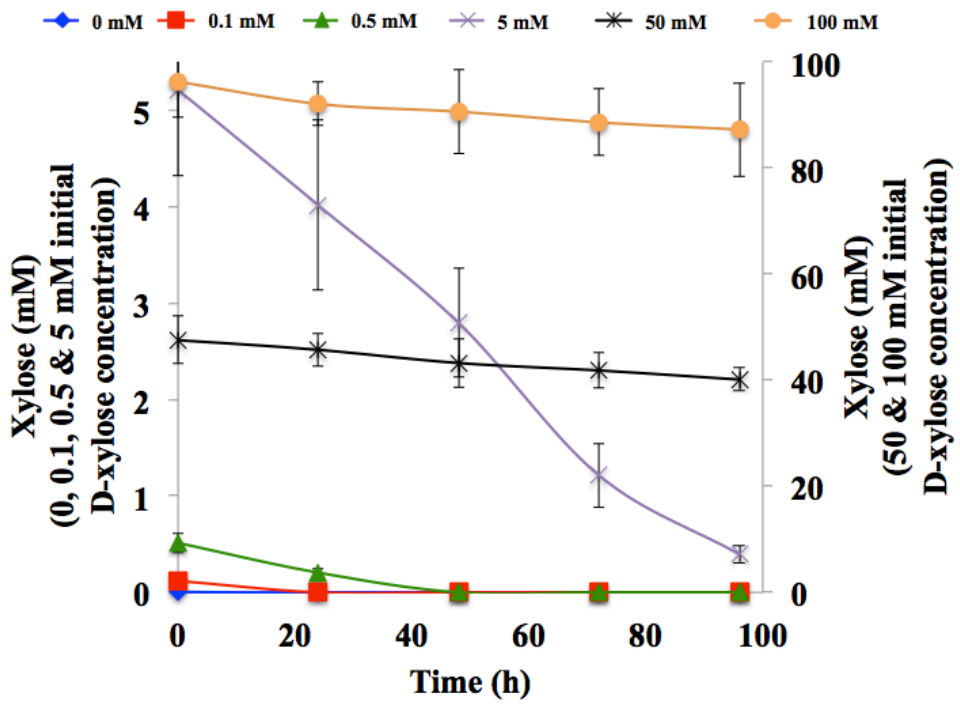

Figure. 5.S4. Xylose concentration profiles during PHB production by strain XM1 harboring the PHB biosynthetic genes *phaCAB*. Cells were cultured in LB and gene expression was induced by the addition of 0.5 mM arabinose. Cells were then resuspended in minimal media with 0 - 100 mM xylose as sole carbon and electron source. Primary y-axis (left) - 0 mM; blue (◆), 0.1 mM; red (■), 0.5 mM; green (▲), 5 mM; violet (x), Secondary y-axis (right) - 50 mM; black (*), 100 mM; orange (●). Error bars represent range of errors in duplicate batch reactors.

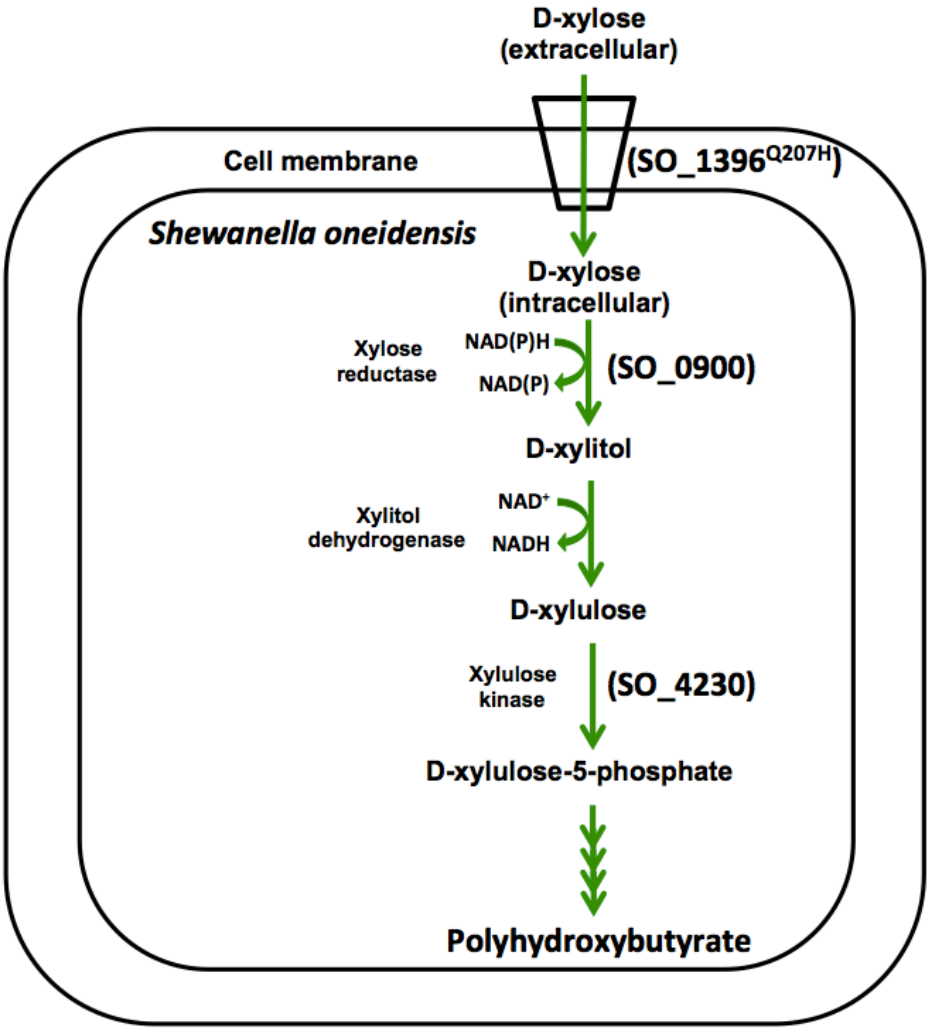

Figure. 5.S5. Working model of the xylose catabolic pathway in strain XM1 including putative xylose transporter SO_1396^{Q207H}, putative xylose reductase SO_0900, and putative xylulose reductase SO_4230 identified in the present study

Table 5.S1. Composition of SM media

Compound	Concentration (mM)
Sodium DL lactate	10
Potassium Phosphate	10
NH_4SO_4	15
$MgSO_4.\ 7H_2O$	1
$CaCl_2.2H_2O$	0.48
EDTA, disodium salt	0.67
$FeSO_4.7H_2O$	0.1
$NaHCO_3$	0.2
$FeCl_3$	0.1
Na_2SeO_4	0.01
H_3BO_3	0.05
$ZnSO_4.7H_2O$	0.005
$Na_2MoO_4.2H_2O$	0.007
$CuSO_4.5H_2O$	0.001
$MnSO_4.H_2O$	0.001
$CoSO_4.7H_2O$	0.05
$NiCl_2.6H_2O$	0.08
NaCl	0.1

Table 5.S2. List of strains and plasmids used in this study

Strains	Feature(s)
Shewanella oneidensis MR-1	Wild type strain
XM1	Xylose-adapted strain
XM1 ΔSO1396^{Q207H}	Xylose-adapted strain with SO1396^{Q207H} gene deleted
XM1 ΔSO1396^{Q207H} + pBBR1MCS-SO1396^{Q207H}	Xylose-adapted strain with SO1396^{Q207H} deleted harboring pBBR1MCS with SO1396^{Q207H} complementation
XM1 ΔSO0900	Xylose-adapted strain with SO0900 gene deleted
XM1 ΔSO4230	Xylose-adapted strain with SO4230 gene deleted
XM1 pBAD-*phaCAB*	Xylose-adapted strain complemented with pBBR1MCS harboring *phaCAB* genes
Escherichia coli β 2155 λ pir	F- *mcrA* Δ(*mrr-hsd*RMS-*mcr*BC) ϕ80d*lac*ZΔM15 Δ*lacX*74 *rec*A1 *end*A1 *ara*D139 Δ(*ara leu*)7697 *gal*U *gal*K λ- *thrB*1004 *pro thi str*A *hsd*S *lac*ZM15 (F9 *lac*ZΔM15 *lacI*^{q} *tra*D36 *pro*A1 *pro*B1) Δ*dapA*::*erm pir*::RP4 Km^{r}
Escherichia coli JM109	*end*A1 *gln*V44 *thi*$^{-1}$ *rel*A1 *gyr*A96 *rec*A1 *mcr*B^{+} Δ(*lac*$^{-}$*pro*AB) e14^{-} [F' *tra*D36 *pro*AB^{+} *lacI*^{q} *lac*ZΔM15] *hsd*R17($r_K^-m_K^+$)
Ralstonia Eutropha	Wild type strain
JM109 pQE80L-0900	JM109 complemented with pQE80L harboring SO0900 genes
JM109 pQE80L-4673	JM109 complemented with pQE80L harboring SO4673 genes
JM109 pQE80L-4230	JM109 complemented with pQE80L harboring SO4230 genes
JM109 pQE80L-2452	JM109 complemented with pQE80L harboring SO2452 genes

Plasmids	
pKO2.0	4.5-kb γR6K, mob RP4 *sac*B Gm^R *lac*Z
pBBR1MCS	4.7-kb Cm^R *lac*Z
pBBR1MCS-1396 ^{Q207H}	Plasmid with SO1396 ^{Q207H} inserted
pQE80L	4.8-kb ColE1 Amp^R *lac*I^q 6xHis (N-terminal)
pQE80L-SO0900	Plasmid under pBAD promoter and SO0900 gene inserted
pQE80L-SO4230	Plasmid under pBAD promoter and SO4230 gene inserted
pQE80L-SO2452	Plasmid under pBAD promoter and SO2452 gene inserted
pBBR1MCS-*phaCAB*	Plasmid under arabinose promoter and phaCAB operon inserted

Table 5.S2 continued

Table 5.S3. List of the primers used in this study. Underline indicates restriction enzyme cutting site

Gene/operon	Sequence (5' – 3')
SO_1396 (Knockout)	CTCGATACCAGCCCATTTACG
	GACTGGATCCGCAATGGACCCTCGGCGATATGC
	CGTCATTATTTGGTATCAATCTCGTGGACGGCTAAGCCTCGAATCGC
	GCGATTCGAGGCTTAGCCGTCCACGAGATTGATACCAAATAATGACG
	GACTGTCGACGGTGATTGATGGCTCGAACAGCTTGG
	GCTGCAAACCAACTTTTCATGG
	GAAGATATTGGCGAATAACCAACC
	GTGGTCGATTCTTTTGAGAACG
	GCCGAGCAATACAGTGCTTGG
	CTCAGCATGACAATAATGTCTG
SO_0900 (Knockout)	GCAGCGCAGTCCACAGGCCACTATTAA
	GACTGGATCCCGTCTAAGCCATTGCAGCGGATCAC
	CTAAGGACAGGGCAATCTAAATTGGCGGTATGCGTCTGTATTCCAT
	ATGGAATACAGACGCATACCGCCAATTTAGATTGCCCTGTCCTTAG
	GACTGTCGACGCTTGCATCACTTGCAACGACTGCGC
	GCTTCAAGCAGGGGATAATCGTCG
SO_4230 (Knockout)	CCACATAGGGCTCACTGG
	GACTGGATCCGGTCTATATGGGTAACACC
	TTAAGAACGGGTTCTTGCTACTGCGGCCACCACATATTTCTTTTGCAC
	GTGCAAAAGAAATATGTGGTGGCCGCAGTAGCAAGAACCCGTTCTTAA
	GACTGTCGACGGAATTAGCCTGAGTTACCAGC
	CCTGTATGACATCAACCATCAGC
SO_0900 (cloning)	GACTGGATCCATGGAATACAGACGCATACCGC
	GACTGTCGACCTAAGGACAGGGCAATCTAAATTG
SO_4673 (cloning)	GACTGGATCCATGAAAGCACTAAGCAAGTTAAAAGC
	GACTGTCGACTTAATCCCAGCTGAGGATGACTTTACC
SO_4230 (cloning)	GACTGGATCCGTGCAAAAGAAATATGTGGTGGCCC
	GACTGGTACCTTAAGAACGGGTTCTTGCTACTGC
SO_1396^{Q207H} (cloning)	CTCGCAGGATCCGCTAAGGAGACGAGAAATTGGGGATATTTTTTA TGAATATC
	CGATGCGTCGACTCAGTATTTTGAAGCTTGCTGGCG
SO_2452 (cloning)	CATGATGGATCC ATGGAGCAACATCAAGTTTGG
	TCCATCGTCGAC ATCTATCACTCGTTTAGGGTTAACACT
phaCAB (cloning)	CTCGCAGCTAGCATGGCGACCGGCAAAGGCGCGGCA
	CGATGCGAATTCTCAGCCCATATGCAGGCCGCCGTT
	CTCGCAGAATTCAAGGGCGAGCTCAAGCTTGAAGGT
	CGATGCGCTAGCGGGTATGTATATCTCCTTCTTAAAGT

Table 5.S4. Blast analysis of SO_1396

	Protein/locus tag	Organism	Size (aa)	Identity (%)	Similarity (%)	e-value	Coverage (%)
	SO_1396 (Template)	*S. oneidensis* MR-1	365				
Top 3 hits in *Shewanella sp*	Sbal223_1289	*S. baltica* OS223	401	78	88	0	99
	AEA42_07100	*Shewanella sp.* Sh95	400	86	94	0	96
	NA	*Shewanella sp*. ZOR0012	400	86	93	0	96
Top 3 hits outside *Shewanella sp*	BG00_17450	*Pseudoalteromonas sp.* SCSIO_11900	361	40	61	3.E-79	95
	AMS57_07405	*Pseudoalteromonas tetraodonis*	361	40	61	4.E-78	95
	ND6B_3400	*Pseudoalteromonas sp.* ND6B	366	40	61	5.E-78	95
Known D-xylose transporters	XylE	*E.coli*	491	29	51	2.E-02	60
	GAL2	*S. cerevisiae*	574	24	48	9.0	6
	XUT1	*S. stipitis*	566	63	79	3.0	9

Table 5.S5. Blast analysis of SO_0900

	Protein/locus tag	Organism	Size (aa)	Identity (%)	Similarity (%)	e-value	Coverage (%)
	SO_0900 (Template)	*S. oneidensis* MR-1	346				
Top 3 hits in *Shewanella sp*	SOHN41_00409	*Shewanella sp.* HN-41	346	97	98	0	100
	Shewmr4_0747	*Shewanella sp.* MR-4	346	98	99	0	100
	Shewmr7_3273	*Shewanella sp.* MR-7	346	99	99	0	100
Top 3 hits outside *Shewanella sp*	AALB_3252	*Agarivorans albus* MKT 106	346	67	81	2.E-172	100
	VIBNISFn118_760019	*Vibrio nigripulchritudo* SFn118	344	66	80	8.E-166	100
	JV59_36730	*Vibrio coralliilyticus*	344	65	78	4.E-160	100
Known D-xylose reductases	ECs0473	*Escherichia coli*	324	31	51	7.E-44	96
	XylR	*Candida tenuis*	322	33	60	4.E-10	32
	ZMO0976	*Zymomonas mobilis*	340	32	48	5.E-29	67

Table 5.S6. Blast analysis of SO_4673

	Protein/locus tag	Organism	Size (aa)	Identity (%)	Similarity (%)	e-value	Coverage (%)
	SO_4673 (Template)	*S. oneidensis* MR-1	341				
Top 3 hits in *Shewanella sp*	AEA42_15490	*Shewanella sp.* Sh95	341	99	99	0	100
	SOHN41_00043	*Shewanella sp.* HN-41	341	99	99	0	100
	Sputcn32_3902	*S. putrefaciens* CN-32	341	99	99	0	100
Top 3 hits outside *Shewanella sp*	VO69_19065	*Aeromonas salmonicida*	342	89	94	0	100
	ERIG_03807	*Escherichia fergusonii* B253	341	89	94	0	100
	SARI_03933	*Salmonella enterica*	341	88	94	0	100
Known D-xylitol dehydrogenases	AGROH133_13378	*Agrobacterium sp.* H13-3	345	28	46	4.E-35	89
	L230_07742	*Staphylococcus aureus* CBD-635	341	22	40	7.E-06	92%
	N42_2157	*Lactococcus lactis*	341	20	42	6.E-07	76%

Table 5.S7. Blast analysis of SO_2452

	Protein/locus tag	Organism	Size (aa)	Identity	Similarity	e-value	Coverage
	SO_2452 (Template)	*S. oneidensis* MR-1	314				
Top 3 hits in *Shewanella sp*	AWJ07_20235	*S. frigidimarina*	335	29%	47%	9.E-23	71%
	Swoo_2967	*S. woodyi*	313	28%	46%	3.E-16	71%
	Sden_2242	*S. denitrificans* OS217	314	27%	41%	1.E-15	92%
Top 3 hits outside *Shewanella sp*	Y702_01970	*Vibrio vulnificus* BAA87	313	71%	84%	1.E-168	99%
	AAY54_06065	*Vibrio metoecus*	313	70%	85%	1.E-167	99%
	VEJY3_09035	*Vibrio sp.* EJY3	313	70%	84%	3.E-166	99%
Known D-xylitol dehydrogenases	Shal_2008	*S. halifaxis*	344	22%	40%	8.E-07	68%
	Spea_2286	*S. pealeana*	344	22%	36%	1.E-05	61%
	AGROH133_13378	*Agrobacterium sp*. H13-3	345	21%	36%	1.E-05	49%

Table 5.S8. Blast analysis of SO_4230

	Protein/locus tag	Organism	Size (aa)	Identity (%)	Similarity (%)	e-value	Coverage (%)
	SO_4230 (Template)	*S. oneidensis* MR-1	494				
Top 3 hits in *Shewanella sp*	SHD_0561	*S. decolorationis* S12	500	96	97	0	100
	Shewana3_3756	*Shewanella sp.* ANA-3	494	96	97	0	100
	Shewmr4_3583	*Shewanella sp.* MR-4	494	96	97	0	100
Top 3 hits outside *Shewanella sp*	Tola_0068	*Tolumonas auensis* DSM 9187	497	75	87	0	99
	WL1483_4080	*Aeromonas shubertii*	504	75	86	0	99
	AH4AK4_1492	*Aeromonas hydrophilia* 4AK4	500	75	86	0	99
Known D-xylulokinases	M943_03795	*Mycobacterium tuberculosis* EAI5	480	28	40	1.E-14	95
	STM3660	*Salmonella enterica Typhimurium*	484	24	42	4.E-26	89
	ECs4447	*Escherichia coli*	484	24	41	2.E-26	97
	GlpK	*Escherichia coli*	502	72	84	0	99

Table 5.S9 Comparison of protein characteristics of SO_0900 and SO_4230 with xylose reductase and xylulokinase from other organisms respectively.

Metabolic function	Protein	Organism	Specific activity (U/mg)	k_m (mM)	V_{max} (U/mg)
Xylose reductase	SO_0900	*S. oneidensis*	2.93 ± 0.17	93 ± 7	3.41 ± 0.21
	XR	*Zymomonas mobilis*	3.4 ± 0.2	258 ± 43	6.9 ± 1.2
	XR	*Pichia stipitis*	16.7	42	16.7
	XR	*S. cerevisiae*	2	142	NA*
	XR	*Neospora crassa*	72.5	34	NA*
Xylulokinase	SO_4230	*S. oneidensis*	0.2 ± 0.013	1.7 ± 0.12	0.52 ± 0.02
	XK	*Escherichia coli*	1.6	0.3	NA*
	XK	*S. cerevisiae*	3	0.31	38.4
	XK	*Mucor circinelloides*	10.8	0.29	32
	XK	*Pichia stipitis* NCYC 1541	21.4	0.52	NA*

CHAPTER 6

CONCLUSIONS AND FUTURE RECOMMENDATIONS

6.1 Conclusions

Due to their high oxidation potential, Fenton reaction-generated HO• radicals oxidatively degrade a wide variety of hazardous organic compounds. Microbially-driven Fenton reactions designed in the present study was based on production of H_2O_2 via microbial O_2 respiration and Fe(II) via microbial Fe(III) reduction alleviate the need for continual addition of H_2O_2 and Fe(II) that drive the chemical Fenton reaction [1-3]. The microbially driven Fenton degradation of 1,4-dioxane was driven by pure cultures of the Fe(III)-reducing facultative anaerobe *S. oneidensis*. *S. oneidensis* batch cultures were provided with lactate, Fe(III), and 1,4-dioxane and were exposed to alternating aerobic and anaerobic conditions. The microbially driven Fenton reaction completely degraded 1,4-dioxane (10 mM initial concentration) in 53 h with an optimal aerobic-anaerobic cycling period of 3 h. Acetate and oxalate were detected as transient intermediates during the microbially-driven Fenton degradation of 1,4-dioxane, an indication that conventional and microbially-driven Fenton degradation processes follow similar reaction pathways (Chapter 2).

The main objective in chapter 3 was to design a new fed batch microbially driven fenton reaction system to simultaneously degrade single, binary and ternery mixtures of TCE, PCE and 1,4-dioxane. In the newly designed reaction system, Fe(II)-generating, H_2O_2-generating, and contaminant degradation phases were separated to minimize contaminant loss due to volatility. Results indicate that the microbially-driven Fenton

reaction system degraded TCE, PCE, and 1,4-dioxane either as single contaminants or as binary and ternary mixtures. In the presence of equimolar concentrations of TCE and PCE, the ratio of the experimentally derived rates of TCE and PCE degradation was nearly identical to the ratio of the corresponding HO• radical reaction rate constants. The new microbially-driven Fenton reaction system may be applied as an *ex situ* platform for simultaneous degradation of co-mingled TCE, PCE, and 1,4-dioxane and provides valuable information for future development of *in situ* remediation technologies.

The main objective in chapter 4 was to apply the newly designed microbially-driven Fenton reactor system to directly pretreat and hydrolyze cellulose and hemicellulose to produce short-chain sugar oligosaccharides. The microbially driven fenton reaction degraded cellulose and hemicellulose to produce a mixture of cellodextrins and xylodextrins as products. We also demonstrated that the individual cellodextrin and xylodextrins degraded to their respective shorter oligosaccharides with lower DP values. The xylose produced as the main byproduct of hemicellulose degradation was fermentable and was coupled to PHB production by XM1. The combined pretreatment and saccharification method for cellulose and xylan developed did not involve the addition of acid, alkali compounds or the use of hydrolyzing enzymes thus being an economically feasible process to directly produce simple fermentable sugars from cellulose and xylan [4]. Microbial Fe(III) reduction is a dominant anaerobic respiratory process in soil and sediments, which suggests that the microbially driven fenton reaction may play an important role in the degradation of decaying plant and woody materials in the natural environment in the presence of fluctuating redox

conditions thus providing a foundation for the study of organic carbon cycling in a natural setting.

The main objective in chapter 5 was to identify the xylose catabolic pathway in *S. oneidensis* genetically engineer xylose-adapted *S. oneidensis* transformants to express the PHB biosynthesis genes (*phaCAB*) of *R. eutropha* and produce PHB (biodegradable plastics) with xylose as sole carbon and energy source. Wild type *S. oneidensis* is unable to utilize xylose as sole carbon and energy source. To overcome this limitation, adaptive evolution approach was followed to generate *S. oneidensis* mutants (XM1) that metabolized xylose as sole carbon and energy source. This study led to the identification of a previously unknown xylose catabolic pathway in *S. oneidensis* including a MFS transporter (SO_1396) and two metabolic enzymes (SO_0900 & SO_4230) through complementary genetic and biochemical techniques. xylose metabolism in XM1 was succensfully coupled to PHB production with an optimum xylose concentration of 5 mM resulting in PHB production yield of 10% mg mg^{-1} DCW. This expansion of metabolic capability to convert xylose to a useful product such as PHB can be beneficial in biotechnological applications to couple multiple carbon sources such as glucose, glycerol and xylose by *S.oneidensis* to improve efficiency of electricity generation, biofuel production and bioremediation of toxic contaminants [5-7].

6.2 Recommendations for future work

6.2.1 Optimization of the current *ex situ* microbially driven Fenton reaction

The current fed-batch reactor configuration is designed to avoid contaminant loss due to high volatility during compressed air and nitrogen inputs. However, the reaction

system to degrade multiplae contaminants is not optimized. The fed-batch reactor could be optimized through a series of modifications to upscale and improve the degradation efficiency. Reaction parameters that could be varied include temperature, pH, concentrations of Fe(III) substrates and concentration of dissolved O_2, Fe(III), electron shuttles, and electron donors (lactate, acetate, or formate). Contaminant concentrations could range from those found in low-concentration plumes to source zone levels (μg/L)(1,4-dioxane: 200-50,000; TCE: 1-15; PCE: 0.5-5 [8, 9]. Fe(III) substrates could include soluble Fe(III)-citrate and solid Fe(III) oxide forms to determine the effects of Fe(III) substrates on the efficiency of the microbially driven Fenton reaction. One key to enhancing microbial Fe(III) reduction activity in the microbially driven Fenton reaction will be to provide soluble electron shuttles to enhance microbial Fe(III) reduction activity, $HO^{\bullet}$ radical production, and contaminant degradation rates. Thus, experiments with solid Fe(III) oxides could be carried out in the presence and absence of both natural (humic acid) and synthetic (anthraquinone-1,6-disulfonate; AQDS) compounds as electron shuttles.

6.2.2 Development of in situ remediation technologies based on the microbially driven Fenton reaction

Following modification of the newly developed fed batch reactor under optimized conditions, flow-through columns could be developed to degrade contaminants under dispersive and advective flow conditions. An efficient flow-through reactor design could entail maintaining reactor O_2 concentrations at approximately 15 μM to facilitate simultaneous O_2 and Fe(III) reduction in the flow-through column. Reactor O_2 concentrations may be changed by varying either O_2 concentrations in the inlet stream or

advective flow rates, which will correspondingly drive changes in microbial O_2 consumption rates and reactor O_2 concentrations. Under these conditions, the flow-through columns may produce $HO^{\cdot}$ radicals and degrade contaminants under steady state conditions.

6.2.3 Development of *S. oneidensis* capable of cometabolizing glucose and xylose mixtures as carbon and energy source

The xylose-adapted XM1 *S. oneidensis* developed in this study (Chapter 5) does not metabolize glucose as sole carbon and energy source. Glucose and xylose are the predominant byproducts from lignocellulosic biomass degradation and hydrolysis. Therefore, simultaneous fermentation of glucose and xylose has been a bottleneck and limits yield and productivity of secondary products such as bioethanol and isobutanol [10]. XM1 strain could be chemically mutagenized to produce genetic mutants that co-metabolize both glucose and xylose to produce secondary chemicals including PHB, bioethanol, isobutanol by genetically engineering *S. oneidensis* with the respective biosynthetic pathways.

6.2.4 Engineering a secretion system and improved acetyl-CoA flux for efficient polyhydroxybutyrate production in XM1

Metabolic engineering is a tool used to produce useful secondary chemicals and improve them with high yield and efficiency. Acetyl CoA is a key intermediate during carbon metabolism and the precursor of the PHB biosynthetic pathway. Therefore, the overall flux of acetyl-CoA may be chanelled to produce high amounts of PHB through identifying and deleting the genes that utilize acetyl-CoA in *S. oneidensis* such as *ackA*,

pta, *gltA*, *mdh* that convert acetyl-CoA to acetylphosphate, acetate, citrate, and malate respectively [11, 12]. XM1 genome does not have PHB depolymerase proteins thus enabling accumulation of intracellular PHB in this study. A PHB secretion system may be engineered into XM1. Intracellular PHB are spherical granules with a hydrophobic core, thus recovery from cells has been a major bottleneck in the past [13]. Current recovery systems include mechanical, chemical and biological treatments that are cost ineffective. A novel secretion system recently reported could be applied in XM1 for efficient secretion of PHB [13].

6.3 References

1. Stefan, M.I. and J.R. Bolton, *Mechanism of the degradation of 1,4-dioxane in dilute aqueous solution using the UV hydrogen peroxide process.* Environmental Science & Technology, 1998. **32**(11): p. 1588-1595.

2. Coleman, H.M., et al., *Degradation of 1,4-dioxane in water using TiO2 based photocatalytic and H2O2/UV processes.* Journal of Hazardous Materials, 2007. **146**(3): p. 496-501.

3. Kim, C.G., H.J. Seo, and B.R. Lee, *Decomposition of 1,4-dioxane by advanced oxidation and biochemical process.* J Environ Sci Health A Tox Hazard Subst Environ Eng, 2006. **41**(4): p. 599-611.

4. Rabemanolontsoa, H. and S. Saka, *Various pretreatments of lignocellulosics.* Bioresource Technology, 2016. **199**: p. 83-91.

5. Sekar, R. and T.J. DiChristina, *Microbially driven fenton reaction for degradation of the widespread environmental contaminant 1,4-dioxane.* Environ Sci Technol, 2014. **48**(21): p. 12858-67.

6. Choi, D., et al., *Metabolically engineered glucose-utilizing Shewanella strains under anaerobic conditions.* Bioresour Technol, 2014. **154**: p. 59-66.

7. Flynn, J.M., et al., *Enabling unbalanced fermentations by using engineered electrode-interfaced bacteria.* MBio, 2010. **1**(5).

8. Reyes, F.d.l., *Impacts of Sampling and Handling Procedures on DNA- and RNA-based Microbial Characterization and Quantification of Groundwater and Saturated Soil*. 2012, SERDP Project ER-1560.

9. Steffan, R.J., *Biodegradation of 1,4-Dioxane*. 2007, SERDP Project ER-1422.

10. Krahulec, S., et al., *Fermentation of mixed glucose-xylose substrates by engineered strains of Saccharomyces cerevisiae: role of the coenzyme specificity of xylose reductase, and effect of glucose on xylose utilization.* Microb Cell Fact, 2010. **9**: p. 16.

11. Geer, L.Y., et al., *The NCBI BioSystems database.* Nucleic Acids Res, 2010. **38**(Database issue): p. D492-6.

12. Kocharin, K., et al., *Engineering of acetyl-CoA metabolism for the improved production of polyhydroxybutyrate in Saccharomyces cerevisiae.* AMB Express, 2012. **2**(1): p. 52.

13. Rahman, A., et al., *Secretion of polyhydroxybutyrate in Escherichia coli using a synthetic biological engineering approach.* J Biol Eng, 2013. **7**(1): p. 24.

VITA

RAMANAN SEKAR

Ramanan Sekar was born in Mysore, Karnataka, India. He received his B.Tech in Chemical Engineering Anna University, Chennai in 2007 M.S degree in Chemical Engineering from SUNY, Buffalo in 2007. In 2011, he joined Georgia Institute of Technology to pursue a Doctoral degree in Biology. Apart from research, Ramanan is an animal lover, loves to play cricket and tennis and has participated in a number of leagues in Atlanta and winning a few of them.